

An Investigation of Yarn Spinning from Electrospun Nanofibres

MOHAMED BASEL BAZBOUZ

A Thesis Submitted in Fulfillment of the Requirement for the
Degree of Doctor of philosophy

Heriot Watt University
The School of Textiles and Design

May 2009

“The copyright in this thesis is owned by the author. Any quotation from the thesis or use of any of the information contained in it must acknowledge this thesis as the source of the quotation or information.”

ABSTRACT

The aim of the thesis is to investigate yarn spinning from electrospun nanofibres. The concepts of staple and core yarn spinning on electrospun nanofibres has been investigated by examining nanofibre uniformity, alignment, twist insertion and yarn take up by engineering and engineering a new take up mechanism. Nylon 6 nanofibres have been fabricated and used throughout this work. The effects of varying the electrospinning parameters such as applied voltage, polymer solution concentration and electrospinning distance on fibre morphology have been established for process optimization. A novel nanofibre aligning mechanism has been devised and systematically revised to enable optimization of alignment process parameters. MWCNTs have been successfully dispersed into nylon 6 nanofibres and have been aligned along the nanofibre body by manipulating the electric and stretching forces with the aid of the alignment mechanism. Novel mechanisms for spinning continuous twisted nanofibre/composite nanofibre yarn and core electrospun yarn have been researched, developed and implemented by making samples. It has been found that defining the velocity and count of the nanofibres entering the spinning zone is important for controlling the yarn count and twist per unit length. By modelling the electrospinning jet, mathematical equations for theoretically calculating the velocity of the jet and nanofibres and their count have been established, necessary for process control. Aspects of practical measurement and comparison of jet and nanofibre velocities have been described and discussed. Tensile testing of single nanofibre and nanofibre mats has been attempted for mechanical characterization. Initial results show the range of tensile strength of nylon 6 nanofibre assemblies and indicate the effect of change of process parameters. A review of those engineering mechanisms related to various nanofibre architectures and their industrial and commercial importance has also been reviewed, described and discussed.

DEDICATION

To my parents, wife, sons (Salah Al Din and Ahmed) and the rest of my family.

ACKNOWLEDGMENTS

There are so many individuals to whom I owe a tremendous amount of thanks and gratitude. I would like to start by expressing my utmost gratitude to my advisor, Prof. George K Stylios for the wisdom and knowledge that he's passed on to me, and for the patience that he has shown throughout this process.

I would like to thank Prof. Roger Wardman, Prof. Robert Christie, Dr. Alex Fotheringham, Dr. Lisa Macintyre, Dr. Robert Mather, Dr Michael Wan, Dr Xiaoming Zhao, Mr Peter sandison, Mr Liang Luo, Mrs Jayne Smith, Mr Andrew McCullough, Mrs Margaret Robson, Dr. Roger Spark and Mrs Eleanour Drummond for their insights and encouragements.

On a more personal note, I want to thank my wife. Thank you for your patience, love and devotion; you are my inspiration. To my sons Salah Al Din and Ahmed, thank you for bringing Daddy so much joy and happiness; I love you both so much.

To my parents, brothers and sisters, thank you for believing in me and for encouraging me all along.

I would like to thank my employer, Aleppo University, and the Syrian Ministry of Education, and my supervisors, Dr. Fayez Al Najjar and Dr. Nawar Kadi, for supporting me through this process.

Thanks to all of my extended family and friends for their thoughts and prayers.

Last, but most importantly, I want to thank God for giving me wisdom and strength, without Him I could do nothing.

DECLARATION STATEMENT

TABLE OF CONTENT

CHAPTER 1: INTRODUCTION OF ELECTROSPINNING NANOFIBRES AND AIMS AND RESEARCH OBJECTIVES

1.1 Introduction	1
1.2 History of electrospinning nanofibres	2
1.3 Electrospinning technique	3
1.3.1 The basic setup of the electrospinning	3
1.3.2 How electrospinning works	4
1.3.3 Process of nanofibres formation	5
1.3.3.1 Electric charges theory	5
1.3.3.2 The initiation of the jet	6
1.3.3.3 The jet travel	7
1.3.3.4 Dividing the jet into many fibres in the splitting region	7
1.3.3.5 Stops in the collection region	9
1.3.4 Effect of electrospinning parameters on nanofibres morphology	10
1.3.4.1 Polymer solution parameters	10
1.3.4.2 Electrospinning process parameters	14
1.3.4.3 Ambient parameters	17
1.4 Diversity of polymers used in electrospinning	17
1.5 Engineering aspects related to the electrospinning of nanofibre assemblies	19
1.5.1 Introduction	19
1.5.2 Nanofibre blended fabric	19
1.5.3 Nonwoven fabrics coated by nanofibre layers	21
1.5.4 Three dimensional nanofibre fabrics	24
1.5.5 Woven nanofibre fabrics.....	26
1.5.6 Core-shell, hollow and porous nanofibres	28
1.5.6.1 Core-shell nanofibres	28
1.5.6.2 Hollow nanofibres	30
1.5.6.3 Porous nanofibres	31
1.5.7 Helical nanofibre assemblies	33
1.5 Aims and research objectives	35
1.6 References	38

CHAPTER 2: INVESTIGATING THE FABRICATION OF NANOFIBRES BY ELECTROSPINNING

2.1 Introduction	53
2.2 Experimental work	53
2.2.1 Materials and electrospinning process parameters	53
2.2.2 Physical properties of the polymer solutions	55
2.2.3 Characterization	55
2.2.3.1 Scanning electron microscopy (SEM)	55
2.2.3.2 Samples preparation	57
2.3 Results and discussion	57
2.3.1 Physical properties of the polymer solutions	57
2.3.2 Morphology of electrospun nonwoven fibre mats	58
2.3.3 Effect of the polymer concentration on the fibre morphology	60
2.3.4 Effect of the voltage and spinning distance on the fibre morphology	62
2.4 Process optimization	63
2.5 References	65

CHAPTER 3: ALIGNMENT OF NANOFIBRES

3.1 Introduction	68
3.2 The concept of nanofibres alignment and reviewing nanofibre alignment	
Mechanisms	68
3.2.1 Nano aligning mechanisms based on dynamic mechanical collection	69
3.2.2 Nano aligning mechanisms based on manipulation of the electric field	71
3.2.3 Nano aligning mechanisms based on combining manipulation of electric field and dynamic collection	75
3.3 Novel mechanism for aligning nanofibres	79
3.4 Experimental work	79
3.4.1 Materials and electrospinning operation	79
3.4.2 Characterization	80
3.5 Results and discussion	81
3.5.1 Alignment of electrospun nanofibres	81
3.5.2 Effect of the collection time and space distance on the degree of alignment	83
3.5.3 Parameters affecting the density of deposited fibres	83
3.6 References	85

CHAPTER 4: NANOFIBRE FILLED WITH CARBON NANOTUBES

4.1 Introduction	90
4.2 Dispersion and alignment of CNTs in the polymer solution	91
4.3 Experimental work	92
4.3.1 Preparation of polymer - MWCNTs solution	92
4.3.2 Electrospinning of the polymer - MWCNTs solution	93
4.3.3 Characterization	93
4.3.3.1 Scanning electron microscopy (SEM)	93
4.3.3.2 Transition electron microscopy (TEM)	93
4.4 Results and discussion	94
4.4.1 Composite aligned nanofibres	94
4.4.2 Challenges of improving the dispersion of MWCNTs in the polymer solution	99
4.5 References	100

CHAPTER 5: SPINNING NANOFIBRE YARNS

5.1 Introduction	104
5.2 Review of mechanisms for spinning nanofibre yarns	105
5.2.1 Nano yarn mechanisms based on dynamic mechanical devices	105
5.2.2 Nano yarn mechanisms based on combining electric field manipulation and dynamic devices	109
5.3 Novel mechanism for spinning continuous twisted nanofibre yarn	113
5.3.1 Experimental work	115
5.3.1.1 Spinning continuous nanofibre yarn / composite continuous nanofibre yarn	115
5.3.2.1 Characterization	117
5.3.2 Results and discussion	117
5.3.2.1 Spinning continuous nanofibre yarn	117
5.3.2.2 Controlling the yarn count and twist per unit length	121
5.3.2.3 Challenges of yarn collection for future work	122
5.4 Core electrospun yarn	125
5.4.1 Novel mechanism for continuous core electrospun nano yarn	126
5.4.2 Experimental work	126
5.4.2.1 Materials and electrospinning operation	126
5.4.2.2 The principle of the core electrospun nano yarn mechanism	127

5.4.2.3 Characterization	129
5.4.3 Results and discussion	129
5.4.3.1 Observations	129
5.4.3.2 Analytical investigation of the parameters of the mechanism on the core electrospun nano yarn morphological structure	129
5.5 Nanofibre production	135
5.5.1 Introduction	135
5.5.2 Mechanisms of nanofibre production	135
5.6 References	144

CHAPTER 6: MODELLING THE ELECTROSPINNING OF NANOFIBRES

6.1 Introduction	151
6.2 Review of mathematical models of the electrospinning process	151
6.2.1 Mathematical models for the initiation of the jet	151
6.2.2 Mathematical models for the straight jet	154
6.2.2.1 Mathematical models for the straight jet based on slender body theory	154
6.2.2.2 Mathematical models for the straight jet based on allometric scaling laws	157
6.2.3 Mathematical models for the instability and splitting of the jet	159
6.2.4 Mathematical models for nanofibres collection	161
6.3 Electrospinning jet/ nanofibres velocity	161
6.3.1 Electrospinning modes theory	162
6.3.2 Practical methods for determining the jet velocity	164
6.4 Novel mathematical model for determining the kinetic features of the electrospinning nanofibres	165
6.5 Experimental work	174
6.5.1 Polymer solution preparation, electrospinning and characterization	174
6.5.2 Theoretical and practical calculation of the jet velocity	177
6.5.3 Practical determination of the collected nanofibres velocity	179
6.6 Discussion	182
6.7 References	184

CHAPTER 7: MECHANICAL CHARACTERIZATION OF NYLON 6 NANOFIBRES

7.1 Introduction	190
7.2 Review of the mechanical testing methods of nanofibres	191

7.2.1 Tensile test method	191
7.2.2 Bending test method	195
7.2.3 The nanoindentation method	197
7.3 Tensile test of nonwoven nylon 6 nanofibre mats	199
7.3.1 Experimental; electrospinning of nylon 6 nanofibres, samples preparation and nano tensile testing	199
7.3.2 Results and discussion	199
7.4 Novel approach for tensile testing of single nanofibre	202
7.4.1 Experimental; electrospinning, samples preparation and nano tensile testing	203
7.4.2 Results and discussion	205
7.4.3 Future work	209
7.5 References	210
CHAPTER 8: GENERAL DISCUSSION AND CONCLUSION	
8.1 Overall project summary	215
8.2 Summary of project results and suggestions for future work	215
APPENDICES	
Appendix A: Potential Applications of Polymer Nanofibres	222

LIST OF TABLES

Table 1.1	The most known polymers electrospun in a solution form	18
Table 1.2	Nanospider™ machine models produced by Elmarco company	23
Table 1.3	Examples of core-shell nanofibres produced by coaxial electrospinning using different materials	29
Table 2.1	Physical properties of nylon 6/formic acid at different concentrations	58
Table 3.1	Nano aligning mechanisms based on dynamic mechanical collection	70
Table 3.2	Nano aligning mechanisms based on manipulation of the electric field	72
Table 3.3	Nano aligning mechanisms based on combining manipulation of electric field and dynamic collection	76
Table 5.1	Nano yarn mechanisms based on dynamic mechanical devices	106
Table 5.2	Nano yarn mechanisms based on combining electric field manipulation and dynamic devices	109
Table 5.3	SEM images of the morphological structure of core electrospun nano yarn with different take up speed and twist under 0° degree core feed- in angle	133
Table 5.4	Schematic diagrams of electrospinning mechanisms for nanofibres production	137
Table 6.1	Definitions and units of measurement for deriving of the jet/ nanofibres velocity equations	166
Table 7.1	Mechanical characterization of single nanofibres	198

LIST OF FIGURES

Figure 1.1	Schematic illustration of the set-up used for the electrospinning process	3
Figure 1.2	A schematic illustration of the initiation steps of the jet	7
Figure 1.3	Photographs of different modes of jets chaotic motion ‘instability’ as they travel towards the grounded collector	8
Figure 1.4	A schematic illustration of the jet travel mechanism in electrospinning	9
Figure 1.5	SEM images of electrospun PEO nanofibres from different polymer solution concentrations	13
Figure 1.6	A schematic drawing and photo show nanofibre blended fabrics	20
Figure 1.7	Photos of conventional nonwoven fabric coated by nanofibres	21
Figure 1.8	SEM images of nano/micro fibres layers used as a filtration membrane	23
Figure 1.9	Schematic illustration of the nanospider™ machine produced by Elmarco ...	24
Figure 1.10	Schematic illustrations and photos of collecting processes for the fabrication of nanofibrous tubes by electrospinning using 3D collectors	26
Figure 1.11	PCL plain weave nanofibre fabric	27
Figure 1.12	Schematic illustration of the electrospinning setup with two coaxial capillaries for spinning nanofibres having a core-shell structure	30
Figure 1.13	SEM images of hollow nanofibres	31
Figure 1.14	SEM images of porous nanofibres	32
Figure 1.15	Schematic drawings of the helical nanofibre fabrications	34
Figure 1.16	SEM images of helical nanofibres	35
Figure 2.1	A photograph of the experimental electrospinning set-up used in the experiments	54
Figure 2.2	Schematic diagram of the SEM	56
Figure 2.3	Average fibre diameter (AFD) at electric fields of 12, 15 and 18 KV and polymer solution concentrations between 15 and 25 wt. % with a constant spinning distance of 5 cm	58
Figure 2.4	Average fibre diameter (AFD) at electric fields of 12, 15 and 18 KV and polymer solution concentrations between 15 and 25 wt. % with a constant spinning distance of 8 cm	59
Figure 2.5	Average fibre diameter (AFD) at electric fields of 12, 15 and 18 KV and polymer solution concentrations between 15 and 25 wt. % with a constant spinning distance of 11 cm	60
Figure 2.6	Relationship between the average fibre diameter and polymer solution concentration at three electric fields with a distance of 8 cm	61
Figure 2.7	Relationship between the average fibre diameter and applied voltage with	

	polymer concentration of 20 wt. % at distances of 5, 8 and 11 cm	62
Figure 2.8	Relationship between the average fibre diameter and distance with an applied voltage of 15 KV at polymer concentrations of 15, 20 and 25 %.....	64
Figure 2.9	SEM image of 20 wt. % nylon 6/ formic acid nanofibres at a voltage of 15 KV and a distance of 8 cm with uniform nanofibre diameters	65
Figure 3.1	Experimental set-up for electrospinning three dimensional aligned nanofibre bundles	80
Figure 3.2	Photograph of an array of aligned Nylon 6/ formic acid nanofibres	81
Figure 3.3	SEM images of aligned nylon 6 nanofibres collected under a 4 cm gap distance at 15, 30, 60 and 120 sec respectively	82
Figure 3.4	SEM images of aligned nylon 6 nanofibres with a constant collection time of 120 sec and different gap spaces between the disks	84
Figure 4.1	Computational image of SWCNTs and MWCNTs	90
Figure 4.2	Photographs of an ultrasonic homogenizer, samples of randomly and aligned nanofibres collected on Cu grids and Philips CM120 TEM	94
Figure 4.3	Photographs of nonwoven nanofibre mats for nylon 6/ MWCNTs composite, with different concentration of filler	95
Figure 4.4	SEM images of randomly collected nylon 6 nanofibres containing various concentrations of MWCNTs from 0 to 4 wt. % respectively	96
Figure 4.5	SEM images of aligned nylon 6 nanofibres containing various concentrations of MWNTs from 1 to 4 wt. % respectively	97
Figure 4.6	TEM images of random and aligned nylon 6 nanofibres containing various concentrations of MWCNTs	98
Figure 5.1	A schematic illustration of the set-up mechanism for spinning continuous nanofibre yarn	114
Figure 5.2	A photograph of the implemented mechanism for twisting highly aligned nanofibres into continuous nanofibre yarn	115
Figure 5.3	Photographs showing how the mechanism was designed step by step	116
Figure 5.4	A schematic illustration of the fibres migration in the helical structure of the yarn	118
Figure 5.5	Photographs of aligned nanofibres suspended conically in the gap between the perpendicular disks, and unequal deposited nanofibres in the spinning zone for spinning continuous yarn	119
Figure 5.6	A microscopic image of continuous nanofibres yarn spun at 750 rpm twist rate and 8 m/min with diameter of 9.40 microns	120
Figure 5.7	A microscopic image and live photograph showing that the spinning triangle was formed and the yarn was twisted during it's take up	121
Figure 5.8	Photographs of suspended aligned MWCNTs/ nylon 6 nanofibres and	

	mechanisms for spinning continuous yarn	122
Figure 5.9	SEM images of electrospun continuous yarns at different twist rates at linear take up speed of 8 m/min	123
Figure 5.10	A photograph of continuous nanofibres yarn spinning zone with replacing the metallic take up spool by glass one and introducing the grounded needle	124
Figure 5.11	Morphological structure of the aimed core electrospun nano yarn which constructed of the man made filament core with the sheath of nanofibres	126
Figure 5.12	A schematic illustration of the mechanism used for spinning core electrospun nano yarn	127
Figure 5.13	A photograph of the installed continuous core electrospun yarn mechanism for twisting in helical form highly aligned nylon 6 nanofibres on a feeding polyester single filament at 0 degree feed in angle	128
Figure 5.14	A photograph of aligned nylon 6 nanofibres deposited in the gap between the perpendicular twist disk and take up disk for producing continuous core electrospun nano yarn	129
Figure 5.15	Recorded photographs showing the concept of the core electrospun nano yarn mechanism developments	131
Figure 5.16	Photographs show three different feed-in angles 0°, 15° and 30° degrees, of the polyester filament into the spinning zone	132
Figure 5.17	SEM images showing how electrospun nylon 6 nanofibres covered helically the polyester filament in the S direction	134
Figure 5.18	SEM image of polyester core electrospun nano yarn covered with nanofibres in a helical sheath with core feed-in angle of 0° degree, take up speed of 1.5 cm/sec and twist of 500 rpm	134
Figure 5.19	Prototype of multiple spinnerets electrospinning apparatus	139
Figure 5.20	Photographs show collected nanofibre fabric mats electrospun from 19 spinnerets at different inter spinneret distances.....	140
Figure 5.21	Photographs of nine spinnerets electrospinning process	140
Figure 5.22	Photographs show steps of electrospinning from polymer solution surface acted by magnetic field	142
Figure 5.23	Photographs show steps of electrospinning from polymer solution surface acted by gas pressure	143
Figure 6.1	Axisymmetrical fluid body kept at constant electric field at a distance 'a' from an equipotential plane	153
Figure 6.2	Momentum balance on a unit section of the jet	155
Figure 6.3	Experimental pictures producing different cone thinning jet profiles	157
Figure 6.4	Mode of single jet thinning	162
Figure 6.5	Photos for the second mode of splitting single jet into multiple jet nanofibre .	162

Figure 6.6	SEM micrographs of multiple neck formation in PEO electrospun nanofibres collected on rotating wheel at linear speed of 5.3 m/sec	164
Figure 6.7	Jet speed measurement by particle tracing	165
Figure 6.8	Schematic drawing of the jet stretching and splitting into uniform branches ..	167
Figure 6.9	Live photograph for the electrospinning process with operation parameters similar to Xu's et. al. electrospinning operation parameters	176
Figure 6.10	Photograph shows a diameter change of the jet as a function of position along the jet, measured by the diffraction of a laser beam	178
Figure 6.11	SEM images of PEO mats collected using a grounded disk collector at constant and different collector linear speeds	181
Figure 6.12	SEM image of PEO mat collected using a constant disk collector	182
Figure 6.13	SEM image of PEO mat collected using a rotated disk collector	183
Figure 7.1	A photograph shows the nano tensile tester (NanoBionix, MTS, USA)	192
Figure 7.2	Images for breaking an electrospun nanofibre during the tensile test	193
Figure 7.3	Mechanical properties of nanofibres measured by AFM cantilever probes ...	194
Figure 7.4	Schematic drawings show examples of bending test method	196
Figure 7.5	Typical stress-strain curves of nylon 6/MWCNTs nanofibre mats	200
Figure 7.6	Schematic drawing of the spring 'transducer' - fibre series configuration	202
Figure 7.7	A schematic drawing and photo show the tensile testing set-up	204
Figure 7.8	Selected individual aligned nanofibres were removed and thus an electrospun single nanofibre is ready for tensile test	205
Figure 7.9	Photographs show the tensile test set-up is conducted step by step	206
Figure 7.10	A schematic of the steps for determining the diameter of the broken single Nanofibre	207
Figure 7.11	Method of calculating the fibre elongation over time	207
Figure 7.12	Average stress - strain curve of single electrospun nylon 6 nanofibre	208

LIST OF PUBLICATIONS

Journals

1. **M.B. Bazbouz**, G.K. Stylios, *Novel mechanism for spinning continuous twisted composite nanofibre yarns*, European Polymer Journal, 44(1), 1-12 (2008)
2. **M.B. Bazbouz**, G.K. Stylios, *Alignment and optimization of nylon 6 nanofibres by electrospinning*, Journal of Applied Polymer Science, 107 (5), 3023-3032 (2008)
3. **M.B. Bazbouz**, G.K. Stylios, *Investigating the spinning of yarn from electrospun nanofibres*, International Journal of Clothing Science and Technology, International Textile and Clothing, Research Register, 18 (6), 21-23 (2006)
4. **M.B. Bazbouz**, G.K. Stylios, *A new mechanism for the electrospinning of nano yarns*, Journal of Applied Polymer Science, Submitted for publication, WILEY InterScience (2009)
5. **M.B. Bazbouz**, G.K. Stylios, *Modeling the effect of jet kinematics in electrospinning of nanofibres*, Journal of Non-Newtonian Fluid Mechanics, Submitted for publication, Elsevier (2009)
6. **M.B. Bazbouz**, G.K. Stylios, *The tensile properties of electrospun nylon 6 single nanofibres*, Journal of Polymer Science Part B: Polymer Physics, Submitted for publication, WILEY InterScience (2009)

Conference Proceedings

1. **M.B. Bazbouz**, G.K. Stylios, *A spinning concept for ultrafine composite nanofibre yarns*, Presented at Green Chemistry & Engineering, The First International Conference on Process Intensification & Nanotechnology, Albany- New York, USA, PP.145-160, BHR Group - ISBN 978 1 85598 101 0 (15th - 18th September 2008)
2. **M.B. Bazbouz**, G.K. Stylios, *Nanofabrication of fibres and fabrics for technical textiles: the challenges in measurements and characterization*, Micro and Nano Characterization of Fibres Conference, University of Ulster, Jordanstown, Belfast, UK, CD Rom, National Physics Laboratory (2nd- 3rd July 2008)
3. **M.B. Bazbouz**, G.K. Stylios, *Significant progress in formation of nano yarn incorporating CNT as reinforcement*, Nanotextiles Conference, Prague, Czech Republic, CD Rom, Pira International (10th December 2007)
4. **M.B. Bazbouz**, G.K. Stylios, *Nanocomposite with multi walled carbon nanotubes*, Composite Materials for Aerospace & Defense & Security Conference, University of Glasgow, Glasgow, UK, CD Rom, National Composites Network (5th December 2007)
5. **M.B. Bazbouz**, *Electrospinning of nanofibres: potential scaffolds for medical applications*, Research in Support of Medicine, Health and Safety Conference, Heriot Watt University, Edinburgh, UK, CD Rom, Heriot Watt University (15 June 2006)

Monograph

1. **M.B. Bazbouz**, G.K. Stylios, *Engineering of nanotextiles by electrospinning*, Textile Progress, Submitted for publication, The Textile Institute, Woodhead Publishers (2009)

CHAPTER 1: INTRODUCTION OF ELECTROSPINNING NANOFIBRES AND AIMS AND RESEARCH OBJECTIVES

1.1 Introduction

Since the beginning of the nineteenth century, metals have been replaced into polymers in various applications for their lightweight and flexibility. In recent years, one dimensional (1D) nanostructures, such as nanowires, nanotubes and nanofibres (NFs) have become a great interesting topic to scientists and engineers. Hence, when the diameter of the polymer fibre is reduced to the nanoscale, several desirable characteristics such as high surface area to volume ratio, flexibility in surface functionalities and superior mechanical properties can be achieved. In fact, there are several techniques of fabricating polymer nanofibres [1]. These fabrication techniques such as electrospinning [2, 3], melt blowing [4], phase separation [5], self assembly [6] and template synthesis [7] have been fulfilled for different purposes. Nanofibres produced by electrospinning among the others are the most industrial and scientific interest due to their length, diameter, pore network and high surface area per unit volume [2]. For instance, one can take the advantage of the porous surface topologies of the nanofibre mat to control the wetting properties and adsorption behavior. Furthermore, the fibres with small diameter have a low bending modulus which manifests the nanofibre mats and yarns a soft fabric hand.

Electrospinning [8-13] provides a straightforward electrohydrodynamical mechanism to produce fibres with diameters less than 100 nm [14], even 5 nm [15]. Under the influence of an electric field, a pendant droplet of the polymer solution at the spinneret is deformed into a conical shape. When the voltage surpasses a threshold value, where electric forces overcome the surface tension, a fine charged jet is ejected. As these electric forces increase, the jet elongates and accelerates by the electric forces. The stretching of the jet is accompanied by a rapid evaporation of the solvent, which leads to a reduction in the diameter of the jet. For that effect, the required physical properties of the solvent for a selected polymer are a good miscibility, low boiling point, low surface tension and high conductivity 'low dielectric constant' [16-21]. Then, the jet undergoes a variety of instabilities, it splits, and deposits as a random nanofibre mat or other geometrical forms on a grounded metallic substrate.

So far, several synthetic and natural polymers, blended polymers and polymers filled with nanoparticles, carbon nanotubes (CNTs) and compounds have been successfully electrospun into nanofibres [22-24]. In addition, while the melt spinning technique is

the preferred method to produce synthetic filaments, efforts have been also made to electrospin nanofibres using polymer melts [25-27]. However, there is currently less research work in electro melt spinning, probably due to its difficulty in fabricating fibres with nanometer diameters [28, 29].

In this chapter, it is aimed to explain in depth the electrospinning technique including its history, principle and parameters. Hence, it is the most versatile and advantageous process for producing continuous nanofibres without purification compared to the other nanofibre fabrication methods [2, 30]. In addition, the aims and research objectives of the present thesis will be highlighted at the end of the chapter.

1.2 History of electrospinning nanofibres

The stability of electrically charged liquid drops and thus the behavior of electrically driven jets have been studied in the past centuries. In 1745, Bose et. al. created an aerosol spray by applying a high electric field to a liquid droplet at the end of a glass capillary tube [31]. In 1882, Raleigh studied the instabilities that occur in electrically charged liquid droplets. He calculated the maximum amount of the charges that a drop of liquid can maintain before the electric forces overcome the surface tension of the drop and lead to the ejection of a jet [32]. In 1917, Zeleny investigated the role of the surface instability of charged droplets in an electric field and the behavior of the ejected thin liquid jet by measuring its path geometrical dimensions [33].

These research studies have led without doubt to the invention of electrospinning threads from polymer solutions. As such, in 1902, Cooley and Morton et. al. patented an electro spraying/electrospinning set-up by using auxiliary electrodes to direct an ejected liquid jet into a rotating collector [34, 35]. In the 1930s, Formhals came out with several innovative set-ups that used multiple spinnerets and parallel electrodes to produce aligned nanofibres and yarns [8-11]. Furthermore, he has introduced an electrospinning design that does not require use of spinneret to produce nanofibres ‘electrospinning from polymer solution surface acted by rotating roller’ [12]. In the 1960s, Taylor et. al. analyzed the conditions at which the point of a droplet is deformed into a conical geometry by an electric field [36-38]. They identified the critical electrical potential field for the electrostatic formation of a cone of liquid at the tip of the spinneret ‘known as a Taylor cone’. Hence, by examining many low molecular weight liquids, they concluded that the conical interface between air and the liquid was stable at a semi-angle conical angle of 49.3° degree. Moreover, they have shown that both conductivity and viscosity of the liquid play a critical role in the electrostatic atomization process

which further influences the equilibrium angle and other aspects of the liquid droplet-jet formation. Taylor cone was considered later as an important part in electrospinning, forasmuch it defines the onset of the extensional velocity gradients in the nanofibre formation process [39].

Before the 1990s, very little research work or publications; however, have been published about electrospinning technique [13]. In the 1990s, Reneker et. al. [14, 40] drew the attention to the electrospinning as a spinning process of fibres at nanoscales. Furthermore, they have established the stepping stones in polymer nanofibres which are revolutionizing the research on materials at nanoscale level and allowing us to scientifically understand and control their geometries and properties without changing their chemical composition.

1.3 Electrospinning technique

1.3.1 The basic set-up of the electrospinning

Figure 1.1, shows a schematic illustration of the basic set-up of electrospinning process. It consists of three major components for fulfilling the process: a high voltage power supply, a spinneret ‘a metallic needle or pipette’ and a collector ‘a grounded metallic substrate’.

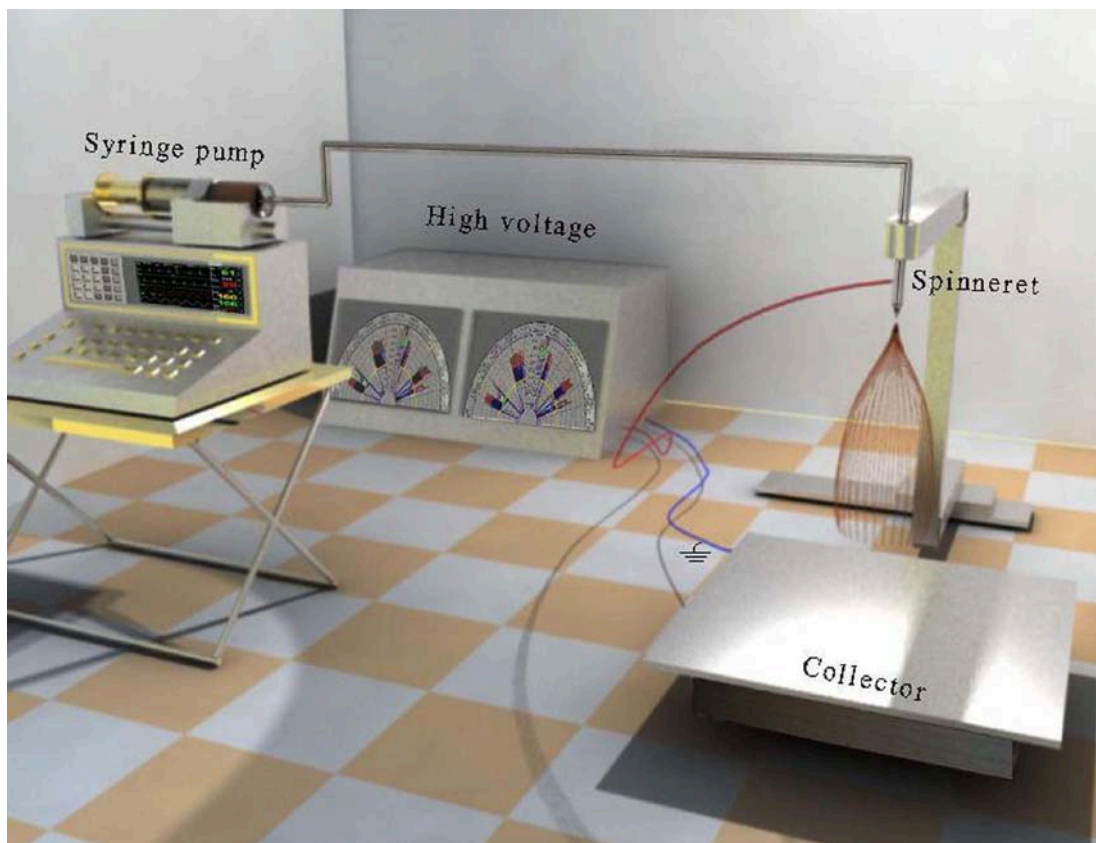


Figure 1.1, Schematic illustration of the set-up used for the electrospinning process.

In the electrospinning process, a high voltage is used to eject an electrically charged jet of polymer solution or melt out of the spinneret. Basically, this can be done by either connecting a metallic wire to the spinneret ‘vertical method’ or immersing the wire in the polymer solution ‘horizontal method’. A direct current (DC) power supply is usually used for electrospinning, nonetheless an alternating current (AC) power supply is also possible [2, 14, 41]. Some set-ups [42] have simply opted to placing the spinneret vertically and laying the collector underneath, letting the polymer liquid flows with help of gravitation [43]. While sometimes, the spinneret is subjected to a defined angle to control the flow [44-46]. Or in other cases, the spinneret is fixed horizontally [47] and a syringe pump is used to initiate the droplet. It can be noted that the syringe pump is also used in the case of vertical feeding [47-50]. Finally, a grounded metallic substrate or any other pre-designed grounded pattern is used to collect the electrospun nanofibres.

More importantly, there are some key points which need to be kept in mind before and during electrospinning addressed herein:

- The viscosity and surface tension of the spinning solution must not be too large preventing the jet from formation, not too small making the polymer solution to drip from the spinneret.
- The high voltage power supply must be high enough to overcome the viscosity and surface tension of the polymer solution and thus to form and sustain the jet from the spinneret, but not too high making the process unstable.
- The grounded collector used to collect the nanofibres must be electrically conductive.
- The gap between the tip of the spinneret and the grounded collector must not be too close, as this will result in collection of wet fibres.
- The solvent present in the spinning solution must evaporate quickly enough allowing the fibre to reach the collector in a dry state, but not too quickly making the fibre to harden before reaching the nanometer scale.
- Some solutions emit harmful smells, so the processes (polymer solution preparation and electrospinning) must be conducted within chambers having a ventilation system.
- A DC voltage in the range of ten to several tens of KV is necessary to generate the electrospinning process, therefore this required careful care to avoid touching any of the charged jet while manipulation [2].

1.3.2 How electrospinning works

Generally, traditional spinning methods of polymer fibres include melt spinning, dry spinning, wet spinning and gel state spinning. These methods rely on mechanical forces

to produce filaments by extruding polymer melt or solution through a spinneret and subsequently drawing the resulting filaments as they solidify or coagulate. Typical filament diameters that result from these methods are in the range of 5-500 μm [51].

Electrospinning process involves polymer science, applied physics, fluid mechanics, electrical, mechanical, chemical and material engineering and rheology [52]. The operational principle of electrospinning is quite simple. In this non-mechanical, electrostatic technique, a high electric field is generated between a polymer solution contained in a spinning dope reservoir 'a spinneret' and a grounded collector. Once the strength of the electric field surpasses a threshold value, the charges on the surface of the suspended droplet is induced. Contraction of the surface charges caused by the counter electrode on the collector generates a force directly opposite to the surface tension of the polymer solution [53]. Subsequently, the hemispherical surface of the droplet at the tip of the spinneret elongates to form a conical shape known as Taylor cone [36-39] and a thread jet is ejected. The electrically charged jet undergoes a series of electrically induced whipping instabilities, which lead the jet to elongate and thin during its travel to the collector. The stretching process is accompanied by a rapid evaporation of the solvent and splitting into many charged jets/fibres in a region at which the radial forces from the electrical charges carried by the jet become larger than the cohesive forces within the jet [42]. It can be noted that in the case of melt electrospinning, the charged jet stretches, splits and the fibres solidify when they travel in the air towards the grounded collector.

1.3.3 Process of nanofibres formation

Electrospinning process essentially includes three stages. In the first stage, a polymer jet ejects from the spinneret. In the second stage, the jet is accelerated and stretched smoothly by the electric forces. In the third stage, splitting and whipping instability of the jets occur making farther the fibres to spiral downstream until they stop in the collection region as nanofibres [54]. Hereinafter, these three stages are described with concise emphasis on their fundamental aspects.

1.3.3.1 Electric charges theory

In an uncharged ionic liquid and if no external electric field is applied, there are the same numbers of positive and negative ions in each volume element of the liquid [55]. In 1960s [36-39], Taylor discovered that it is impossible to account that any liquid is either a complete insulator or perfect conductor. The reason is that any dielectric liquid

still contains nonzero free charges. These charges are existent in the interfaces of the liquid. If there is also a nonzero electric field tangent to the interface, then there will be a nonzero tangential stress on the interface. The only possible force that can balance the tangential stress is the viscous force. As a result, the liquid will be necessarily in motion under these conditions [56]. This has become known as the ‘leaky dielectric model’ for the electrically driven liquids theory [39]. Therefore, when an external electric field is applied to the polymer solution, the voltage polarizes the ions. In other words, negative ions are forced towards the positive electrode, and positive ions are forced towards the negative electrode. The difference in the number of positive and negative ions in a specific region is called the excess charges [55]. Usually, adding a soluble salt increase the electrical conductivity of the solution through increasing the number of ions per unit volume. The higher conductivity, decreases the time required for the excess charge to move to a further region in response to a change in the electric field [55].

1.3.3.2 The initiation of the jet

Due to the surface tension forces, the polymer solution droplet is initially in equilibrium with the gravitational forces, thus the polymer solution will be prevented from flowing out of the spinneret [31]. Reneker et. al. have demonstrated that when a high electric field is applied to the polymer solution in the spinneret, the charges in the solution are forced to aggregate at the surface of the droplet. As a result, the surface is pulled into the approximate shape of ‘*a section of sphere*’. When the electrical forces overcome the surface tension, a bulge forms and the charges move through the liquid and concentrate on this protruding part of the surface [14]. The accumulation of the charges causes the surface to protrude more forming a conical shape that was mathematically described by Taylor and referred as Taylor cone [36-39]. As the applied electric field is increased, a thread jet of liquid is pulled from the tip of the spinneret, and the electrospinning process begins, as shown in figure 1.2. The jet is elongated by the electric forces and gravity, while surface tension, viscosity and inertia forces also play apart [54].

Reneker et. al. have concluded that the base region stabilises at a size and a shape determined by the rate at which liquid is supplied to the tip of the spinneret. In addition, the flow pattern in the base and parameters such as elongation flow and time dependent elasticity of the liquid affect critically on the diameter and shape of the base [55]. It has been also reported, that at sufficient high voltages; multiple jets from the spinneret were observed during the electrospinning process [57, 58].

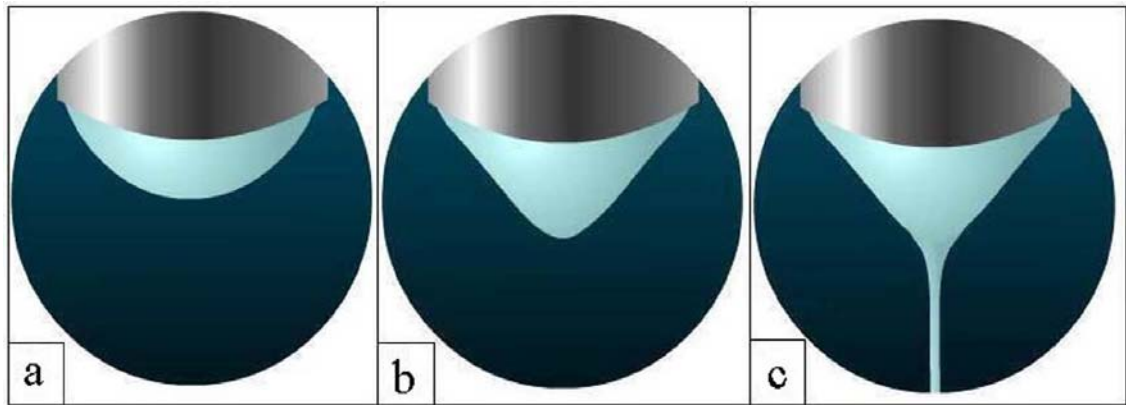


Figure 1.2. A schematic illustration of the initiation steps of the jet. (a) Under the electric field the surface is pulled into the approximate shape of a section of a sphere, (b) the accumulation of the charges causes the surface to protrude more forming Taylor cone, (c) a thread jet of liquid is pulled from the tip of the spinneret.

1.3.3.3 The jet travel

Upon initiation, the charges which are embedded in the direction of the electric field transfer the forces from the electric field to the polymer solution mass. If the electric field is strong enough, a jet of liquid is ejected and accelerated from a surface that was essentially semi sphere before applying the electric field. The acceleration of the jet is mediated by the transfer of the forces through the viscoelastic jet in which the viscoelastic state is changing at the same time as the solvent evaporates from the jet. During the jet travel, its diameter decreases and its length increases in a way that the amount of mass per unit time passing any point in the z axis remains constant [14]. Feng has proposed that as the jet thins the surface charge density varies which in turn affects the electric field and the pulling force and increases the viscosity slowly along the straight part of the jet. As both the surface charge density and the jet radius vary away from the tip of the spinneret ‘jet thins’, the stability characteristics of the jet is also changed [54, 59].

This is the mechanism in which the electric charges carry the polymer solution from the spinneret to the collector, and thereby a complete electrical circuit which provides the energy is needed to drive the flow, accelerate the jet and increase its surface area. In fact, the best calculation of the jet velocity is from measurement of the mass of the nanofibres that are collected in a known time interval the diameter of the jet and concentration of the solution [14], which will be investigated later on in this thesis.

1.3.3.4 Dividing the jet into many fibres in the splitting region

As mentioned above, stretching and evaporating of the solvent molecules cause the jet diameter to become smaller. It must be noted that the charges on the jet expand the jet in the radial direction and stretch it in the axial direction. Furthermore, the radial forces from the charges become large enough to overcome the cohesive forces of the jet [14]. Based on this concept, as the diameter decreases the radial forces increase to split the jet into two or more charged jets which are approximately equal in diameters and charges per unit length [42]. Each smooth segment that is straight or slightly curved suddenly develops an array of whips. After a short sequence of an unstable whipping back and forth, each jet follows a bending, winding, spiralling and looping path in three dimensions [55]. In other words, the jet in each branch grows longer and thinner as the loop diameter and circumference increases, similar to, but at a smaller scale than the first. As a result, the motion velocity increases and the evaporation process strongly intensifies. Concisely, the jet splitting process which is the result of complicated interaction of variables that include viscosity, surface tension, electric forces, air friction and gravity occurs several times in fast succession and produces a large number of super fine fibres ‘nanofibres’ moving towards the collector, as shown in figure 1.3 [59, 60].

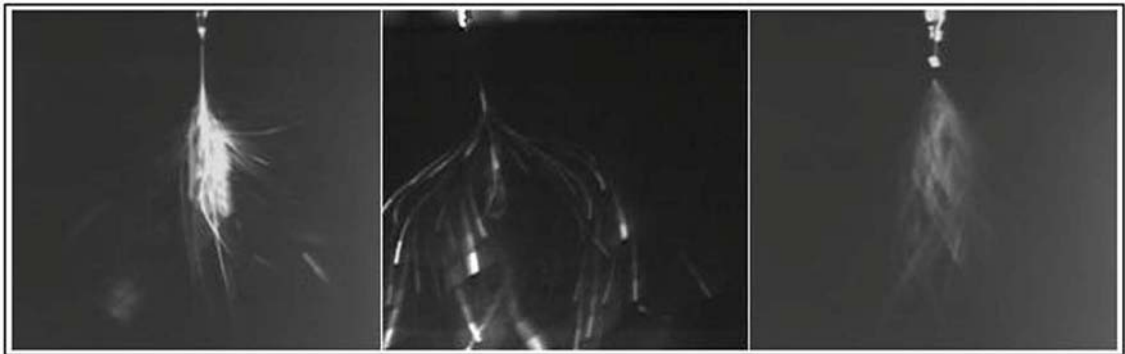


Figure 1.3, Photographs of different modes of jets chaotic motion ‘instability’ as they travel towards the grounded collector [60].

An analogy to the jet travel mechanism in electrospinning has been recently described by He et. al. in the following manner, as shown in figure 1.4 [61]. When the fibre moves to the boundary AB (conical envelope), for example at M, the velocity in the x direction becomes zero. The reason was explained as the following: at point M, there are three main forces acting on the fibre; viscous force, electric force and inertia force. Hence, the direction of viscous force is in the inverse direction of its motion, i.e., in the direction of MA and the direction of electric force and inertia force is in z direction. Now, based on

the parallelogram law, the combining force moves in the direction of its diagonal, i.e. the direction of MO. At the point M, it has the maximal acceleration, and when it reaches the point O, the velocity in the x direction takes the maximum value while its acceleration becomes zero, and due to inertia force it moves to the other boundary AC. Concisely, He et. al. have described the instability motion in electrospinning like pendulum motion ‘a parachute jump’.

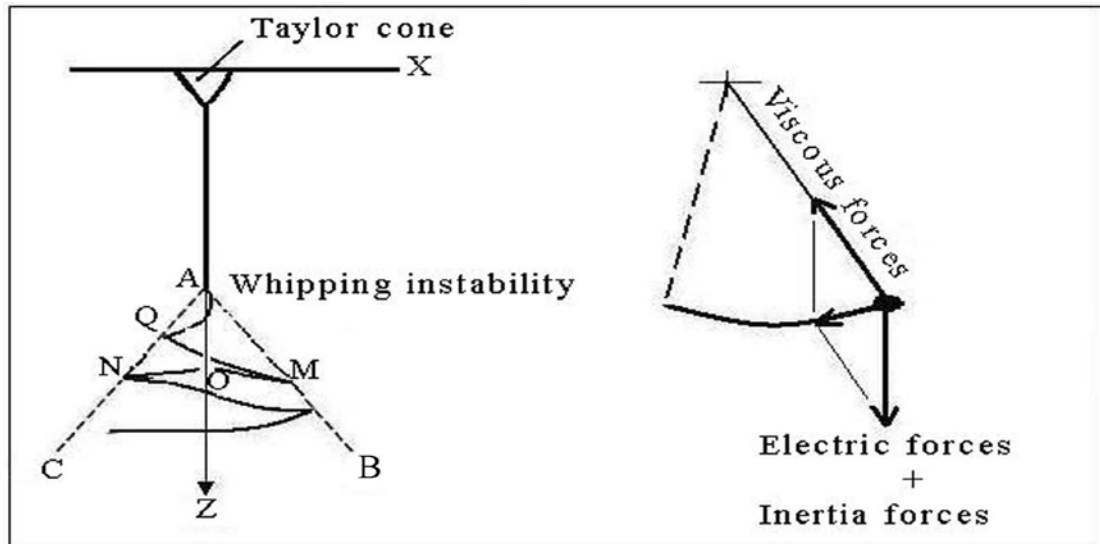


Figure 1.4. A schematic illustration of the jet travel mechanism in electrospinning [61].

1.3.3.5 Stops in the collection region

As described above, electrospun nanofibres are charged during flight and travel downward until they impact with the collector to form a nonwoven mat ‘fabric’ of disordered nanofibres. Actually, the nanofibres lying on the collector tend to repel the fibres that arrive later, due to repulsion forces [55]. If the nanofibres arrived with a high velocity onto a stationary collector; the nanofibres tend to coil or fold [62]. The collected coils and loops provide information about the sizes of the whipping instabilities that occurred. The integrity of the nonwoven nanofibre mat depends on the random overlapping of the fibres and interactions between the fibres that occur at the contact points between the fibres. Therefore the structure of the collected nano-web is usually irregular.

In order to obtain ordered and aligned nanofibres, special collector patters are necessary to be designed. Rotating rollers and aerodynamic currents have been used for collecting aligned nanofibres. In addition, conductive, nonsolvent liquids, water or other appropriate liquids have been also utilized to remove the solvent and coagulate the polymer fibres resulting in a wet electrospinning ‘electro wet spinning’ [63-65].

1.3.4 Effect of electrospinning parameters on nanofibres morphology

Electrospinning process, polymer solution and ambient parameters have been noted to have the role of successful electrospinning and controlled nanofibres morphology (nanofibre diameters and nanofibre diameters uniformity).

Polymer solution parameters which are related to the polymer solution properties are:

- Polymer [type, molecular weight, molecular weight distribution and structure (branched, linear, etc.)].
- Solvent (types, vapor pressure, miscibility), additives (surfactants, salts).
- Polymer solution concentration.
- Polymer solution properties (rheological behavior, relaxation time, viscosity, surface tension, electric conductivity and dielectric permittivity).

Electrospinning process parameters which are related to the operational conditions are:

- The applied electric field (strength, geometry).
- Distance from the spinneret to the collector 'electrospinning distance'.
- Volume feed rate of the polymer solution.
- Spinneret orifice internal diameter.
- The motion of the collector.

Ambient parameters are:

- Environmental temperature.
- Relative humidity.
- Air velocity in the electrospinning chamber.

1.3.4.1 Polymer solution parameters

As nanofibres are produced from evaporation or solidification of the polymer liquid jet, the nanofibres morphology depends primarily on the polymer contents in the jet and its physical and chemical properties.

The polymer type, molecular weight, and its structure play an important role in determining the minimum polymer concentration to electrospin fine continuous nanofibres. Hence, a polymer with large molecular weight is subjected to a high degree of number of the entanglements within the polymer chains [28]. It is therefore more

difficult for the electric forces to pull on individual polymer chains into fibre. As a result, larger fibre diameters are formed. It has been agreed that as the molecular weight decreased the fibres diameter decreased [24]. Furthermore, the nanofibres production rate increases when dissolving polymer with low molecular weight, hence high polymer solution concentration can be achieved.

As electrospinning is 'electro dry spinning' process which uses solvents to dissolve the polymers, the solvent vapor pressure plays a critical role in the evaporation rate of solvent from the jet. Truly, decreasing of the evaporation rate of the solvent from the jet during electrospinning allows the charged jet to remain liquid, to continue, to stretch and to become thinner and thus fibres at nanoscale level. On the other hand, low evaporation rate results in collecting wet nanofibres.

Practically, polymer solution concentration plays the most important role in determining the nanofibres morphology. Electrospinning results showed that the diameter of the electrospun nanofibres dramatically decreases with decreasing polymer solution concentration [24]. In comparison, as the polymer solution concentration increases, the viscosity increases and higher electrical forces are required to overcome both the surface tension and the viscoelastic forces for stretching the jet into nanofibres. Hence, the spinnability of polymer solution is relevant to its viscoelastic properties [68].

Although the range of polymer solution concentrations that produce nanofibres obviously varies with the polymer used, the viscosity and surface tension forces determine the upper and lower limits of polymer solution concentration, provided all other parameters are held constant. At the low polymer concentration, too dilute solution in the absence of polymer chain entanglements will result in the jet breaking into droplets and give rise to the spherical liquid particles instead of continuous fibres on the grounded collector. As a result, the fibres will have an irregular and undulating morphology with large variations in diameters along the fibre length. Moreover, nanofibres produced from lower concentrated polymer exhibit more beads formation [17]. The practical reason is that at lower polymer concentration, electrospun nanofibres are harder to dry before reaching the collector. Even the measured mass of collected nanofibres was found to decrease as the polymer concentration decreased. On the other hand, at the high polymer solution concentration, the nanofibres have a regular, cylindrical morphology and in average a larger and more uniform diameter [16]. Hence, viscoelastic forces resist formation of beads and allow formation of smooth nanofibres.

While when the polymer solution concentration is too high, the high viscosity and the rapid evaporation of the solvent make the extension of the jet more difficult and thereby wider fibre diameters are formed. Experimentally, research reports have addressed a strong linear relationship between nanofibre diameters and polymer solution concentration. Deitzel et. al. have demonstrated that the average nanofibre diameters is related to the polymer solution concentration in a power law relationship with an exponent of about 0.5 [71]. While Demir et. al. have reported a power law relationship with an exponent of 3 [58]. However, literature publications have reported initial polymer solution concentrations ranging from 1 to 40 wt. %, and typically most of them were less than 30 wt. % [16, 17, 66-72].

Polymer solution viscosity and surface tension play an important role in determining the range of polymer solution concentrations from which continuous uniform fibres can be obtained in electrospinning. The experimental referenced works show that increasing the zero-shear viscosity, whether by a higher molecular weight polymer or higher polymer solution concentration, will increase the resulting fibre diameter [16, 71]. While the spinnability or 'solution viscosity' will be poor if the polymer solution concentration is low. Moreover, when the solution viscosity is too low, electrospun nanofibres will be unstable and form beaded texture [16] or cups [73]. At low viscosities of (0.1 Pa.sec), surface tension is the dominant factor on the fibre morphology and below a certain polymer solution concentration attributed to this viscosity value, drops are formed instead of fibres [77]. At high viscosities of (6 Pa.sec), processing the jet is prohibited by the inability to control and maintain the flow of the polymer solution out of the spinneret and by the cohesive nature of the high viscose polymer solution [2]. It has also been demonstrated that increasing the polymer solution concentration (and consequently the viscosity) and thus lowering the surface tension favor the formation of beads-free uniform fibres [58, 75, 76]. This is consistent in reality with most properly chosen electrospun polymer solutions, where the viscoelastic forces completely dominate the surface tension. In other words, a direct correlation has been observed between uniform fibre diameter and polymer solution viscosity [58, 74]. In comparison, when low molecular weight polymers are used or polymer solution concentration is significantly reduced, the viscoelastic forces dramatically diminish and thereby the surface tension plays a strong role in the morphology of the resulting fibres. Hence, when the surface tension forces are dominant, they attempt to reduce surface area per unit mass, and thus beaded fibres are consequently produced [78].

Beads are known as defect structures, because they disturb the unique property of electrospun nanofibres and decrease the surface area to volume ratio [58]. The formation of beaded fibres is attributed to the instability of the jet associated with the poor spinnability of the polymer solution and the domination of the surface tension forces over viscose forces [3]. Reneker et. al. [16, 77] have systematically investigated the influence of polymer solution properties of polyethylene oxide (PEO) on the density of beads contained in the electrospun nanofibres. They have recognized that, higher polymer concentration produce fewer beads, as shown in figure 1.5. In addition, they have found that viscose forces prevented the formation of beads and allowed for the formation of smooth nanofibres.

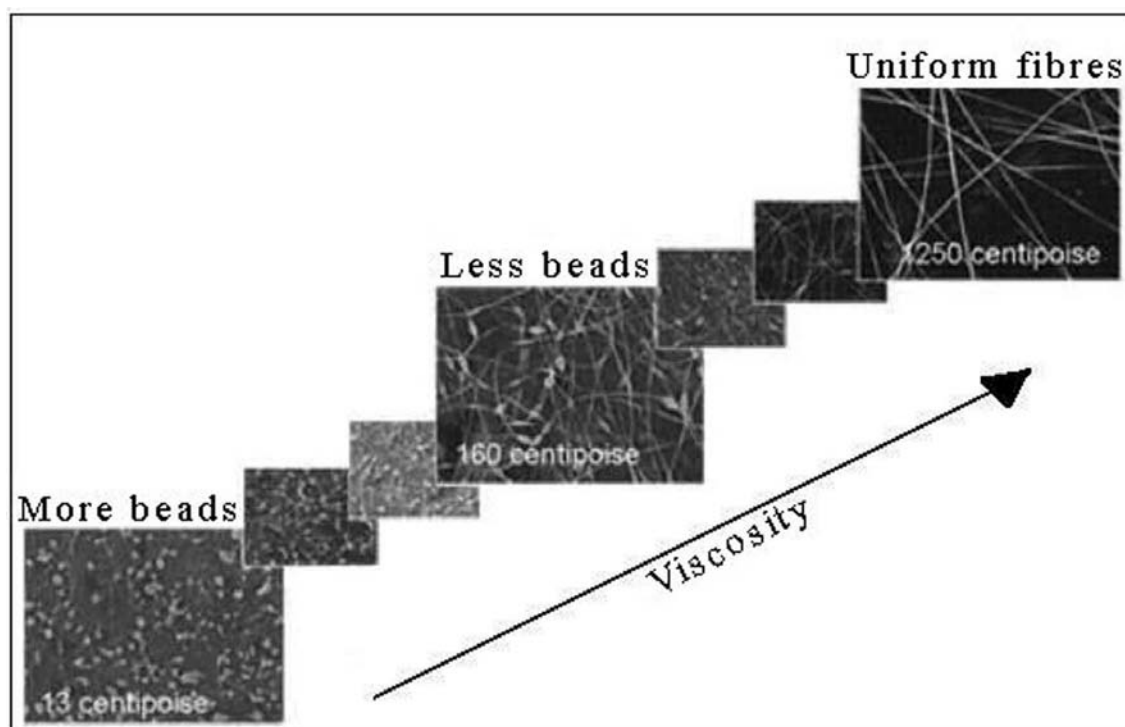


Figure 1.5, SEM images of electrospun PEO nanofibres from different polymer solution concentrations, in which the lowest viscosity (13 centipoises) corresponded to 1 wt. % PEO, whereas the highest viscosity (250 centipoises) corresponded to 4 wt. % PEO [77].

Hsiao et. al. have reported that the overall tension in the electrospun fibres depends on the self-repulsion of the excess charges on the jet [79]. Thus, smaller fibre diameters can be also produced with higher electrical conductivity of the polymer solution. As a matter of fact, the electrical conductivity of the polymer solution mirrors the charges density on the jet and thus higher elongation forces are imposed to the fibres under an

applied electrical field. In other words, under the same applied voltage and spinning distance, a polymer solution with higher electrical conductivity will cause higher elongation to the jet along its length and thus electrospinning fibres with smaller diameter. For instance, Ramakrishna et. al. have showed a significant drop in the diameters of the electrospun PLLA nanofibres when the electrical conductivity of the polymer solution (PLLA/ dichloromethane) was increased by adding DMF or pyridine [24]. Beads were also observed in their experiments at low conductive polymer solution. They explained the reason that, a low conductive polymer solution reflects an insufficient elongation of the fibres by the electrical forces to produce uniform fibres without beads. He et. al. have also concluded that as the charges density increased, the beads became smaller and more spindle like - smooth fibres were formed [80]. It has been recommended that adding a salt to the polymer solution increases the net charges density and thus enhances the electrical conductivity of the polymer solution [81]. Briefly, the electrical conductivity of the polymer solution is a key factor in determining the electrospinning current, net charges density and fibres morphology [66].

1.3.4.2 Electrospinning process parameters

It has been already reported that electrospun nanofibre diameters are not dramatically changed when the applied electric field is varied [58, 82-86]. It has been found that applied electric field may affect some factors such as polymer solution mass fed out the spinneret, elongation level of the jet and morphology of the jet (a single or multiple jets), etc. [24]. However, a balance between these factors determines the final diameter of the electrospun fibres [78].

In fact, two distinguish concepts have been issued related to the applied electric field effect. Firstly, the electrospun fibre diameters slightly decrease as the electric field strength increases due to the increasing of the pulling and stretching forces [78, 87]. Secondly, increasing the applied electric field does increase the electric forces and create more elongation; but it also draws more polymer solution out of the spinneret and in turn the fibre diameters will increase, as reported by Demir et. al. [58]. It has been concluded that the nanofibre diameters are a combination result of the polymer solution feeding rate and the applied electric field, provided all other variables are held constant [24]. Nevertheless, based on the literature works, the applied electric field affects on the length of the liquid jet, number of the jets ejected from the droplet surface and the jet speed [17, 55]. In addition, applying a higher electric field is shortened the length of the jet path, thus the whipping instability and splitting will happen earlier which results in a

chaotic motion to a larger extent [16]. The other interesting phenomenon is that, under a higher electric field multiple jets are generated from the droplet at the spinneret tip which will provide smaller diameter of electrospun fibres, but non uniform fibre diameters distribution [52]. It has been also noted that with too high level of electric field, the resulting nanofibres became beaded and rougher [71]. The reason can be attributed to the increase of the jet instability at the spinneret tip under too high electric field. Briefly, increasing the applied electric field to a high level would change the shape of the pendant drop from which the jet originated, and thus a stable shape could not be achieved. As a result, the stability of the liquid jet would be weakened which might lead to an increase in the density of the beads in the electrospun nanofibres.

Generally, it has been found that electrospinning distance performs a role on the nanofibres structure and morphology [78]. It can be noted that the electric field strength increases when the electrospinning distance decreases, provided the applied voltage remains constant. It can be also pointed that during the fibres travel towards the collector 'electrospinning distance', the electric field strength has the opportunity to stretch the fibres more and thus produce thinner fibres. In addition, due to the extent of the solvent evaporation; the consequent drying, depositing and orienting of the fibres 'nanofibre properties' can be affected by varying the electrospinning distance.

It has been indicated that in case of a short electrospinning distance, the drying time is not long enough to fully evaporate the solvent before depositing the nanofibres. As a result, partially dried fibres are spread on the collector and formed a densely packed membrane instead of a porous nanofibrous membrane [88]. Megelski et. al. have also observed beads formation in electrospun PS nanofibres and thick ribbon shaped morphology when the electrospinning distance is decreased [89]. On contrast, as the electrospinning distance is increased, the time for solvent evaporation is increased. As a result, dry solid nanofibres can be collected at the grounded collector. It has also been proved that when the electrospinning distance increases the jet undergoes a larger amount of electrically driven whipping and bending instabilities and thus an increase in the jet branches and a decrease in the nanofibre diameters [55, 90]. Moreover, the resulting nanofibrous web is with irregular fibre diameters. Systematic optimization for the electrospinning process showed that the optimum spinneret tip to collector distance is attributed to the polymer solution concentration, its flow rate and the applied electric field [78]. However, several literature research works have reported in their experimental set-ups an electrospinning distance of 50 to 500 mm [16, 17, 66-71, 89].

The volume feed rate of the polymer solution from the spinneret is an important process parameter which influences the jet stability, path and velocity. Literature research works have reported somewhat conflicting results in either increase or decrease in the jet diameter with varying the volume feed rate of the polymer solution [67-69].

With too high volume feed rate, the pendant droplet size increases, and then the possibility of the multi jets generation becomes larger. In addition, higher jet mobility, (vibrated dancing) around the Taylor cone can be observed. As a result, the jet undergoes a capillary instability and develops beads [91]. In other words, the volume of the Taylor cone fluctuates with time during electrospinning and a steady volume is never reached, giving the possibility to the intermittent jet formation. Moreover, transforming a large spherical-shaped into convex-shaped cone requires a higher applied electric field to reach critical surface charges for issuing a jet from the apex of the spinneret. It has been argued that the volumetric charges density and the volume feed rate interact with each other to play a significant role in the morphology of the electrospun nanofibres [70]. This can be explained by the competition between polymer solution feed rate, its volumetric charges density and the droplet shape from which the jet emanates. In addition, electrospinning under high volume feed rate does not render a sufficient viscous stretching for the fibres by the electric forces. On the other hand, with too low volume feed rate, the pendant droplet may be disappeared and the jet is generated from the sidewall of the spinneret tip. This is possibly due to the insufficient polymer solution delivered to the cone volume after the jet has formed at the apex of the spinneret. It has been also found that the lower the polymer solution volume feed rate is, the smaller the fibres are formed [68, 70, 92]. Most importantly, a certain minimum value of the polymer solution volume suspended at the tip of the spinneret must be maintained constant during electrospinning in order to form equilibrium for the Taylor cone. Under constant electric field, the optimum volume feed rate for a stable cone-jet mode is depended on the conductivity, surface tension and viscosity of the polymer solution. Practically, a steady liquid jet can be observed when a volume feed rate of 0.1 ml/hr to 5 ml/hr is used for a single spinneret [16, 21, 40, 67-70, 92, 93].

It has been reported that the spinneret orifice internal diameter which supplies the polymer solution to the droplet shaped as Taylor cone affects on the initial jet radius. Three orifice internal diameters ranging from 0.29 to 0.59 mm were used to determine their effect on the nanofibre diameters, while all other variables remained constant among each experiment by Ko et. al. [84]. The results displayed an increasing trend to

the final fibre diameters corresponding to the increase in the initial jet diameter when spinneret orifice size was increased. However, based on our knowledge, the initial jet diameter at the tip of the Taylor cone is significantly affected by the applied electric field. Therefore, spinneret orifice internal diameter cannot be considered as an independent parameter for changing the jet diameter when the applied electric field remains constant.

1.3.4.3 Ambient parameters

The ambient parameters around the spinneret, such as temperature, relative humidity and air velocity in the electrospinning chamber influence on the structure and morphology of the electrospun nanofibres. The ambient relative humidity in the electrospinning chamber plays an important role in determining the solvent evaporation rate in a charged jet during its flight towards the collector. The evaporation rate from the charged jet decreases at higher relative humidity, which consequently allows the jet to continue and elongate. It has been demonstrated that fibre diameters become smaller when evaporation and solidification rates are slow because of the higher relative humidity [94, 95]. On the other hand, the charged jet and consequently the fibres solidify at larger diameters when are electrospun at low relative humidity due to the rapid solvent evaporation. In 1971, Baumgarten et. al. reported that a relative humidity in the range of 30-40 % RH were needed for electrospinning of acrylic fibres of diameters in the range of 1.1 - 50 μm [13]. They have found that in a dry air ($\text{RH} < 5\%$), the electrospinning droplet dried out and electrospinning process could be carried out for only 1 - 2 min. On the other hand, in a humid air ($\text{RH} > 60\%$); the polymer solution did not dry properly and the electrospun nanofibres remarkably tangled. Moreover, humid air decreases the pore size of the deposited fibres web compared to nanofibres electrospun under a low relative humidity of 30 %. Huan et. al. have added a furnace to their electrospinning set-up in order to control the ambient parameters [96]. In this case, a gradual temperature and controllable air velocity attenuate and adjust the jet stability, solvent evaporation and thus nanofibres solidification.

1.4 Diversity of polymers used in electrospinning

A wide range of polymers such as biopolymers, modified biopolymers, water- soluble synthetic polymers, organo-soluble synthetic polymers, biodegradable polymers, natural polymers, gels consisting of a variety of natural and synthetic polymers and composite polymers have been successfully electrospun into nanofibres having many different

nanostructures. In addition, proteins, enzymes, drugs, fullerenes, carbon nanotubes, metals, and semiconductors are processed by electrospinning as blends with synthetic and natural polymers. Specific conditions are often necessary, such as the use of special solvents or the processing of the polymers as blends for a successful electrospinning. Out of dry electrospinning, however, melt electrospinning process can electrospin polymers in the melt form. Table 1.1, shows the most known polymers that have been electrospun with their solvents and proposed applications.

Table 1.1 The most known polymers electrospun in a solution form.

No	Polymer	Polymer classification	Solvent	Application	Ref *
1-	Collagen	Biopolymer	Hexafluoroisopropyl alcohol	Tissue engineering	97
2-	Regenerated silk (Bombyx mori)	Biopolymer	Hexafluoroacetone	Wound dressing	98
3-	Silk fibroin	Biopolymer	Formic acid	Wound dressing	99
4-	chitosan	Biopolymer	Formic acid or acetic acid	Wound dressing	100
5-	Cellulose	Biopolymer	NMO/water	Membranes	101
6-	Cellulose acetate, CA	Biopolymer	acetic acid	Membranes	76
7-	Polyethylene oxide, PEO	Synthetic polymer	water	Biomedical applications	102
8-	Polyvinyl alcohol, PVA	Synthetic polymer	water	Chemical applications	103
9-	Polyvinyl phenol, PVP	Synthetic polymer	water	Antimicrobial agents	104
10-	Polylactic acid, PLA	Biodegradable polymer	Dimethylformamide, DMF	Medical applications	24
11-	Polycaprolactone, PCL	Biodegradable polymer	Chloroform: Methanol (3: 1)	Tissue engineering	105
12-	Aliphatic PA (Nylon 6)	Organosoluble synthetic polymer	Formic acid	Filteration	78
13-	Polyacrylonitrile, PAN	Organosoluble synthetic polymer	Dimethylformamide, DMF	Protective textiles	106
14-	Polycarbonate, PC	Organosoluble synthetic polymer	Dimethylformamide: tetrahydrofuran (1: 1)	Filteration	107
15-	Polystyrene, PS	Organosoluble synthetic polymer	Dimethylformamide, DMF	Filteration	108

16-	Polybenzimidazole, PBI	Organosoluble synthetic polymer	Dimethylacetamide, DAA	Protective clothing	109
17-	Polyethylene Terephthalate, PET	Organosoluble synthetic polymer	Dichloromethane	Composites	110
18-	Polyurethanes, PU	Organosoluble synthetic polymer	Dimethylformamide, DMF	Protective clothing	111
19-	Polyvinylchloride, PVC	Organosoluble synthetic polymer	Dimethylformamide: tetrahydrofuran	Protective clothing	112
20-	Polyvinylidene fluoride, PVDF	Organosoluble synthetic polymer	Dimethylformamide: Dimethylacetamide	Flat ribbons	43

*: The most up-to-date reference.

1.5 Engineering aspects related to the electrospinning of nanofibre assemblies

1.5.1 Introduction

Electrospinning is currently a well established technique in university laboratories and industry that can fabricate continuous fibres with diameters down to a few nanometers. These nanofibres possess one of the highest surface areas to mass ratios among all cohesive porous materials due to their small diameters, and mats made of nanofibres can be highly porous with excellent pore interconnection void volume in the range of 50 % to even greater than 90 % [113, 114]. Moreover, electrospinning can be applied to synthetic and natural polymers, polymer alloys, metals, ceramics and polymers functionalized by the addition of drugs, nanoparticles and active agents [115]. The unique characteristics of nanofibres and the functionalities from the polymers themselves make nanofibres as a required candidate for many advanced applications [116-123].

1.5.2 Nanofibre blended fabrics

Hybrid nanofibrous fabrics with nano layered structures were fabricated by either sequential or simultaneous electrospinning. In addition to the increase in the production rate, multiple spinnerets arranged in either side by side [124, 126-129] or opposite sides [130, 131] have been used to electrospin nanofibres from dissimilar polymers onto a rotating collector for making blended fabric. It has been noted that spinning different fibres from opposite sides spinnerets arrangement require different electrospinning parameters, as shown in figure 1.6. The weight ratio of each polymer fibre resulted in the blended fabric and fibre mixture and distribution throughout the depth of the fabric

can be controlled by changing the number ratio and position of the spinnerets [130]. In fact, combination of the advantageous properties of each polymer is a promising solution for the preparation of novel nanofibrous fabrics for many applications. Furthermore, blending of different polymer nanofibres provides a strategy for controlling porosity and pore size distribution through the fabric. For instance, Frey et. al. have electrospun nylon 6 and PEO from opposite sides spinnerets to produce blended nanofibres fabric, as shown in figure 1.6 [130]. Then PEO component was removed by immersing nanofibrous fabric into the water for 24 hours followed by drying in a vacuum oven for another 24 hours to increase the void volume and associated pore size. They have reported a change in the voids volume from a narrow distribution of pores less than 200 nm in diameter to a broad distribution of pores ranging from 100 nm to 1 micron in diameter.

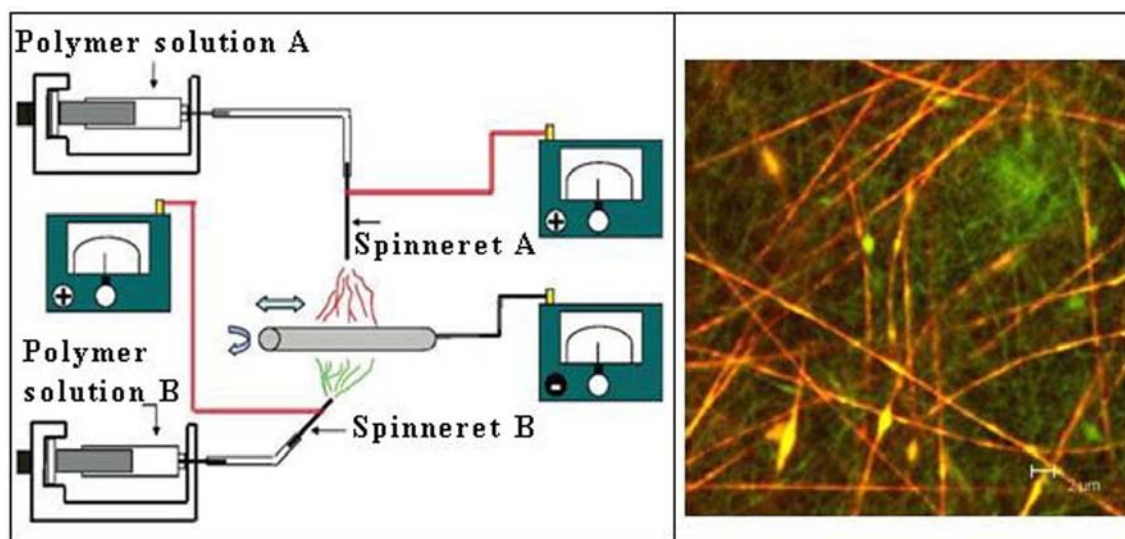


Figure 1.6, (Left) Two electrospinning apparatuses were set on opposite sides of a spinning collector, rotating the collector blends the nanofibres in the resulting nonwoven fabric [131]. (Right) confocal laser scanning microscope image of dyed nylon 6 / PEO nanofibrous fabric [130].

Researches have reported many examples of nanofibres blending to get the benefit of each polymer such as water-resistant hybrid nanofibrous fabric [128]. In addition, thin collagen nanofibres as the inner layer and thick PU fibres as the outer layer have been cylindrically constructed to serve as a good carrier tissue for artificial blood vessels [129]. Wagner et al. have constructed nanofibrous fabric from biodegradable poly (ester urethane) urea (PEUU) as an elastomeric polymer and poly (lactide-co-glycolide) (PLGA) to reduce the shrinkage ratio [131].

Briefly, these studies indicate a useful progress in controlling the nanofibrous fabric physical properties and its voids through blending of different polymers. To do so, electrospinning applied voltage, spinneret to collector distance, volume feed rate and polymer solution concentration must be optimized for every polymer.

1.5.3 Nonwoven fabrics coated by nanofibre layers

As previously mentioned, the nanofibrous mat provides a well interconnected porous network with a surface area per unit mass that is about 100 - 1000 times larger than that of carbon or glass fibres [132]. Moreover, this high specific area enhances the bonding area between the nanofibres and the surrounding environment [114, 115]. Based on this concept, conventional nonwoven fabrics are coated by electrospun nanofibre membranes to modify the properties of these textile fabrics, as shown in figure 1.7. The new nanofibre coating technology can be applied to any nonwoven base polymers, such as glass [133], natural or synthetic fibres [125] and even paper [134].

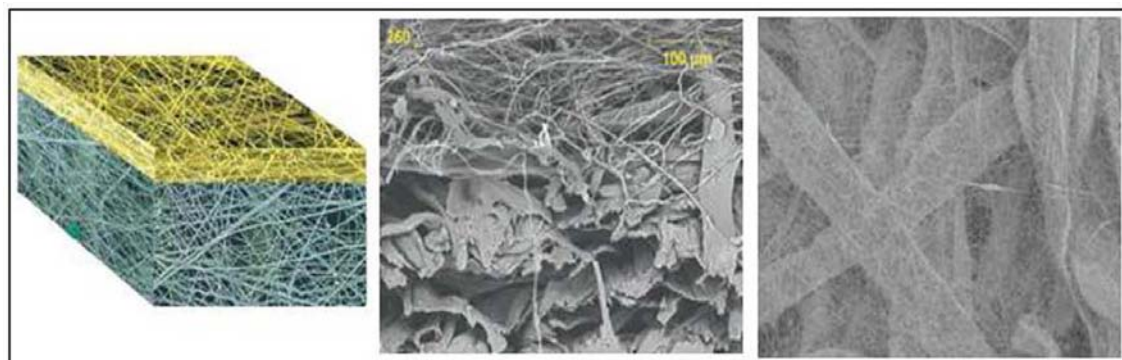


Figure 1.7, (Left) mode of a conventional nonwoven fabric coated by nanofibres [125], (middle) side view SEM image consisting of layered nanofibres nonwoven material developed by Hollingsworth-Vose Co. [51], (right) top view SEM image of nanofibres web density which can be adapted and controlled versus the microfibrils nonwoven base [135].

A second nanofibre layer applied on nonwoven fabric can enhance the thermal insulation [115], change the water vapor permeability ‘waterproof or breathable fabric’ [115], increase the barrier properties [114], absorb acoustic and antinoise resources [125] and achieve the desired structural, physical and mechanical properties such as pores size, durability and stiffness [136]. Furthermore, functional nanoparticles ‘enzymes’ can be added into a polymer solution before electrospinning the nanofibres to

give the composed fabric a specific functionality such as protection against chemical or biological hazards and aerosol filtrations.

However, as the electrospun nanofibre layer has two dimensional structure that lacks the z-direction depth, it offers little strength and bonding adhesion with the base fabric. Due to this configuration, surface loading stability is required for preventing damage or dislodge from the base fabric; there is still a need for enhancing nanofibre - fabric base adhesion. To overcome this deficiency, two solutions have been applied technically by the industry. Firstly, for protecting nanofibres against mechanical damage, an extra layer of nonwoven coarse 'micro' fibres has been applied. In other words, new three layers 'in which both the base and the top are coarse fibre layers for supporting the mid nanofibre layer' have been interconnected [137]. Or to provide a smoother surface to the top coating layer, the top layer can be replaced into few layers of the nanofibrous structures that electrospun with thinner fibre diameters than the mid layer as shown in figure 1.8 [114]. Secondly, before electrospinning the nanofibre layer onto the nonwoven fabric, the fabric can be dipped in an adhesive solution and compressed by either a compression roller, a heating embossing roller, a high pressure water injection, by electromagnetic waves, ultrasonic waves or plasma. Then after delivering of the nanofibre, the composed fabric is dried and bonded [137].

Further discussed are the advantages of using nanofibre coating for different applications. Coating the filter material with a layer of nanofibres has been used to improve depth filtration and self-cleaning or pulse-cleaning ability. Hajra et al. have reported that the filtration performance 'efficiency and pressure drop' of glass fibres filter was not improved by coating of coarse fibres with average diameter of 7 μm on the glass filter, but significantly improved by the same mass of nanofibres with average diameters of 150 nm [138]. Hsiao et al. have also reported an improvement in the oil/water filtration performance by using a crosslinked electrospun PVA nanofibrous substrate as a mid layer [139]. In addition, fabrics for protective clothing applications are also coated by different nanofibrous layers to improve many specific properties such as mechanical support and resistance against air and moisture transport [132].

In fact, the potential impact of nanofibre coating is extensive. Elmarco and others have developed many machine models with different production rates for integrating nanofibres on line onto coarse fibre nonwoven fabrics for building a three dimensional structure, as shown in figure 1.9. An example of the industrial nanofibres coating machines made by Elmarco is shown in table 1.2.

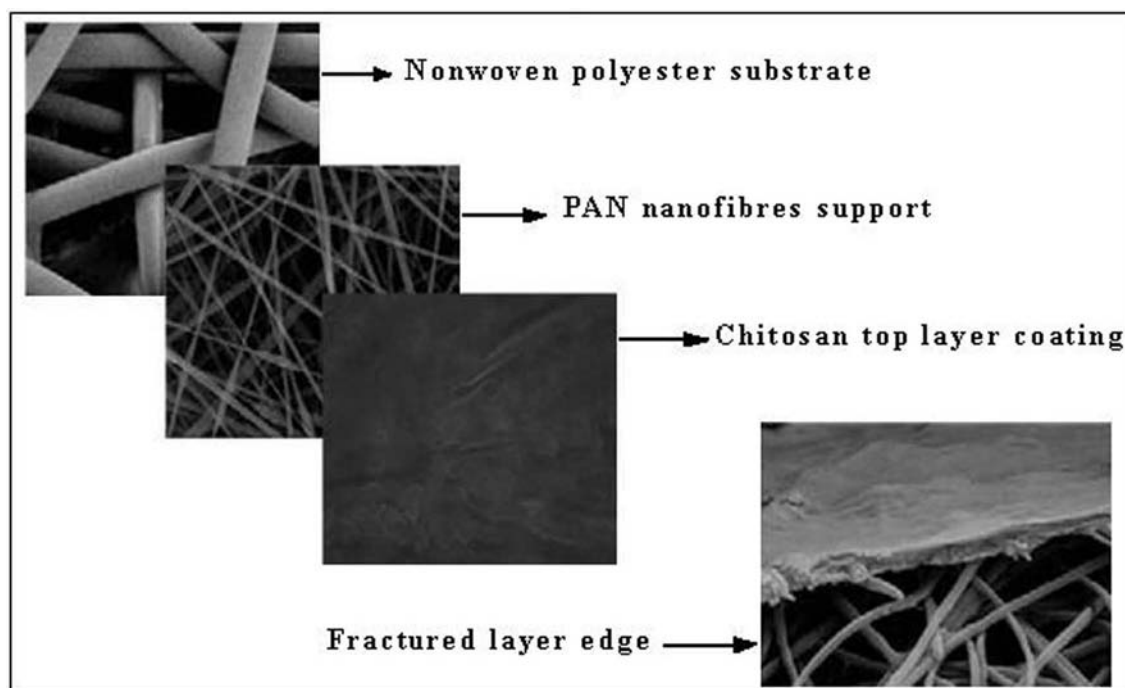


Figure 1.8, SEM images of three layers used as a filtration membrane in which a melt blown nonwoven polyester base is used as a support layer, PAN electrospun nanofibres as a mid layer, and a top coating layer of chitosan [114].

Table 1.2, Nanospider™ machine models produced by Elmarco company [125].

Machine model	NS 8A 1600	NS 16A 1600
Number of spinning units	2	4
Number of spinning heads	8	16
Width	1.6 m	1.6 m
Type of polymer	PA6	PA6
Fibre diameter	0.03 g/ m ² , fibres 50-150 nm	0.03 g/ m ² , fibres 50-150 nm
Linear speed	18 m/min	33 m/min
Operation cycle	16 h	16 h
Dimensions	(L 4.1, W 2.6, H 2.5) m	(L 8.1, W 2.6, H 2.5) m

In summary, the study presented here indicates the useful progress in developing the physical, mechanical and structural properties of nonwoven fabrics through coating the fabric by electrospun nanofibres. Hence the transition from microfibre to nanofibre nonwovens led to a significant change in the transport properties as a result of the reduction in the pore size and the large increase in the inner surface area. So a lightweight, hydrophilic, hydrophobic, breathable, permeable and highly resistant to deadly chemicals fabric can be achieved. To do so successfully, homogeneity in the size

diameter distribution of nanofibres and uniform nanofibre coating thickness are required. Furthermore, bonding and adhering the nanofibre layer onto the nonwoven fabric are still great challenge which needs further investigation.



Figure 1.9, Schematic illustration of the nanospiderTM machine produced by Elmarco company [125], (upper left) photograph of nanospiderTM machine [125], (upper middle) technical electrospinning set-up with a large scale width presented in TransMIT-Marburg- Germany [117], (upper right) technical textile fabrics coated by electrospun nanofibres [117].

1.5.4 Three dimensional nanofibre fabrics

Typically, as shown previously, electrospun nanofibre assemblies are collected as a two dimensional form with randomly arranged structures. In addition, it is difficult to control the density of nanofibres in the direction of thickness, thus fabricating a solid three dimensional structure form through electrospinning is hard to achieve. So far,

however, the only electrospun three dimensional structure form with proper length, width and height that has been successfully fabricated is a nanofibrous tube. Nevertheless, some solid three dimensional nanofibrous fabrics have also been fabricated with some success.

Recently, researchers have reported three dimensional construction fabric forms via electrospinning by using different methods. They have used a micro patterned template as a collector [140], a chemical blowing agent with heat post treatment [141], combination of electrospinning and wet spinning 'electro wet spinning' [142] and a three dimensional collecting template as an assistant collector [143]. Hereinafter, a brief explanation about the most recent effective methods for fabricating three dimensional nanofibre fabrics is presented.

Kobayashi et. al. have established a novel system based on electro wet spinning for the three dimensional structure control of nanofibre fabric [142]. After electrospinning nanofibres in the liquid bath, the collected nanofibre fabric was frozen and then vacuum-freeze dried. A three dimensional spongiform fabric with remarkable low bulk density in comparison with the nonwoven electrospun fabric has been produced. They have demonstrated, within this system, that the apparent density, porosity and formation of the fabric depend critically on the surface tension of the liquid bath. Hence, for instance, when water was used as a liquid bath, the nanofibres floated on the water surface due to its high surface tension.

Chang et. al. have designed a novel method for fabricating nanofibrous tubes with different three dimensional tubular architectures by controlling the configuration of the collectors [143]. They have used three dimensional collecting templates (a working collector with similar configuration of the desired fibrous tubes and a stick assistant collector) in order to manipulate the electric field and the electric forces 'Coulomb interactions', as shown in figure 1.10. As a result, tubular structures with different lengths, diameters, cross sectional shapes and multiple interconnected patterns have been synchronously fabricated. They have demonstrated, in this design, that formation of the tube architecture depends on the electrospinning solvent permittivity, feeding rate, applied voltage, charge density and the correlated nanofibre velocity.

In fact, with the ability to fabricate three dimensional structure fabrics, many effective applications such as tissue organ scaffolds can be achieved. However, three dimensional nanofibre fabrics still have some problems in controlling the fabric's thickness density for commercial and industrial applications, and need further research.

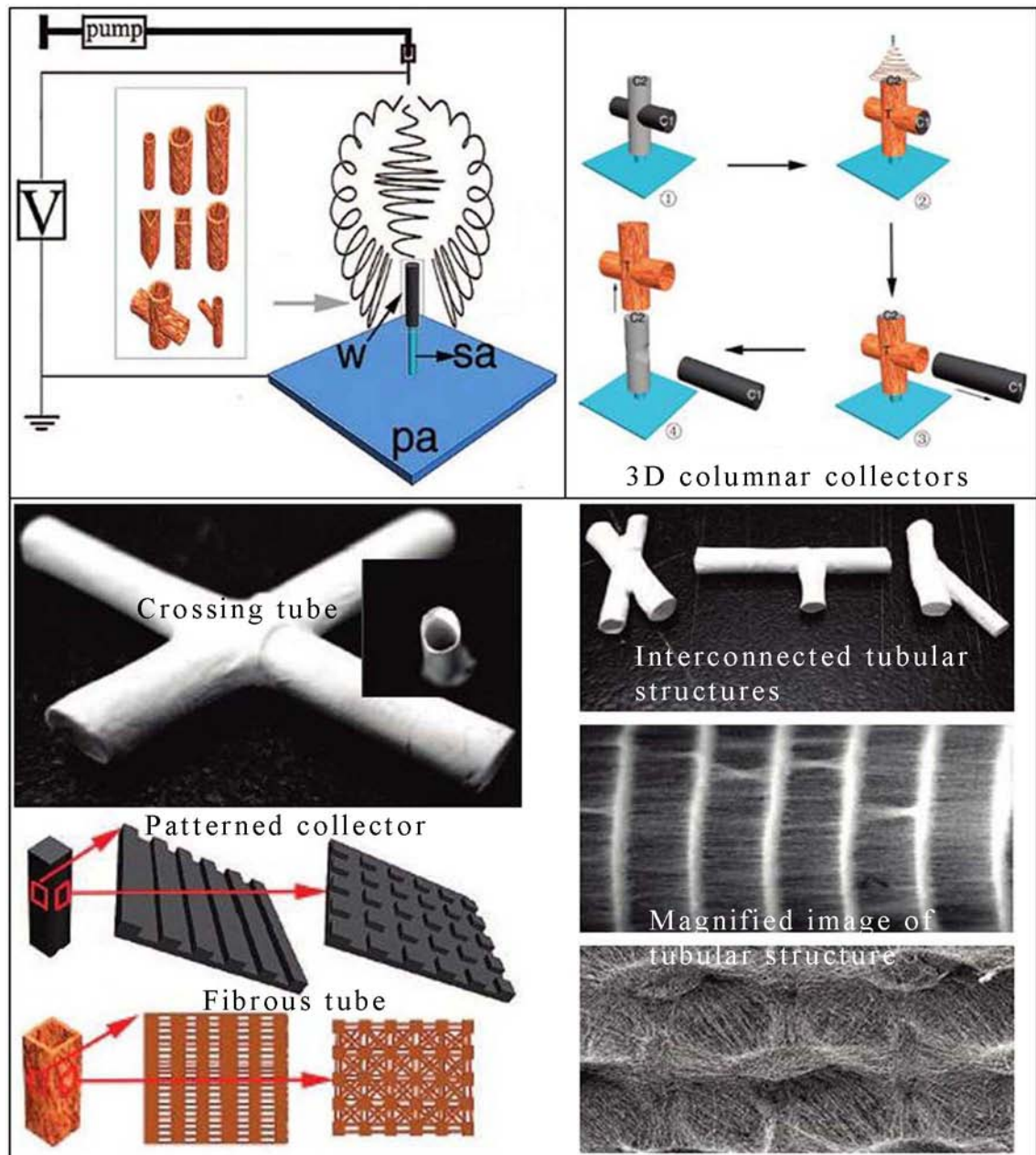


Figure 1.10, Schematic illustrations and photos of collecting processes for the fabrication of nanofibrous tubes with different patterns by electrospinning using 3D collectors, ((w) is the working collector, (pa) is the plane assistant collector, and (sa) is the stick assistant collector) [143].

1.5.5 Woven nanofibre fabrics

As previously shown from the literature on nanofibre fabrics, it is found that most developments have focused on functionality and engineering of nonwoven nanofibre fabrics. So far, however, nanofibres have not been widely used in woven fabric formation. Hence, according to the weaving process fundamentals, single nanofibres cannot be applied directly due to their geometrical structure and physical properties. In

other words, manufacturing of woven nanofibre fabrics is mainly based on spinning nanofibre yarns with controlled orientation and architecture. In fact, as shown previously in chapter five, spinning continuous twisted nanofibre yarn at acceptable production rates and mechanically suitable for weaving process requirements is a serious challenge which needs further systematic research.

Nevertheless, researchers have recently demonstrated the feasibility of weaving nanofibre bundles or tows ‘oriented yarns’ into three dimensional woven fabrics. Kim et. al. have constructed plain woven fabric based on polycaprolactone nanofibre bundles [144]. In their work, electrospun porous PCL nanofibres were produced using electro wet spinning. After delivering and coagulating, the nanofibres were drawn out from the coagulant bath (distilled water) by means of a roller rotating at 30 m/min and dried in a vacuum oven at 20°C. Then the plain woven fabric was constructed with interlacing warp yarns and filling yarns at right angles, as shown in figure 1.11. They have claimed that the produced PCL woven fabric provides an engineering scaffold able to support cells-tissue proliferation.

However, having a low production rate (the highest nanofibre yarn spinning speed of 63 m/min [145] is still much slower than that of the industrial dry spinning for yarn of 1500 m/min [146]) and the unclear physical and mechanical properties of nanofibre yarns, the ability to fabricate woven nanofibre fabric remains a challenge. Moreover, imparting the twist and thus producing continuous twisted nanofibre yarn with good strength is another crucial role in manufacturing woven fabric.

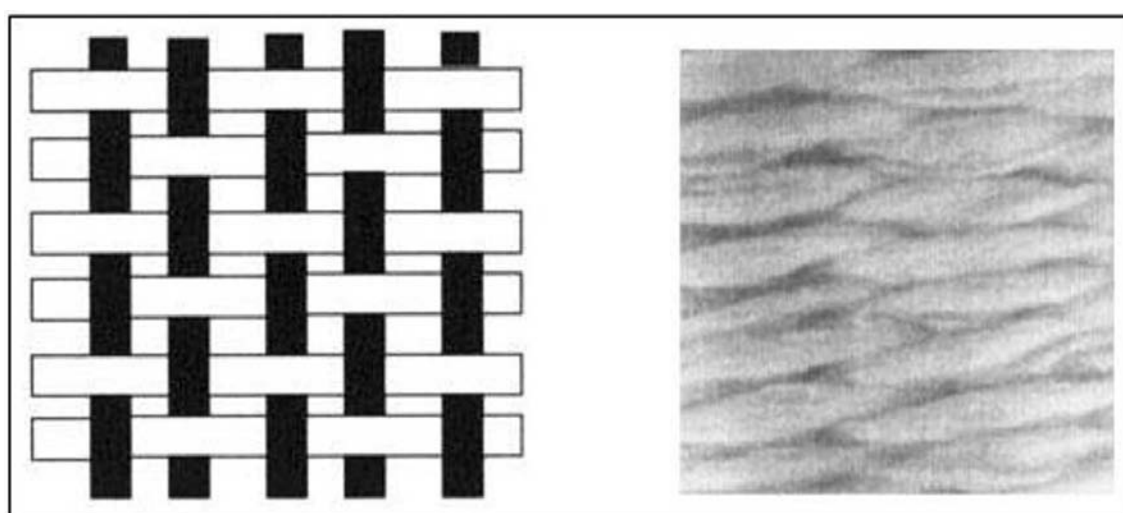


Figure 1.11, (Left) Schematic diagram of the plain weave fabric, (right) close photo of PCL plain weave nanofibre fabric [144].

1.5.6 Core-shell, hollow and porous nanofibres

Electrospun nanofibres usually have a solid interior body and smooth surface. Recently, researchers have demonstrated that nanofibres with controllable hierarchical (such as core-shell, bicomponent, hollow and porous) structures could be produced if proper processing parameters or designs of spinnerets were implemented. Functionalizing nanofibre by different materials or controlling nanofibre body size, mass and content has produced nanofibres with super active surface properties. Hierarchical organization in nanofibre morphologies and textures can be utilized in advanced applications such as nanofluidics, catalysis, drug delivery and release, nano supports, energy storage and gas sensors. Herein, from the engineering point of view, these types of nanofibre structures with an emphasis on their formation mechanisms and functionality are reviewed.

1.5.6.1 Core-shell nanofibres

To impart functional properties to the nanofibres, two components consisting of two or more different types of polymers, polymer/nanoparticles, polymer/(bacterias, viruses, cells and enzymes carrying specific functions) and polymer/nonpolymeric Newtonian liquid have been electrospun. To synthesize this tubular or core-shell 'core-sheath' (cable-like) nanofibre structure, different methods including multi steps template synthesis [147, 148], surface initiated atom transfer radical polymerization 'ATRP' [149] and coaxial electrospinning [150-159] have been utilized. Coaxial electrospinning has been considered as the most versatile method for producing compound core-shell nanofibres [115]. Table 1.3, shows examples of the core-shell nanofibres produced by coaxial electrospinning.

In coaxial electrospinning, two concentrically aligned capillary channels located coaxially one inside the other are used for the simultaneous electrospinning of two different immiscible liquids. One of the liquids flows through the inner capillary and the other liquid flows through the annular gap between the outer and the inner capillary. When the same voltage is applied to both capillaries, a jet is generated on the tip of the deformed droplet. The jet stretches and the solvent evaporates causing the jet to solidify, thus producing compound core-shell nanofibres, as shown in figure 1.12.

It can be noted that by using a concept similar to the coaxial spinneret, the spinneret can be designed with two capillaries side by side in order to electrospin bicomponent nanofibres [126, 160, 161]. It has been demonstrated within this system that the feed rate ratio of the two components must be constant along the length of the fibre for preventing the fluctuations of the jet on the surface of the Taylor cone [117].

Table 1.3, Examples of core-shell nanofibres produced by coaxial electrospinning using different materials.

Synthesis method	Core	Shell	Ref.
Coaxial spinneret	Heavy mineral oil	Poly(vinylpyrrolidone)(PVP)	[150, 153]
Coaxial spinneret	Poly(styrene-block-isopreneblock-styrene)	Poly(methylmethacrylate-co-methacrylic acid)	[152]
Coaxial spinneret	Polystyrene (PS)	Poly(phenylenevinylene)PPV	[154]
Coaxial spinneret	Poly(vinyl alcohol)(PVA)	Poly(phenylenevinylene)PPV	[154]
Coaxial spinneret	Poly(anilinesulfonic acid)(PASA)	Poly(ethylene oxide) (PEO)	[155]
Coaxial spinneret	Poly(acrylonitrile) (PAN)	Poly(ethylene oxide) (PEO)	[155]
Coaxial spinneret	Poly(methylmethacrylate) (PMMA)	Poly(acrylonitrile) (PAN)	[156]
Coaxial spinneret	Paraffin oil	Poly(vinylpyrrolidone)(PVP)	[157]
Coaxial spinneret	Cellulose acetate (CA)	Poly(ethylene oxide) (PEO)	[158]
Coaxial spinneret	Poly(methylmethacrylate) (PMMA)	Polypyrrole (PPY)	[159]

During coaxial electrospinning, the nanofibre core diameter and shell thickness can be conveniently varied by controlling the flow rates of liquids in the inner and the outer capillaries. In general, the physical pattern of coaxial electrospinning depends on the compound droplet suspended at the edge of a core-shell spinneret. The compound droplet must be elongated at the same magnitude in order to obtain core-shell nanofibres with continuous and uniform diameters. Common problems that may occur in the coaxial electrospinning are; if, due to the weakness of the electric forces, the outer droplet is transformed into a jet while the inner droplet is not transformed. In that case, the deformation of the inner droplet into a core is left to viscous forces only [115]. In addition, when the shell liquid is a polymeric solution and the core liquid is a normal liquid (e.g. oil, water), the core jet may break into droplets as the shell stretches quickly [155]. Hence, rapid stretching of the shell may cause strong viscous stress tangential to the core [150].

In summary, in this new electrospinning system, parameters of electrospinning and liquids properties such as size of core-shell capillaries, applied electric field, volume feed rate, immiscibility of the core-shell liquids and their viscosity and conductivity play crucial roles in determining the uniform formation of core-shell jet and the

morphology of the produced nanofibres. However, more systematic work is still required in order to control the process and to achieve a better understanding.

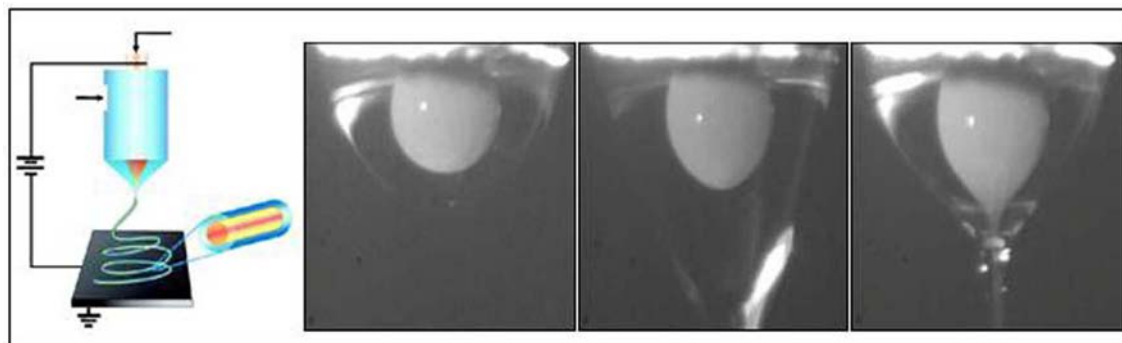


Figure 1.12, (Left) Schematic illustration of the electrospinning setup with two coaxial capillaries for spinning nanofibres having a core-shell structure [157], (right) series photos of the formation of the compound conical electrified coaxial jet, the liquids are a PVP solution as a shell and a mineral oil as a core [155].

1.5.6.2 Hollow nanofibres

Nanofibres with hollow interiors ‘like tubes’ are of great technical importance for many applications such as nanofluidics and hydrogen storage [162]. Recently two effective methods have been used to synthesize hollow “electrospun” nanofibres from a wealth of materials. Coaxial electrospinning of two immiscible liquids followed by dissolving the core with a selective solvent [150, 151], by dissolving and calcining ‘heating treatment’ the core [163, 164] or by calcining the core [157, 165] has been successfully utilized. For instance, with the use of coaxial electrospinning, nanofibres made of TiO_2/PVP as a shell and mineral oil as a core were obtained. Removal of the oil phase by solvent extraction resulted in the formation of hollow nanofibres consisting of TiO_2/PVP composite walls [150]. In this method, the size and wall thickness of these nanofibres can be varied by controlling the process parameters such as feeding rate of the core liquid. Most importantly, choosing the right solvent and calcining the electrospun nanofibres with controlling the heating rate and the dwell time for extracting the core are crucial steps for successful hollow nanofibres synthesis [166]. In the second method, electrospun polymer fibres are used as template for the preparation of hollow nanofibres. Then this template is coated with one or more layers ‘a layer-by-layer technique’ of polymers, metals, or even oxygen plasma irradiation [167] as a sheath to the nanofibre core. With a similar concept, the sacrificial template material is extracted by dissolving and heat drying [167], dissolving and centrifugal rotation drying

[168, 169] or by calcining [170, 171] to synthesize the hollow nanofibre structure. It has been demonstrated that the quality of the resultant hollow nanofibres is strongly dependent on the yield and control of coating and etching steps [170]. Figure 1.13, shows hollow nanofibre images synthesized by different methods which are adapted from the open literature.

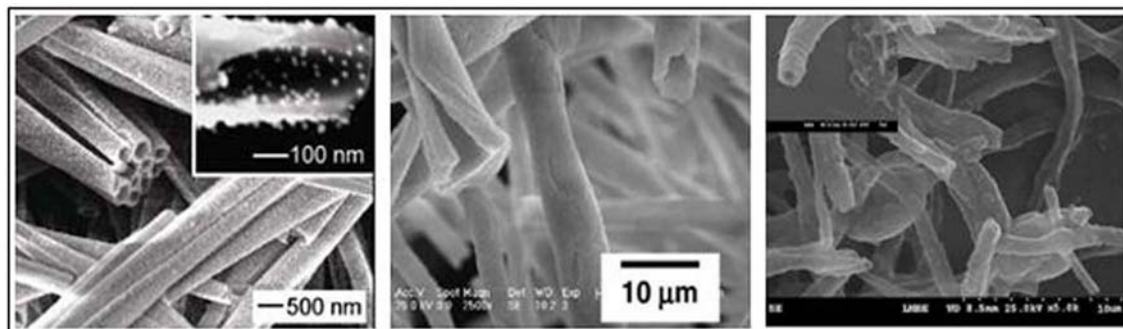


Figure 1.13, (Left to right) SEM images of hollow titania nanofibres functionalized with amino-terminated silane and gold nanoparticles [151], 8YSZ hollow nanofibres calcined at 1400 °C [170], hollow multilayer (PEI/TiO₂)₄ nanofibres [169].

In fact, the hollow nanofibre synthesis facilitates functionalization of the inner and outer surfaces of the hollow nanofibres with salts, ferrofluids, enzymes, dyes, and precursors [162]. Moreover, the surface area measurements gave hollow nanofibres a BET surface area ‘a technique for the measurement of the specific surface area of a material m²/g’ larger than (approximately two times) those of the solid core-shell nanofibres [165].

1.5.6.3 Porous nanofibres

The surface area of nanofibre can be greatly enhanced when its topology is transformed into a porous structure. Increase of surface areas expands nanofibre scope for a range of beneficial applications such as modifying the wetting properties for filtration and altering the biodegradation kinetics of bioerodible nanofibres. [115]. As such, several researchers have generated porous nanofibres with different topologies by selecting particular solvents or solvent mixtures, or polymer mixtures under controlled environmental mediums.

It has been reported by Xia et. al. that by electrospinning immiscible polymers and miscible solvents, highly porous nanofibres could be obtained [151]. In their work, the PS solution in a mixture of DMF/THF was used as a core liquid and a PVP/TiO₂ solution in ethanol was used as the shell liquid. As the solvents evaporated during electrospinning, the two polymer phases were separated to generate nanofibres of PS

embedded in a PVP/TiO₂ matrix. Then, by calcining the fibres; the PS phase had been removed to form highly porous nanofibres with no defined core-shell morphology, as shown in figure 1.14, (right). It can be noted that if a mixture of immiscible polymers is electrospun from the same solvent, binodal or spinodal nanofibre structures have been produced after evaporation of the solvent and phase separation. Consequently, by using a specific solvent; porous nanofibres with periodic thickness fluctuations and fractal surfaces can be obtained, as shown in figure 1.14, (middle) [115].

Researchers have also produced porous nanofibres by electrospinning polymer blends, followed by selective removal of one component. Wendorff et. al. have produced porous nanofibres of PLA/PVP blend solution [172]. They have reported that the degree of nanofibre porosity can be controlled by varying the amounts of the two polymers loaded into the polymer solution. Furthermore, by exploiting this concept, Khan et. al. have reported that removal of the salt from electrospun nanofibres of nylon 6/ GaCl₃ blend using water or other solvents resulted in nanopores with controlled pore size along the surface of the nanofibres [173].

Another method of obtaining porous structures could be by electrospinning nanofibres in a bath of liquid (such as nitrogen) [174]. Here, phase separation of the polymer and the solvent occurs and thus porous nanofibres are formed by removing the solvent under vacuum. Finally, using either a highly volatile solvent [175] or a swelling agent [176] or injecting tiny droplets of water under a very humid environment [177] within the polymer solution followed by drying the electrospun nanofibres has also led to porous structures. Figure 1.14, shows some examples of porous nanofibres formed by different methods (referred to their references) which are adapted from the open literature.

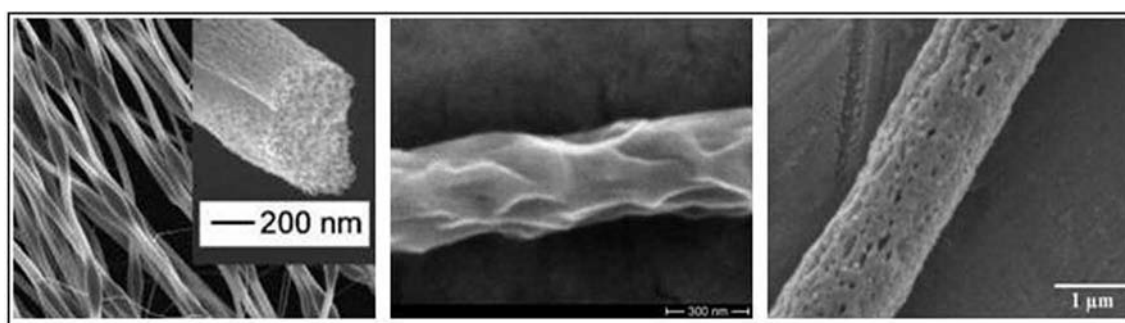


Figure 1.14, (Left to right) SEM images of porous Titania nanofibres fabricated by calcining fibres electrospun from PS in DMF/THF in the core with a titanium/PVP in the outer shell [151], electrospun nanofibre of a PLA/PVP blend after the selective extraction of PVP [115], porous nylon 6 nanofibres after removing the salt from the nylon 6/ GaCl₃ [173].

In summary, porous nanofibres enlarge of the inner surface and thus the average surface area for the fibre matrix. For instance, Khan et. al. found that the BET surface area of the electrospun nanofibres is $1.8 \text{ m}^2/\text{g}$, whereas the BET surface area for the same nanofibres but porous is $12 \text{ m}^2/\text{g}$, reflecting an increase of a factor of 6 [173]. Moreover, their structure feature possesses the functionality to make porous nanofibres an important candidate for tissue engineering, catalysis and drug delivery and release applications.

1.5.7 Helical nanofibre assemblies

With the development of numerous novel electrospinning setups, great success has been achieved in controlling the fluffy texture of the nanofibres. Recently, architectural nanofibres including sinuous and zigzag folding, helical coiling and meandering, nanospring, coiled and surprising shish-kebab structures have been fabricated. In order to produce nanofibres with controlled configurations, electrospinning modification or polymer crystallization synthesis must be applied.

It has been demonstrated that the helical structures of nanofibres can be formed when the jets hit the collector surface during electrospinning [178]. Hence, when the jets impinged on the collector surface; the jets are under longitudinal compressive forces and thus the nanofibres recoil ‘buckling instability’. Based on this concept, and to elucidate this helical transformation mechanism; Reneker et. al. established an electrospinning set-up with a varied spinneret to collector distance of 1.5 cm to 5 cm, as shown in figure 1.15 (left) [179]. They have reported that the buckling frequency and wavelength, packing density ‘dense or loose’ and coils characteristic vary with this distance. In addition, they have observed that highly conductive, charged and viscous jets produced highly tightly looped buckling patterns.

Kim et. al. and another research group have introduced splitting the electric field in electrospinning as a method for helical structures formation [180, 181]. Particularly, by introducing unique set-ups consisting of parallel electrodes or one electrode and tilted glass slide as shown in figure 1.15 (middle and right), the nanofibre morphology changed into aligned helical coiling structures. They have also found that the coiling patterns were dependant on the jet viscosity and the geometric configuration of the collector electrodes.

Other research groups have produced helical nanofibre structures by electrospinning two components polymer solution, one conducting polymer (e.g. polyaniline sulfonic acid PASA) and one nonconducting polymer (e.g. PEO) from either single spinneret

[182, 183] or side by side bicomponent spinneret [161] on a conducting collector. It has been suggested that the viscoelastic shrinkage and the charge neutralization on the conductive phase were responsible for the formation of the helical structures.

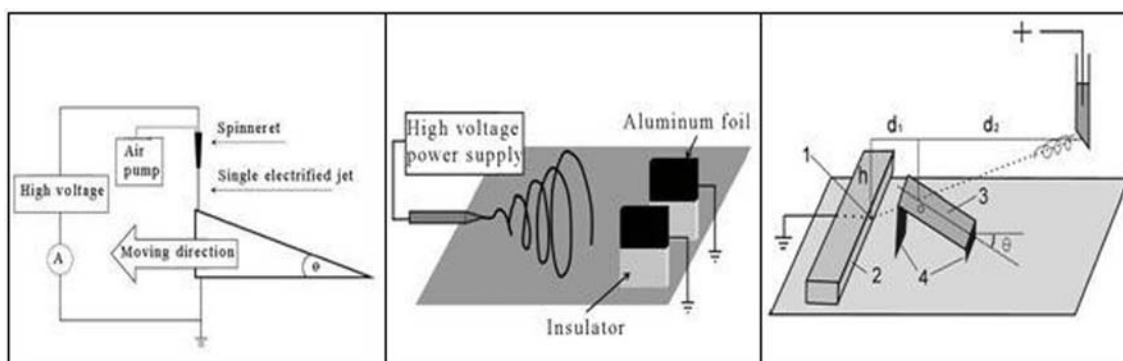


Figure 1.15, Schematic drawings of the helical nanofiber fabrications, (left) jets hitting [179], (middle) electric field splitting by parallel electrodes [180], (right) electric field splitting by one electrode and tilted glass slide [181].

Li et. al. have recently fabricated fancy hierarchical nanofibres by combining electrospinning and polymer crystallization technique [184]. They have decorated shish-kebab nanofibres by either an incubation (slow crystallization) or a solvent evaporation (fast crystallization) method. In fact, in this method, they have presented an effective strategy for fabricating well controlled fancy nanofibres. Hence, the hierarchical shape can be controlled by adjusting the crystallization conditions such as crystallization time, temperature and concentration.

Most recently, Wendorff and Bahnmüller et. al. have precisely made parallel, rectangular, undulating, buckling and fancy nanofiber structures on a high speed displaced silicon wafer collector [185]. In this method, the collector was ordered to a rapid displacement along the x-axis followed by a sequential rapid shift along the y-axis, and so on. They have claimed that by controlling the spinneret-collector distance, the applied voltage and the resolution of the displacement velocity in all directions, different pattern architectures can be fabricated. Figure 1.16, shows overview images of the different architectural nanofibres fabricated by the above mentioned methods.

In conclusion, these architectural nanofibres render a three dimensional feature and provide higher surface areas with spacer porosity control compared with a nonwoven nanofiber mat. Furthermore, they open the road towards novel applications such as sensorics, optical components and nanoelectromechanical systems.

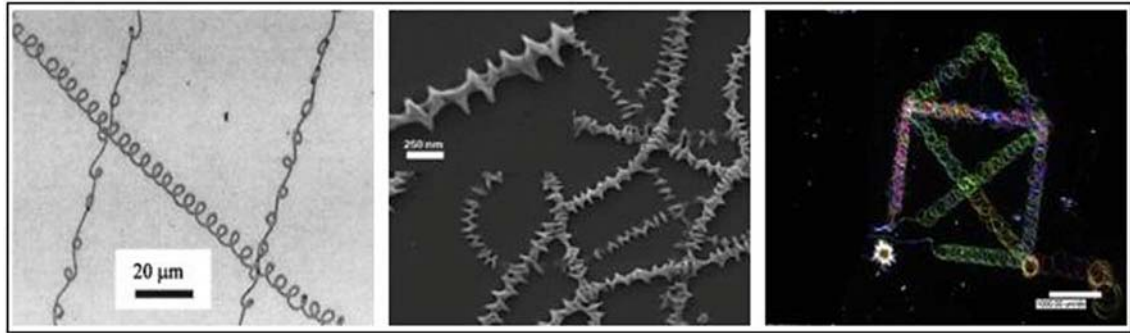


Figure 1.16, (Left to right) Images of helical nanofibres [182], shish-kebab nanofibres [184], (House of Santa Claus) written by nanofibres using the displaced collector method [185].

1.6 Aims and research objectives

The main aim of the thesis is to investigate yarn spinning from electrospun nanofibres. Based on the concept of staple yarn spinning, random fibres are aligned, drafted and twisted by devising a suitable spinning mechanism. This concept has been applied on electrospun nanofibres, by studying the morphology of nanofibres, alignment and orientation of nanofibres and finally the application of twist into the nanofibres and the taking up of the resulted yarn. The control of the yarn linear density and twist per unit length are important process requirements for optimum yarn design. Mechanical characterization of the electrospun nanofibres and techniques for enhancing their strength and functionality by (CNTs) also need to be studied for effective yarn production.

These research objectives are being fulfilled in six chapters, the arrangements of which are described below.

Chapter 2: *Investigating the fabrication of nanofibres by electrospinning*: the thesis focus on nylon 6 polymer for electrospinning nylon 6 nanofibres and for further spinning them into continuous yarn. Although other polymers have been investigated and could be used, we felt that consistency throughout of this research was important.

In this chapter, the physical properties of the polymer solution and the electrospinning process parameters are investigated in order to establish their effect on nylon 6 nanofibre morphology, average diameter and uniformity. The polymer solution concentration, applied voltage and electrospinning distance are optimized to enable uniform nanofibre diameter distribution. Consequently, uniform diameter nanofibres can be produced for alignment and parallelization for the next step of this study.

Chapter 3: *Alignment of nanofibres*: in this chapter, a comprehensive review on the design and use of manifold nano mechanisms for the alignment of nanofibres is provided. We revise and further develop a novel nano alignment and parallelization mechanism for nanofibres by considering its further use for nanofibre twist insertion necessary for later; steps of this research. We systematically scrutinize the degree of alignment of nanofibres, nanofibres length and linear density of collected nylon 6 nanofibres. This enables us to optimize the alignment mechanism by characterizing the nanofibres alignment morphology. Thus, the optimum parameters of the alignment mechanism are in agreement with the requirements for the continuous nanofibre yarn making for the following research step.

Chapter 4: *Nanofibres filled with carbon nanotubes (CNTs)*: in this chapter, we aim to functionalize and strengthen the aligned nylon 6 nanofibres before gathering them into a continuous yarn. We have used multiwall carbon nanotubes (MWCNTs) as filler nanoparticles, because CNTs are suitable candidates due to their hardness, strength, thermal and electrical conductivity to enhance yarn characteristics. We used a high speed shearing method to improve the dispersion of MWCNTs into the polymer solution under a loading. We have manipulated the electric forces during electrospinning and the stretching forces on the fibres by the alignment mechanism to enable better alignment of the MWCNTs along the nanofibre axis. We have characterized microscopically the morphology of electrospun nanofibres and the dispersion of the MWCNTs and their alignment inside the nanofibre body. This enabled us to look into how to twist and collect nanofibres for yarn making, discussed in the next chapter.

Chapter 5: *Spinning nanofibre yarns*: in this chapter, we provide a comprehensive review on the design of various nano mechanisms for nanofibre yarns. In this chapter two techniques for making yarn have been examined; the conventional spun and the core spun concepts. We design and implement a novel mechanism for spinning nanofibre/composite nanofibre yarn as a further development of the alignment mechanism. We characterized microscopically the resulted yarn and further examined the inserted twist and the yarn linear density. We explained how we can control different yarn geometries such as yarn linear density and twist per unit length.

Another technique investigation was the one based on the conventional core spun yarn concept where we devised a new electro mechanical mechanism for spinning ‘core

electrospun nano yarns'. We have characterized microscopically the helical wraps of nanofibres wound around the core filament. We have analytically investigated the parameters of this mechanism such as feed-in angles, twist speeds and take up speeds for optimum spinning of core electrospun nano yarns.

Although the results fulfilled the objectives and were pushing the electrospinning of yarn further, it was necessary to try to theoretically and mechanically explain some process parameters for a more generic and robust process optimization. To that effect modeling of the jet and mechanical measurement of the fibres and mats were undertaken.

Chapter 6: *Modelling the electrospinning of nanofibres*: In practice, controlling yarn linear density and twist per unit length requires defining of the velocity of the nanofibres entering the spinning zone. To fulfil these requirements we aim in this chapter to establish mathematically the velocity; 'kinematics feature' of the nanofibres prior to collection. We have provided a comprehensive review on the mathematical models of electrospinning from jet initiation to nanofibre collection. In addition, we examine the electrospinning modes theory and their kinetic features. We were able to establish a mathematical model for recognizing and calculating theoretically the jet velocity at its splitting point, the number of nanofibres generated from the jet and their velocities. The accuracy of this model and its equations has been validated by considering the actual jet and the collected nanofibre velocities.

Chapter 7: *Mechanical characterization of nylon 6 nanofibres*: in this chapter, we aim to mechanically characterize the nanofibres by tensile testing of a single nanofibre and nanofibre mat. We start by providing a critical review of the developed mechanical characterization testing methods of single nanofibre. We have carried out a tensile test for nanofibre/ composite MWCNTs nanofibre mats to further characterize the effect of the MWCNTs filling fibre architecture. In addition, we design and implement a novel simple laboratory set-up for performing tensile test of single nanofibres. As a result, we have established the stress - strain curve for single nylon 6 nanofibres allowing us to define the tensile strength, axial tensile modulus and ultimate strain of these fibres. Finally, we explained how we can improve the mechanical properties of nylon 6 nanofibres and discussed how to overcome the tensile testing challenges of nanofibres.

Chapter 8: *General discussion and conclusion*: in this chapter, we try to summarize and conclude the investigation by answering the questions of the research aims and objectives. We discuss what was achieved in this study and state the challenges we faced in this work and how we have overcome these challenges, and discuss the new challenges of future work related to this study and further.

1.7 References

- [1.1] A. Vaseashta, *In nanostructured and advanced materials*, Edited by A. Vaseashta, D. Malinowska, J.M. Marshall, Dordrecht, **204**, 1-30 (2005)
- [1.2] Z.M. Huang, Y.Z. Zhang, M. Kotaki, S. Ramakrishna, *A review on polymer nanofibres by electrospinning and their applications in nanocomposites*, *Composites Science Technology*, **63**, 2224-2253 (2003)
- [1.3] D. Li, Y. Xia, *Electrospinning of nanofibres: reinventing the wheel*, *Advanced Materials*, **16**, 1151-1170 (2004)
- [1.4] T. Ondarcuhu, C. Joachim, *Drawing a single nanofibre over hundreds of microns*, *EPL-Europhysics Letters*, **42**, 215-220 (1998)
- [1.5] P.X. Ma, R. Zhang, *Synthetic nano-scale fibrous extracellular matrix*, *Journal of Biomedical Materials Research*, **46**, 60-72 (1999)
- [1.6] G.M. Whitesides, B.J. Grzybowski, *Self-assembly at all scales*, *Science*, **295**, 2418-2421 (2002)
- [1.7] C.R. Martin, *Membrane-based synthesis of nanomaterials*, *Chemistry of Materials*, **8**, 1739-1746 (1996)
- [1.8] A. Formhals, *Method and apparatus for spinning*, US Patent, **2160962** (1939)
- [1.9] A. Formhals, *Artificial thread and method of producing same filed*, US Patent, **2187306** (1940)
- [1.10] A. Formhals, *Producing of artificial fibres from fibre forming liquids*, US Patent, **2323025** (1943)
- [1.11] A. Formhals, *Method and apparatus for spinning*, US Patent, **2349950** (1944)
- [1.12] A. Formhals, *Process and apparatus for preparing artificial threads*, US Patent, **1975504** (1934)
- [1.13] P.K. Baumgarten, *Electrostatic spinning of acrylic microfibrils*, *Journal of Colloid and Interface Science*, **36**, 71-79 (1971)
- [1.14] D.H. Reneker, I. Chun, *Nanometre diameter fibres of polymer produced by electrospinning*, *Nanotechnology*, **7**, 216-223 (1996)

- [1.15] Y. Zhou, M. Freitag, J. Hone, C. Staii Jr, A.T. Johnson, N.J. Pinto, A.G. MacDiamid, *Fabrication and electrical characterization of polyaniline-based nanofibres with diameter below 30 nm*, Applied Physics Letters, **83**, 3800-3802 (2003)
- [1.16] H. Fong, I. Chun, D.H. Reneker, *Beaded nanofibres formed during electrospinning*, Polymer, **40**, 4585-4592 (1999)
- [1.17] W.K. Son, J.H. Youk, T.S. Lee, W.H. Park, *The effects of solution properties and polyelectrolyte on electrospinning of ultrafine poly(ethylene oxide) fibres*, Polymer, **45**, 2959-2966 (2004)
- [1.18] S.J. Kim, C.K. Lee, S.I. Kim, *Effect of ionic salts on the processing of poly(2-acrylamido-2-methyl-1-propane sulfonic acid) nanofibres*, Journal of Applied Polymer Science, **96**, 1388-1393 (2005)
- [1.19] K.H. Lee, H.Y. Kim, H.J. Bang, Y.H. Jung, S.G. Lee, *The change of bead morphology formed on electrospun polystyrene fibres*, Polymer, **44**, 4029-4034 (2003)
- [1.20] T. Lin, H. Wang, X. Wang, *The charge effect of cationic surfactants on the elimination of fibre beads in the electrospinning of polystyrene*, Nanotechnology, **15**, 1375-1381 (2004)
- [1.21] L. Wannatong, A. Sirivat, P. Supaphol, *Effects of solvents on electrospun polymeric fibres: preliminary study on polystyrene*, Polymer International, **53**, 1851-1859 (2004)
- [1.22] C. Huang, S. Chen, C. Lai, D.H. Reneker, H. Qiu, Y. Ye, H.Q. Hou, *Electrospun polymer nanofibres with small diameters*, Nanotechnology, **17**, 1558-1563 (2006)
- [1.23] Y.Z. Zhang, J. Venugopal, Z.M. Huang, C.T. Lim, S. Ramakrishna, *Crosslinking of the electrospun gelatin nanofibres*, Polymer, **47**, 2911-2917 (2006)
- [1.24] S.H. Tan, R. Inai, M. Kotaki, S. Ramakrishna, *Systematic parameter study for ultra-fine fibre fabrication via electrospinning process*, Polymer, **46**, 6128-6134 (2005)
- [1.25] L. Larrondo, R.S.J. Manley, *Electrostatic fibre spinning from polymer melts: I, experimental observations on fibre formation and properties*, Journal of Polymer Science part B: Polymer Physics, **19**, 909-920 (1981)
- [1.26] L. Larrondo, R.S.J. Manley, *Electrostatic fibre spinning from polymer melts: II, examination of the flow field in an electrically driven jet*, Journal of Polymer Science part B: Polymer Physics, **19**, 921-932 (1981)
- [1.27] L. Larrondo, R.S.J. Manley, *Electrostatic fibre spinning from polymer melts: III, electrostatic deformation of a pendent drop of polymer melt*, Journal of Polymer Science part B: Polymer Physics, **19**, 933-940 (1981)

- [1.28] J. Lyons, C. Li, F. Ko, *Melt- electrospinning part I: processing parameters and geometric properties*, *Polymer*, **45**, 7597-7603 (2004)
- [1.29] J.E. Sanders, S.E. Lamont, A. Karchin, S.L. Golledge, B.D. Ratner, *Fibro-porous meshes made from polyurethane micro-fibres: effects of surface charge on tissue response*, *Biomaterials*, **26**, 813-818 (2005)
- [1.30] Y. Dzenis, *Spinning continuous fibres for nanotechnology*, *Science*, **304**, 1917-1919 (2004)
- [1.31] V.I. Kozhenkov, N.A. Fuks, *Electrohydrodynamic atomization of liquids*, *Russian Chemical Reviews*, **45**, 1179-1184 (1976)
- [1.32] F. Raleigh, *On the equilibrium of liquid conducting masses charged with electricity*, *Philosophical Magazine*, **14**, 184-186 (1882)
- [1.33] J. Zeleny, *Instability of electrified liquid surfaces*, *Physical Review Letters*, **10**, 1-6 (1917)
- [1.34] J.F. Cooley, *Apparatus for electrically dispersing fluids*, US Patent, **692631** (1902)
- [1.35] W.J. Morton, *Method of dispersing fluids*, US Patent, **705691** (1902)
- [1.36] G. I. Taylor, *Disintegration of water drops in an electric field*, *Proceedings of the Royal Society of London Series A*, **280**, 383-397 (1964)
- [1.37] G. I. Taylor, *The circulation produced in a drop by an electric field*, *Proceedings of the Royal Society of London Series A*, **291**, 159-166 (1966)
- [1.38] G. I. Taylor, *Electrically driven jets*, *Proceedings of the Royal Society of London Series A*, **313**, 453-475 (1969)
- [1.39] J.R. Melcher, G.I. Taylor, *Electrohydrodynamics: a review of the role of interfacial shear stresses*, *Annual Review of Fluid Mechanics*, **1**, 111-122 (1969)
- [1.40] J. Doshi, D.H. Reneker, *Electrospinning process and applications of electrospun fibres*, *Journal of Electrostatics*, **35**, 151-160 (1995)
- [1.41] R. Kessick, J. Fenn, G. Tepper, *The use of AC potentials in electrospaying and electrospinning processes*, *Polymer*, **45**, 2981-2984 (2004)
- [1.42] A. Frenot, I.S. Chronakis, *Polymer nanofibres assembled by electrospinning*, *Current Opinion in Colloid & Interface Science*, **8**, 64-75 (2003)
- [1.43] S. Koombhongse, W. Liu, D.H. Reneker, *Flat ribbons and other shapes by electrospinning*, *Journal of Polymer Science part B: Polymer Physics*, **39**, 2598-2606 (2001)
- [1.44] A. Buer, S.C. Ugbolue, S.B. Warner, *Electrospinning and properties of some nanofibres*, *Textile Research Journal*, **71**, 323-328 (2001)

- [1.45] A.G. MacDiarmid, W.E. Jones, I.D. Noris, *Electrostatically-generated nanofibres of electronic polymers*, Synthetic Materials, **119**, 27-30 (2001)
- [1.46] D. Diaz, M.J. Leon, *Electrospinning nanofibres of polyaniline and polyaniline/polystyrene and polyethylene oxide blends*, National Conference of Undergraduate Research, University of Kentucky, Lexington, USA (2001)
- [1.47] M. Bognitzki, H. Hou, M. Ishaque, *Polymer-metal and hybrid nano-and Mesotubes by coating degradable polymer template fibres*, Advanced Materials, **12**, 637-640 (2000)
- [1.48] M. Bognitzki, T. Frese, M. Steinhart, A. Greiner, J.H. Wendorff, *Preparation of fibres with nanoscaled morphologies: electrospinning of polymer blends*, Polymer Engineering Science, **41**, 982-989 (2001)
- [1.49] M. Bognitzki, J.H. Wendorff, A. Greiner, *Submicrometer shaped polylactide fibres by electrospinning*, Polymer Materials Science Engineering, **82**, 115-116 (2000)
- [1.50] S.B. Warner, A. Buer, S.C. Ugbohue, G.C. Rutledge, M.Y. Shin, *A fundamental investigation of the formation and properties of electrospun fibres*, M98-D01, Department of Chemical Engineering and Material Sciences, Massachusetts Institute of Technology, Cambridge (2000)
- [1.51] A. Ziabicki, *Fundamentals of fibre formation*, John Wiley & Sons, London (1976)
- [1.52] S.Y. Gu, J. Ren, G.J. Vancso, *Process optimization and empirical modeling for electrospun polyacrylonitrile (PAN) nanofibre precursor of carbon nanofibres*, European Polymer Journal, **41**, 2559-2568 (2005)
- [1.53] X. Fang, D.H. Reneker, *DNA fibres by electrospinning*, Journal of Macromolecular Science part B: Physics, **36**, 169-173 (1997)
- [1.54] J.J. Feng, *The stretching of an electrified non-Newtonian jet: a model for electrospinning*, Physics of Fluids, **14**, 3912-3926 (2002)
- [1.55] D.H. Reneker, A.L. Yarin, H. Fong, S. Koombhongse, *Bending instability of electrically charged liquid jets of polymer solutions in electrospinning*, Journal of Applied Physics, **87**, 4531-4547 (2000)
- [1.56] M.M. Hohman, M.Y. Shin, G.C. Rutledge, M. Brenner, *Electrospinning and electrically forced jets I: stability theory*, Physics of Fluids, **13**, 2201-2220 (2001)
- [1.57] I. Hayati, A.I. Bailey, T.F. Tadros, *Investigation into the mechanisms of electrohydrodynamic spraying of liquids*, Journal of Colloid and Interface Science, **117**, 205-221 (1987)

- [1.58] M.M. Demir, I. Yilgor, E. Yilgor, B. Erman, *Electrospinning of polyurethane fibres*, *Polymer*, **43**, 3303-3309 (2002)
- [1.59] J.M. Deitzel, D. Kleinmeyer, J.K. Hirvanen, N.C.B. Tan, *Controlled deposition of electrospun poly (ethylene oxide) fibres*, *Polymers*, **42**, 8163-8170 (2001)
- [1.60] T.A. Kowalewski, A.L. Yarin, S. Blonski, *Experiments and modelling of electrospinning process*, The 5th Euromech Fluid Mechanics Conference, 24-28, Toulouse, France (2003)
- [1.61] J.H. He, Y.Q. Wan, J.Y. Yu, *Allometric scaling and instability in electrospinning*, *International journal of nonlinear and numerical Simulation*, **5**, 243-252 (2004)
- [1.62] S.V. Fridrikh, J.H. Yu, M.P. Brenner, G.C. Rutledge, *Controlling the fibre diameter during electrospinning*, *Physics Review Letters*, **90**, 144502-1 - 144502-5 (2003)
- [1.63] G. Srinivasan, D.H. Reneker, *Structure and morphology of small diameter electrospun aramid fibres*, *Polymer International*, **36**, 195-201 (2003)
- [1.64] M.S. Khil, S.R. Bhattarai, H.Y. Kim, S.Z. Kim, K.H. Lee, *Novel fabricated matrix via electrospinning for tissue engineering*, *Journal of Biomedical Materials Research part B: Applied Biomaterials*, **72**, 117-124 (2005)
- [1.65] J. Kameoka, H.G. Craighead, *Fabrication of oriented polymeric nanofibres on planar surfaces by electrospinning*, *Applied Physics Letters*, **3**, 371-373 (2003)
- [1.66] S. Theron, E. Zussman, A.L. Yarin, *Experimental investigation of the governing parameters in the electrospinning of polymer solutions*, *Polymer*, **45**, 2017-2030 (2004)
- [1.67] W. Zuo, M. Zhu, W. Yang, H. Yu, Y. Chen, Y. Zhang, *Experimental study on relationship between jet instability and formation of beaded fibres during electrospinning*, *Polymer Engineering and Science*, **45**, 704-709 (2005)
- [1.68] T. Jarusuwannapoom, W. Hongrojjanawiwat, S. Jitjaicham, L. Wannatong, M. Nithitanakul, C. Pattamaprom, *Effect of solvents on electrospinnability of polystyrene solutions and morphological appearance of resulting electrospun polystyrene fibres*, *European Polymer Journal*, **41**, 409-421 (2005)
- [1.69] K. Arayanarakul, N. Choktaweasap, D. Aht-Ong, C. Meechaisue, P. Supaphol, *Effects of poly(ethylene glycol) inorganic salt sodium dodecyl sulfate and solvent system on electrospinning of poly(ethylene oxide)*, *Macromolecular Materials and Engineering*, **291**, 581-591 (2006)
- [1.70] J.H. Yu, S.V. Fridrikh, G.C. Rutledge, *The role of elasticity in the formation of electrospun fibres*, *Polymer*, **47**, 4789-4797 (2006)

- [1.71] J.M. Deitzel, J.D. Kleinmeyer, D. Harris, N.C. Tan, *The effect of processing variables on the morphology of electrospun nanofibres and textiles*, *Polymer*, **42**, 261-272 (2001)
- [1.72] E.D. Boland, G.E. Wnek, D.G. Simpson, K.J. Palowski, G.L. Bowlin, *Tailoring tissue engineering scaffolds using electrostatic processing techniques: A study of poly (glycolic acid) electrospinning*, *Journal of Macromolecular Science Pure Applied Chemistry*, **A38**, 12, 1231-1243 (2001)
- [1.73] J. Liu, S. Kumar, *Microscopic polymer cups by electrospinning*, *Polymer*, **46**, 3211-3214 (2005)
- [1.74] M.G. McKee, G.L. Wilkes, R.H. Colby, T.E. Long, *Correlations of solution rheology with electrospun fibre formation of linear and branched polyesters*, *Macromolecules*, **37**, 1760-1767 (2004)
- [1.75] K.H. Lee, H.Y. Kim, Y.M. La, D.R. Lee, N.H. Sung, *Influence of a mixing solvent with tetrahydrofuran and N,N-dimethylformamide on electrospun poly(vinyl chloride) nonwoven mats*, *Journal of Polymer Science part B: Polymer Physics*, **40**, 2259-2268 (2002)
- [1.76] H. Liu, Y.L. Hsieh, *Ultrafine fibrous cellulose membranes from electrospinning of cellulose acetate*, *Journal of Polymer Science part B: Polymer Physics*, **40**, 2119-2129 (2002)
- [1.77] H. Fong, D.H. Reneker, *Elastomeric nanofibres of styrene-butadiene- styrene triblock copolymer*, *Journal of Polymer Science part B: Polymer Physics*, **37**, 3488-3493 (1999)
- [1.78] M.B. Bazbouz, G.K. Stylios, *Alignment and optimization of nylon 6 nanofibres by electrospinning*, *Journal of Applied Polymer Science*, **107**, 3023-3032 (2008)
- [1.79] X. Zong, K. Kim, D. Fang, S. Rana, B.S. Hsiao, B. chu, *Structure and process relationship of electrospun bioabsorbable nanofibre membranes*, *Polymer*, **43**, 4403-4412 (2002)
- [1.80] J. He, Y. Wan, J.Y. Yu, *Scaling law in electrospinning relationship between electric current and solution flow rate*, *Polymer*, **46**, 2799-2801 (2005)
- [1.81] X.H. Qin, S.Y. Wang, T.S.D. Lukas, *Effect of LiCl on the stability length of electrospinning jet by PAN polymer solution*, *Materials Letters*, **59**, 3102-3105 (2005)
- [1.82] X.M. Mo, C.Y. Xu, M. Kotaki, S. Ramakrishna, *Electrospun (PLLA-CL) nanofibre: a biomimetic extracellular matrix for smooth muscle cell and endothelial cell proliferation*, *Biomaterials*, **25**, 1883-1890 (2004)

- [1.83] C.J. Buchko, L.C. Chen, Y. Shen, D.C. Martin, *Processing and microstructural characterization of porous biocompatible protein polymer thin films*, *Polymer*, **40**, 7397-7407 (1999)
- [1.84] D.S. Katti, K.W. Robinson, F.K. Ko, C.T. Laurencin, *Bioresorbable nanofibre based systems for wound healing and drug delivery: optimization of fabrication parameters*, *Journal of Biomedical Materials Research*, **70B**, 286-296 (2004)
- [1.85] S. Kidoaki, I.K. Kwon, T. Matsuda, *Mesosopic spatial designs of nano and microfibre meshes for tissue-engineering matrix and scaffold based on newly devised multilayering and mixing electrospinning techniques*, *Biomaterials*, **26**, 37-46 (2005)
- [1.86] S.F. Fennessey, R.J. Farris, *Fabrication of aligned and molecularly oriented electrospun polyacrylonitrile nanofibres and the mechanical behavior of their twisted yarns*, *Polymer*, **45**, 4217-4225 (2004)
- [1.87] B. Ding, H.Y. Kim, S.C. Lee, C.L. Shao, D.R. Lee, S.J. Park, *Preparation and characterization of a nanoscale poly (vinyl alcohol) fibre aggregate produced by an electrospinning method*, *Journal of Polymer Science part B: Polymer Physics*, **40**, 1261-1268 (2002)
- [1.88] G.G. Chase, D.H. Reneker, *Nanofibres in filter media*, *Fluid / Particle Separation Journal*, **16**, 105-117 (2004)
- [1.89] S. Megelski, J.S. Stephens, D.B. Chase, J.F. Rabolt, *Micro- and nanostructure surface morphology on electrospun polymer fibres*, *Macromolecules*, **35**, 8456-8466 (2002)
- [1.90] D.H. Reneker, W. Kataphinan, A. Theron, E. Zussman, A.L. Yarin, *Nanofibre garlands of polycaprolactone by electrospinning*, *Polymer*, **43**, 6785-6794 (2002)
- [1.91] A.L. Yarin, S. Koombhongse, D.H. Reneker, *Taylor cone and jetting from liquid droplets in electrospinning of nanofibres*, *Journal of Applied Physics*, **90**, 4836-4846 (2001)
- [1.92] P. Supaphol, C. Mit-Uppatham, M. Nithitanakul, *Ultrafine electrospun polyamide-6 fibres: effect of emitting electrode polarity on morphology and average fibre diameter*, *Journal of Polymer Science Part B: Polymer Physics*, **43**, 3699-3712 (2005)
- [1.93] C. Mit-Uppatham, M. Nithitanakul, P. Supaphol, *Effects of solution concentration, emitting electrode polarity, solvent type, and salt addition on electrospun polyamide-6 fibres: a preliminary report*, *Macromolecular Symposia*, **216**, 293-299 (2004)

- [1.94] C.L. Casper, J.S. Stephens, N.G. Tassi, D.B. Chase, J.F. Rabolt, *Controlling surface morphology of electrospun polystyrene fibres: effect of humidity and molecular weight in electrospinning process*, *Macromolecules*, **37**, 573-580 (2004)
- [1.95] S. Tripatanasuwan, Z. Zhong, D.H. Reneker, *Effect of evaporation and solidification of the charged jet in electrospinning of poly(ethylene oxide) aqueous solution*, *Polymer*, **48**, 5742-5746 (2007)
- [1.96] J.H. He, Y.Q. Wan, J.Y. Yu, *Application of vibration technology to polymer electrospinning*, *International Journal of Nonlinear Science and Numerical Simulation*, **5**, 253-261 (2004)
- [1.97] K.S. Rho, L. Jeong, G. Lee, B.M. Seo, Y.J. Park, S.D. Hong, S. Roh, J.J. Cho, W.H. Park, B.M. Min, *Electrospinning of collagen nanofibres: effects on the behavior of normal human keratinocytes and early-stage wound healing*, *Biomaterials*, **27**, 1452-1461 (2006)
- [1.98] J. Ayutsede, M. Gandhi, S. Sukigara, M. Micklus, H.E. Chen, F. Ko, *Regeneration of bombyx mori silk by electrospinning part 3: characterization of electrospun nonwoven mat*, *Polymer*, **46**, 1625-1634 (2005)
- [1.99] L. Jeong, K.Y. Lee, J.W. Liu, W.H. Park, *Time-resolved structural investigation of regenerated silk fibroin nanofibres treated with solvent vapor*, *International Journal of Biological Macromolecules*, **38**, 140-144 (2006)
- [1.100] K. Ohkawa, D. Cha, H. Kim, A. Nishida, H. Yamamoto, *Electrospinning of Chitosan*, *Macromolecular Rapid Communication*, **25**, 1600-1605 (2004)
- [1.101] C.W. Kim, M.W. Frey, M. Marquez, Y.L. Joo, *Preparation of submicron-scale electrospun cellulose fibres via direct dissolution*, *Journal of Polymer Science part B: Polymer Physics*, **43**, 1673-1683 (2005)
- [1.102] V.K. Daga, M.E. Helgeson, E. Matthew, N.J. Wagner, *Electrospinning of neat and laponite-filled aqueous poly(ethylene oxide) solutions*, *Journal of Polymer Science part B: Polymer Physics*, **44**, 1608-1617 (2006)
- [1.103] S.L. Shenoy, W.D. Bates, G. Wnek, *Correlation between electrospinnability and physical gelatin*, *Polymer*, **46**, 8990-9004 (2005)
- [1.104] Q. Yang, Z. Li, Y. Hong, Y. Zhao, S. Qiu, C. Wang, Y. Wei, *Influence of solvents on the formation of ultrathin uniform poly(vinyl pyrrolidone) nanofibres with electrospinning*, *Journal of Polymer Science part B: Polymer Physics*, **42**, 3721-3726 (2004)

- [1.105] Z.M. Huang, C.L. He, A. Yang, Y. Zhang, X.J. Han, J. Yin, Q. Wu, *Encapsulating drugs in biodegradable ultrafine fibres through co-axial electrospinning*, Journal of Biomedical Materials Research part A, **77**, 169-179 (2006)
- [1.106] J. McCann, M. Marquez, Y. Xia, *Highly porous fibres by electrospinning into a cryogenic liquid*, Journal of the American Chemical Society, **128**, 1436-1437 (2006)
- [1.107] R.V.N. Krishnappa, K. Desai, C. Sung, *Morphological study of electrospun polycarbonates as a function of the solvent and processing voltage*, Journal of Materials Science, **38**, 2357-2365 (2003)
- [1.108] S.C. Baker, N. Atkin, P.A. Gunning, N. Granville, K. Wilson, D. Wilson, J. Southgate, *characterization of electrospun polystyrene scaffolds for three-dimensional in vitro biological studies*, Biomaterials, **27**, 3136-3146 (2006)
- [1.109] H.L. Schreuder-Gibson, P. Gibson, K. Senecal, M. Sennett, J. Walker, W. Yeomans, D. Ziegler, P.P. Tsai, *Protective textile materials based on electrospun nanofibres*, Journal of Advanced Materials, **34**, 44-55 (2002)
- [1.110] K.H. Hong, T.J. Kang, *Hydraulic permeabilities of PET and nylon 6 electrospun fibre webs*, Journal of Applied Polymer Science, **100**, 167-177 (2006)
- [1.111] S. Kidoaki, I.K. Kwon, T. Matsuda, *Structural features and mechanical properties of in situ-bonded meshes of segmented polyurethane electrospun from mixed solvents*, Journal of Biomedical Materials Research part B, **76**, 219-229 (2006)
- [1.112] R. Ramaseshan, S. Sundarrajan, Y. Liu, R.S. Barhate, N.L. Lala, S. Ramakrishna, *Functionalized polymer nanofibre membranes for protection from chemical warfare stimulants*, Nanotechnology, **17**, 2947-2953 (2006)
- [1.113] F. Jian, N.H. Tao, L. Tong, W.X. Gai, *Applications of electrospun nanofibres*, Chinese Science Bulletin, **53**, 2265-2286 (2008)
- [1.114] C. Burger, B.S. Hsiao, B. Chu, *Nanofibrous materials and their applications*, Annual Review Materials Research, **36**, 333-368 (2006)
- [1.115] A. Greiner, J.H. Wendorff, *Electrospinning: a fascinating method for the preparation of ultrathin fibres*, Angewandte Chemie International Edition, **46**, 5670-5703 (2007)
- [1.116] Z.M. Huang, Y.Z. Zhang, M. Kotaki, S. Ramakrishna, *A review on polymer nanofibres by electrospinning and their applications in nanocomposites*, Composites Science and Technology, **63**, 2223-2253 (2003)
- [1.117] S. Agarwal, J.H. Wendorff, A. Greiner, *Use of electrospinning technique for biomedical applications*, Polymer, **49**, 5603-5621 (2008)

- [1.118] S. Ramakrishna, K. Fujihara, W. Teo, T. Yong, Z. Ma, R. Ramaseshan, *Electrospun nanofibres: solving global issues*, *Materials today*, **9**, 40-50 (2006)
- [1.119] C.P. Barnes, S.A. Sell, E.D. Boland, D.G. Simpson, G.L. Bowlin, *Nanofibre technology: designing the next generation of tissue engineering scaffolds*, *Advanced Drug Delivery Reviews*, **59**, 1413-1433 (2007)
- [1.120] J. Lannutti, D. Reneker, T. Ma, D. Tomasko, D. Farson, *Electrospinning for tissue engineering scaffolds*, *Materials Science and Engineering C*, **27**, 504-509 (2007)
- [1.121] T.J. Sill, H.A. Recum, *Electrospinning: Applications in drug delivery and tissue engineering*, *Biomaterials*, **29**, 1989-2006 (2008)
- [1.122] I.S. Chronakis, *Novel nanocomposites and nanoceramics based on polymer nanofibres using electrospinning process-a review*, *Journal of Materials Processing Technology*, **167**, 283-293 (2005)
- [1.123] W. Sigmund, J. Yuh, H. Park, V. Maneeratana, G. Pyrgiotakis, A. Daga, J. Taylor, J.C. Nino, *Processing and structure relationships in electrospinning of ceramic fibre systems*, *Journal of American Ceramic Society*, **89**, 395-407 (2006)
- [1.124] D.J. Smith, D.H. Reneker, A.T. McManus, A.L.S. Gibson, C. Mello, M.S. Sennett, *Electrospun fibres and an apparatus therefore*, US Patent, **6753454** (2004)
- [1.125] Elmarco company, www.elmarco.com, accessed 18/02/2009
- [1.126] P. Gupta, G.L. Wilkes, *Some investigations on the fibre formation by utilizing a side-by-side bicomponent electrospinning approach*, *Polymer*, **44**, 6353-6361 (2003)
- [1.127] B. Ding, E. Kimura, T. Sato, S. Fujita, S. Shiratori, *Fabrication of blend biodegradable nanofibrous nonwoven mats via multi-jet electrospinning*, *Polymer*, **45**, 1895-1902 (2004)
- [1.128] M. Ignatova, N. Manolova, N. Markova, I. Rashkov, *Electrospun non-woven nanofibrous hybrid mats based on chitosan and PLA for wound-dressing applications*, *Macromolecular Bioscience*, **9**, 102-111 (2009)
- [1.129] S. Kidoaki, I.K. Kwon, T. Matsuda, *Mesoscopic spatial designs of nano- and microfibre meshes for tissue-engineering matrix and scaffold based on newly devised multilayering and mixing electrospinning techniques*, *Biomaterials*, **26**, 37-46 (2005)
- [1.130] W.M. Frey, L. Li, *Electrospinning and porosity measurements of nylon-6/poly(ethylene oxide) blended nonwovens*, *Journal of Engineered Fibres and Fabrics*, **2**, 31-37 (2007)
- [1.131] Y. Hong, K. Fujimoto, R. Hashizume, J. Guan, J.J. Stankus, K. Tobita, W.R. Wagner, *Generating elastic biodegradable polyurethane /poly (lactide-co-glycolide)*

- fibrous sheets with controlled antibiotic release via two stream electrospinning*, Biomacromolecules, **9**, 1200-1207 (2008)
- [1.132] L. Liu, Z.M. Huang, C.L. He, X.J. Han, *Mechanical performance of laminated composites incorporated with nanofibrous membranes*, Materials Science and Engineering A, **435–436**, 309-317 (2006)
- [1.133] C. Shin, G.G. Chase, *Water-in-oil coalescence in micro-nanofibre composite filters*, AIChE Journal, **50**, 343-350 (2004)
- [1.134] A. Kumar, C. Asemota, J. Padilla, M. Invernale, T.F. Otero, G.A. Sotzing, *Photopatterned conjugated polymer electrochromic nanofibres on paper*, 4th World Congress on Biomimetics, Artificial Muscles and Nano-Bio Conference, **127**, 012014-1 – 012014-6 (2008)
- [1.135] Hollingsworth-Vose Company, www.hollingsworth-vose.com, accessed 19/02/2009
- [1.136] H.T. Grafe, K.M. Graham, *Nanofibre webs from electrospinning*, presented at the Nonwovens in Filtration - Fifth International Conference, Stuttgart, Germany (2003)
- [1.137] Finetex Technology CO. Ltd., www.finetextech.com, accessed 19/02/2009
- [1.138] M.G. Hajra, K. Mehta, G.G. Chase, *Effects of humidity, temperature, and nanofibres on drop coalescence in glass fibre media*, Separation and Purification Technology, **30**, 79-88 (2003)
- [1.139] X. Wang, X. Chen, K. Yoon, D. Fang, B.S. Hsiao, B. Chu, *High flux filtration medium based on nanofibrous substrate with hydrophilic nanocomposite coating*, Environmental Science and Technology, **39**, 7684-7691 (2005)
- [1.140] S. Igarashi, J. Tanaka, H. Kobayashi, *Micro-patterned nanofibrous biomaterials*, Journal of Nanoscience and Nanotechnology, **7**, 814-820 (2007)
- [1.141] G. Kim, W. Kim, *Highly porous 3D nanofibre scaffold using an electrospinning technique*, Journal of Biomedical Materials Research Part B: Applied Biomaterials, **81B**, 104-113 (2007)
- [1.142] Y. Yokoyama, S. Hattori, C. Yoshikawa, Y. Yasuda, H. Koyama, T. Takato, H. Kobayashi, *Novel wet electrospinning system for fabrication of spongiform nanofibre 3-dimensional fabric*, Materials Letters, Article in press (2009)
- [1.143] D. Zhang, J. Chang, *Electrospinning of three-dimensional nanofibrous tubes with controllable architectures*, Nano Letters, **8**, 3283-3287 (2008)
- [1.144] M.S. Khil, S.R. Bhattarai, H.Y. Kim, S.Z. Kim, K. Hyung Lee, *Novel fabricated matrix via electrospinning for tissue engineering*, Journal of Biomedical Materials Research Part B: Applied Biomaterials, **72B**, 117-124 (2005)

- [1.145] W. Teo, R. Gopal, R. Ramase, K. Fujihar, S. Ramakrishna, *A dynamic liquid support system for continuous electrospun yarn fabrication*, *Polymer*, **48**, 3400-3405 (2007)
- [1.146] V.B. Gupta, V.K. Kothari, *Manufactured fibre technology*, Chapman and Hall, London (1997)
- [1.147] H. Hou, Z. Jun, A. Reuning, A. Schaper, J.H. Wendorff, A. Greiner, *Poly(p-xylylene) nanotubes by coating and removal of ultrathin polymer template fibres*, *Macromolecules*, **35**, 2429-2431 (2002)
- [1.148] R.A. Crauso, J.H. Schattka, A. Greiner, *Titanium dioxide tubes from sol-gel coating of electrospun polymer fibres*, *Advanced materials*, **13**, 1577-1579 (2001)
- [1.149] G.D. Fu, J.Y. Lei, C. Yao, X.S. Li, F. Yao, S.Z. Nie, E.T. Kang, K.G. Neoh, *Core-sheath nanofibres from combined atom transfer radical polymerization and electrospinning*, *Macromolecules*, **41**, 6854-6858 (2008)
- [1.150] D. Li, Y. Xia, *Direct fabrication of composite and ceramic hollow nanofibres by electrospinning*, *Nano Letters*, **4**, 933-938 (2004)
- [1.151] J.T. McCann, D. Li, Y. Xia, *Electrospinning of nanofibres with core-sheath, hollow, or porous structures*, *Journal of Materials Chemistry*, **15**, 735-738 (2005)
- [1.152] M. Ma, V. Krikorian, J.H. Yu, E.L. Thomas, G.C. Rutledge, *Electrospun polymer nanofibres with internal periodic structure obtained by microphase separation of cylindrically confined block copolymers*, *Nano Letters*, **6**, 2969-2972 (2006)
- [1.153] S. Zhan, D. Chen, X. Jiao, *Co-electrospun SiO₂ hollow nanostructured fibres with hierarchical walls*, *Journal of Colloid and Interface Science*, **318**, 331-336 (2008)
- [1.154] Y. Xin, Z. Huang, W. Li, Z. Jiang, Y. Tong, C. Wang, *Core-sheath functional polymer nanofibres prepared by co-electrospinning*, *European Polymer Journal*, **44**, 1040-1045 (2008)
- [1.155] J.E. Diaz, A.F. Nieves, A. Barrero, M. Marquez, I.G. Loscertales, *Fabrication of structured micro and nanofibres by coaxial electrospinning*, 4th World Congress on Biomimetics Artificial Muscle and NanoBio Conference, **127**, 012008-1 – 012008-8 (2008)
- [1.156] E. Zussman, A.L. Yarin, A.V. Bazilevsky, R. Avrahami, M. Feldman, *Electrospun polyaniline/poly(methyl methacrylate)-derived turbostratic carbon micro-/nanotubes*, *Advanced Materials*, **18**, 348-353 (2006)
- [1.157] J. Di, H. Chen, X. Wang, Y. Zhao, L. Jiang, J. Yu, R. Xu, *Fabrication of Zeolite hollow fibres by coaxial electrospinning*, *Chemistry of Materials*, **20**, 3543-3545 (2008)

- [1.158] L. Zhang, Y.L. Hsieh, *Ultra-fine cellulose acetate/poly (ethylene oxide) bicomponent fibres*, Carbohydrate Polymers, **71**, 196-207 (2008)
- [1.159] H. Dong, W.E. Jones, *Preparation of submicron polypyrrole/poly(methyl methacrylate) coaxial fibres and conversion to polypyrrole tubes and carbon tubes*, Langmuir, **22**, 11384-11387 (2006)
- [1.160] H.S. Gibson, P. Gibson, P. Tsai, P. Gupta, G. Wilkes, *Cooperative charging effects of fibres from electrospinning of electrically dissimilar polymers*, INJ Winter, **13**, 39-45 (2004)
- [1.161] T. Lin, H. Wang, X. Wang, *Self-crimping bicomponent nanofibres electrospun from polyacrylonitrile and elastomeric polyurethane*, Advanced materials, **17**, 2699-2703 (2005)
- [1.162] D. Li, Y. Xia, *Electrospinning of nanofibres: reinventing the wheel*, Advanced Materials, **16**, 1151-1170 (2004)
- [1.163] S. Zhan, D. Chen, X. Jiao, C. Tao, *Long TiO₂ hollow fibres with mesoporous walls: sol gel combined electrospun fabrication and photocatalytic properties*, Journal of Physical Chemistry B, **110**, 11199-11204 (2006)
- [1.164] S. Zhan, D. Chen, X. Jiao, S. Liu, *Facile fabrication of long α -Fe₂O₃, α -Fe and γ -Fe₂O₃ hollow fibres using sol-gel combined co-electrospinning technology*, Journal of Colloid and Interface Science, **308**, 265-270 (2007)
- [1.165] Y. Gu, F. Jian, *Hollow LiNi_{0.8}Co_{0.1}Mn_{0.1}O₂-MgO coaxial fibres: sol gel method combined with co-electrospun preparation and electrochemical properties*, Journal of Physical Chemistry C, **112**, 20176-20180 (2008)
- [1.166] Y. Zhang, Q. Li, H. Li, Y. Cheng, J. Zhang, X. Cao, *Sintering-resistant hollow fibres of LaMgAl₁₁O₁₉ prepared by electrospinning*, Journal of Crystal Growth, **310**, 3884-3889 (2008)
- [1.167] A.M. Rahmathullah, E.J. Robinette, H. Chen, Y.A. Elabd, G. R. Palmese, *Plasma assisted synthesis of hollow nanofibres using electrospun sacrificial templates*, Nuclear Instruments and Methods in Physics Research B, **265**, 23-30 (2007)
- [1.168] L. Gea, C. Pan, H. Chena, X. Wang, C. Wang, Z. Gua, *The fabrication of hollow multilayered polyelectrolyte fibrous mats and its morphology study*, Colloids and Surfaces A: Physicochemistry Engineering Aspects, **293**, 272-277 (2007)
- [1.169] T. Zhang, L. Ge, X. Wang, Z. Gu, *Hollow TiO₂ containing multilayer nanofibres with enhanced photocatalytic activity*, Polymer, **49**, 2898-2902 (2008)

- [1.170] J.Y. Li, Y. Tan, F.M. Xu, Y. Sun, X.Q. Cao, Y.F. Zhang, *Hollow fibres of yttria-stabilized zirconia (8YSZ) prepared by calcination of electrospun composite fibres*, *Materials Letters*, **62**, 2396-2399 (2008)
- [1.171] C. Qizheng, D. Xiangting, W Jinxian, L. Mei, *Direct fabrication of cerium oxide hollow nanofibres by electrospinning*, *Journal of Rare Earth*, **26**, 664-669 (2008)
- [1.172] M. Bognitzki, T. Frese, M. Steinhart, A. Greiner, J.H. Wendorff, A. Schaper, M. Hellwig, *Preparation of fibres with nanoscaled morphologies: electrospinning of polymer blends*, *Polymer Engineering and Science*, **41**, 982 – 989 (2004)
- [1.173] A. Gupta, C.D. Saquing, M. Afshari, A.E. Tonelli, S.A. Khan, R. Kotek, *Porous nylon-6 fibres via a novel salt-induced electrospinning method*, *Macromolecules*, **42**, 709-715 (2009)
- [1.174] J.T. McCann, M. Marquez, Y. Xia, *Highly porous fibres by electrospinning into a cryogenic liquid*, *Journal of American Chemical Society*, **128**, 1436-1437 (2006)
- [1.175] C.L. Casper, J.S. Stephens, N.G. Tassi, D.B. Chase, J.F. Rabolt, *Controlling surface morphology of electrospun polystyrene fibres: effect of humidity and molecular weight in the electrospinning process*, *Macromolecules*, **37**, 573-578 (2004)
- [1.176] P. Dayal, J. Liu, S. Kumar, T. Kyu, *Experimental and theoretical investigations of porous structure formation in electrospun fibres*, *Macromolecules*, **40**, 7689-7694 (2007)
- [1.177] S. Megelski, J.S. Stephans, C.D. Bruce, J.F. Rabolt, *Micro-nanostructured surface morphology on electrospun polymer fibres*, *Macromolecules*, **35**, 8456-8466 (2002)
- [1.178] D.H. Reneker, A.L. Yarin, *Electrospinning jets and polymer nanofibres*, *Polymer*, **49**, 2387-2425 (2008)
- [1.179] T. Han, D.H. Reneker, A.L. Yarin, *Buckling of jets in electrospinning*, *Polymer*, **48**, 6064-6076 (2007)
- [1.180] M.K. Shin, S.I. Kim, S.J. Kim, *Controlled assembly of polymer nanofibres: from helical springs to fully extended*, *Applied Physics Letters*, **88**, 223109-1 - 223109-3 (2006)
- [1.181] J. Yu, Y. Qiu, X. Zha, M. Yu, J. Yu, J. Rafique, J. Yin, *Production of aligned helical polymer nanofibres by electrospinning*, *European Polymer Journal*, **44**, 2838-2844 (2008)
- [1.182] R. Kessick, G. Tepper, *Microscale polymeric helical structures produced by electrospinning*, *Applied Physics Letters*, **84**, 4807- 4809 (2004)

- [1.183] Y. Xin, Z.H. Huang, E.Y. Yan, W. Zhang, Q. Zhao, *Controlling poly p-phenylene vinylen/polyvinyl pyrrolidone composite nanofibres in different morphologies by electrospinning*, Applied Physics Letters, **89**, 053101-1 – 053101-3 (2006)
- [1.184] B. Wang, B. Li, J. Xiong, C.Y. Li, *Hierarchically ordered polymer nanofibres via electrospinning and controlled polymer crystallization*, Macromolecules, **41**, 9516-9521 (2008)
- [1.185] C. Hellmann , J. Belardi, R. Dersch, A. Greiner, J.H. Wendorff, S. Bahnmueller, *High precision deposition electrospinning of nanofibres and nanofibre nonwovens*, Polymer, Article in press (2009)

CHAPTER 2: INVESTIGATING THE FABRICATION OF NANOFIBRES BY ELECTROSPINNING

2.1 Introduction

Fibre diameters in the nanorange have great advantages in volume to space and strength to weight ratios. Although conventional textile fibres have a fibre diameter ranging from 1000 to 50000 nm [1], electrospinning is one of those technologies that enable the production of continuous nanofibres of the order of 100 nm to even 5 nm from polymer solutions or melts in high electric fields [2-7].

Although nanofibres of more than 100 different types of polymers have been successfully produced by electrospinning [8], a systematic study of electrospinning parameters for optimizing nylon 6 is yet to be achieved. It has been found that the morphology, such as the fibre diameter and uniformity of electrospun polymer fibres are dependent on polymer solution properties, electrospinning processing parameters and ambient conditions [9, 10].

The polymer jet trajectory has a very complicated three dimensional whipping and bending instability form [11]. As a result, most nanofibres obtained so far are in a nonwoven form, which can be useful for many applications such as filtration [12-14], tissue scaffolds [15], implant coating films [16], and wound dressing [17]. Design of polymeric nanofibres to meet specific needs for useful applications requires a thorough knowledge of the electrospinning parameters and their effect on nanofibre diameters and morphologies.

In order to optimize and predict the morphology of the electrospun nylon 6 nanofibres, design of the experiments has been employed in the present chapter. Consequently, the effects of the solution properties and processing parameters on the morphology of electrospun nylon 6 nanofibres have been systematically studied to produce a wide range of fibre diameters with a uniform fibre diameters distribution [10].

2.2 Experimental work

2.2.1 Materials and electrospinning process parameters

Nylon 6 has a good resistance to many commercial solvents and can be only dissolved in a few solvents such as formic acid [18]. It has been also found that water molecules in the atmosphere did not act as a solvent for nylon 6 during electrospinning [19].

Nylon 6 and formic acid were purchased from Sigma–Aldrich (Gillingham, United Kingdom). The polymer solution was fed from a 5 mL capacity syringe (Fisher Co.,

Leicestershire, United Kingdom) to a vertically orientated (25 gauge) blunt-ended metal needle 'spinneret' via Teflon tubing. The volume feed rate was digitally controlled by a positive displacement microprocessor syringe pump (M22 PHD 2000, Harvard Apparatus, Edenbridge Kent, United Kingdom). The needle was connected to one electrode of a high voltage direct-current power supply (MK35P2.0-22, Glassman, New Jersey, USA).

Various polymer solution concentrations ranging from 15 to 25 wt. % were prepared by the dissolution of the polymer in formic acid. Nanofibres were obtained with an earthed collection system, which consisted of a copper collector plate measuring 150 mm × 150 mm. Typical operating regimes were flow rates of 0.2 mL/h, applied voltages of 12, 15 and 18 kV, and a spinning working distance of 5, 8 and 11 cm. The experiments were conducted under ambient condition at room temperature and 25 % RH humidity.

Figure 2.1, shows the designed system used in the experiments. This system was built to house the electrospinning apparatus in order to control the safe release of solvent and prevent turbulent air from disturbing the collection of nanofibres.



Figure 2.1, A photograph of the experimental electrospinning set-up used in the experiments.

2.2.2 Physical properties of the polymer solutions

Polymer solutions viscosity was determined by a rheometer instrument (AR-1000 Rheometer, TA instruments, UK). The measurements were conducted in a continuous ramp mode at room temperature 25° C using cone and plate geometry. Each sample was placed between a fix Peltier plate and a rotating cone (diameter of 40 mm, vertex angle of 2°) attached to a driving motor spindle. Changes of shear stress and thus viscosity versus changes in shear rate were measured. A computer interfaced to the rheometer instrument was used to record the resulting shear stress and shear rate data. Viscosity of the polymer solutions was reported from 2.842 to 4.856 Pa.sec.

Surface tension for each polymer solution concentration was measured by the torsion balance instrument using surface and interfacial tension measurement method. A 40 mm circumference platinum ring supplied by (Torsion balance, UK) has been used for these measurements. The surface tension of the polymer solution concentrations was reported from 44.8 to 53.0 mN/m.

Electrical conductivity of the polymer solutions was measured by using the four probe method. The charge induction and charge retention characteristics are various according to the polymer solution concentration. Therefore, when an identical voltage was applied to the polymer solution, electrical responses were different. The electric conductivity of the polymer solution (k, mS/m) was calculated from the following equation [29]:

$$k = \frac{1}{r} = \frac{L}{RS} \quad (2.1)$$

Where r is the specific resistance of the solution (m Ohm. m), R is the electric resistance of the solution (m Ohm), L is the distance between the electrodes (m) and S is the surface area of the electrode (m²). The electric conductivity of the polymer solutions was reported from 445 to 116 mS/m.

2.2.3 Characterization

2.2.3.1 Scanning electron microscopy (SEM)

All scanning electron microscopes work basically at the same principle. The SEM consists of a gun section, a column section and a chamber section as shown in figure 2.2.

The gun section is under a vacuum that ranges from 1 x 10⁻³ Pascal to 1 x 10⁻⁹ Pascal [20]. The column section can be under a full vacuum of the gun section or under a partial pressure as the case of environmental SEM.

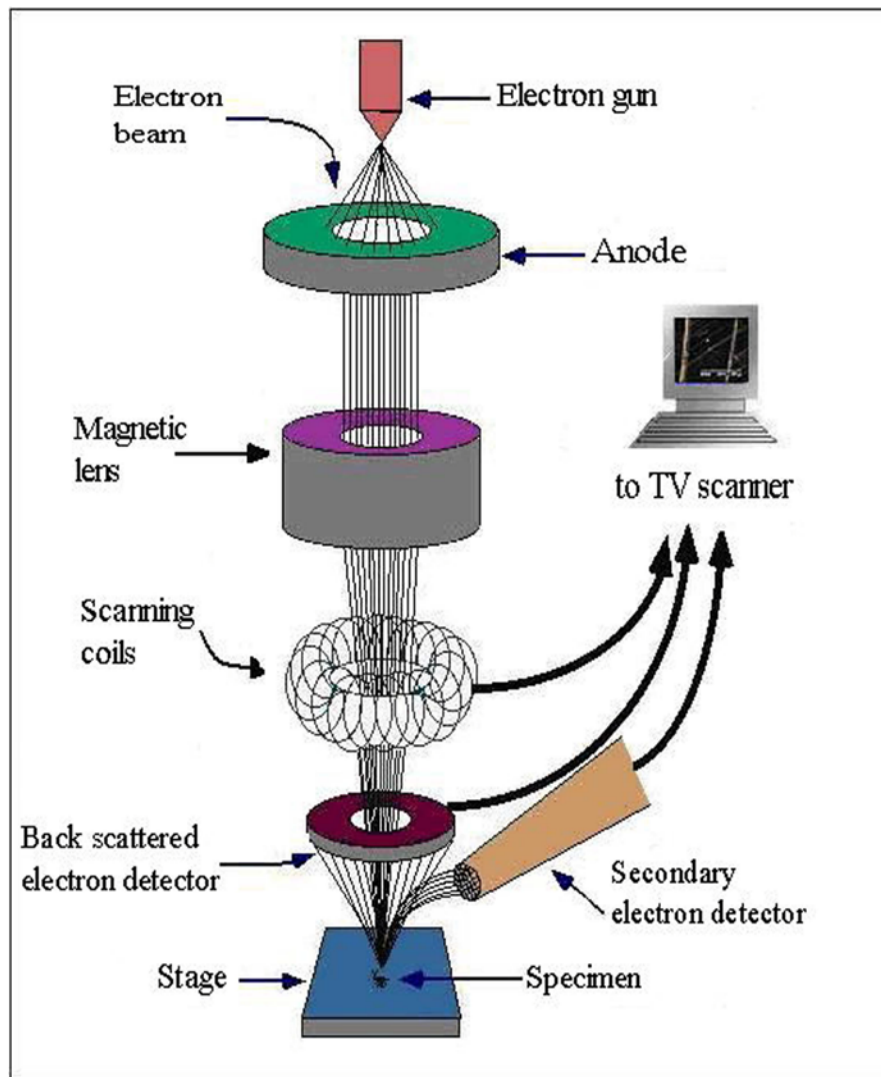


Figure 2.2, Schematic diagram of the SEM.

There are three types of electron guns: Tungsten, LaB6 and field emission, all of which produce electrons for imaging of the specimen, therefore they have different characteristics and imaging capabilities. Among the three gun types; field emission gun produces the highest brightness as compared to the tungsten and LaB6 guns [20].

The gun emits a large amount of electrons that are gathered in the gun chamber and passed into the column where they are focused into a tight beam, in the order of 1 nanometer. Then these electrons impinge on the surface of the sample where several processes occur simultaneously. Electrons from the beam enter the sample and bounce back to the surface to be sent to the monitor. These electrons are called primary or backscattered electrons, and they usually carry information about the sample such as atomic number contrast. Another electrons signal that occurs is the secondary electrons, which is the most frequently collected. Secondary electrons come from inelastic scattering inside the sample with the sample own electrons to give us the sample surface

picture. This scattering causes liberating of the sample electrons into the chamber where they are withdrawn into the secondary electron detector. These electrons are then sent to the monitor where they are placed back in order to be viewed.

Important notes must be mentioned here, under normal working conditions, the microscope scans the electron beam in a square pattern on the sample. With this scanning, there must be synchronization between the beam and the monitor for giving us a true image for the sample. In addition, X-ray signals are generated during imaging of any sample in the electron microscope. These x-rays are from the inelastic scattering collisions that generate the image and are characteristic of the element from which they came and can be analyzed based on their wavelength or their energy.

2.2.3.2 Samples preparation

Samples of random nanofibres were collected on aluminium stubs. These samples were sputter coated with gold palladium for 45 sec at 18 mA using a sputter coater (Polaron Sc7620, Quorum technologies Ltd, UK). Nanofibre samples were examined by SEM (Hitachi S-530, Berkshire, UK) at an accelerating voltage of 10 kV. Micrographs were taken at three random areas of each sample between 20,000 and 40,000 magnifications. Photographs were processed using imaging software (Corel paint shop pro X version 10.00, UK). For measuring the average diameter of the fibres viewed on a photograph, a transect line was drawn from the bottom right to the top left of the SEM image and fibre diameters were measured at the point the line transected, perpendicular to the fibre length. These results were used to compile fibre diameters distribution profiles.

2.3 Results and discussion [10]

2.3.1 Physical properties of the polymer solutions

The viscosity and surface tension of the polymer solutions were based on the polymer/solvent system used. Table 2.1 shows viscosity and surface tension of nylon 6 dissolved in formic acid at different concentrations; they were 2.842 - 4.856 Pa.s and 44.8 - 53.0 mN/m, respectively. These values increased with increasing polymer solution concentration. Specifically, the viscosity increased from 3.358 to 4.856 Pa.s when a polymer solution concentration increased from 20 to 25 wt. %.

The electric conductivity of polymer solutions was 116 - 445 m Siemens/m. The electric conductivity decreased with increasing polymer solution concentration due to the high dielectric constant (58.5 at 15° C) and dipole moment (1.41 Debye) of formic acid [21].

Table 2.1 Physical properties of nylon 6/ formic acid at different concentrations.

Nylon 6 / formic acid concentration (wt.%)	Viscosity [Pa.s]	Surface tension [mN/m]	Electric conductivity [mS/m]
15	2.842	44.8	445
20	3.358	48.5	294
25	4.856	53.0	116
Formic acid (96 %)	0.00178	37.67	9000

2.3.2 Morphology of electrospun nonwoven fibre mats

Figures 2.3 - 2.5, show a series of SEM images of the micro morphology of the

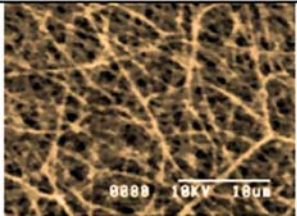
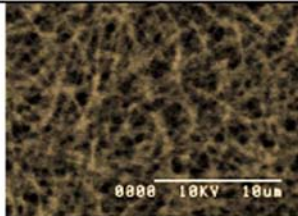
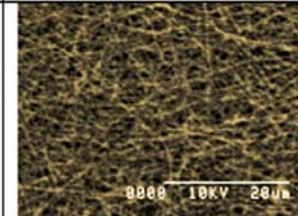
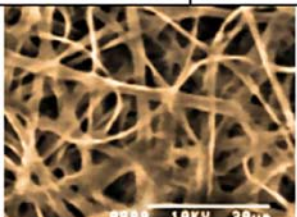
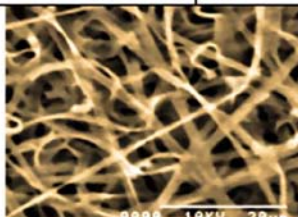
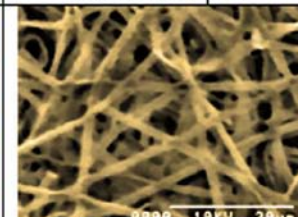
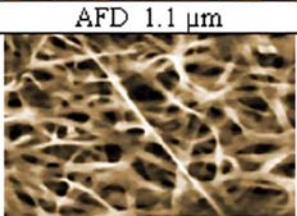
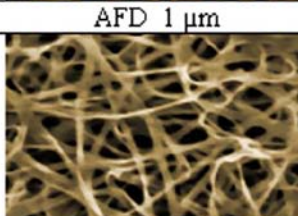
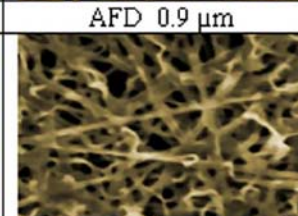
The morphology of fibers with a spinning distance of 5 cm			
Concentration (wt %)	Applied voltage (KV)		
	12	15	18
15	 AFD 0.5 μm	 AFD 0.4 μm	 AFD 0.35 μm
20	 AFD 1.1 μm	 AFD 1 μm	 AFD 0.9 μm
25	 AFD 1.3 μm	 AFD 1.2 μm	 AFD 1 μm

Figure 2.3, Average fibre diameter (AFD) at electric fields of 12, 15 and 18 KV and polymer solution concentrations between 15 and 25 wt. % with a constant spinning distance of 5 cm.

nanofibres obtained from the electrospinning of nylon 6 solutions with three different concentrations. Different fibre morphologies occur at different concentrations and have a significant effect on the surface area to the volume ratio of the fibre. At a 15 % concentration, fibres less than 200 nm in diameter are formed, with some spindle-like beads ‘drops of polymer over the nonwoven mat’ being formed at lower voltage. These beads disappear as the fibre diameter is increased with increasing polymer concentration.

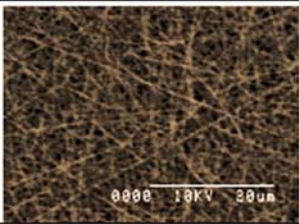
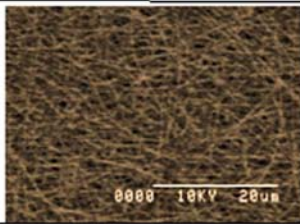
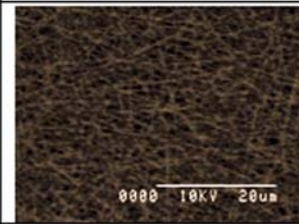
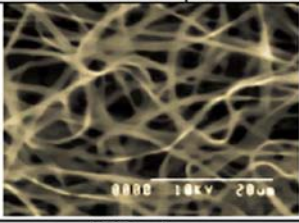
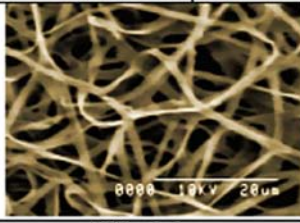
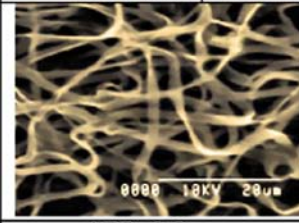
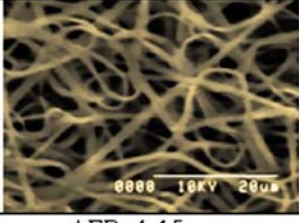
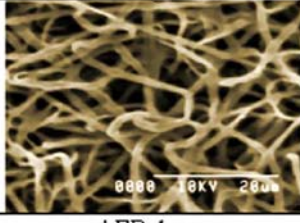
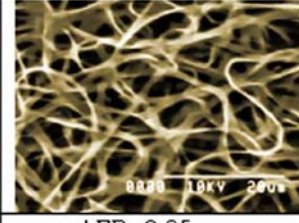
The morphology of fibers with a spinning distance of 8 cm			
Concentration(wt %)	Applied voltage(KV)		
	12	15	18
15			
	AFD 0.4 μm	AFD 0.3 μm	AFD 0.25 μm
20			
	AFD 1 μm	AFD 0.9 μm	AFD 0.8 μm
25			
	AFD 1.15 μm	AFD 1 μm	AFD 0.95 μm

Figure 2.4, Average fibre diameter (AFD) at electric fields of 12, 15 and 18 KV and polymer solution concentrations between 15 and 25 wt. % with a constant spinning distance of 8 cm.

It has been found that the average fibre diameter has a similar tendency to viscosity and surface tension [10]. In other words, the average fibre diameter becomes gradually broader with increasing concentration, which is in consistency with the results obtained by Ryu et. al. [22]. The average fibre diameter has increased from 200 to 1300 nm for 15 - 25 wt. % nylon 6 solutions. Electrospinning using high concentrated nylon 6 solutions produces smooth and curled nanofibres with thicker fibre diameters. A nylon 6

concentration of 25 wt. % or more results in ribbon like nanofibres (see figure 2.3). The formation of ribbon like nanofibres is due to rapid solvent vaporization from the surface of the jet and has previously been described [23]. It has been also observed that as the wet nanofibres are no longer strained by the electric field when they are laid on the collector, they undergo a solidification process as a result of the surface tension and the relaxation process controlled by the viscoelastic property of the wet nanofibres.

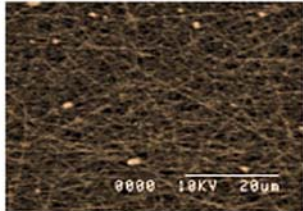
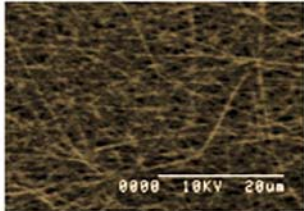
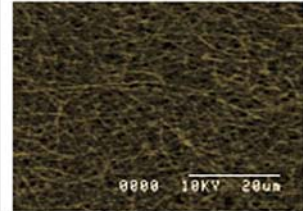
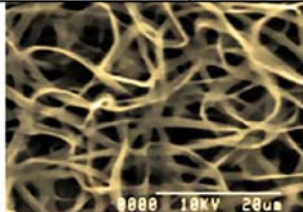
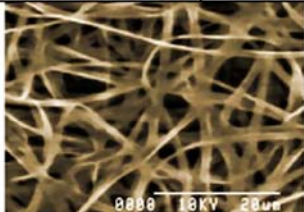
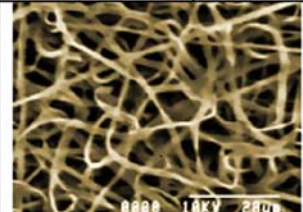
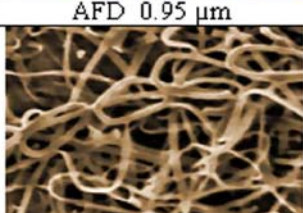
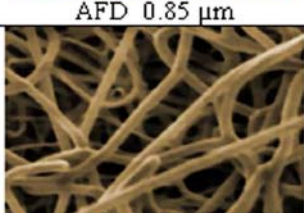
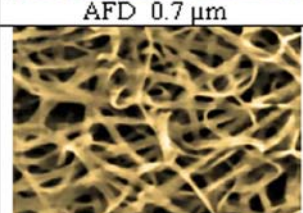
The morphology of fibers with a spinning distance of 11 cm			
Concentration(wt %)	Applied voltage(KV)		
	12	15	18
15			
	AFD 0.3 μm	AFD 0.25 μm	AFD 0.2 μm
20			
	AFD 0.95 μm	AFD 0.85 μm	AFD 0.7 μm
25			
	AFD 1.1 μm	AFD 1 μm	AFD 0.95 μm

Figure 2.5, Average fibre diameter (AFD) at electric fields of 12, 15 and 18 KV and polymer solution concentrations between 15 and 25 wt. % with a constant spinning distance of 11 cm.

Briefly, the morphology of electrospun nylon 6 nanofibre mats changes from curled at high concentration, to one containing beads at low concentration.

2.3.3 Effect of the polymer concentration on the fibre morphology

As the electrospinning results shown in figure 2.6, the diameter of the electrospun fibres dramatically decreases with decreasing polymer concentration. When the spinning distance is small and the polymer solution has a low concentration (15 wt. %), the solution reaches the collection plate before full evaporation of the solvent. This explains

the formation of droplets and beads at the low polymer concentration and short spinning distance. Fewer beads were observed in electrospun fibres at higher concentration. The changing of the fibre morphology can probably be attributed to a competition between the surface tension and viscosity.

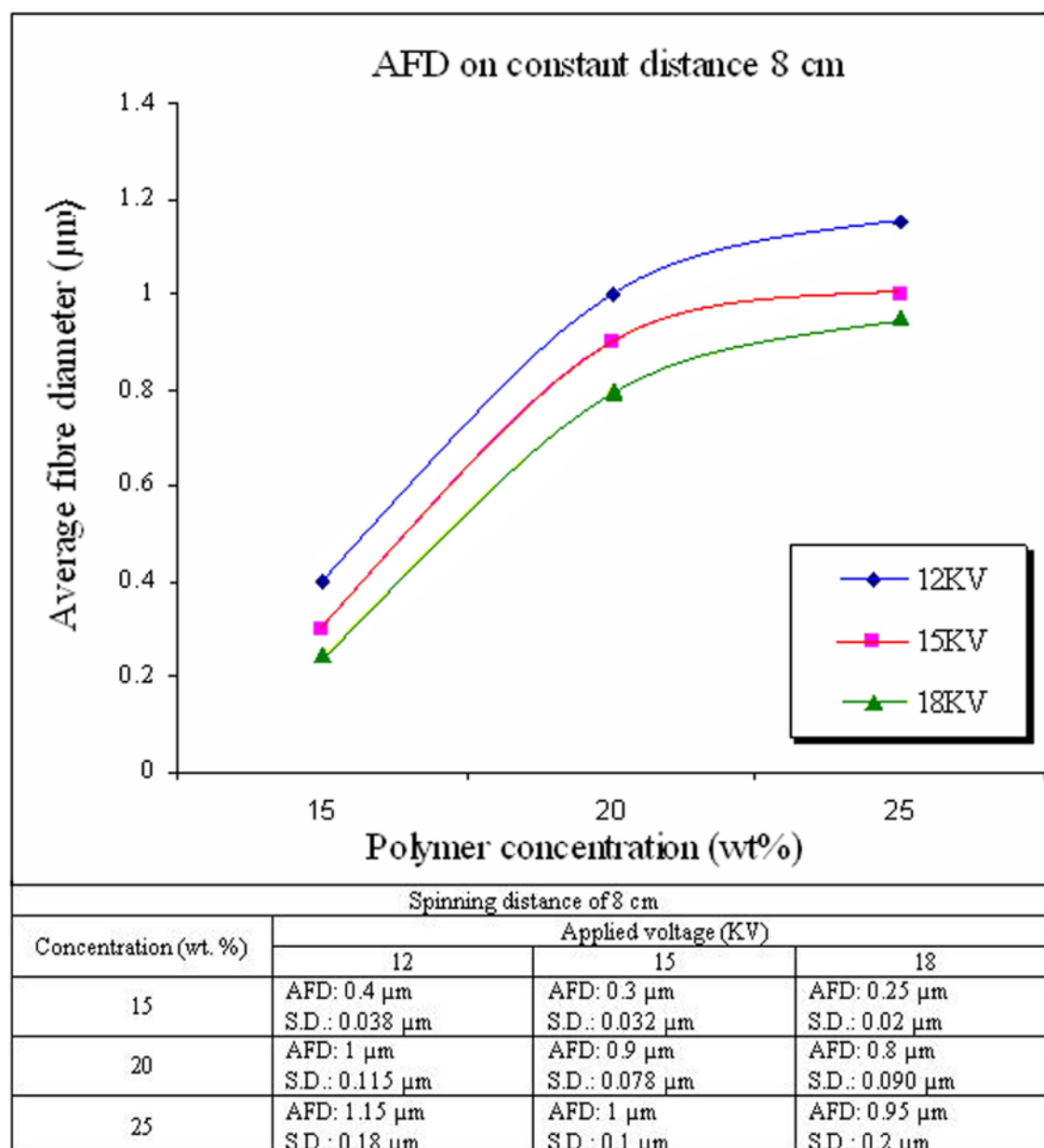


Figure 2.6, Relationship between the average fibre diameter (AFD) and polymer solution concentration at three electric fields with a constant spinning distance of 8 cm.

Reneker et. al. systematically investigated the influence of solution properties of polyethylene oxide (PEO) on the density of beads contained in the electrospun fibres [24]. It has been found that the viscosity and surface tension are the most important factors that affect the morphology of the resultant fibres [24, 25]. Vancso et. al.

indicated that viscoelastic forces prevented the formation of beads and allowed the formation of smooth fibres [26].

2.3.4 Effect of the voltage and spinning distance on the fibre morphology

We optimized the process parameters by studying the influence of the electric field and spinning distance on fibres morphology. Figure 2.7, shows the relationship between the average fibre diameter and applied voltage with a constant concentration of 20 wt. %.

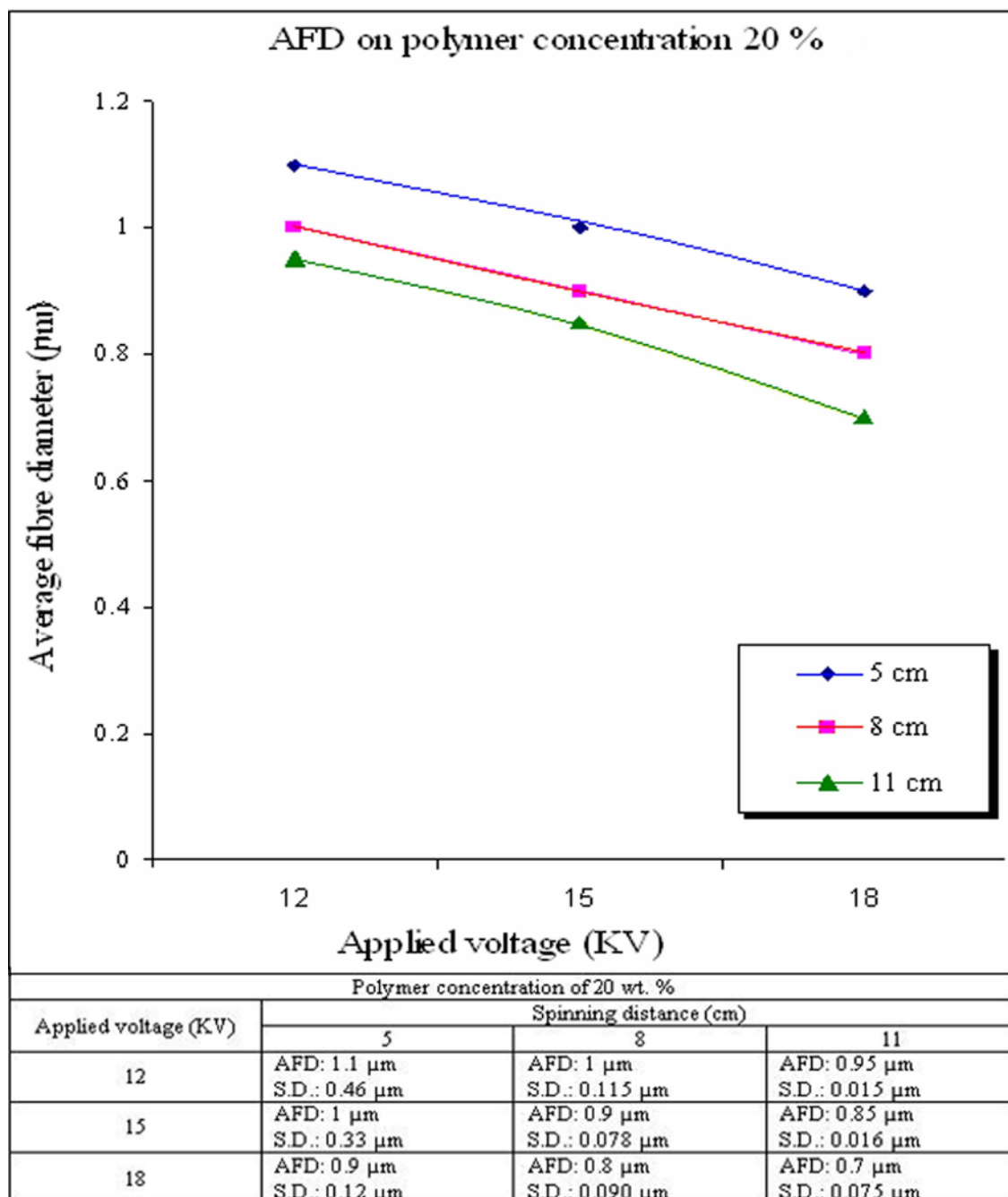


Figure 2.7. Relationship between the average fibre diameter (AFD) and applied voltage with polymer solution concentration of 20 wt. % at spinning distances of 5, 8 and 11 cm.

Figure 2.8, shows the relationship between the average fibre diameter and spinning distance with an applied voltage of 15 KV. The fibre diameter is not changed dramatically with various applied voltages.

Comparing the fibre diameters at 5 and 8 cm spinning distances with the same applied voltage and concentration (see figure 2.7) shows that fibre diameters obtained at 8 cm spinning distance are lower than those obtained at 5 cm spinning distance in the concentration range of 15 - 25 wt. %. For 20 wt. % nylon 6 concentration, an increase in the applied voltage from 15 to 18 kV leads to a decrease in the average fibre diameter from 850 to 800 nm and from 850 to 750 nm under 8 and 11 cm spinning distances, respectively. One might suggest that this result is due to the longer spinning distance, which enables the solvent to evaporate more efficiently even at the same electric field strength, thus leading to a smaller fibre diameter in comparison with the fibre diameter obtained at a 5 cm spinning distance.

The applied voltage may affect some factors such as the mass of polymer fed from the tip of the spinneret, the elongation level of the jet by an electrical force and the morphology of the jet (single or multiple jets), etc [9]. A balance among these factors may determine the final diameter of the electrospun fibres.

Increasing the applied voltage does increase the electrical force and create smaller fibre diameters, but it also draws more polymer solution out of the spinneret. If the increasing electrical force draws much more polymer solution out of the spinneret, the fibre diameter will increase with increasing applied voltage, as reported by Demir et. al. [27]. In general, increasing the applied voltage to a certain level changes the shape of the pendant droplet from which the jet originates, so a stable shape can not be achieved. As a result, the stability of the liquid jet is weakened, and this might lead to an increase in the density of beads in the electrospun nanofibres.

2.4 Process optimization [10]

Processing parameters need be optimized to electrospin nylon 6 into nanofibres with the desired morphology. The applied voltage reflects on the force to pull a solution out from the spinneret, so a higher applied voltage causes higher polymer solution consumption.

On the other hand, the applied voltage affects the charge density and thus the electrical force, which influences the elongation of the jet during electrospinning. Briefly, electrospun nanofibres with a smaller diameter can be produced with a lower polymer solution concentration, but nonuniform/ beaded fibres are found if these parameters were either too high or too low.

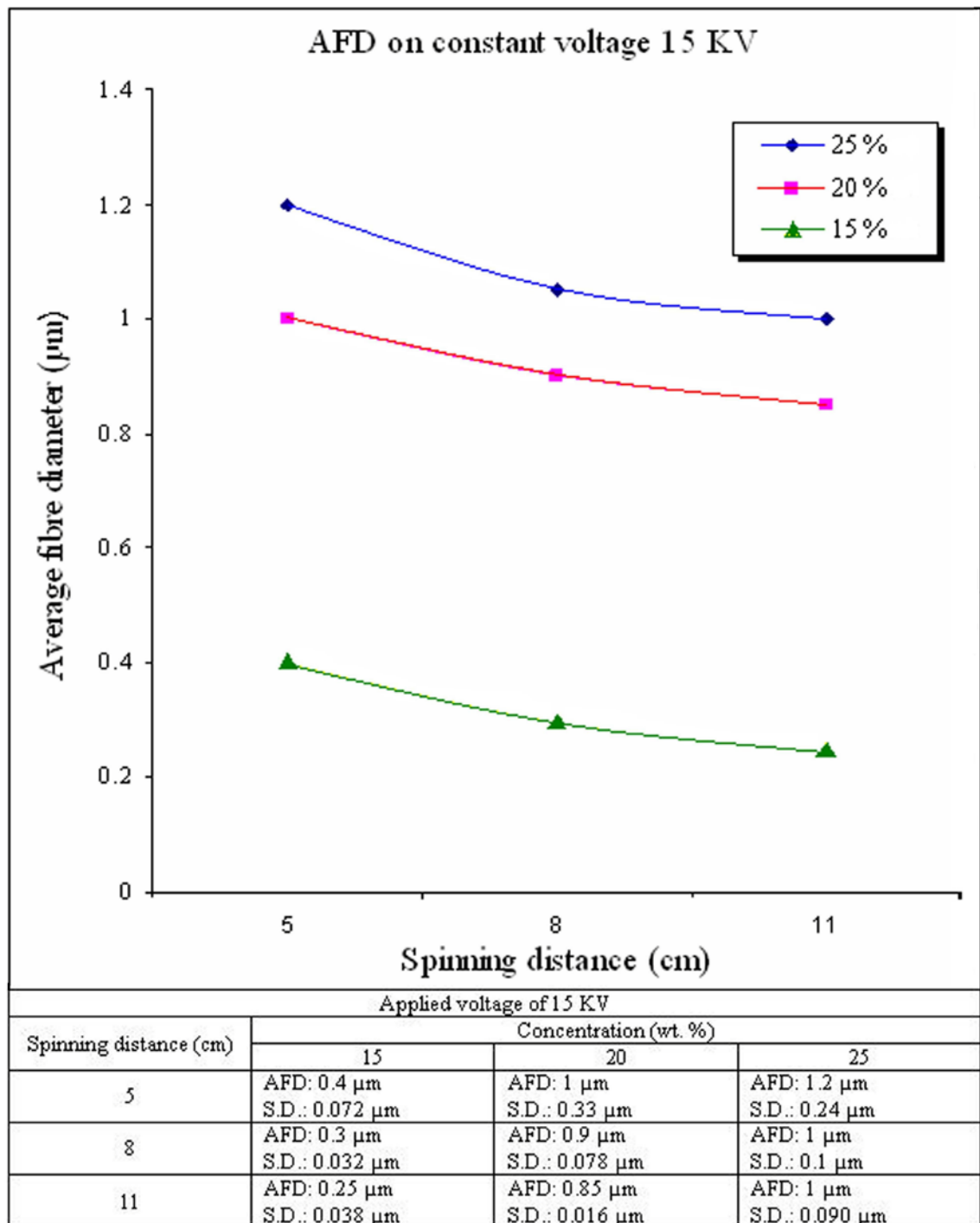


Figure 2.8, Relationship between the average fibre diameter (AFD) and spinning distance with an applied voltage of 15 KV at polymer solution concentrations of 15, 20 and 25 wt. %.

For obtaining a uniform fibre structure, higher polymer concentration and lower electrical field strength are preferred. These results are in agreement with published reports for polymers other than nylon 6 [7, 27-29].

The analyzed SEM image shown in figure 2.9, indicates that the optimal conditions for producing a uniform fibre diameters distribution are a polymer solution concentration of

20 wt. %, an applied voltage of 15 kV, volume feed rate of 0.2 mL/h and a spinning distance of 8 cm. These parameters were made constant for producing uniform nylon 6 fibres, which assisted the subsequent investigation of the alignment of nylon 6 nanofibres.

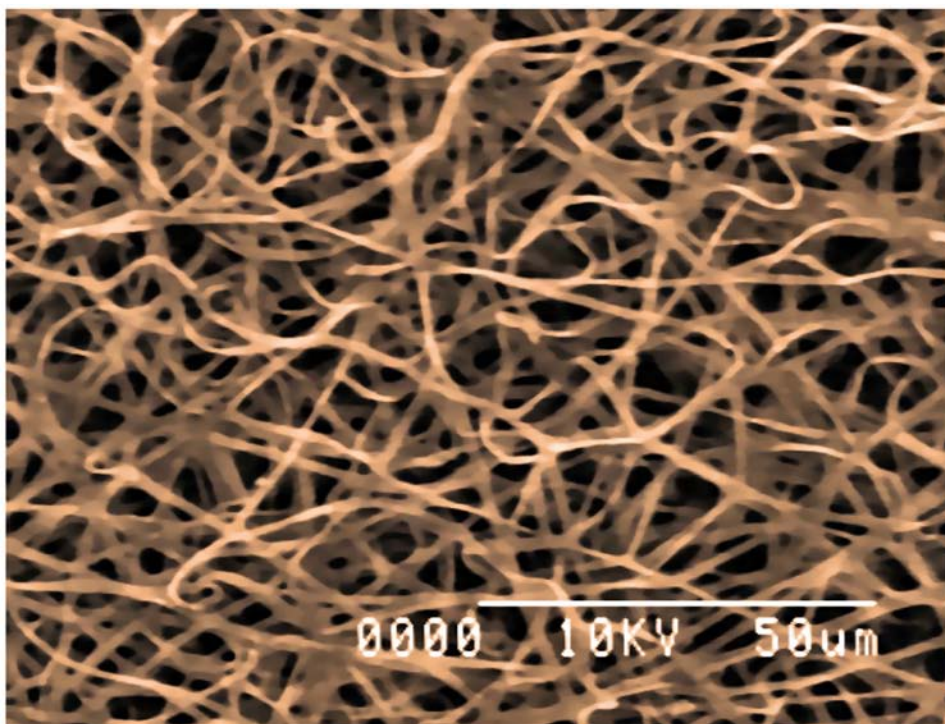


Figure 2.9, SEM image of 20 wt. % nylon 6/ formic acid nanofibres at a voltage of 15 KV and a distance of 8 cm with a uniform nanofibre diameters distribution of 900 ± 50 nm.

2.5 References

- [2.1] A. Ziabicki, *Fundamentals of fibre formation*, John Wiley & Sons, London (1976)
- [2.2] A. Formhals, *Process and apparatus for preparing artificial threads*, US Patent, **1975504** (1934)
- [2.3] A. Formhals, *Method and apparatus for spinning*, US Patent, **2160962** (1939)
- [2.4] A. Formhals, *Artificial thread and method of producing same filed*, US Patent, **2187306** (1940)
- [2.5] A. Formhals, *Producing of artificial fibres from fibre forming liquids*, US Patent, **2323025** (1943)
- [2.6] A. Formhals, *Method and apparatus for spinning*, US Patent, **2349950** (1944)
- [2.7] D.H. Reneker, I. Chun, *Nanometer diameter fibres of polymer produced by electrospinning*, *Nanotechnology*, **7**, 216-223 (1996)

- [2.8] A. Greiner and J.H. Wendorff, *Electrospinning: a fascinating method for the preparation of ultrathin fibres*, *Angewandte Chemie International Edition*, **46**, 5670-5703 (2007)
- [2.9] S.H. Tan, R. Inai, M. Kotaki, S. Ramakrishna, *Systematic parameter study for ultra-fine fibre fabrication via electrospinning process*, *Polymer*, **46**, 6128-6134 (2005)
- [2.10] M.B. Bazbouz, G.K. Stylios, *Alignment and optimization of nylon 6 nanofibres by electrospinning*, *Journal of Applied Polymer Science*, **107**, 3023-3032 (2008)
- [2.11] D.H. Reneker, A.L. Yarin, H. Fong, S. Koombhongse, *Bending instability of electrically charged liquid jets of polymer solutions in electrospinning*, *Journal of Applied Physics*, **87**, 4531-4547 (2000)
- [2.12] S.A. Angadjiv, M.G. Schwartz, P.D. Eitzman, M.E. Jones, *Method and apparatus for making a nonwoven fibrous electret web from free fibre and polar liquid*, US Patent, **6375886** (2002)
- [2.13] P.W. Gibson, H.L.S. Gibson, D. Riven, *Electrospun fibre mats: transport properties*, *The American Institute of Chemical Engineers (AIChE) Journal*, **45**, 190-195 (1999)
- [2.14] Y.C. Ahn, S.K. Park, G.T. Kim, Y.J. Hwang, C.G. Lee, H.S. Shin, J.K. Lee, *Development of high efficiency nanofilters made of nanofibres*, *Current Applied Physics*, **6**, 1030-1035 (2006)
- [2.15] A. Fertala, W.B. Han, F.K. Ko, *Mapping critical sites in Collagen II for relational design of gene-engineered proteins for cell-supporting materials*, *Journal of Biomedical Materials Research*, **57**, 48-58 (2001)
- [2.16] C.J. Buchko, L.C. Chen, Y. Shen, D.C. Martin, *Processing and micro structural characterization of porous biocompatible protein polymer thin films*, *Polymer*, **40**, 7397-7407 (1999)
- [2.17] H.J. Jin, S. Fridrikh, G.C. Rutledge, D. Kaplan, *Electrospinning Bombyx Mori silk with poly (ethylene oxide)*, *Abstracts of Papers - American Chemical Society*, **224**, 408-420 (2002)
- [2.18] C. Mit-uppatham, M. Nithitanakul, P. Supaphol, *Ultrafine electrospun polyamide-6 fibres: effect of solution conditions on morphology and average fibre diameter*, *Macromolecular Chemistry and Physics*, **205**, 2327-2338 (2004)
- [2.19] D. Lin, C. Chang, C. Lee, L. Cheng, *Fine structure and crystallinity of porous nylon 66 membranes prepared by phase inversion in the water/formic acid/nylon 66 system*, *European Polymer Journal*, **42**, 356-367 (2006)

- [2.20] www.en.wikipedia.org/wiki/Scanning_electron_microscope accessed 29/07/2008
- [2.21] A.D. John, S. Lange, *Handbook of chemistry (15th edition)*, McGraw-Hill, New York, 5-118 (2001)
- [2.22] Y.J. Ryu, H.Y. Kim, K.H. Lee, H.C. Park, D.R. Lee, *Transport properties of electrospun nylon 6 nonwoven mats*, *European Polymer Journal*, **39**, 1883-1889 (2003)
- [2.23] S. Koombhongse, W. Liu, D.H. Reneker, *Flat polymer ribbons and other shapes by electrospinning*, *Journal of Polymer Science part B: Polymer Physics*, **39**, 2598-2606 (2001)
- [2.24] H. Fong, I. Chun, D.H. Reneker, *Beaded nanofibres formed during electrospinning*, *Polymer*, **40**, 4585-4592 (1999)
- [2.25] D. Li, Y.N. Xia, *Electrospinning of nanofibres: reinventing the wheel*, *Advanced Materials*, **16**, 1151-1162 (2004)
- [2.26] S.Y. Gu, J. Ren, G.J. Vancso, *Process optimization and empirical modeling for electrospun polyacrylonitrile (PAN) nanofibre precursor of carbon nanofibres*, *European Polymer Journal*, **41**, 2559-2568 (2005)
- [2.27] M.M. Demir, I. Yilgor, E. Yilgor, B. Erman, *Electrospinning of polyurethane fibres*, *Polymer*, **43**, 3303-3309 (2002)
- [2.28] S.V. Fridrikh, J.H. Yu, M.P. Brenner, G.C. Rutledge, *Controlling the fibre diameter during electrospinning*, *Physical Review Letters*, **90**, 1445021-1445025 (2003)
- [2.29] S.A. Theron, E. Zussman, A.L. Yarin, *Experimental investigation of the governing parameters in the electrospinning of polymer solutions*, *Polymer*, **45**, 2017-2030 (2004)

CHAPTER 3: ALIGNMENT OF NANOFIBRES

3.1 Introduction

Deposition of electrospun nanofibres on a flat collector is essentially random and disordered due to the chaotic and unstable motion of the electrospinning jet as it travels to the collector [1]. However, this is generally useful for membrane and filtrations, due to the small pore size obtained by the random morphology of the formation of the nonwoven electrospun nanofibres mat. The disordered structure of the electrospun nanofibres is problematic for producing highly ordered architectures, yarn forms and unique electrical and optical devices for microelectronics and photonics [2, 3]. Moreover, there is interest for some applications in achieving parallel and oriented nanofibres with highly improved mechanical properties [4].

Considering the chaotic nature of the electrospun jet motion, the buildup of electrical surface charges on the collector and the nanometer size of the electrospun fibres into account, the collector design can control the electrospun nanofibres architecture. By also controlling the geometrical shape and strength of the macroscopic electric field between the spinneret and the collector, it should be possible to control the jet path, to improve its stability and to achieve aligned nanofibres [5]. In recent years, researchers have developed several collection mechanisms to control the deposition of the electrospun nanofibres and to obtain continuous fibre alignment by manipulating the dynamic motion of the collector or the electric field strength and geometrical shape or both [6, 7]. To that effect, alignment of nanofibres which is the focus of this chapter is extremely important for engineering nano structures and enabling the twisting of aligned fibre bundles into yarn.

In this chapter, a comprehensive useful review is presented on the design of various mechanisms for nanofibres alignment, followed by an effective mechanism of generation of a bundle of aligned three-dimensional nanofibres over a large area by the introduction of a gap between two known surfaces. In addition, morphology of the electrospun aligned nanofibres and mechanism parameters affecting the nanofibres density, nanofibres length and degree of alignment are investigated.

3.2 The concept of nanofibres alignment and reviewing nanofibre alignment mechanisms

The importance of fibre alignment has been understood by man for centuries, when for the formation of coarse yarns made by hand spinning, the wool fibres had to be as

aligned as possible, which was achieved by stretch drawing, using our hands. This process has been mechanized during the industrial revolution and it has also been adopted nowadays for the nano formation of fibres and yarns.

3.2.1 Nano aligning mechanisms based on dynamic mechanical collection

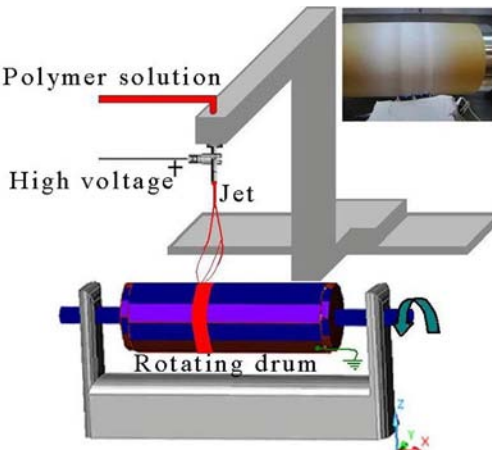
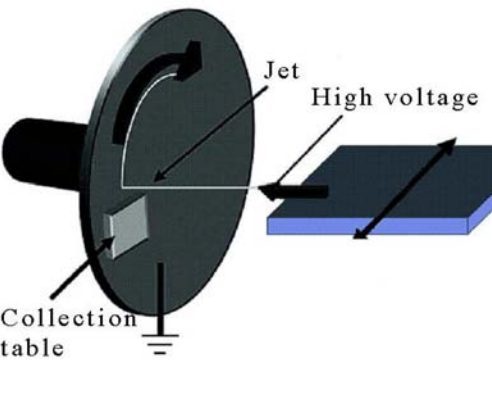
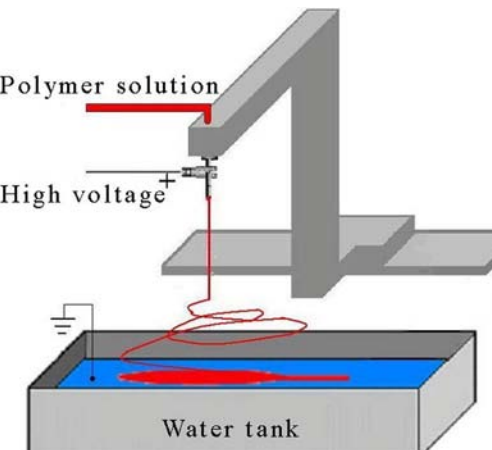
Several researchers have shown that it is possible to obtain aligned nanofibres by using a rotating cylinder [8-20, 55-57], rapidly oscillating a grounded frame [21] and flow of liquid [24, 25]. A schematic diagram of these mechanisms is shown in table 3.1.

It has been suggested that by rotating the cylinder collector at very high speed, up to thousands of revolutions per minute, electrospun nanofibres could be aligned circumferentially [8-20]. Matthews et. al. demonstrated that when the linear speed of the cylinder was approximately 1.4 m/sec, collagen nanofibres showed significant alignment along the axis of the fibre [9]. Kim et. al. examined the effect of the linear speed of the rotating cylinder on the crystallinity, mechanical properties and alignment of electrospun polyethylene terephthalate (PET) [10]. PET electrospun nanofibres were found to be more oriented, however, with increasing cylinder linear speed up to 30 m/min. Problems of this mechanism occur when the surface speed of the cylinder is slower than the stretching speed; and thus randomly deposited fibres are being collected. On the other hand, when the rotating speed of the cylinder is too high, continuous fibres cannot be collected due to fibre breaks. Even so, the degree of alignment achieved with this method is limited to partial alignment only and it still needs improving. Kessick et. al. addressed the reasons of the presence of disordered nanofibres on a rotating cylinder to the residual charge accumulation between the deposited fibres and the incoming fibres. In order to reduce the residual charge accumulation on the rotating cylinder they used an alternating current (AC) high voltage power supply to charge the polymer solution for electrospinning [19].

A newly developed scanned electrospinning mechanism that enables rapid fabrication of aligned polymeric nanowires is described by Kameoka et. al. [22, 23]. Although this presents new opportunities for the manufacture and applications of nanowire devices, the electrospinning process conditions (spinning distance and solvent vaporization) for obtaining dry nanofibres should be investigated.

Reneker et. al. and other researchers used water as a coagulation bath to collect the electrospun nanofibres [24, 25]. In this mechanism, electrospinning took place over a water bath. Electrospun fibres first fell on the surface of the water bath and subsequently drawn by the motion of the water bath or a rotating cylinder inside the

Table 3.1, Nano aligning mechanisms based on dynamic mechanical collection.

<p>1- Rotating drum</p> 	<p><u>Advantages</u> Large area of aligned fibres may be fabricated.</p> <p><u>Disadvantages</u> Highly aligned fibres may be difficult to achieve. Fibre breakages may occur if rotating drum speed is too high. Twist can not be applied for yarn spinning. [8-20, 55-57], photograph reprinted from [19].</p>
<p>2- Scanned disk fabrication [22, 23]</p> 	<p><u>Advantages</u> Rapid fabrication of aligned polymeric nanowires.</p> <p><u>Disadvantages</u> Vaporization of solvent is not complete. Thicker jet formation. Twist cannot be applied to form a yarn.</p>
<p>3- Coagulation bath collector</p> 	<p><u>Advantages</u> Nanofibres can be collected without sticking.</p> <p><u>Disadvantages</u> Applicable to some polymers. Partial alignment of fibres. Growth of bead deposits. Twist cannot be applied to form a yarn. [24, 25].</p>

bath. Visual analysis showed achieving aligned electrospun fibres in the direction of the water flow.

3.2.2 Nano aligning mechanisms based on manipulation of the electric field

As mentioned earlier, the movement of nanofibres is due to the electric field between the spinneret and the collector. By manipulating the strength, frequency, position and geometric shape of the electric field and the polarity of the charges, aligned and pre-ordered nanofibres can be achieved. A schematic diagram of the mechanisms based on electric field manipulation is shown in table 3.2.

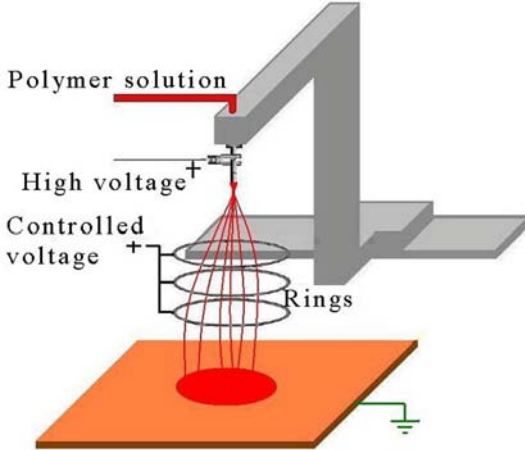
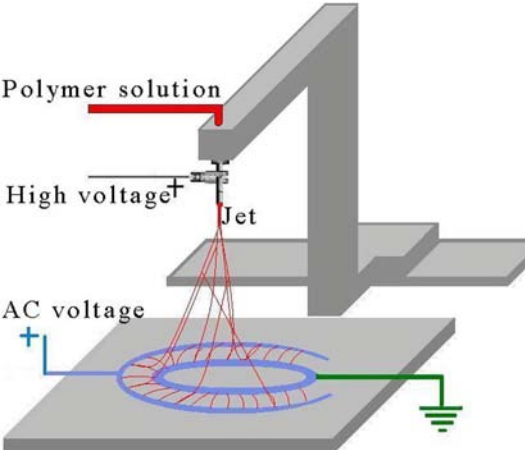
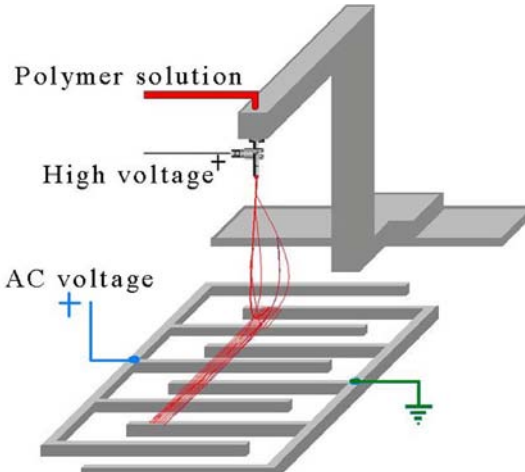
Deitzel et. al. [26, 27] used metallic rings placed below the tip of the spinneret as auxiliary electrodes and charged them with positive applied voltage, positively charging the collector, in their first experiment. The positively charged rings created a cylindrical electrical field that prevented the electrospinning jet from travelling out of its drawn path. In their second experiment they applied negative charges to the collector creating a pulling force on the electrospinning jet, through the charged rings. Stankus et. al. [28] also used a single positively charged cylindrical steel mesh near the tip of the spinneret to control the deposition area on a negatively charged collector. Although electric rings were employed to stabilize and focus the charged jets to generate oriented fibres with precise patterning, the deposition fibre area was reduced. This mechanism however offers advantages of fibre formation in controlled locations. This is important because the chaotic flight of the electrospinning jet and the residual charge accumulation on the deposited fibres may cause the fibres to deposit on areas outside the collector.

In another effort by Kim et. al. and other researchers [29, 30], the collector electrodes were modified. They presented a simple mechanism of fabricating aligned polycaprolactone nanofibres. Suspended aligned nanofibres were generated on a dielectric substrate by controlling of the electric field between the collector electrodes, which were subjected to an applied alternating-current field. The alignment of nanofibres was dependent on the applied frequency, field strength, and shape of the collector electrode.

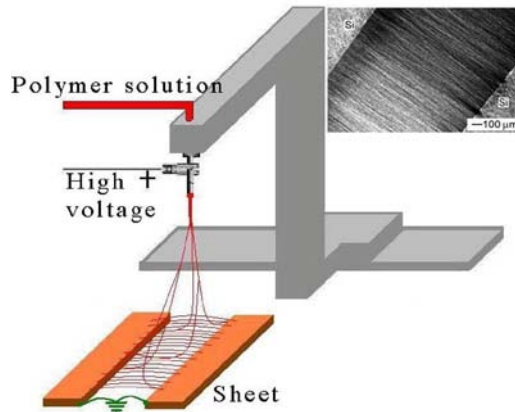
Another approach to fibre alignment was developed as early as 1938 by Formhals et. al. who patented an electrospinning set-up where bars were placed in parallel with gaps between them as a collector. By changing the geometric shape of the electric field of the collector, aligned fibres can be formed between the bars [31]. Haung et. al. [32] simply placed a rectangular frame structure under the spinning jet for collecting aligned nanofibres. Further work was done by the rotation of this frame on which electrospun polyethylene oxide nanofibres were deposited continuously. Xia et. al. and other researcher later on [2, 33-39, 58, 59] demonstrated the importance of the geometrical configuration of a conductive collector on the alignment of electrospun nanofibres. A

simple and versatile mechanism that generates uniaxially aligned nanofibres over large areas by introducing a gap in a charged collector has been presented. This exerts a pulling force on the electrospinning jet across the gap towards the parallel electrodes.

Table 3.2, Nano aligning mechanisms based on manipulation of the electric field.

<p>1- Auxiliary rings electrodes</p> 	<p><u>Advantages</u> Controlled fibres deposition area and location. Twist can be applied.</p> <p><u>Disadvantages</u> Complicate assembly. Small deposited area. [26-28].</p>
<p>2- Auxiliary AC circular electrodes</p> 	<p><u>Advantages</u> Highly aligned fibres are easily obtained. Aligned fibres are easily transferable.</p> <p><u>Disadvantages</u> Complicated set-up. Thicker layer of aligned fibres are not possible. There is a limit in the length of the fibres Twist can not be applied to spin a yarn. [29, 30].</p>
<p>3- Auxiliary AC parallel electrodes</p> 	<p><u>Advantages</u> Highly aligned fibres are easily obtained. Aligned fibres are easily transferable. No limit in the length of fibres produced</p> <p><u>Disadvantages</u> Complicated set-up. Thicker layer of aligned fibres are not possible. [29, 30].</p>

4- Parallel auxiliary electrodes



Advantages

Simple set-up.

Highly aligned fibres are easily obtained.

Aligned fibres are easily transferable.

Disadvantages

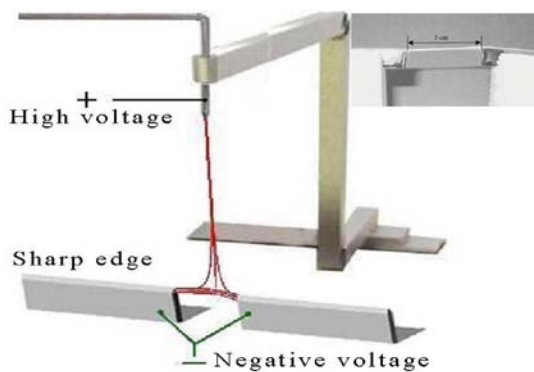
Thicker layer of aligned fibres are not possible.

There is a limit in the length of the fibres produced.

Twist can not be applied to spin a yarn.

[2, 31-39, 58, 59], photo reprinted from [2].

5- Negative parallel auxiliary electrodes



Advantages

Highly aligned fibres are easily obtained.

Aligned fibres are easily transferable.

Twist can be applied to spin a yarn

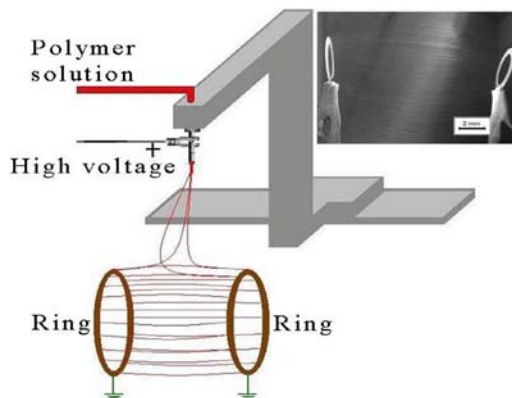
Disadvantages

There is a limit in the length of the fibres produced.

Application of negative voltage.

[41], photograph reprinted from [41].

6- Ring parallel electrodes



Advantages

Simple set-up.

Highly aligned fibres are easily obtained.

Aligned fibres are easily transferable.

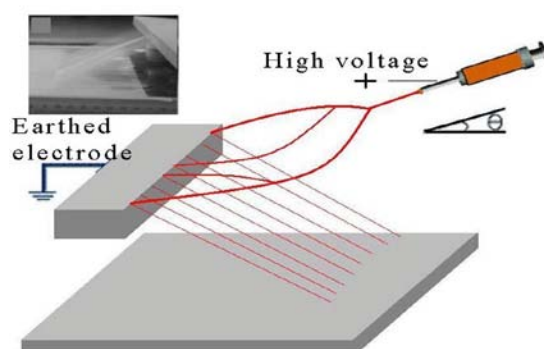
Twist can be applied to spin a yarn.

Disadvantages

There is a limit in the length of the fibres produced.

[42], photograph reprinted from [42].

7- Auxiliary electrode with support plate



Advantages

Simple set-up.

Highly aligned fibres are easily obtained.

Aligned fibres are easily transferable.

Big area of aligned fibres is possible.

Disadvantages

Twist cannot be applied to spin a yarn.

[43], photograph reprinted from [43].

By alternating the configuration of electric forces acting on the fibres spanning across the gap, nanofibres are stretched across the gap to form a parallel array. The effects of the gap width and applied voltage on the degree of fibre alignment were investigated by Morshed et. al. [39]. They experimented with the electrospinning conditions (i.e., the tip-to-collector distance, voltage, and gap width) that produce high alignment of fibres for 10-15 wt. % polyacrylonitrile/ dimethylformamide concentrations. It has been reported that 11 kV provides the highest alignment of nanofibres with a fixed corresponding concentration of 15 wt. % and gap 'space' width of 3 cm. The length of the aligned electrospun fibres across a gap is controlled by the gap distance, which is typically less than 10 cm. At a greater distance, the electrospinning jet may fail to deposit fibres across the gap or the fibres may break under their own weight, especially if the fibres are of smaller diameter [2]. When parallel electrodes are used as collectors however, aligned fibres become more random with increasing the deposition of fibres along the electrodes [40]. This is probably due to the accumulation of residual charges on the deposited fibres distorting the desired electric field shape.

The set-up of Ramakrishna et. al. [41] consisted of placing two blades in line with one another and with a gap between them. Negative charges were applied to the blades to create greater attractive forces on the positively charged jet and thus a highly aligned fibre bundle was collected. An important advantage of this mechanism is that the two ends connecting the fibre bundle to the electrodes are precise and consistent; this can help in collecting stretched fibres and provides the opportunity for subsequent testing their strength.

Dalton et. al. [42] used two parallel rings to collect highly aligned fibres suspended across the gap along the circumference of the rings. By rotating one of the rings after the fibres were deposited, they were able to obtain twisted multi-filament yarn.

Yu et. al. [43] used one earthed electrode and support plate surface to collect well aligned nanofibres of more than 25 cm long over a lateral range as large as 63 cm. In this mechanism the rear part of the fibre moves towards the support plate due to the combined inertia, electrical, and gravitational forces. It was found that the aligning process was greatly affected by the geometrical shape of the collector such as height and length. In addition, it is expected that the production throughput of aligned nanofibres may be greatly increased by arranging multi-spinnerets and multi-collecting electrodes.

3.2.3 Nano aligning mechanisms based on combining manipulation of electric field and dynamic collection

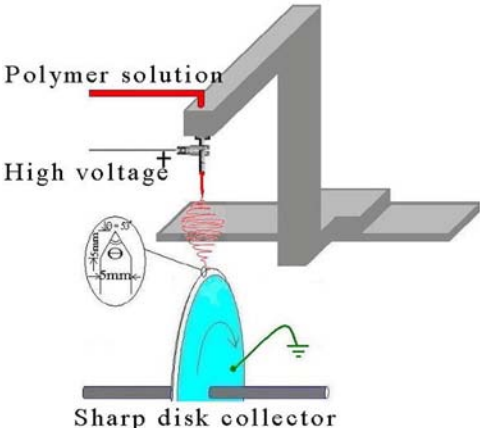
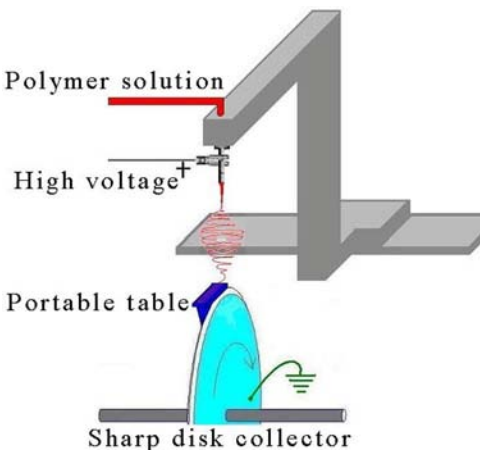
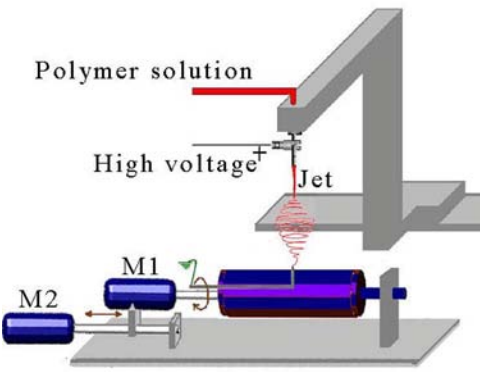
By controlling the geometric profile and strength of the electric field and by using different dynamic collecting systems, greater alignment in the nanofibres assembly can be achieved. Researchers successfully fabricated fibrous assemblies by using of both rotating collectors and manipulation of the electric field profile. A schematic diagram of the mechanisms based on combining electric field manipulation and dynamic collection is shown in table 3.3.

Zussman et. al. and other researchers [44-46] modified the design of a cylinder collector and used a tapered disk, with knife like edge, as a collector. The disk edge substantially improves the concentration of the electrical field and thus the electrospinning jet converged towards the disk attracting almost all nanofibres. The charged nanofibres are continuously wound on the edge of the rotating disk at a relatively high speed. When a nanofibre is attached to the disk edge, it exerts a repulsive force on the next fibre attracted to the edge. This repulsion results in a separation between the deposited nanofibres. Hence the nanofibre diameter and charges are not completely identical, the repulsive force will vary, which may explain the variation in distance separating the nanofibres. Zussman et. al. demonstrated later that at high rotational speed of the knife edge disk collector, necking of the electrospun nanofibres was observed [47]. Therefore the disk rotational speed and fibre alignment have a direct influence on the mechanical properties of the engineered fibres. They have further reported on a technique for a hierarchical assembly of nanofibres into crossbar nanostructures [48, 49, 60]. The collector disk is equipped with glass cover slips or any non conducting table that collects the nanofibres and can be rotated about the z axis. In this technique, the uniaxially aligned arrays of nanofibres could be stacked to a cross-bar in a layer-by-layer fashion to generate a 3D net structure. The area in which the nanofibres are deposited is limited and needs further investigation. With the understanding that the manipulation of the electric field could exert some control to the alignment of the nanofibres deposited on the rotating cylinder, Sundaray et. al. used a sharp needle as a counter electrode placed on an insulating rotating cylinder [50]. This method allows a tube made of circumferentially aligned nanofibres to be obtained. As the layer of fibres increases, however, the counter electrode does not hold a significant draw on the fibres. As a result, the thickness of the aligned fibres obtained is restricted.

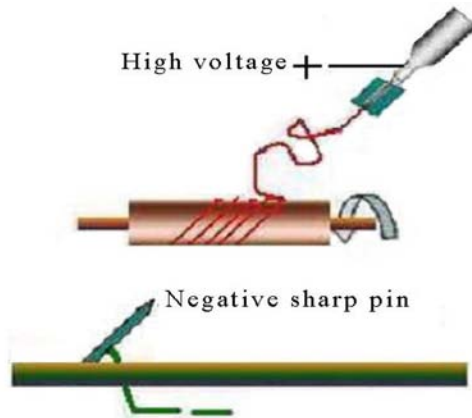
Teo et. al. [51] demonstrated the effect of a sharp needle auxiliary electrode on the deposition of electrospun fibres on the rotating cylinder. Instead of having the electrode

directly below the spinneret, they placed the needle under the rotating cylinder to direct the trajectory of the fibres for achieving greater degree of alignment. A tubular structure with well aligned nanofibres in a circumferential direction and at an angle to the longitudinal axis of a tube has been proposed.

Table 3.3, Nano aligning mechanisms based on combining manipulation of electric field and dynamic collection.

<p>1- Sharp disk collector</p>  <p>Polymer solution High voltage Sharp disk collector</p>	<p><u>Advantages</u> Highly aligned fibres are possible. Able to fabricate array of fibres by attaching a rotatable table on the disk.</p> <p><u>Disadvantages</u> Unable to retain high fibre alignment at the same rotating speed when the deposited fibres are thicker. Twist cannot be applied to spin a yarn [44-47].</p>
<p>2- Sharp disk collector with attached table</p>  <p>Polymer solution High voltage Portable table Sharp disk collector</p>	<p><u>Advantages</u> Highly aligned fibres are possible. Able to fabricate array of fibres.</p> <p><u>Disadvantages</u> Unable to retain high fibre alignment at the same rotating speed when the deposited fibres are thicker. Twist cannot be applied to spin a yarn. [48, 49, 60].</p>
<p>3- Rotating drum with sharp pin on it</p>  <p>Polymer solution High voltage Jet M1 M2 Rotating drum with sharp pin on it</p>	<p><u>Advantages</u> Large area of fibre arrays can be fabricated.</p> <p><u>Disadvantages</u> Set-up is complicated. Thicker area of fibre arrays assembly may not be possible. Twist cannot be applied to spin a yarn. [50].</p>

4- Rotating drum with needle as an auxiliary electrode



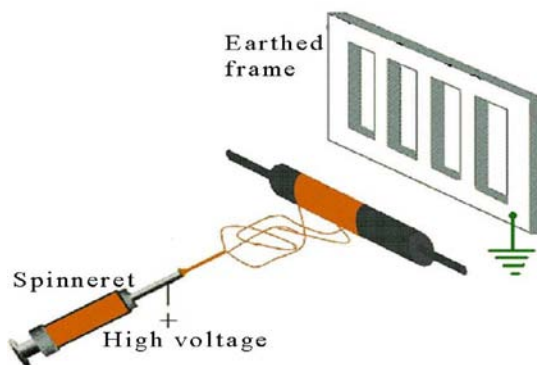
Advantages

Direction of alignment can be controlled.
Tubular structure can be fabricated.

Disadvantages

Thicker area of aligned fibre assembly may not be possible.
Twist cannot be applied to spin a yarn. [51].

5- Rotating drum with earthed frame as an auxiliary electrode



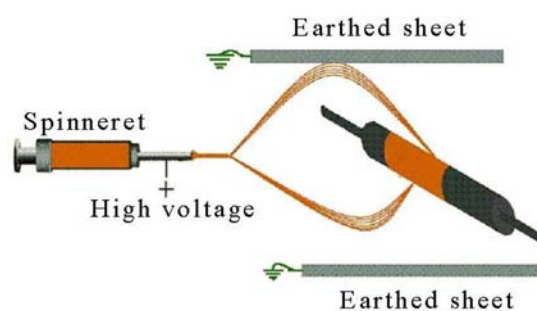
Advantages

Tubular structure can be fabricated.

Disadvantages

Thicker area of aligned fibre assembly may not be possible.
Twist cannot be applied to spin a yarn. [52].

6- Rotating drum with parallel surface plates as auxiliary electrodes



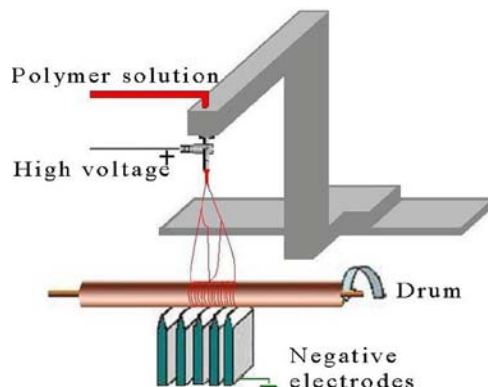
Advantages

Large area of aligned fibres can be fabricated.
Tubular structure can be fabricated.
Thicker area of aligned fibre assembly may be possible.

Disadvantages

Set-up is complicated.
Twist cannot be applied [52].

7- Rotating drum with sharp edge plates as auxiliary electrodes



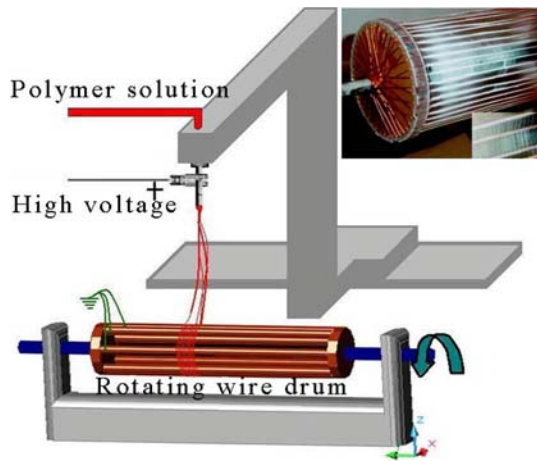
Advantages

Large area of aligned fibres can be fabricated.
Tubular structure can be fabricated.
Thicker area of aligned fibre assembly may be possible.

Disadvantages

Set-up is complicated.
Twist cannot be applied to spin a yarn. [51, 53].

8- Rotating wire drum collector



Advantages

Highly aligned fibres are possible.

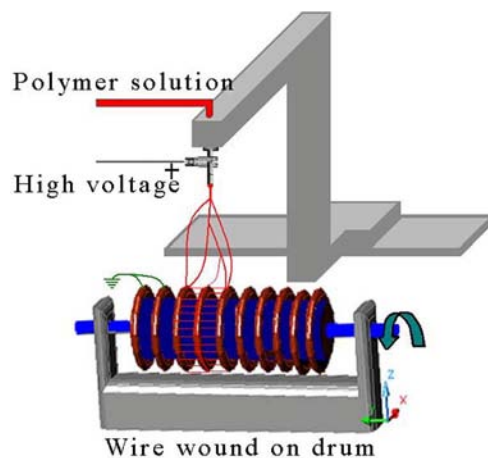
Disadvantages

Thicker layer of aligned fibres are not possible.

Fibres may not be aligned throughout the whole assembly.

Twist cannot be applied to spin a yarn. [40], photograph reprinted from [40].

9- Drum collector with wire wound on it



Advantages

Highly aligned fibres are possible.

Area of aligned fibres is adjustable by the wire thickness.

Disadvantage

Aligned fibres are concentrated on the wire instead of the whole drum.

Twist cannot be applied to spin a yarn. [54].

In a U.S. patent, it has been reported that by the asymmetric placement of a rotating and charged cylinder between two charged plates, electrospun nanofibres can be produced circumferentially to the longitudinal axis of the cylinder forming a tubular structure [52].

In a similar mechanism, a conventional rotating collector was employed with the addition of an auxiliary electrode positioned directly behind the collector to direct the fibre alignment [52]. The auxiliary electrode opposite to the spinning spinneret was designed to stretch the charged electrospun fibres by forming a strong electrostatic field between the nozzle and the collector. The electrospun fibres were focused between the gaps of the two electrodes to form parallel fibres, which were collected conveniently onto the rotating collector.

Ramakrishna et. al. [51] placed conducting parallel knife-edged as auxiliary electrodes under a rotating collector. They have demonstrated that the strength of the electric field is directly related to the quantity of electrodes and inversely related to the distance from the electrodes, the electric field lines will never cross each other and the density of lines

at a specific location represents the strength of the electric field. With the help of auxiliary electrodes, Carnell et. al. controlled the width of the aligned nanofibre mat collected on the rotating cylinder [53].

In another report, a successful mechanism for spinning sheets of 1 cm wide strips of aligned nanofibres was presented by Chase et. al. [40]. In this mechanism, copper wires spaced evenly in the form of a circular drum as a collector of nanofibres have been used. A further investigation of this work is needed on the effects of the rotation speed, gap distance between the wires, wire diameter, and polymer type. It has been noted that after 15 min of electrospinning, the alignment of nanofibres was reduced probably due to the increase in the residual charges accumulated on the collected nanofibres.

Bhattarai et. al. [54] produced highly aligned fibres of controllable size by winding a copper wire as an electrode on an insulating cylinder to collect a highly aligned fibre bundle by rotating the cylinder at an optimum speed of 2000 rpm. The length of the fibre bundle was said to be controlled by varying the wire diameter and the wire wraps step. Although highly aligned fibres can be obtained, the deposited fibres on the wire are difficult to extract.

3.3 Novel mechanism for aligning nanofibres [7]

Having established the optimum electrospinning conditions for uniform nylon 6 nanofibres which are a polymer solution concentration of 20 wt. %, an applied voltage of 15 kV, a volume feed rate of 0.2 mL/h and an electrospinning distance of 8 cm, we present a novel mechanism that is based on a three dimensional alignment principle shown in figure 3.1.

The nanofibres alignment mechanism involves collecting the electrically charged nanofibres between two faced-electrically grounded collector disks. Two copper circular disks (30 mm outer diameter, 2 mm thick) were used as collection disks. They were positioned by grounded alligator clips, with the top of the disks being 8 cm from the spinneret. In this mechanism, changing of the geometrical shape of the electric field by placing the two grounded disks under the spinneret splits the vertical electric field lines into two parts and thus aligns the electrospun nanofibres between the two disks.

3.4 Experimental work

3.4.1 Materials and electrospinning operation

The polymer solution (Nylon 6 and formic acid at concentration of 20 wt. %) was fed from a 5 mL capacity syringe to a vertically orientated (25 gauge) blunt ended metal

needle ‘spinneret’ via Teflon tubing. The volume feed rate was digitally adjusted using the Harvard syringe pump to be 0.2 mL/h. The spinneret was connected to one electrode of the power supply at a high voltage of 15 kV. The two disks were positioned 8 cm down from the spinneret.

Investigations of the effect of the disks gap width and collection time on the degree of alignment and the density of fibres were carried out. The gap width was set at 2, 3, 4, 5 and 6 cm at 15, 30, 60 and 120 sec collection times. A heating lamp was employed to dry the collected nylon 6 nanofibres during the electrospinning process.

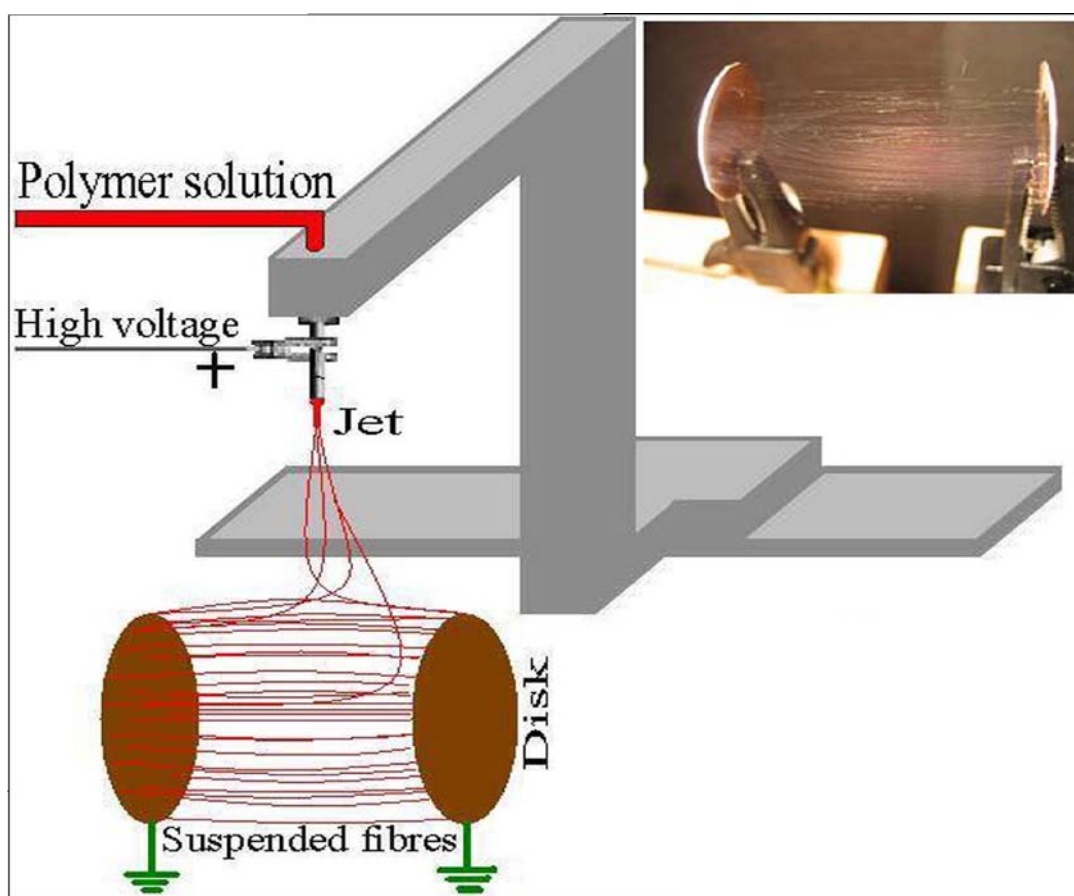


Figure 3.1, Experimental set-up for electrospinning three dimensional aligned nanofibre bundles.

3.4.2 Characterization

Samples of aligned nanofibres were collected on aluminium stubs. The aluminium stubs with parallel strips of super-glue tapes were passed through the suspended fibres between the collection disks. These samples were sputter coated with gold palladium for 45 sec at 18 mA. Nanofibres were examined by a Hitachi S-530 scanning electron microscope at an accelerating voltage of 10 kV. Micrographs were taken at three different areas of each sample between 20,000 and 40,000 magnifications.

3.5 Results and discussion

3.5.1 Alignment of electrospun nanofibres

Unlike electrospun fibres directly deposited onto a grounded collector as a random mesh, centimetres long fibre bundles were deposited in a curved parallel path between two copper disks in seconds, as shown in figure 3.1. After 15 sec of spinning, parallel aligned nanofibres between the two disks were observed. The magnified micrograph in figure 3.2, shows that the aligned nanofibres are perpendicular to the axis of the collection disks and have a uniform diameter distribution.

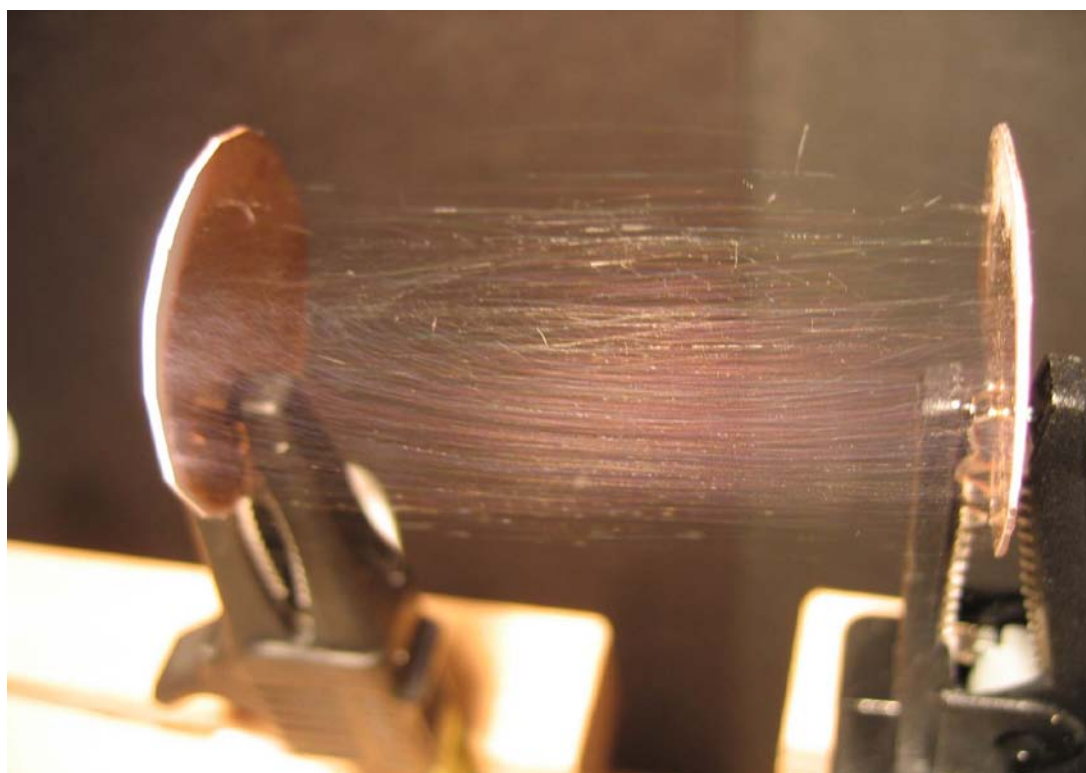


Figure 3.2, Photograph of an array of aligned (20 wt. % Nylon 6/ formic acid) nanofibres, 5 cm in length, deposited between two charged disks after 120 sec with an applied voltage of 15 KV and an electrospinning distance of 8 cm. The obtained fibre diameter was 800 ± 40 nm.

Alignment and stretching of the fibres are derived by electrostatic interactions between the positive electrode on the spinneret and the grounded disks. As a result, the polymer fibre travels toward the disk collector, one end of the fibre is attached to one of the disks, and the other end of the fibre is pulled toward the other disk. In other words, the bending shape of the flying nanofibres is transformed into a linear shape between the grounded circular disks. Once the charged fibres have moved into the gap between the

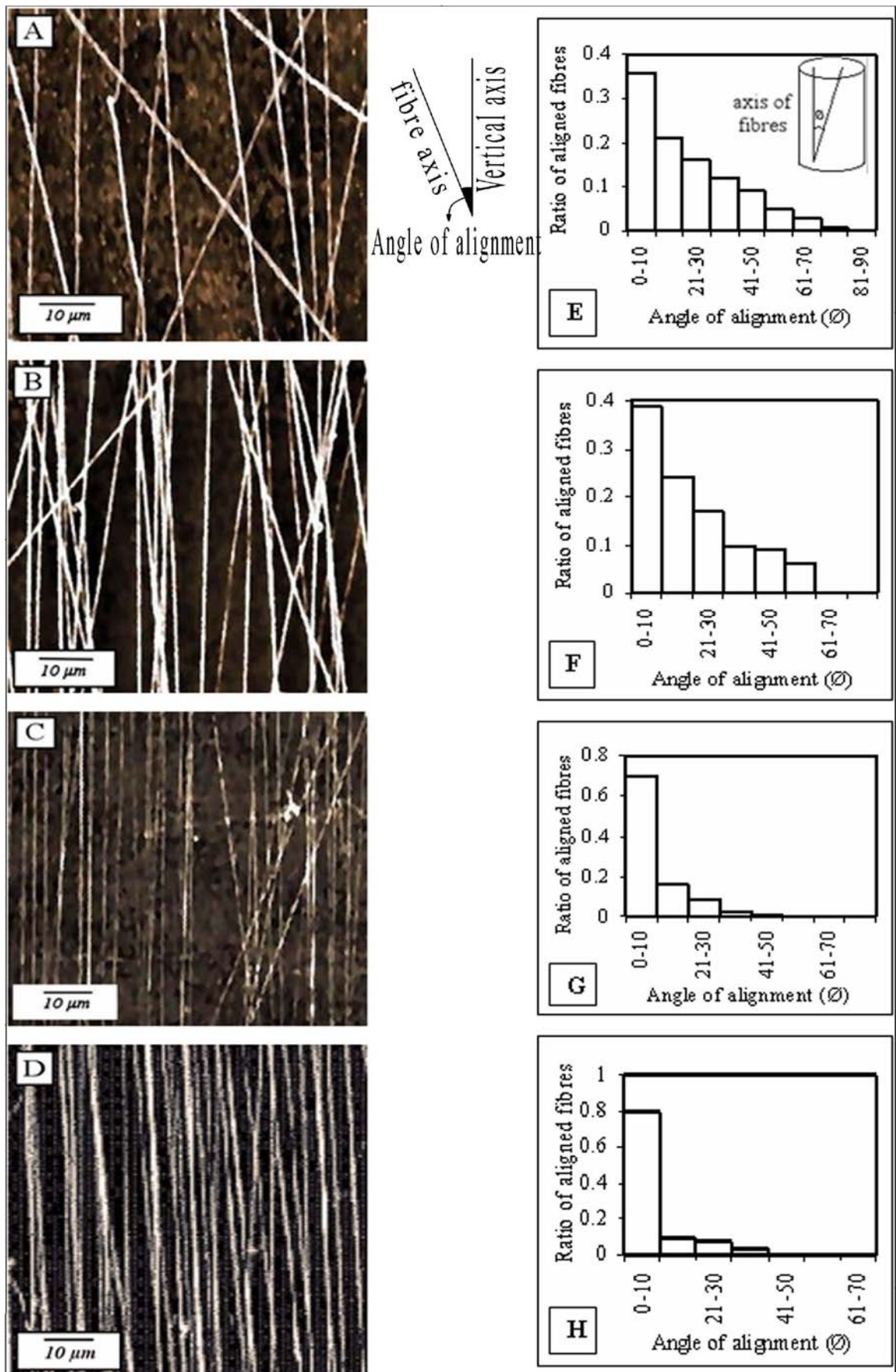


Figure 3.3. (A-D) SEM images of aligned nylon 6 nanofibres collected under a 4 cm gap distance at 15, 30, 60 and 120 sec respectively, and (E-H) charts of the ratio of aligned nanofibres per angle of alignment related to the SEM images.

disks, the fibres will induce opposite charges on the surface of the disks. These opposite charges will attract the fibres to the grounded disks, leading to the alignment of the fibres in the gap between the grounded circular disks. The nanofibres suspended across the gap remain highly charged after deposition, thus the electrostatic repulsion between the deposited and the upcoming fibres can further enhance the alignment mechanism. The SEM images in figure 3.3, show that well-aligned nanofibres have been formed, having diameters in the range of 800 ± 40 nm over four different collection times. The aligned fibres collected have lower average fibre diameters because their relaxation and expansion values are lower than in the case of random collection, leading to a decrease in the fibre diameters. Additionally, this confirmed that the nanofibres were physically stretched and thinned by the electric fields associated with the parallel grounded disks.

3.5.2 Effect of the collection time and space distance on the degree of alignment

The degree of parallelism of the aligned fibres was measured by image analysis. The experiments indicated that the collection time had a major effect on the alignment-parallelism degree of the fibres. Figure 3.3 (A), shows that the fibres are not well aligned along the axis of the fibres bundle, whereas perfectly parallel nanofibres can be seen in figure 3.3 (D). This means that the degree of fibre alignment increases with the collection time. On the other hand, because of the electrostatic repulsion force increasing between the deposited fibres with time, a long collection time will lead to worse alignment. Figure 3.4, shows SEM images of electrospun nanofibres after 120 sec of spinning, with gap (space) distance between the disks ranging between 2 and 6 cm. These images indicate a greater degree of alignment with the increase in disk space and the significant effect of the collection time.

3.5.3 Parameters affecting the density of deposited fibres

The experiment carried out shows that the number of nanofibres distributed in the bundle depends on parameters such as the collection time and the gap width. However, the applied voltage, spinning distance and flow rate, are the main effects on the mass of the deposited fibres and the number of branches generated from the electrospinning jet. With an increase in the applied voltage for a given spinning distance, nanofibre branching will increase, resulting in difficulties for aligning nylon 6 nanofibres. On the other hand, with an increase in the voltage, the drawing forces will increase, improving the alignment across the gap. The images in figures 3.3, and 3.4, show that as the deposition time is increased and the width of the gap is decreased, the number of nylon

6 fibres increases, and this makes the bundle denser. In fact, this can be explained by the theory of mass conservation.

The results obtained by Morshed et. al. [39] showed a low relative proportion of aligned polyacrylonitrile nanofibres mass for all electrospun polyacrylonitrile nanofibres (ca. 10-20 wt. %) with changes of the gap width. These results are expected because the conductive metallic collector surfaces are small; the metallic collector will not have a significant drawing on the fibres as the layer of fibres increases. In this mechanism, a higher proportion of aligned nanofibre mass has been obtained because of the large effective face surfaces of the disks, which stretch and span the fibres across the gap of the disks.

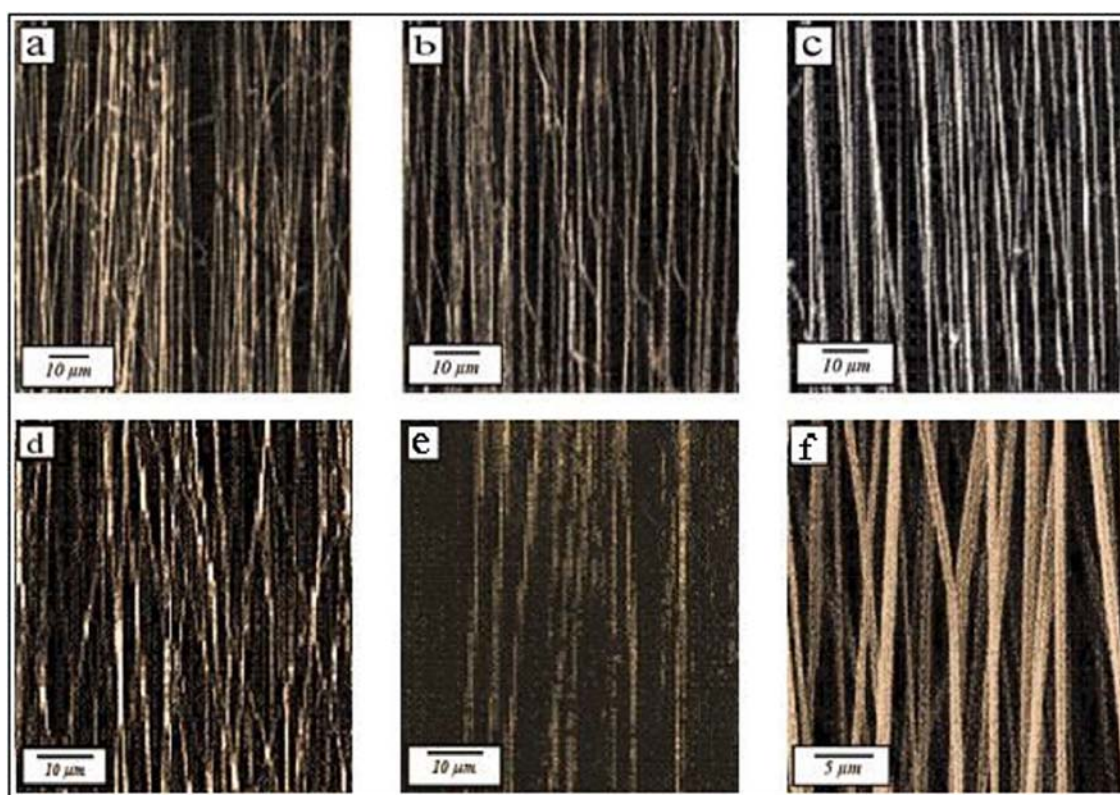


Figure 3.4, SEM images of aligned nylon 6 nanofibres with a constant collection time of 120 sec and gap spaces between the disks of (a) 2 cm, (b) 3 cm, (c) 4 cm, (d) 5 cm and (e) 6 cm. (f) SEM image of approximately uniform fibres 800 ± 40 nm in diameter with a 5 cm gap space and 120 sec collection time.

It has been noted that at a gap distance of 10 cm, few nylon 6 nanofibres were collected across the gap of the collection disks. When the collection disks were separated by a distance larger than 10 cm, the electrospinning jet had difficulty in depositing the nylon 6 fibres across the gap of the collection disks.

In conclusion, the optimum disk distance for spinning nylon 6 nanofibres is 4-5 cm. This provides the basis for twisting the nanofibre bundle for the formation of uniform nano yarns.

3.6 References

- [3.1] D.H. Reneker, A.L. Yarin, H. Fong and S. Koombhongse, *Bending instability of electrically charged liquid jets of polymer solutions in electrospinning*, Journal of Applied Physics, **87**, 4531-4547 (2000)
- [3.2] D. Li, Y. Wang, Y. Xia, *Electrospinning of polymeric and ceramic nanofibres as uniaxially aligned arrays*, Nano Letters, **3**, 1167-1171 (2003)
- [3.3] F. Kim, S. Kwan, J. Akana, P. Yang, *Langmuir-Blodgett nanorod assembly*, Journal of the American Chemical Society, **123**, 4360-4361 (2001)
- [3.4] L.M. Bellan, J. Kameoka, H.G. Craighead, *Measurement of the Young's moduli of individual polyethylene oxide and glass nanofibres*, Nanotechnology, **16**, 1095-1099 (2005)
- [3.5] D. Li, Y.N. Xia, *Electrospinning of nanofibres: reinventing the wheel*, Advanced Materials, **16**, 1151-1162 (2004)
- [3.6] W.E. Teo, S. Ramakrishna, *A review on design and nanofibre assemblies*, Nanotechnology, **17**, R89-R106 (2006)
- [3.7] M.B. Bazbouz, G.K. Stylios, *Alignment and optimization of nylon 6 nanofibres by electrospinning*, Journal of Applied Polymer Science, **107**, 3023-3032 (2008)
- [3.8] E.D. Boland, G.E. Wnek, D.G. Simpson, K.J. Palowski, G.L. Bowlin, *Tailoring tissue engineering scaffolds using electrostatic processing techniques: A study of poly (glycolic acid) electrospinning*, Journal of Macromolecular Science: part A Pure and Applied Chemistry, **38**, 1231-1243 (2001)
- [3.9] J.A. Matthews, G.E. Wnek, D.G. Simpson, G.L. Bowlin, *Electrospinning of Collagen nanofibres*, Biomacromolecules, **3**, 232-238 (2002)
- [3.10] K.W. Kim, K.H. Lee, M.S. Khil, Y.S. Ho, H.Y. Kim, *The effect of molecular weight and the linear velocity of drum surface on the properties of electrospun poly (ethyleneterephthalate) nonwovens fibre*, Polymer, **5**, 122-128 (2004)
- [3.11] Y.J. Wen, E.K.F. Yim, K. Leong, *Sustained release of proteins from electrospun biodegradable fibres*, Biomacromolecules, **6**, 2017-2022 (2005)
- [3.12] L. Wannatong, A. Sirivat, P. Supaphol, *Effects of solvents on electrospun polymeric fibres: preliminary study on polystyrene*, Polymer International, **53**, 1851-1857 (2004)

- [3.13] B. Ding, H.Y. Kim, S.C. Lee, D.R. Lee, K.J. Choi, *Preparation and characterization of nanoscaled poly(vinyl alcohol) fibres via electrospinning*, *Fibres and Polymers*, **3**, 73-79 (2002)
- [3.14] R. Dersch, T. Liu, A.K. Schaper, A. Greiner, J.H. Wendorff, *Electrospun nanofibres: Internal structure and intrinsic orientation*, *Journal of Polymer Science part A: Polymer Chemistry*, **41**, 545-553 (2003)
- [3.15] K.J. Shields, M.J. Beckman, G.L. Bowlin, J.S. Wayne, *Mechanical properties and cellular proliferation of electrospun Collagen type II*, *Tissue Engineering*, **10**, 1510-1517 (2004)
- [3.16] W.A. Yee, M. Kotaki, Y. Liu, X. Lu, *Morphology, polymorphism behavior and molecular orientation of electrospun poly(vinylidene fluoride) fibres*, *Polymer*, **48**, 512-521 (2007)
- [3.17] G. Wang, Z.K. Tan, X.Q. Liu, S. Chawda, J.S. Koo, V. Samuilov, M. Dudley, *Conducting MWNT/poly(vinyl acetate) composite nanofibres by electrospinning*, *Nanotechnology*, **17**, 5829-5835 (2006)
- [3.18] J. Doshi, D.H. Reneker, *Electrospinning process and applications of electrospun fibres*, *Journal of Electrostatics*, **35**, 151-160 (1995)
- [3.19] R. Kessick, J. Fenn, G. Tepper, *The use of AC potentials in electrospraying and electrospinning processes*, *Polymer*, **45**, 2981-2984 (2004)
- [3.20] H.S. Shim, S.I. Na, S.H. Nam, H.J. Ahn, H.J. Kim, D.Y. Kim, W.B. Kim, *Efficient photovoltaic device fashioned of highly aligned multilayers of electrospun TiO₂ nanowire array with conjugated polymer*, *Applied Physics Letters*, **92**, 183107-1 - 183107-3 (2008)
- [3.21] H. Fong, L. Weidong, C.S. Wang, R.A. Vaia, *Generation of electrospun fibres of nylon 6 and nylon 6-montmorillonite nanocomposite*, *Polymer*, **43**, 775-780 (2002)
- [3.22] J. Kameoka, D. Czaplewski, H. Liu, H.G. Craighead, *Polymeric nanowire architecture*, *Journal of Materials Chemistry*, **14**, 1503-1505 (2004)
- [3.23] J. Kameoka, R. Orth, Y. Yang, D. Czaplewski, R. Mathers, G.W. Coates, H.G. Craighead, *A scanning tip electrospinning source for deposition of oriented nanofibres*, *Nanotechnology*, **14**, 1124-1129 (2003)
- [3.24] G. Srinivasan, D.H. Reneker, *Structure and morphology of small diameter electrospun aramid fibres*, *Polymer International*, **36**, 195-201 (1995)
- [3.25] M. Gorantla, S.E. Boone, M. El-Ashry, D. Younga, *Continuous polymer nanofibres by extrusion into a viscous medium: A modified wet-spinning technique*, *Applied Physics Letters*, **88**, 0731151- 0731153 (2006)

- [3.26] J.M. Deitzel, D. Kleinmeyer, J.K. Hirvanen, N.C.B. Tan, *Controlled deposition of electrospun poly (ethylene oxide) fibres*, *Polymer*, **42**, 8163-8170 (2001)
- [3.27] J. Kleinmeyer, J. Deitzel, J. Hervonen, *Electrospinning of submicron diameter polymer filaments*, US Patent, **7086846** (2006)
- [3.28] J.J. Stankus, J. Guan, W.R. Wagner, *Fabrication of biodegradable elastomeric scaffolds with sub-micron morphologies*, *Journal of Biomedical Materials Research part A*, **70A**, 603-614 (2004)
- [3.29] G. Kim, W. Kim, *Formation of oriented nanofibres using electrospinning*, *Applied Physics Letters*, **88**, 2331011-2331013 (2006)
- [3.30] Y. Ishii, H. Sakai, H. Murata, *A new electrospinning method to control the number and a diameter of uniaxially aligned polymer fibres*, *Materials Letters*, **62**, 3370-3372 (2008)
- [3.31] A. Formhals, *Method and apparatus for spinning*, US Patent, **2160962** (1939)
- [3.32] Z.M. Huang, Y. Z. Zhang, M. Kotaki, S. Ramakrishna, *A review on polymer nanofibres by electrospinning and their applications in nanocomposites*, *Composites Science and Technology*, **63**, 2223-2253 (2003)
- [3.33] D. Li, Y. Wang and Y. Xia, *Electrospinning nanofibres as uniaxially aligned arrays and layer- by-layer stacked films*, *Advanced Materials*, **16**, 361-365 (2004)
- [3.34] S.J. Lee, N.I. Cho, D.Y. Lee, *Effect of collector grounding on directionality of electrospun Titania fibres*, *Journal of the European Ceramic Society*, **27**, 3651-3654 (2007)
- [3.35] M.V. Kakade, S. Givens, K. Gardner, K.H. Lee, D.B. Chase, J.F. Rabolt, *Electric field induced orientation of polymer chains in macroscopically aligned electrospun polymer nanofibres*, *Journal of the American Chemical Society*, **129**, 2777-2782 (2007)
- [3.36] Q. Zhang, Z. Chang, M. Zhu, X. Mo, D. Chen, *Electrospun carbon nanotube composite nanofibres with uniaxially aligned arrays*, *Nanotechnology*, **18**, 115611-1 - 115611-6 (2007)
- [3.37] H.W. Lu, W. Zeng, Y.S. Li, Z.W. Fu, *Fabrication and electrochemical properties of three-dimensional net architectures of anatase TiO₂ and spinel Li₄Ti₅O₁₂ nanofibres*, *Journal of Power Sources*, **164**, 874-879 (2007)
- [3.38] Y. Xin, Z. Huang, J. Chen, C. Wang, Y. Tong, S. Liu, *Fabrication of well-aligned PPV/PVP nanofibres by electrospinning*, *Materials Letters*, **62**, 991-993 (2008)
- [3.39] R. Jalili, M. Morshed, S.A.H. Ravandi, *Fundamental parameters affecting electrospinning of PAN nanofibres as uniaxially aligned fibres*, *Journal of Applied Polymer Science*, **101**, 4350-4357 (2006)

- [3.40] P. Katta, M. Alessandro, R.D. Ramsier, G.G. Chase, *Continuous electrospinning of aligned polymer nanofibres onto a wire drum collector*, Nano Letters, **4**, 2215-2218 (2004)
- [3.41] W.E. Teo, S. Ramakrishna, *Electrospun fibre bundle made of aligned nanofibres over two fixed points*, Nanotechnology, **16**, 1878-1884 (2005)
- [3.42] D. Paul, D. Dalton, D. Klee, M. Möller, *Electrospinning with dual collection rings*, Polymer, **46**, 611-614 (2005)
- [3.43] J. Rafique, J. Yu, J. Yu, G. Fang, *Electrospinning highly aligned long polymer nanofibres on large scale by using a tip collector*, Applied Physics Letters, **91**, 0631261-0631263 (2007)
- [3.44] A. Theron, E. Zussman, A.L. Yarin, *Electrostatic field-assisted alignment of electrospun nanofibres*, Nanotechnology, **12**, 384-390 (2001)
- [3.45] C.Y. Xu, R. Inai, M. Kotaki, S. Ramakrishna, *Aligned biodegradable nanofibrous structure: a potential scaffold for blood vessel engineering*, Biomaterials, **25**, 877-884 (2004)
- [3.46] S. Chen, P. Hu, A. Greiner, C. Cheng, H. Cheng, F. Chen, H. Hou, *Electrospun nanofibre belts made from high performance copolyimide*, Nanotechnology, **19**, 015604-1 - 015604-9 (2008)
- [3.47] E. Zussman, D. Rittel, A.L. Yarin, *Failure modes electrospun nanofibres*, Applied Physics Letters, **82**, 3958-3960 (2003)
- [3.48] A. Theron, E. Zussman, A.L. Yarin, *Formation of nanofibre crossbars in electrospinning*, Applied Physics Letters, **82**, 973-975 (2003)
- [3.49] R. Inai, M. Kotaki, S. Ramakrishna, *Structure and properties of electrospun PLLA single nanofibres*, Nanotechnology, **16**, 208-213 (2005)
- [3.50] B. Sundaray, V. Subramanian, T.S. Natarajan, R.Z. Xiang, C.C. Chang, W.S. Fann, *Electrospinning of continuous aligned polymer fibres*, Applied Physics Letters, **84**, 1222-1224 (2004)
- [3.51] W.E. Teo, M. Kotaki, X.M. Mo, S. Ramakrishna, *Porous tubular structures with controlled fibre orientation using a modified electrospinning method*, Nanotechnology, **16**, 918-924 (2005)
- [3.52] J.P. Berry, *Electrostatically produced structures and methods of manufacturing*, US Patent, **4965110** (1990)
- [3.53] Y.Q. Wu, L.A. Carnell, R.L. Clark, *Control of electrospun mat width through the use of parallel auxiliary electrodes*, Polymer, **48**, 5653-5661 (2007)

- [3.54] N. Bhattarai, D. Edmondson, O. Veisoh, F.A. Matsen, M. Zhang, *Electrospun chitosan- based nanofibres and their cellular compatibility*, *Biomaterials*, **26**, 6176-6183 (2005)
- [3.55] H.B. Wang, M.E. Mullins, J.M. Cregg, A. Hurtado, M. Oudega, M.T. Trombley, R.J. Gilbert, *Creation of highly aligned electrospun poly-L-lactic acid fibres for nerve regeneration applications*, *Journal of Neural Engineering*, **6**, 016001-1 – 016001-15 (2009)
- [3.56] L.S. Carnell, E.J. Siochi, N.M. Holloway, R.M. Stephens, C. Rhim, L.E. Niklason, R.L. Clark, *Aligned mats from electrospun single fibres*, *Macromolecules*, **41**, 5345-5349 (2008)
- [3.57] L.S. Carnell, E.J. Siochi, R.A. Wincheski, N.M. Holloway, R.L. Clark, *Electric field effects on fibre alignment using an auxiliary electrode during electrospinning*, *Scripta Materialia*, **60**, 359-361 (2009)
- [3.58] Y. Ishii, H. Sakai, H. Murata, *A new electrospinning method to control the number and a diameter of uniaxially aligned polymer fibres*, *Materials Letters*, **62**, 3370-3372 (2008)
- [3.59] T.J. Shan, L.Y. Ze, L.M. Meng, *Preparation of aligned polymer micro/nanofibres by electrospinning*, *Chinese Physics Letters*, **25**, 3067-3070 (2008)
- [3.60] W.A. Yee, A.C. Nguyen, P.S. Lee, M. Kotaki, Y. Liu, B.T. Tan, S. Mhaisalkar, X. Lu, *Stress-induced structural changes in electrospun polyvinylidene difluoride nanofibres collected using a modified rotating disk*, *Polymer*, **49**, 4196-4203 (2008)

CHAPTER 4: NANOFIBRE FILLED WITH CARBON NANOTUBES

4.1 Introduction

Electrospinning nanofibres are not as strong as desired because of their small diameter and unoptimized molecular chain orientation along the fibre. The elongation balance theory in textile engineering [1] and composite analysis [2] suggests that incorporating materials with fillers provides the most effective means of transferring tensile properties.

Based on this theory concept, research work has shown that the addition of filler into the fibre body leads to an increase of the strength of the fibre.

Carbon nanotubes (CNTs) which are made up of carbon atoms arranged in graphitic sheets structure have been received great attention since their discovering in 1991 by a Japanese microscopist Sumio Iijima of NEC [3. 4]. Figure 4.1, shows computational image of single wall carbon nanotubes SWCNTs and multi wall carbon nanotubes MWCNTs.

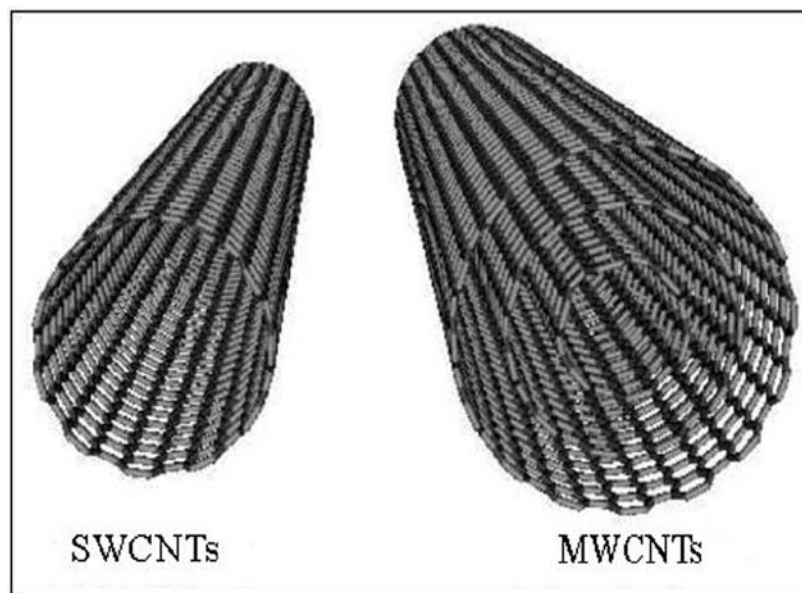


Figure 4.1, Computational image of SWCNTs and MWCNTs [5].

SWCNTs and MWCNTs are similar in structure except that MWCNTs are composed of more than one wall arranged concentrically like rings of tree trunk and held together by weak van der Waals bonds [5]. The diameter and length of carbon nanotubes CNTs varies depending on their production method 'synthesization'. SWCNTs can be produced with diameter in the range of $\sim 0.4 - 3$ nm; with ~ 1.2 nm as an average diameter. On the other hand, MWCNTs are produced with diameter in the range of

several nanometers to tens of nanometers. The length of CNTs are typically in the micrometers range which normally result in aspect ratio of >100 to as high as 10,000 depending on synthesizing method [6]. CNTs are proven to have magnificent mechanical properties such as; high aspect ratio of 10,000, young's modulus of 1 TPa for SWCNTs and 0.3 - 1 TPa for MWCNTs, tensile strength of 30 GPa for MWCNTs and fracture strains of 10 % - 30 % [6]. In other words, the tensile strength of CNTs can be as high as 100 times that of steel, and the graphene sheet is as stiff as diamond at low strain. They have been observed to have thermal conductivity of about 28.9 W/cm.k [7], electrical conductivity of 10^7 amp/cm², specific surface area of 10 - 20 m²/g and very good thermal stability [8].

It has been found that incorporating CNTs as filler into polymer fibres allows one or more or all of the above properties to be achieved [9]. In recent years, significant effort has been made into fabricating polymer fibre-carbon nanotube composites for improving the composite physical properties [10-17], mechanical properties [18-27] and electrical properties [28-31]. Composite nanofibres have been successfully electrospun with diameters as low as several tens of nanometers to as high as several micrometers depending on the polymer type, polymer molecular weight, electrospinning dope properties and electrospinning conditions.

For many applications of industrial fibres, CNTs composite nanofibres have been electrospun using different polymers such as; nylon 6 [25, 29], nylon 4, 6 [32], PAN [30, 33-35], PVA [26, 36], epoxy resins [37-40], silk [41, 42], thermo plastic polymers [43, 44], polypropylene [45] and blends of PVA with PEO [46].

However, separation of CNTs bundles, their dispersion and their alignment are still critical issues with regard to the mechanical and functional properties of any polymer CNTs composite. The main challenge for processing nanofibre composites at the present time is to improve the dispersion and alignment of CNTs in the polymer matrix for enhancing mechanical and electrical properties of the nanofibres [37, 47]. It has been indicated that stretching of the nanofibres during collection is a promising method for both improving the alignment of CNTs across the fibre body and fibre's molecular orientation [34, 44, 49, 50].

4.2 Dispersion and alignment of CNTs in the polymer solution

It is essential to have a good dispersion, uniform distribution and alignment of the CNTs in the polymer solution in order to optimize the mechanical, electrical and thermal properties of the final composite. To obtain a stable and uniform suspension of CNTs in

the polymer solution, several strategies have been employed to disperse the CNTs which include chemical modification of CNTs through attaching functional groups to the surface of the CNTs, non-chemical functionalization of CNTs through wrapping the CNTs with a surfactant and optimum physical blending ‘high speed shearing’ of CNTs and polymer solution [48].

The organization of nanofillers ‘parallel to each other’ into the nanofibre body serves not only as a mean of properties translation factor but also as helpful factor in designing and predicting properties of the final composite. The flow of the polymer solution, the presence of electrostatic charge, and the nanometer diameter of fibre are critical parameters in electrospinning for aligning CNTs into the fibre. It has been also researched that applying geometrical stretching to the electrospun nanofibres during collection improves the alignment of CNTs across the nanofibre body [50].

Scientifically, SWNTs have smooth and uniform interaction surfaces along their length, therefore they have high affinity to attract each other and aggregate forming packed ropes or entangles into their networks due to strong inter tube van der Waals attraction [5]. Moreover, the fineness of the SWNTs promotes agglomeration and formation of unoriented ropes, which prevents full translation of properties [48]. Having these properties into account, it is easier to uniformly disperse and align MWCNTs in the polymer solution.

In this chapter, ultrasound dispersion combined with high speed shearing is used to disperse MWCNTs into nylon 6 solution. As it has been found the simplest and most convenient method to improve the dispersion of CNTs in a polymer matrix [48]. By manipulating the electrical forces during electrospinning and applying geometrical stretching to the electrospun nanofibres by the alignment mechanism, high polymer chain orientation and better alignment of MWCNTs along the fibre axis is achieved [50].

4.3 Experimental work

4.3.1 Preparation of polymer - MWCNTs solution

Nylon 6 solution of 20 wt. % concentration was prepared by dissolving the polymer in 98 % formic acid. MWCNTs (Sunnano Co Ltd, China) with a diameter of 20 ± 10 nm and length of 1-10 μm of 95 % purity were dispersed to disrupt possible agglomerates using an ultrasonic homogenizer (model 300 V/T, Biologics INC, UK) operating at 25 Hz, as shown in figure 4.2. Different masses of MWCNTs were added to 20 ml of formic acid and sonicated for 3 hours. Specific amounts of nylon 6 were weighted and

added to certain quantities of formic acid for maintaining the desired polymer weight ratio. These mixtures were stirred for 2 hours and kept in an air tight bottle to prevent evaporation of formic acid for a period of time until the polymer was uniformly dissolved in the solvent. The sonicated and stirred solutions of MWCNTs and nylon 6 in formic acid were mixed by stirring. The final solutions produced contained varying concentrations of MWNTs from 0 to 4 wt. % in 20 wt. % nylon 6 solution.

4.3.2 Electrospinning of the polymer - MWCNTs solution

The MWCNTs/ nylon 6 solution was fed through a 5 mL capacity syringe to a vertically orientated (25-gauge) blunt-ended metal needle via Teflon[®] tubing and the flow rate was controlled using a digitally controlled, positive displacement syringe pump (Harvard Apparatus M22 PHD 2000). The needle was held by one electrode connected to a high voltage DC power supply (Glassman MK35P 2.0-22). Typical operating regimes at volume feed rate of 0.2 ml/hr, applied voltages of 15 KV and a working electrospinning distance of 8 cm were employed. These parameters were used for producing uniform diameter distribution of nylon 6 nanofibres, based on own published research [51]. Various polymer nanofibre collection system ranging from random fibres collection on a copper plate measuring 15cm × 15cm, to aligned fibres collection over two circular electrically grounded disks separated by 4 cm space distance and collection time of 120 sec were investigated.

4.3.3 Characterization

4.3.3.1 Scanning electron microscopy (SEM)

Samples of both aligned and random nanofibres were collected on aluminum stubs. For collecting the aligned nanofibres, aluminum stubs with parallel strips of super glue tapes were passed through the suspended fibres between the collection disks. These samples were sputter coated with gold palladium for 45 seconds at 18 mA. Nanofibres were examined using a Hitachi S-530 scanning electron microscope at an accelerating voltage of 10 kV. Micrographs were taken at three random areas of each sample between 20,000 and 40,000 times magnification.

4.3.3.2 Transition electron microscopy (TEM)

A TEM was utilized to qualitatively determine the size distribution and structure of carbon nanotubes in the composite nanofibre on 100 square mesh Cu grids for samples of randomly collected nanofibres, and 100 parallel mesh Cu grids for samples of aligned

collected nanofibres as shown in figure 4.2. The TEM (Philips CM120, Eindhoven, The Netherlands) as shown in figure 4.2, was used with an accelerating voltage of 120 KV. Micrographs were developed, digitally scanned, and presented without any other image manipulation.

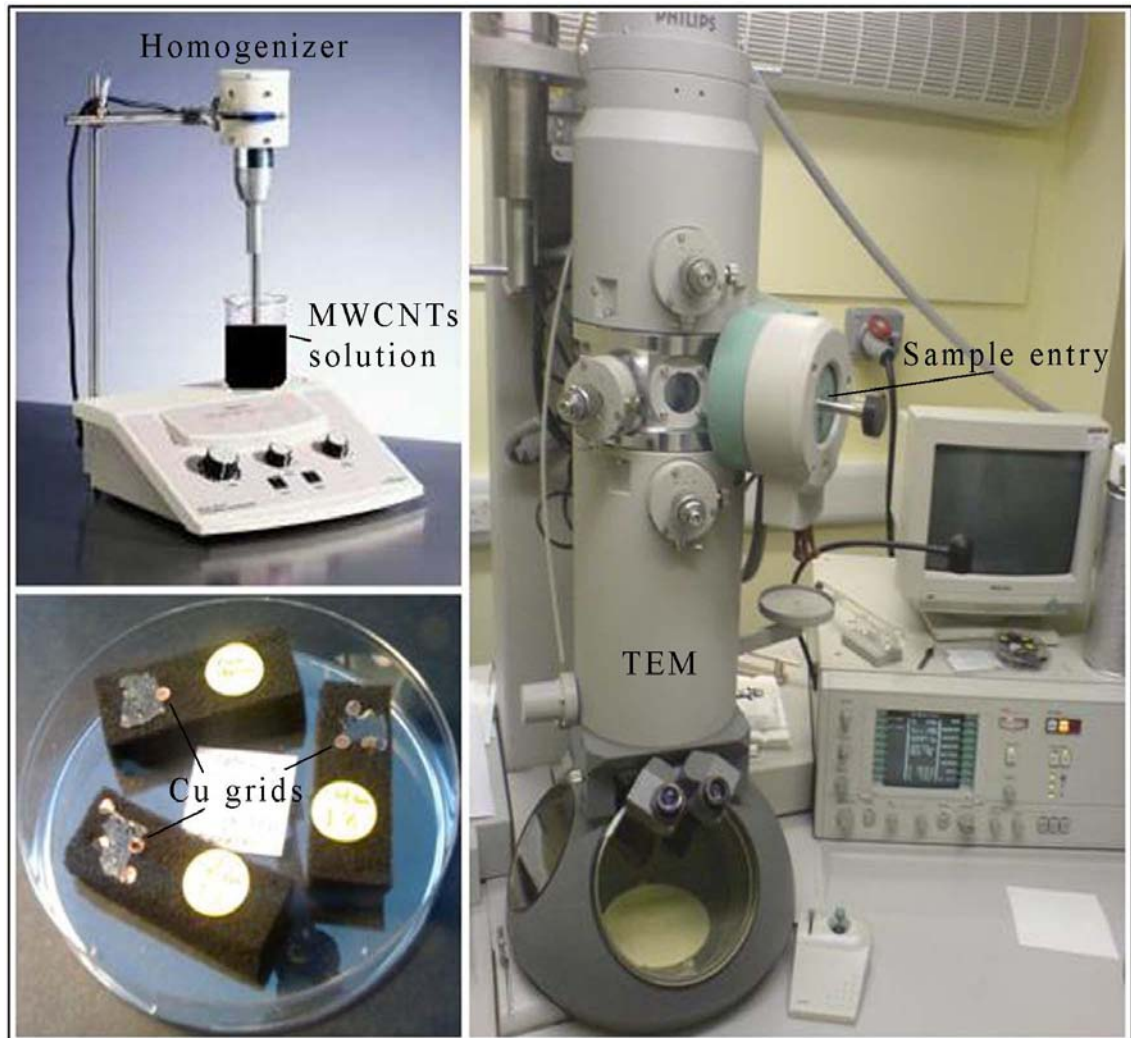


Figure 4.2, Photographs from the left to the right are: an ultrasonic homogenizer model 300 V/T, samples of randomly and aligned nanofibres collected on 100 square and parallel mesh Cu grids and Philips CM120 transition electron microscope used in the experimental work.

4.4 Results and discussion [50]

4.4.1 Composite aligned nanofibres

Figure 4.3, shows recorded photographs of randomly collected nylon 6 nanofibres containing various concentrations of MWCNTs from 0 to 4 wt. % in 20 wt. % nylon 6 solution. They have showed that as the loading of the carbon nanotubes is increased, the surface colours of the nanofibre mats changed from colourless 'white' to grey/black.

Figure 4.4, shows a series of micro morphological SEM images of randomly collected nylon 6 nanofibres containing various concentrations of MWNTs from 0 to 4 wt. % in 20 wt. % nylon 6 solution. Visual analysis of these images shows that as the loading of the carbon nanotubes is increased, the surface morphology of the nanofibres become rougher, because MWCNT particles were only partly dispersed in the nanofibre matrix.

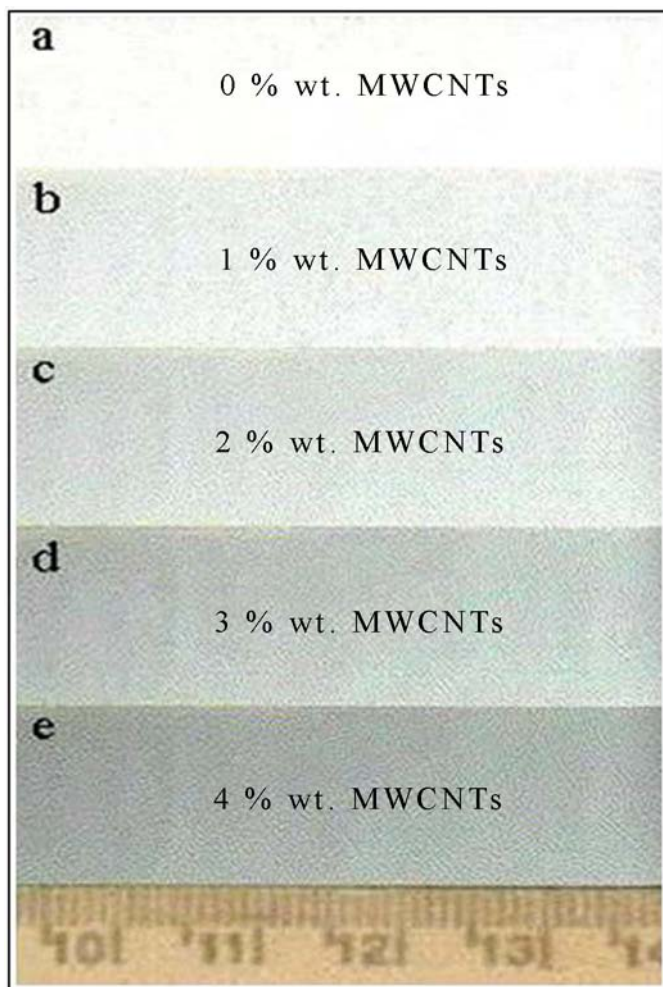


Figure 4.3. Recorded photographs of nonwoven nanofibre mats for (a) nylon 6 and (b-e) nylon 6/ MWCNTs composite, with increasing concentration of fillers from to (a) colourless of 0 wt. % MWCNTs, (b) ash/grey of 1 wt. % MWCNTs, (c) dirty grey of 2 wt. % MWCNTs, (d) deep grey of 3 wt. % MWCNTs and (e) grey/black of 4 wt. % MWCNTs.

It has been confirmed that [33], successful dispersing of the nanotubes inside the fibre body and orienting them along the axis of the fibre will minimize the protruded segments which are not embedded within the nanofibre. Achieving uniform distribution of MWCNT particles which is attributed to the fine dispersion of the nanotubes in the composite fluid is critical for preventing MWCNTs protrusion, notches and beads

across the fibre body. Although the electrospinning mechanism provides the electrostatic stretching forces (whipping elongation) for overcoming any entanglement of MWCNTs, applying other stretching forces can enhance the alignment of the nanotubes along the fibre axis within the nanofibre. This was achieved by the novel mechanism which described in the previous chapter [51].

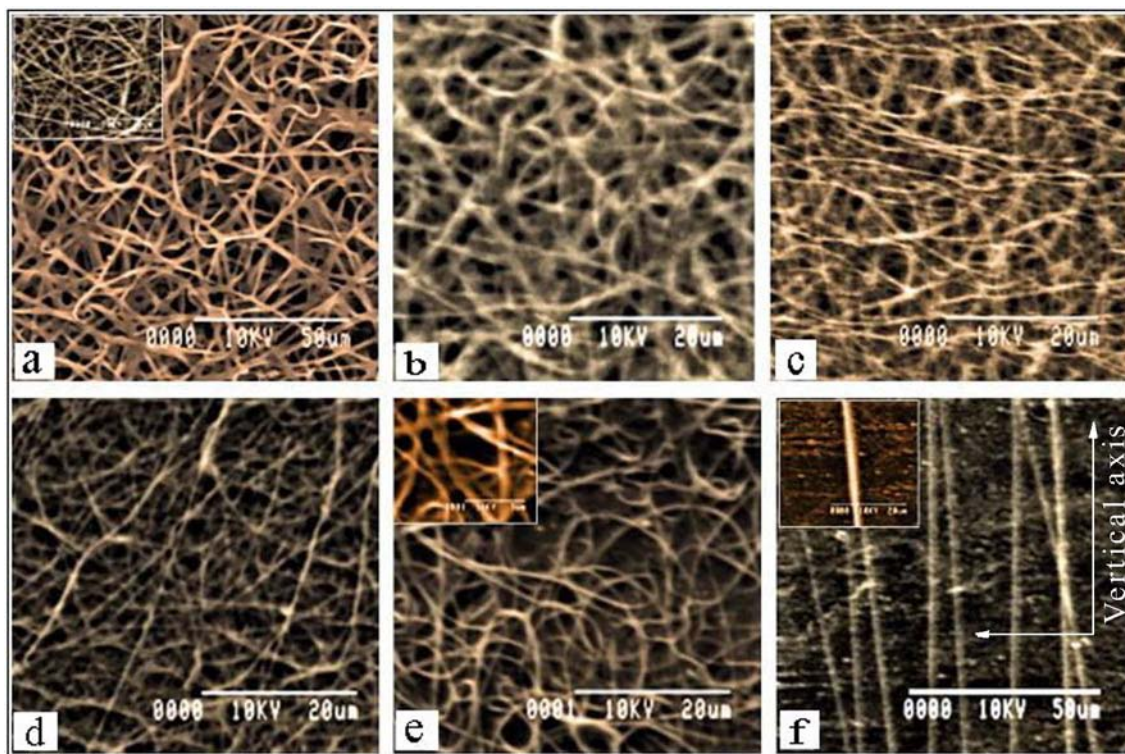


Figure 4.4. (a-e) are SEM images of randomly collected nylon 6 nanofibres containing various concentrations of MWCNTs from 0 to 4 wt. % respectively in 20 wt. % nylon 6/ formic acid solution, at 0.2 mL/h volume feed rate, 15 KV applied voltage and 8 cm electrospinning distance. (f) SEM image of aligned nylon 6 nanofibres with approximately uniform fibres diameter of 850 ± 50 nm at 4 cm space distance between the collection disks.

Figure 4.5, shows SEM images of aligned nylon 6 nanofibres containing various concentrations of MWCNTs from 1 to 4 wt. % in 20 wt. % nylon 6 solution, which are electrospun over the circular electrically grounded disks separated by a 4 cm distance [50]. The magnified images in figure 4.5, show that the aligned nanofibres are perpendicular to the axis of the collection disks and have a uniform fibre diameters distribution of $850 \text{ nm} \pm 50$ nm. These images also indicate that the enhanced stretching applied by the alignment mechanism could lead to a high polymer chain orientation and a better arrangement of the MWCNTs inside the fibre itself.

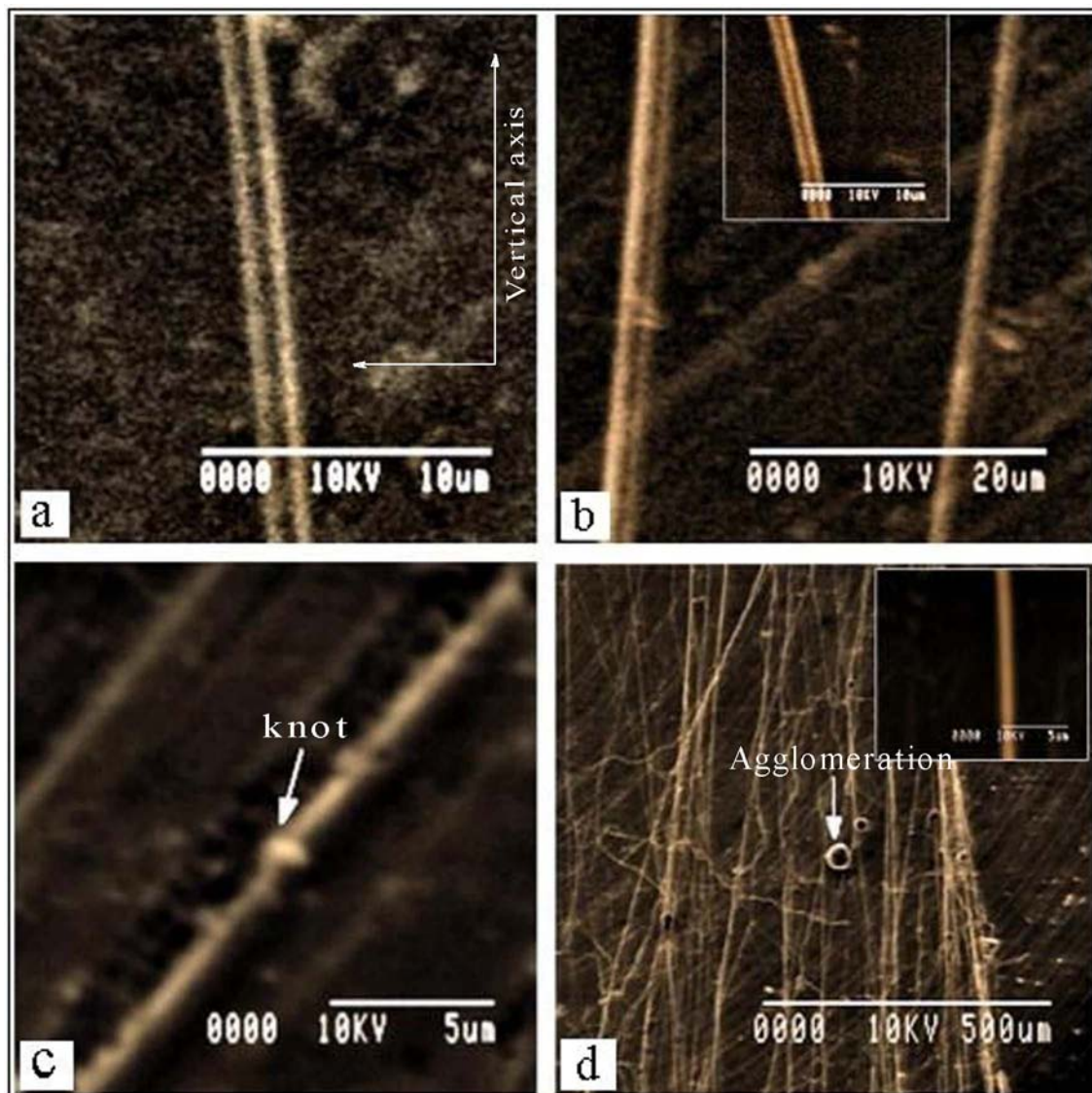


Figure 4.5, (a-d) are SEM images of aligned nylon 6 nanofibres containing various concentrations of MWNTs from 1 to 4 wt. % respectively; in 20 wt. % nylon 6/ formic acid solution, at 0.2 mL/h volume feed rate, 15 KV applied voltage and 8 cm electrospinning distance, electrospun between two circular disks at 4 cm distance between them. The protruded segments of MWCNTs which are not embedded and dispersed inside the nanofibre body are indicated by arrows in images (c), (d).

Due to different densities between MWCNTs and nylon 6, TEM images can show the MWCNTs inside the body of the electrospun nanofibres. Figure 4.6, shows TEM images of random and aligned nylon 6 nanofibres containing various concentrations of MWCNTs from 1 to 4 wt. % in 20 wt. % nylon 6 solution. Analysis of a large number of nanofibres, indicated by arrows in these images, shows that multi wall carbon nanotube particles were embedded well within the fibres as the loading of MWCNTs

decreases in the nylon 6 nanofibres. We can also observe that MWCNTs are aligned and straight along the direction of the fibre axis in the aligned nanofibres samples, whilst curvatures or knots are observed in the randomly collected nanofibre samples. We can conclude that by applying both electrostatic drawing (whipping) by electrospinning and geometrical-mechanical stretching by the alignment mechanism, a perfect longitudinal alignment of MWCNTs can be achieved across the fibre. Moreover, good insertion and uniform longitudinal distribution will improve the thermal conductivity, electrical conductivity and mechanical property of the MWCNTs/ polymer composite [35, 48]. It has been found by the TEM images however, that poor dispersion and interfacial contact of the MWCNTs occurs as the loading concentration increases more than 3 wt. %.

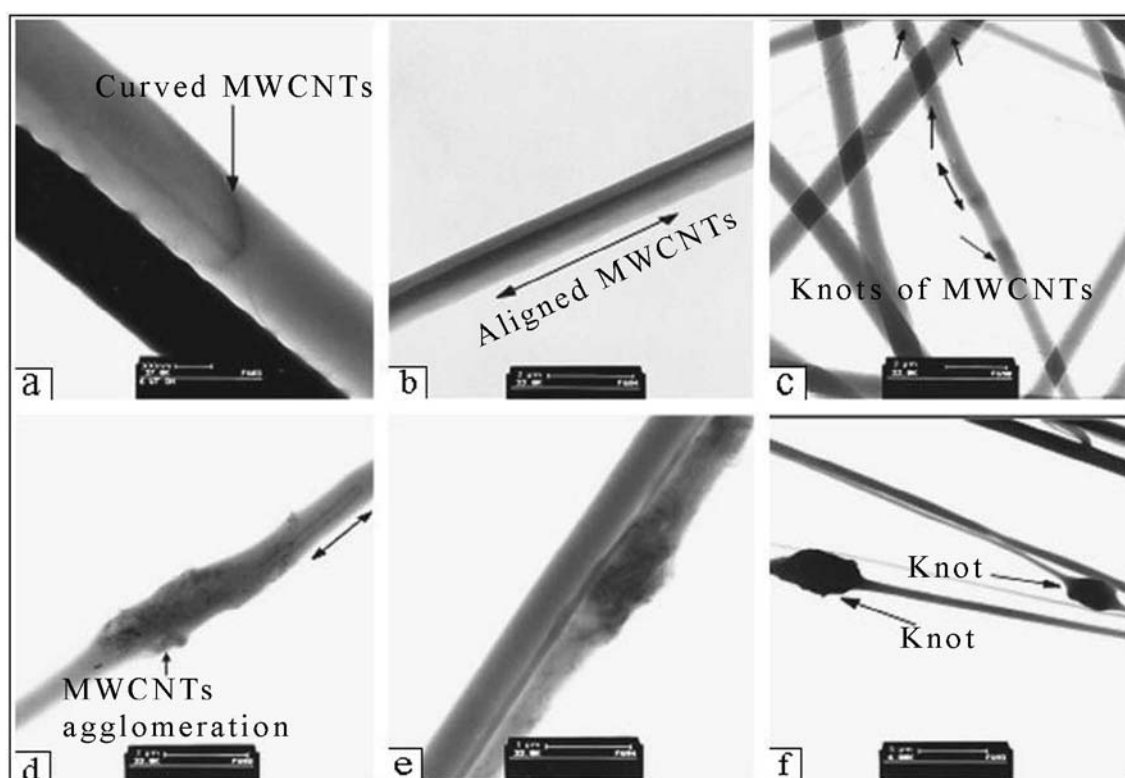


Figure 4.6, TEM images of random and aligned nylon 6 nanofibres containing various concentrations of MWCNTs; 1 to 4 wt. % in 20 wt. % nylon 6 solution. (a, b) show random and aligned nanofibres respectively with 1 wt. % of MWCNTs in nylon 6 nanofibres, (c) shows random nanofibres with 2 wt. % of MWCNTs, (d) shows individual nanofibres with 3 wt. % of MWCNTs, (e, f) show aligned nanofibres with 4 wt. % of MWCNTs. The arrows indicate that MWCNTs are straight in the direction parallel to the fibre axis being subjected to aligned collection, while curvature or knots are observed in the randomly collected nanofibres. (e, f) show poor dispersion for the MWCNTs with loading concentration more than 3 wt. %.

In fact, this is to be expected for two reasons: firstly, the stress resulted from agglomeration of MWCNTs at high load concentration and secondly, high loading of MWCNTs will increase the surface tension and viscosity of the polymer composite solution, leading to difficulties during the electrospinning process. Consequently, the optimum MWCNTs concentration for spinning aligned nylon 6 nanofibres composite is 1 wt. %. This provides the basic composite nanofibre material for the spinning of continuous yarns in the next chapter.

4.4.2 Challenges of improving the dispersion of MWCNTs in the polymer solution

Although, the properties of CNTs are well researched and understood, but uniform dispersion of CNTs into individual tube in the polymer solution remains a critical challenge. It has been argued that a technique for disrupting the surface uniformity ‘surface modification’ of the CNTs thereby reducing the van der Waals interaction between the tubes and preventing the tubes from re-agglomeration is needed to overcome this challenge [12]. Moreover, surface modification of CNTs induces tube matrix interaction resulting in better interfacial bonding and allowing load transferring across the CNTs matrix interface.

To do so, researchers have used a chemical modification through attaching functional groups to the surface of the CNTs, or a non chemical functionalization through wrapping the CNTs with a surfactant [12, 48].

Chemical modification is a chemical reaction process where the atoms on the surface of the tube are oxidized to carboxylic acid groups thus making covalent bonds to the polymer by esterification [48]. This process is time-consuming; hence it involves breaking the covalent bonds on the wall of the CNTs and forming new ones. Most importantly, it tends to damage the pristine structure of the nanotube and greatly reduce the tube properties [48].

While non chemical modification reduces the van der Waals attraction between tubes resulting in well separated tubes in the solution. Consequently, based on this modification technique, changing the polymer solution concentration or finding a specific surfactant ‘agent’ to be chemically suitable for the polymer solution is a solution key for optimum dispersion. Gum Arabic, as a dispersing agent, is one of the surfactant examples that being used in experimental research work [52].

Furthermore, investigating other dispersion agents and higher loading concentration of CNTs in the polymer solution will be an interesting further investigation, for improving nanofibres composite field.

4.5 References

- [4.1] F.K. Ko, K. Krauland, F. Scardino, *Weft insertion warp knit for hybrid composites*, Progress in Science and Engineering of Composites, Fourth International Conference on Composites, Japan Society for Composite Materials, Tokyo, Japan (1982)
- [4.2] J. Averston, G. Cooper, A. Kelly. *Properties of fibre composites*, National Physical Laboratory, IPC Science and Technology, Guildford, UK (1971)
- [4.3] S. Iijima, *Helical microtubules of graphitic carbon*, Nature, **354**, 56-58 (1991)
- [4.4] S. Iijima, *Single-shell carbon nanotubes of 1-nm diameter*, Nature, **363**, 603-604 (1993)
- [4.5] http://www.en.wikipedia.org/wiki/Carbon_nanotube accessed 04/08/2008
- [4.6] M.F. Yu, B.S. Files, S. Arepalli, R.S. Ruoff, *Tensile loading of ropes of single wall carbon nanotubes and their mechanical properties*, Physical Review Letters, **84**, 5552-5555 (2008)
- [4.7] J. Che, T. Cagin, W.A. Goddard, *Thermal conductivity of carbon nanotubes*, Nanotechnology, **11**, 65-69 (2000)
- [4.8] S. Frank, P. Poncharal, Z.L. Wang, W.A. Heer, *Carbon nanotube quantum resistors*, Science, **280**, 1744-1746 (1998)
- [4.9] K. Laxminarayana, N. Jalili, *Functional nanotube-based textiles: pathway to next generation fabrics with enhanced sensing capabilities*, Textile Research Journal, **75**, 670-680 (2005)
- [4.10] R. Andrews, M.C. Wiesenberger, *Carbon nanotube polymer composites*, Current Opinion in Solid State and Materials Science, **8**, 31-37 (2004)
- [4.11] P.J.F. Harris, *Carbon nanotube composites*, International Materials Reviews, **49**, 31-43 (2004)
- [4.12] H. Farzana, M. Hojjati, O. Masami, G.E. Russell, *Polymer-matrix nanocomposites, processing, manufacturing and application: an overview*, Journal of Composite Materials, **40**, 1511-1575 (2006)
- [4.13] M. Moniruzzaman, K.I. Winey, *Polymer nanocomposites containing carbon nanotubes*, Macromolecules, **39**, 5194-5205 (2006)
- [4.14] Z. Jia, Z. Wang, C. Xu, J. Liang, B. Wei, D. Wu, S. Zhu, *Study on poly(methyl methacrylate)/carbon nanotube composites*, Materials Science & Engineering, a: Structural Materials: properties, microstructure and processing, **A 271**, 395-400 (1999)
- [4.15] B. Safadi, R. Andrews, E.A. Grulke, *Multiwalled carbon nanotube polymer composites: synthesis and characterization of thin films*, Journal of Applied Polymer Science, **84**, 2660-2669 (2002)

- [4.16] P. Potschke, T.D. Fornes, D.R. Paul, *Rheological behavior of multiwall carbon nanotube polycarbonate composites*, *Polymer*, **43**, 3247-55 (2002)
- [4.17] O.N. Dong, D. Jae, D.H. Lee, J.Y. Lee, J.K. Jong, M. Jong, *Morphological characteristics of electrospun poly (methyl methacrylate) nanofibres containing multi-walled carbon nanotubes*, *Molecular Crystals and Liquid Crystals*, **464**, 137-144 (2007)
- [4.18] L.S. Schadler, S.C. Giannaris, P.M. Ajayan, *Load transfer in carbon nanotube epoxy composites*, *Applied Physics Letters*, **73**, 3842-3844 (1998)
- [4.19] D. Qian, E.C. Dickey, R. Andrews, T. Rantell, *Load transfer and deformation mechanisms in carbon nanotube-polystyrene composites*, *Applied Physics Letters*, **76**, 2868-2870 (2000)
- [4.20] K. Lozano, E.V. Barrera, *Nanofibre-reinforced thermoplastic composites I, Thermoanalytical and Mechanical Analyses*, **79**, 125-133 (2000)
- [4.21] Z. Jin, K.P. Pramoda, G. Xu, S.H. Goh, *Dynamic mechanical behavior of melt processed multi-walled carbon nanotubes/ poly (methyl methacrylate) composite*, *Chemical Physical Letters*, **337**, 43-47 (2001)
- [4.22] C. Bower, R. Rosen, L. Jin, J. Han, O. Zhou, *Deformation of carbon nanotubes in nanotube- polymer composites*, *Applied Physics Letters*, **74**, 3317-3319 (1999)
- [4.23] E. William, D. Russell, E. Gorga, *Morphological and mechanical properties of carbon nanotube polymer composites via melt compounding*, *Journal of Polymer Science part B: Polymer Physics*, **44**, 864-878 (2006)
- [4.24] G.E. Russell, R.E. Cohen, *Toughness enhancements in poly (methyl methacrylate) by addition of oriented multiwall carbon nanotubes*, *Journal of Polymer Science part B: Polymer Physics*, **42**, 2690-2702 (2004)
- [4.25] J. Moncy, V. Steinert, W. Brian, V. Thomas , R.D. Derrick, M.A. Abdalla, G. Price, G.M. Janowski, *Morphology and mechanical properties of nylon 6/MWNT nanofibres*, *Polymer*, **48**, 1096-1104 (2007)
- [4.26] J.S. Jeong, J.S. Moon, S.Y. Jeon, J.H. Park, P.S. Alegaonkar, J.B. Yoo, *Mechanical properties of electrospun PVA /MWNTs composite nanofibres*, *Thin Solid Films*, **515**, 5136-5141 (2007)
- [4.27] A. Agic, B. Mijovic, *Mechanical properties of electrospun carbon nanotube composites*, *Journal of Textile Institute*, **97**, 419-427 (2006)
- [4.28] B. Sundaray, V. Subramanian, T.S. Natarajan, *Electrical conductivity of a single electrospun fibre of poly (methyl methacrylate) and multiwalled carbon nanotube nanocomposite*, *Applied Physics Letters*, **88**, 143114-1 - 143114-3 (2006)

- [4.29] J.S. Jeong, S.Y. Jeon, T.Y. Lee, J.H. Park, J.H. Shin, P.S. Alegaonkar, A.S. Berdinsky, J.B. Yoo, *Fabrication of MWNTs/nylon conductive composite nanofibres by electrospinning*, *Diamond and Related Materials*, **15**, 1839-1843 (2006)
- [4.30] J.A.R. Eun, H. Kay, K.K. Kim, S.Y. Lee, H. Young, *Anisotropic electrical conductivity of MWCNT/PAN nanofibre paper*, *Chemical Physics Letters*, **413**, 188-193 (2005)
- [4.31] G.T. Wang, L. Zhongkui, C. Xueqing, K. Samrat, S. Ja-Seung, V.D. Michael, *Conducting MWNT poly (vinyl acetate) composite nanofibres by electrospinning*, *Nanotechnology*, **17**, 5829-5835 (2006)
- [4.32] M.M. Bergshoef, G.J. Vancso, *Transparent nanocomposites with ultrathin, electrospun nylon-4, 6 fibre reinforcement*, *Advanced Materials*, **11**, 1362-1365 (1999)
- [4.33] H.G. Hou, J. Jason, J. Zeng, Q. Li, D.H. Reneker, A.C. Greiner, Z.D. Stephen, *Electrospun polyacrylonitrile nanofibres containing a high concentration of well-aligned multiwall carbon nanotubes*, *Chemistry of Materials*, **17**, 967-973 (2005)
- [4.34] Z. Qinghua, C. Zhenjun, Z. Meifang, M. Xiumei, C. Dajun, *Electrospun carbon nanotube composite nanofibres with uniaxially aligned arrays*, *Nanotechnology*, **18**, 115611-1 – 115611-6 (2007)
- [4.35] F. Ko, Y. Gogotsi, A. Ali, N. Naguib, H. Ye, G. Yang, C. Li, P. Willis, *Electrospinning of continuous carbon nanotube-filled nanofibre yarns*, *Advanced Materials*, **15**, 1161-1165 (2003)
- [4.36] P. Kannan, S.J. Eichhorn, R.J. Young, *Deformation of isolated single-wall carbon nanotubes in electrospun polymer nanofibres*, *Nanotechnology*, **18**, 235707-1 - 235707-7 (2007)
- [4.37] S. Allaoui, H. Bai, M. Cheng, J.B. Bai, *Mechanical and electrical properties of a MWNT/epoxy composite*, *Composites Science and Technology*, **62**, 1993-1998 (2002)
- [4.38] T. Natsuki, M. Endo, T. Takahashi, *Percolation study of orientated short-fibre composites by a continuum model*, *Physica: A Statistical Mechanics and its Applications*, **352**, 498-508 (2005)
- [4.39] J.K.W. Sandler, J.E. Kirk, I.A. Kinloch, M.S.P. Shaffer, A.H. Windle, *Ultra-low electrical percolation threshold in carbon-nanotube-epoxy composites*, *Polymer*, **44**, 5893-5899 (2003)
- [4.40] F.H. Gojny, M.H.G. Wichmann, U. Köpke, B. Fiedler, K. Schulte, *Carbon nanotube-reinforced epoxy-composites: enhanced stiffness and fracture toughness at low nanotube content*, *Composites Science and Technology*, **64**, 2363-2371 (2004)

- [4.41] J.G.M. Ayutsede, S. Sukiraga, H.H. Ye, M. Chen, Y. Gogotsi, F. Ko, *Carbon nanotube reinforced Bombyx Mori silk nanofibres by the electrospinning process*, *Biomacromolecules*, **7**, 208-214 (2006)
- [4.42] F. Ko, S. Sachiko, G. Milind, A. Jonathan, *Electrospun carbon nanotube reinforced silk fibres*, World Intellectual Property Organization Patent, **WO045122** (2005)
- [4.43] C. Bower, R. Rosen, L. Jin, J. Han, O. Zhou, *Deformation of carbon nanotubes in nanotube-polymer composites*, *Applied Physics Letters*, **74**, 3317-3319 (1999)
- [4.44] L. Jin, C. Bower, O. Zhou, *Alignment of carbon nanotubes in a polymer matrix by mechanical stretching*, *Applied Physics Letters*, **73**, 1197-1199 (1998)
- [4.45] J.C. Kearns, R.L. Shambaugh, *Polypropylene fibres reinforced with carbon nanotubes*, *Journal of Applied Polymer Science*, **86**, 2079-2084 (2002)
- [4.46] Z.W.W. Yulong, W. Fei, L. Guohua, Q. Weizhong, *Elastic deformation of multiwalled carbon nanotubes in electrospun MWCNTs-PEO and MWCNTs- PVA nanofibres*, *Polymer*, **46**, 12689-12695 (2005)
- [4.47] S.D. McCullen, D.R. Stevens, R. Derrick, R.A. Wesley, O.S. Satyajeet, L.I. Clarke, G.E. Russell, *Morphological, electrical, and mechanical characterization of electrospun nanofibre mats containing multiwalled carbon nanotubes*, *Macromolecules*, **40**, 997-1003 (2007)
- [4.48] X.L. Xie, Y.M. Wing, X.P. Zhou, *Dispersion and alignment of carbon nanotubes in polymer matrix: a review*, *Materials Science and Engineering*, **49**, 89-112 (2005)
- [4.49] C.A. Cooper, D. Ravich, D. Lips, J. Mayer, H.D. Wagner, *Distribution and alignment of carbon nanotubes and nanofibrils in a polymer matrix*, *Composites Science and Technology*, **62**, 1105-1112 (2002)
- [4.50] M.B. Bazbouz, G.K. Stylios, *Novel mechanism for spinning continuous twisted composite nanofibre yarns*, *European Polymer Journal*, **44**, 1-12 (2008)
- [4.51] M.B. Bazbouz, G.K. Stylios, *Alignment and optimization of nylon 6 nanofibres by electrospinning*, *Journal of Applied Polymer Science*, **107**, 3023-3032 (2008)
- [4.52] W. Salalha, Y. Dror, R.L. Khalfin, Y. Cohen, A.L. Yarin, E. Zussman, *Single-walled carbon nanotubes embedded in oriented polymeric nanofibres by electrospinning*, *Langmuir*, **20**, 9852-9858 (2004)

CHAPTER 5: SPINNING NANOFIBRE YARNS

5.1 Introduction

Electrospinning enables production of continuous nanofibres, nonwoven fabrics and functionalized composite fibres and yarns. The art of changing the process parameters and applying and modifying different collection mechanisms enable researchers to develop interesting and novel materials with unique properties for a number of end uses. Although collection of random nanofibres is already being used for membranes, filtrations, tissue scaffolds and wound dressings, the application of these nanofibres need highly ordered and aligned architectures for yarn formation. Currently, various ordered structures such as aligned nanofibres, arrayed nanofibres and controlled deposition of the electrospun fibres have been achieved using different mechanical collection devices and the manipulation of the electric field [1-3].

Alignment of nanofibres is important for engineering nano structures, but most importantly, for enabling the twisting of aligned fibre bundles in achieving the ultimate formation of continuous nano yarns, which is the focus of this thesis. Due to the chaotic nature of the electrospinning jet motion and the nanometer size of the electrospun nanofibres, there had been very few attempts to spin yarns that are made out of electrospun nanofibres [3-5]. Despite considerable effort in trying to form yarns from nanofibre oriented bundles, further improvements in architecture, mechanical geometry, dimensions and dynamic motion of the collection system are needed for effective fibres assembling, orienting and yarn formation.

This chapter provides a critical account of the existing mechanisms for electrospun nanofibre yarn formation, and it also puts forward own design mechanisms as a stepping stone to the ultimate formation of continuous nano yarns. Nylon 6 aligned nanofibres and nylon 6 aligned nanofibres filled with MWCNTs at concentrations of 1 wt. % are electrospun into continuous yarn using a novel electro mechanical collection mechanism. The continuous yarn can be collected at a production rate of over 8 m/min. Basic studies in optimizing the yarn parameters such as twist speed and yarn linear density are investigated and further discussed. In addition, a novel electro mechanical mechanism for spinning core electrospun nano yarn is designed, investigated and implemented. These nano yarns are expected to find many applications in industrial and medical textiles for artificial muscles, actuators, protective clothing, high performance fabrics, tissue engineering, composites, automotive, aerospace and civil engineering applications.

5.2 Review of mechanisms for spinning nanofibre yarns

Several mechanisms have been developed to control the deposition of the electrospun nanofibres moving away from collecting disordered nanofibres to collecting ordered yarns by changing from static collection to dynamic collection or manipulating of the electric field with dynamic collection [3-5]. The results are promising, but further improvements are needed for effective fibre alignment in the yarn body architecture.

In this review, it is focused on the different designed mechanisms to obtain various modifications of nanofibre assemblies. This will allow researchers in the nanofibre engineering field to gain knowledge on the various concepts of nanofibre assemblies and how they are constructed for fabrication of yarn forms for meeting specific needs.

5.2.1 Nano yarn mechanisms based on dynamic mechanical devices

A schematic diagram of the mechanisms based on dynamic mechanical devices is shown in table 5.1.

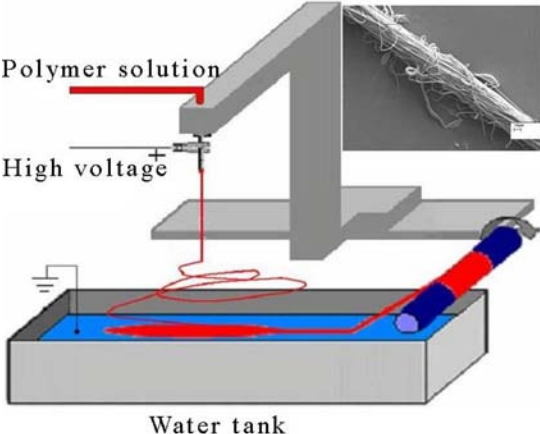
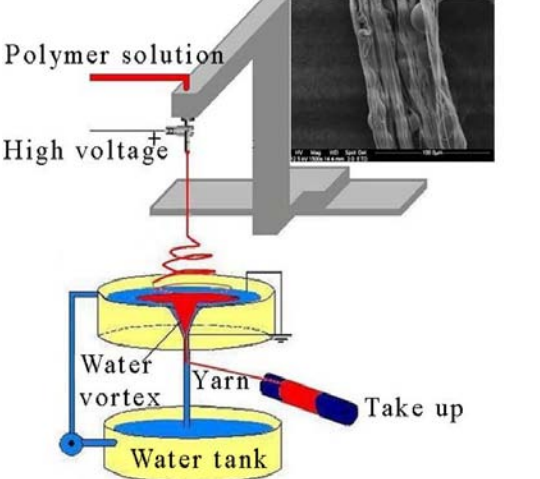
It has been suggested that a strand of electrospun porous filaments of nanofibres can be fabricated by spinning a polymer on the surface of a static water or organic solvent as a coagulation bath, then drawing it manually to a revolving take up roller [6-9]. In other words, a new mechanism which consists of a coagulating bath, a guiding bar system for guiding the nanofibre bundles and a take up winder is designed to make uniaxial nanofibres bundles of yarn.

Smit et. al. obtained a three dimensional round yarn structure by electrospinning nanofibres via a water bath and subsequently drawing the nonwoven web 'mesh' of nanofibres with the aid of a glass rod across the surface of the water and scooped off into air to a rotating roller above it [6]. The resulting yarn was drawn slowly by hand to a take up roller, then the roller was rotated at a speed of 3 m/min. The tension applied by the roller elongated the nanofibres in the direction of the length of the yarn. Yarns were fabricated with a textured appearance from electrospun polyvinyl acetate, polyvinylidene fluoride and polyacrylonitrile nanofibres using this mechanism. Khil et. al. used a similar set-up and fabricated porous filaments yarn but at a speed of 30 m/min [7]. They introduced electro wet spinning as a new possibility, based on the principle of phase separation in the polymer solution [10].

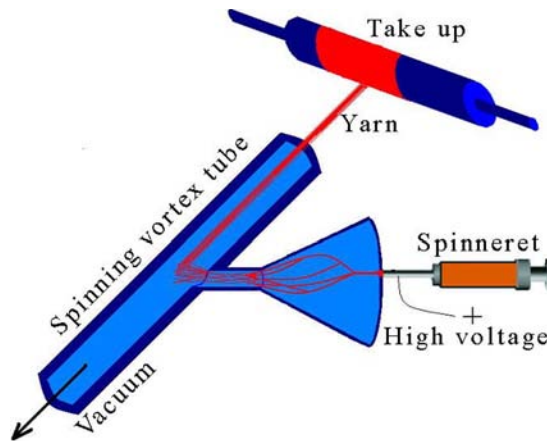
By using both distilled water and a mixture of distilled water/methanol to collect the nanofibres, they did not show any differences in the structure of the collected yarns. Polycaprolactone plain woven fabric was constructed with interlacing warp and filling filament yarns for tissue engineering. An air turbulence twister has been applied to the

resulted filaments yarn by other researchers for increasing cross linking between the nanofibres [11]. The yarn structure of this mechanism was observed to depend on many parameters such as the diameter of the electrospun nanofibres, the surface tension and viscosity of the liquid in the collection bath and the type of polymer. Surface tension of the liquid causes the fibre mesh to collapse into a yarn when it is lifted from the liquid surface to the rotating roller. Additionally, the viscose liquid may cause a higher drag force on the electrospun nanofibres as they are drawn to the edge of the collection bath and wound onto the roller. It should be observed however that, by randomly depositing fibres on the liquid surface, then rearranging them across the surface of the liquid and scooping them off in the air, before winding them by hand onto a take up roller, the act of spinning is being lost.

Table 5.1, Nano yarn mechanisms based on dynamic mechanical devices.

<p>1- Yarn collected by liquid bath.</p>  <p>Polymer solution</p> <p>High voltage +</p> <p>Water tank</p>	<p><u>Advantages</u> Simple mechanism. High production rate.</p> <p><u>Disadvantages</u> Bundled yarn. Liquid properties may cause arrangement difficulties. Manual collection. Lose the art of spinning. [6-9, 11], photograph reprinted from [6].</p>
<p>2- Yarn collected by dynamic liquid bath [13].</p>  <p>Polymer solution</p> <p>High voltage +</p> <p>Water vortex</p> <p>Yarn</p> <p>Water tank</p> <p>Take up</p>	<p><u>Advantages</u> High production rate.</p> <p><u>Disadvantages</u> Complicated mechanism. Bundled yarn. A few fibres do not stick tightly on the yarn. Manual collection. [12, 13], photograph reprinted from [13].</p>

3- Core electrospun yarn by air vortex tube.



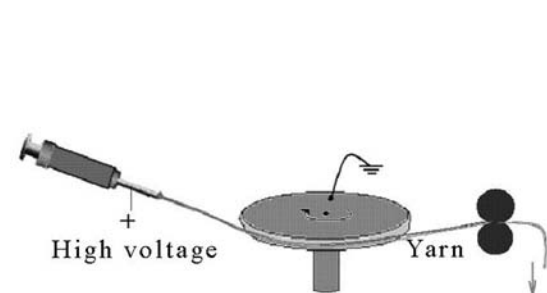
Advantages

Tubular structure.
Variety of applications.

Disadvantages

Low production rate as nanofibres stick on the wall of the tube.
Complicate mechanism and parameters.
Yarn helix is unclear.
[14].

4- Yarn collected with the aid of disk.



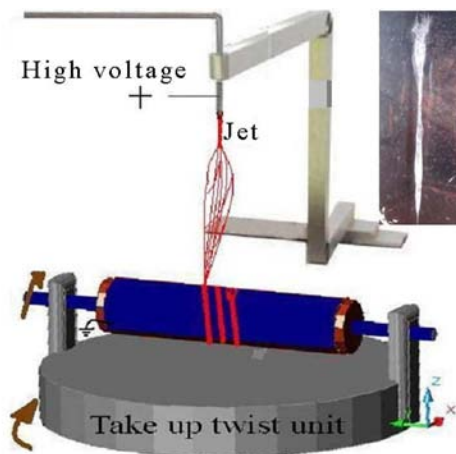
Advantages

No advantages.

Disadvantages

Difficult to apply.
Very low production rate.
Most nanofibres stick on the wall of the first delivering disk.
Yarn structure is unclear.
[16].

5- Yarn collected by compound rotated collector.



Advantages

Simple mechanism

Disadvantages

Entangled and unoriented nanofibres in the yarn body.
Wet yarn.
Yarn will stick on the surface of the collector.
[17, 18], photograph reprinted from [18].

Ramakrishna et. al. patented a modified dynamic liquid winding mechanism by using a vortex created from water flowing out from the bottom of a container 'basin' [12, 13]. The vortex was formed on the container through a hole of 5 mm diameter. A pump was used to recirculate the water from the tank back to the container and a rotating winder was revolved at a speed of over 60 m/min to collect the yarn emerging from the bottom

of the container. As the deposited nanofibres flow within the vortex, the nanofibre mesh elongates and consolidates in the direction of the flow of the water. In fact, in this mechanism, liquid properties such as surface tension, viscosity and hydrodynamic motion of the liquid play a great part in controlling the yarn structure. For example, when the random deposition of the nanofibres around the edge of the vortex is faster than the flowing water through the hole, entangled fibres will result in the yarn body, while with much faster vortex, the amount of fibres drawn down from the vortex become inconsistent. Although this is an improved mechanism, its main drawbacks are manual taking up of the fibres, unoriented and untwisted fibres in the yarn body and difficult control of the parameters.

Scardino et. al. also designed a mechanism by using an air vortex tube. They applied an air vortex spinning tube to impart twist to the drawn nanofibres as a sheath on a core filament, forming core filament yarn [14]. Although they presented a core electrospun yarn, no detailed discussion of the structure of the resultant yarn is given. It is observed that controlling the air vortex for depositing the nanofibre on the filament core in a helical manner is very difficult.

In a recent paper, Fennessey et. al. described the making of twisted 32 cm × 2 cm unidirectional electrospun nanofibres tow into yarn using an electrical twister [15]. Although they researched the effect of twist angle on the tensile strength and other mechanical properties of the yarn, no detailed description and discussion of the structure of the resultant yarn is given.

Some researchers have shown that it is possible to obtain continuous yarn by using a rotating earthed disk for delivering the electrospun nanofibres and an unearthed rotated roller separated at a certain distance for taking up the resulting yarn [16]. We can observe that it seems to be very difficult to implement this mechanism because the electrospun nanofibres stick on the surface of the delivering disk.

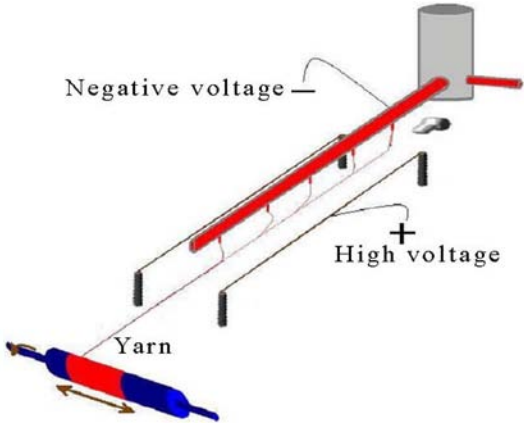
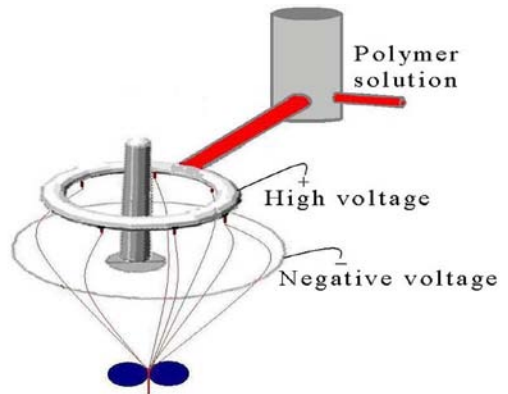
Ko et. al. developed continuous composite yarns of polylactic acid (PLA) and polyacrylonitrile (PAN) with single wall carbon nanotubes by collecting the electrospun nanofibres on a Z-Y plane rotated cylinder based on a rotated plate at X-Y plane [17, 18]. In accordance with their work wet, entangled and unoriented nanofibres were found in the yarn body. This is due to the evaporation rate of the solvent which should be studied in depth in further work.

5.2.2 Nano yarn mechanisms based on combining electric field manipulation and dynamic devices

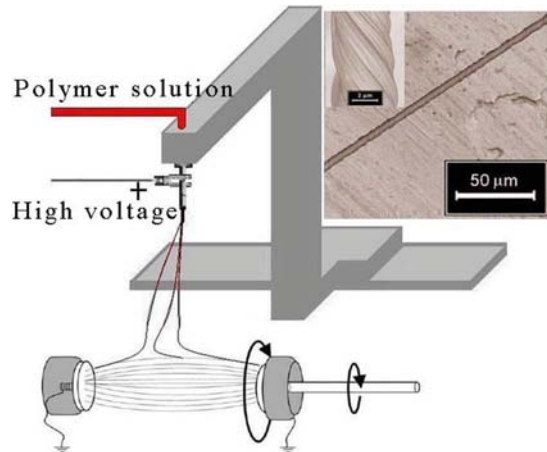
The manipulation of the geometric shape of the electric field and the dynamic motion of the collector make precise control of the deposition of electrospun nanofibres almost possible. A schematic diagram of the mechanisms based on combining electric field manipulation with dynamic devices is shown in table 5.2.

In the late 1930s, Formhals et. al. discussed many mechanisms for making continuous nanofibres yarn using parallel electrodes [19-21]. We have investigated these mechanisms in the experiments, and found that they are not able to spin uniform yarns. Multifilament twisted yarn has also been spun by suspending the electrospun nanofibres between two earthed plate electrodes and by rotating one of the electrodes [22, 23]. Although the yarn made from this mechanism has a very uniform helix and the fibres are aligned in the direction of the length of the yarn, the yarn was of limited length limiting its end use.

Table 5.2, Nano yarn mechanisms based on combining electric field manipulation and dynamic devices.

<p>1- Yarn Based on parallel electrodes.</p> 	<p><u>Advantages</u> Simple mechanism. High production rate.</p> <p><u>Disadvantages</u> Difficult yarn collection. Inapplicable. Nanofibres may be suspend between the two electrode wires. [19-21].</p>
<p>2- Yarn fabricated using negative ring electrodes.</p> 	<p><u>Advantages</u> Simple mechanism. High production rate.</p> <p><u>Disadvantages</u> Difficult yarn collection. Nanofibres may stick on the negative ring. [19-21].</p>

3- Yarn collected by rotating one of the dual electrodes form 1 [22].



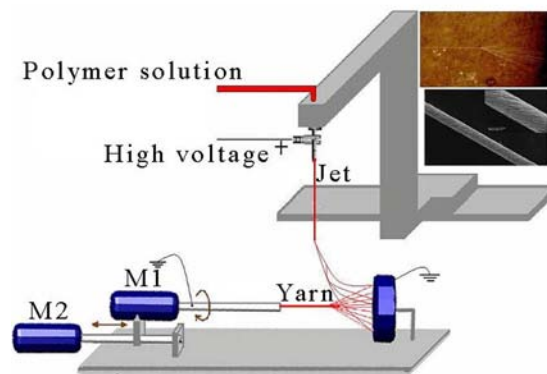
Advantages

- Simple mechanism.
- Ability to control the twist direction.
- Yarn structure with uniform helix.
- Nanofibres are aligned in the direction of the length of the yarn.

Disadvantages

- Yarn with limited length.
- Photograph reprinted from [22].

4- Yarn collected by rotating one of the dual electrodes form 2.



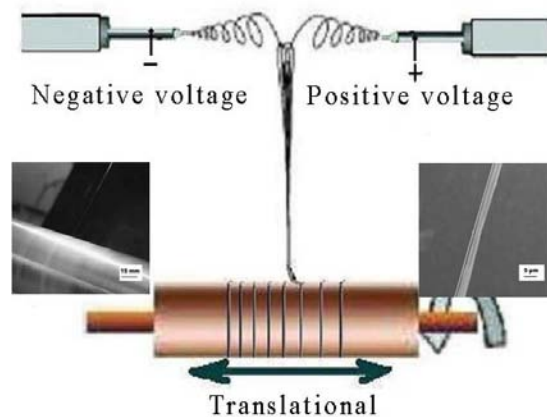
Advantages

- Simple mechanism.
- Ability to control the twist direction.
- Yarn structure with uniform helix.
- Nanofibres are aligned in the direction of the length of the yarn.

Disadvantages

- Yarn with limited length.
- [23], photograph reprinted from [23].

5- Yarn fabricated by opposite charged needles.



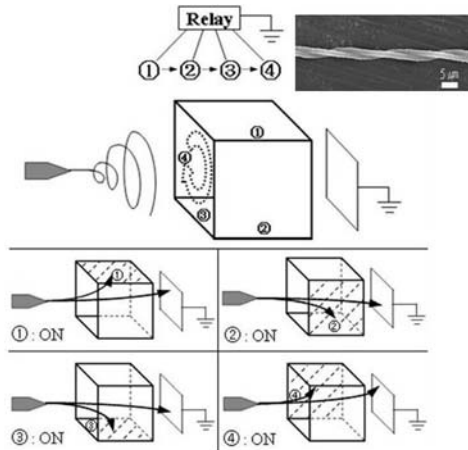
Advantages

- Simple mechanism.

Disadvantages

- Difficult to apply.
 - Entangled and unoriented nanofibres in the yarn body.
 - Curly yarn structure.
 - Manual yarn collection.
 - Difficult yarn extraction.
- [24], photograph reprinted from [24].

6- Yarn fabricated using polygonal electrode and relay [25].



Advantages

Ability to control the twist direction.

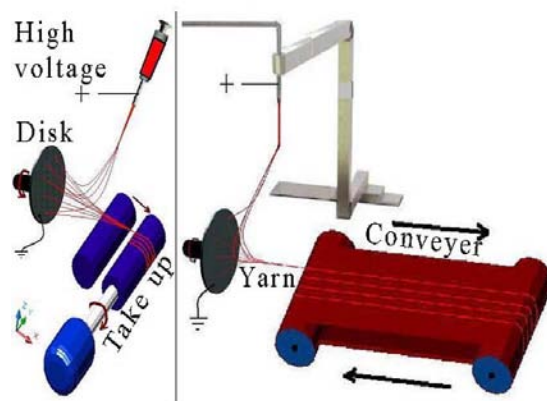
Disadvantages

Complicate mechanism.

Manual yarn collection.

Low production rate.

7- Continuous yarn collected by rotating one of the dual electrodes.



Advantages

Simple mechanism.

Ability to control the twist direction.

Continuous yarn.

Yarn structure with uniform helix.

Nanofibres are aligned in the direction of the length of the yarn.

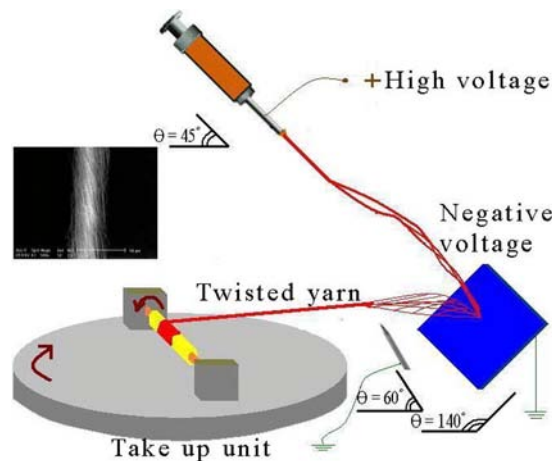
Disadvantages

Aligned nanofibres collected instead of Yarn.

Random jet suspension.

[26].

8- Yarn fabricated by manipulating the electric field via grounded bar.



Advantages

Continuous yarn.

Ability to control the twist direction.

Yarn structure with uniform helix.

Nanofibres are aligned in the direction of the length of the yarn.

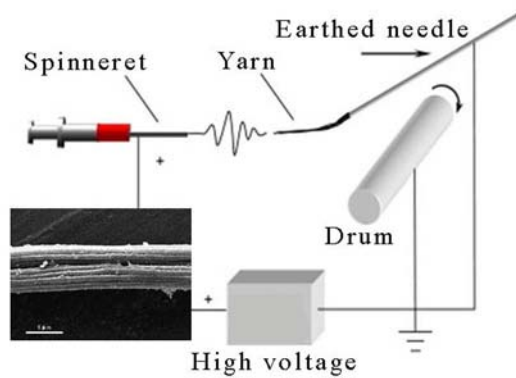
Disadvantages

Complicate mechanism.

Low production rate as most nanofibres stick on the negative surface.

[27], photograph reprinted from [27].

9- Self bundled yarn spun by manipulating the electric field via grounded bar [28].



Advantages

No advantages.

Disadvantages

Complicate mechanism.

First manual help.

Random jet suspension.

Difficult yarn extraction.

Difficult to apply, when it was tried.

Entangled and unoriented nanofibres in the yarn body.

[28].

Li et. al. presented a novel mechanism of manufacturing continuous yarn by using two oppositely placed metallic needles connected to a positive and negative voltage [24]. In this mechanism, positively charged nanofibres come into contact with negatively charged ones; they stick to each other at the center of the two needles after short time of electrospinning and then towed manually and wound onto a cylindrical collector rotating at a linear speed of 0.9 m/sec, forming continuous yarn. After towing the bundle of fibres manually to the rotating collector, the yarn is elongated by the mechanical tension of the rotating cylinder. In their experiment, they have indicated that the yarn structure is curly and that some fibres in the yarn body are not aligned well. It can also be observed that extracting the deposited yarn from a solid substrate without damaging the yarn is very difficult.

Kim et. al. reported a mechanism for fabricating twisted nanofibre yarn using polygonal electrode with four faces connected to a relay that transforms the applied electric field sequentially in the range of 0.001 to 1.0 sec [25]. When the electrical field was applied to each face of the electrode in a step-by-step way, the electric field was sequentially rotated around the electrode. In this mechanism, changing the direction of twist in the resulting yarn occurs by changing the direction of the electric field through limiting of the electrode and the relay time. However, this mechanism is complicated and sticking of the nanofibres on the electrode faces is difficult to overcome.

Another interesting mechanism for spinning continuous twisted yarn which has been patented [26], is using a rotated earthed disk and an unearthed rotated roller separated at a certain distance. However, no results on any yarn formation have been reported.

Ravandi et. al. designed a mechanism for spinning continuous uniaxially aligned PAN nanofibre yarn by electric field manipulation [27]. By employing a negative charged bar with a diameter of 0.3 mm in the electric field between the positive charged spinneret and negative charged delivering surface, nanofibres suspended between the negative surface and the take up unit as shown in table 5,2 (8). The bar was 21 cm below the spinneret, the negative surface was located 23 cm from the spinneret and 12 cm from the bar, the area of the negative surface was 6 cm×12 cm and the linear take up speed 14.064 m/h. Based on the experimental investigation, the unearthed take up unit used in this mechanism produced random deposition of fibres on the spinning surfaces.

Wang et. al. provided a simple mechanism for spinning continuous aligned electrospun nanofibre yarn using a grounded needle to induce the self bundling in the electrospinning process [28]. They have indicated that if a grounded metallic needle was used between the spinneret and the rotating collector, then self bundled nanofibre yarn will be formed. By pulling a yarn back and wind it on a grounded rotating collector, a nanofibre yarn is manufactured. They have concluded, however, that at the beginning of the process, as the surface speed of the rotating collector increases and as the conductivity of the polymer solution decreases, the electrospun nanofibres will only be deposited on the surface of the needle. In other words, the self bundling process will be broken down and as the electrospinning jet starts random whipping, random deposition of nanofibres is formed. Bent fibre loops were also observed in the yarn body making fluffy yarn appearance. Briefly, the stability of self bundling and the alignment of fibres in the yarn could be achieved for specific polymer solutions and operating parameters making this mechanism promising for some end uses.

Despite considerable efforts in trying to form yarn from nanofibre oriented bundles, further improvements in architecture, mechanical geometry, dimensions and dynamic motion of the collection system are needed for effective fibre assembling, orienting and spinning into a yarn.

5.3 Novel mechanism for spinning continuous nanofibre yarn [4]

Most of yarn mechanisms described above, involve at least three distinct steps, namely; aligned nanofibre manipulation, followed by twist insertion by means of an electric motor and take up unit.

Based on the alignment mechanism described in chapter 3, changing of the geometrical shape of the electric field by placing the two grounded disks under the spinneret splits the vertical electric field lines into two parts and thus aligns the electrospun nanofibres

between the two disks [2]. Through this concept, by rendering the first grounded disk as a twist disk and the second disk as a take up disk, spinning continuous nano yarn has been achieved. A schematic drawing of this mechanism is shown in figure 5.1.

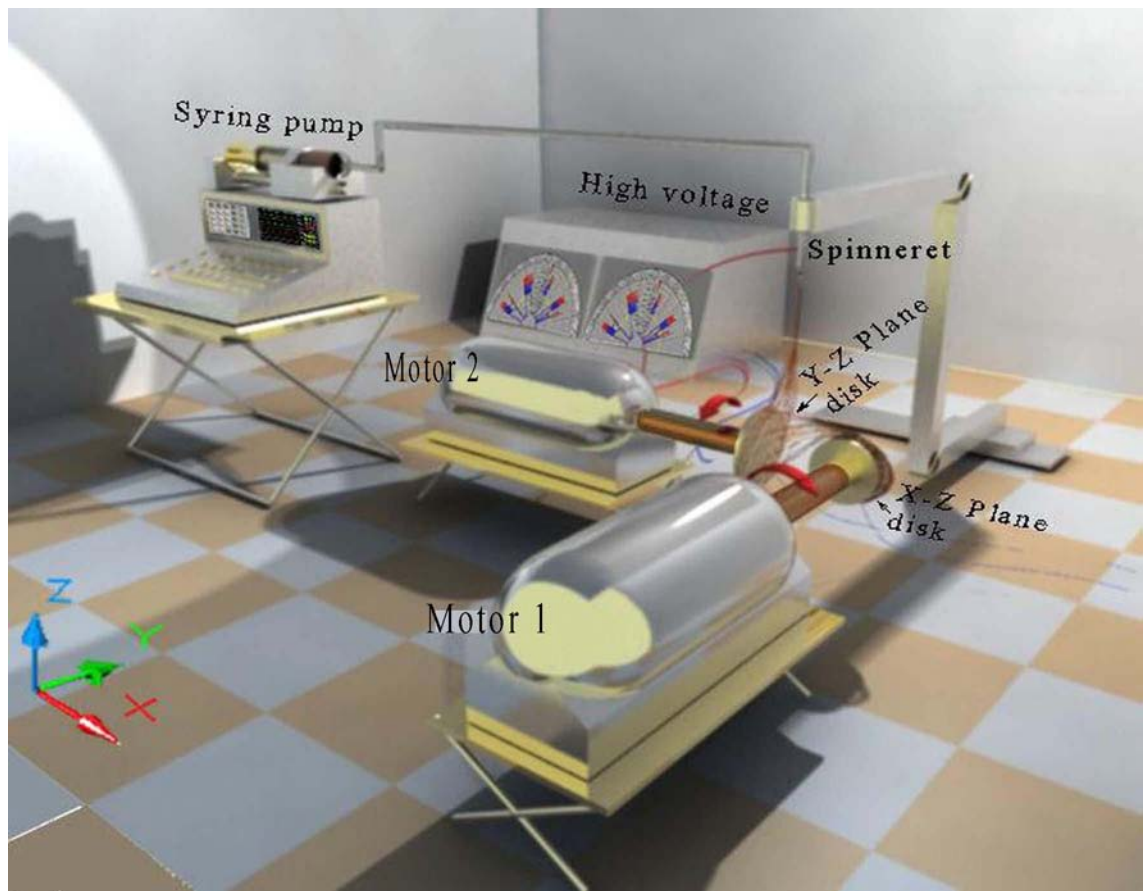


Figure 5.1, A schematic illustration of the set-up mechanism for assembling highly aligned nanofibres, suspended between two perpendicularly Y-Z plane to X-Z plane electrically grounded collector disks, for enabling spinning of continuous nanofibre yarn [4].

We have implemented an experimental spinning continuous nanofibre yarn mechanism by modification of the electric field in three dimensional domains in the space between the spinneret and the yarn twist and take up zone, as shown in figure 5.2.

The continuous yarn spinning mechanism involves collecting the electrically charged nanofibres between two perpendicularly Y-Z plane to X-Z plane electrically grounded collector disks.

The two disks are circular; the first is an earthed copper circular disk with dimensions of 60 mm diameter, 0.5 mm thickness and the second is a wider earthed circular disk with dimension of 40 mm diameter, 4 mm thickness separated by a distance of 4 cm from each other. The first copper circular disk is rotated around its axis by attaching it to a

motorized insulated shaft set to run at a controllable rotary speed to twist the fibre bundle into a nanofibre yarn. The yarn was wound on the take up disk which is also attached to a motorized insulated shaft set to run at a rotary speed equivalent to a linear take up speed of 8 m/min.

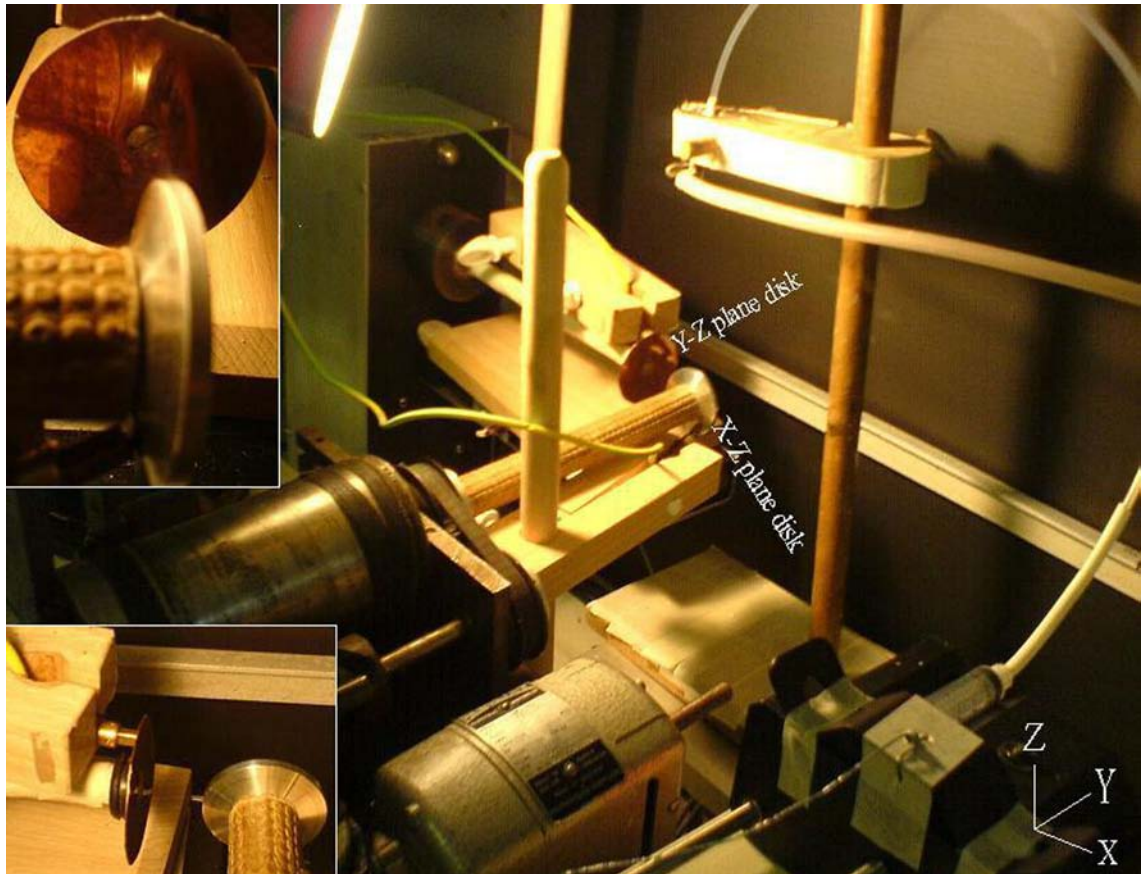


Figure 5.2, Photograph of the implemented mechanism used in the experiments for twisting highly aligned nanofibres suspended between two perpendicularly electrically grounded collector disks into continuous nanofibre yarn. The copper disk is the twist disk and the aluminium one is the take up disk, each disk is attached to a motorized insulated shaft to run at a controllable rotary speed.

This mechanism has been designed after careful consideration of literature and by investigating step by step the requirements for spinning continuous nano yarn, as shown in figure 5.3.

5.3.1 Experimental work

5.3.1.1 Spinning continuous nanofibre yarn / composite continuous nanofibre yarn

Nylon 6 solution of 20 wt. % concentration was prepared by dissolving the polymer in 98% formic acid. Nylon 6 solution for first case and nylon 6/MWCNTs solution with

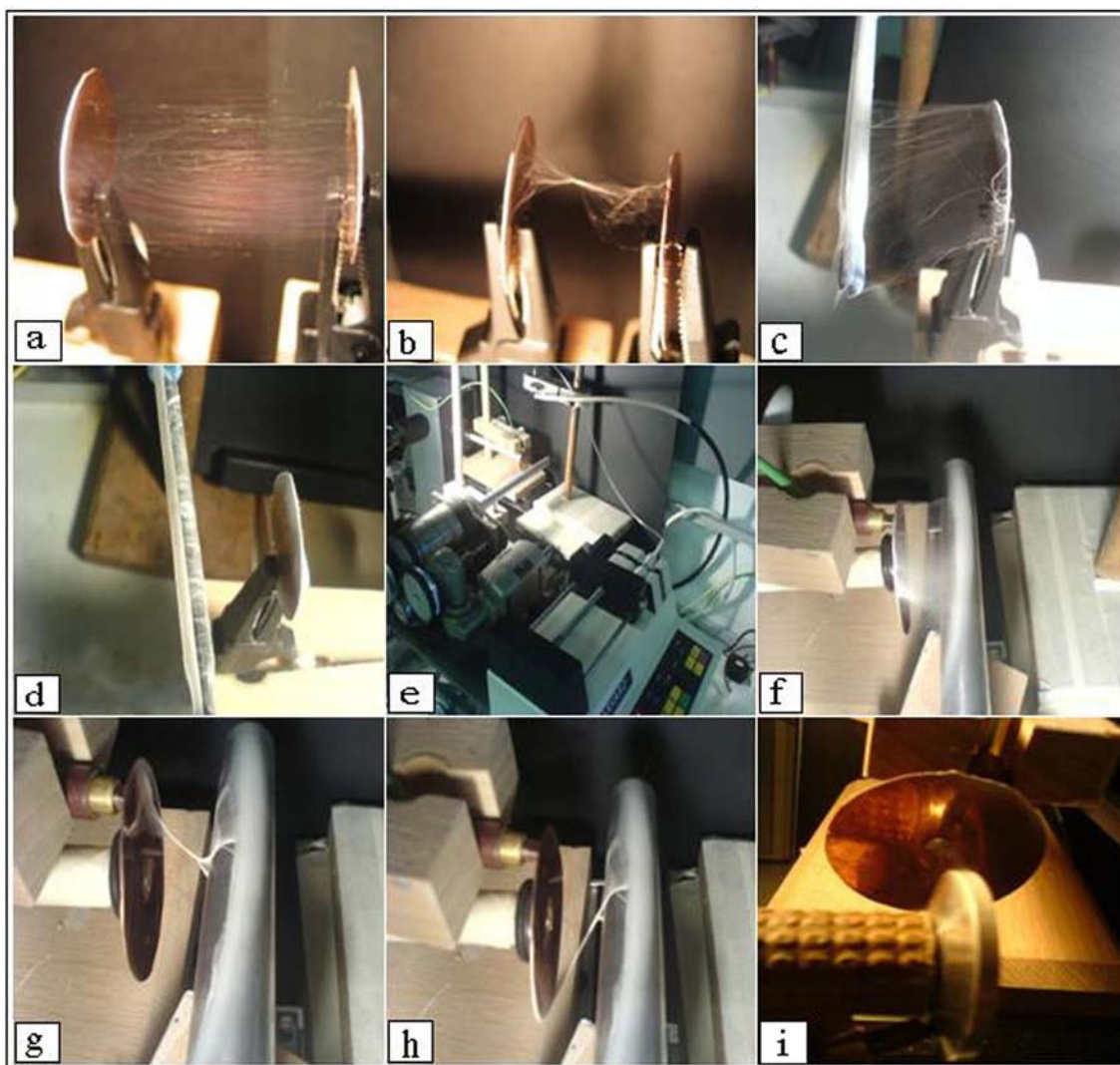


Figure 5.3, Recorded photographs showing how the mechanism was designed step by step, (a) shows highly aligned nanofibres suspended between grounded disks, (b) by rotating one of the disks, a twisted yarn was created, (c) one of the disks was replaced by glass rod for enabling continuous yarn production, (d) when the glass rod was rotated, broken yarns were taken up, (e) a mechanism was fulfilled consisting of a grounded disk and a grounded metallic rod instead of glass rod, (f) highly aligned nanofibres were suspended between the grounded disk and the grounded metallic rod, (g, h) failure in collecting continuous yarn by applying twist to the aligned nanofibres between the disk and the rod and thus the mechanism failed, (i) a continuous yarn mechanism has been developed.

optimized concentration of 1 wt. % for second case were fed through a 5 mL capacity syringe to a vertically orientated (25-gauge) blunt-ended metal needle via Teflon[®] tubing and the flow rate was controlled using a digitally controlled, positive displacement syringe pump Harvard apparatus M22 PHD 2000 (Harvard apparatus Ltd,

Edenbridge Kent, UK). The needle ‘spinneret’ was held by one electrode connected to a high voltage DC power supply; a Glassman MK35P2.0-22 (Glassman High voltage INC, New Jersey, USA). Typical operating regimes at flow rates of 0.2 ml/hr, applied voltages of 15 KV and a working distance of 8 cm were employed. These parameters were used for producing uniform diameter distribution of nylon 6 nanofibres based on chapter two and three [2]. Conically aligned fibres were appeared perpendicularly over Y-Z plane and X-Z plane electrically grounded disks which are separated by 4 cm space distance. The yarn was wound on take up disk which is set to run at a rotary speed equivalent to a linear speed of 8 m/min. The twist effect on the yarn was investigated by changing the rotation speed of the Y-Z plane disk of 100, 250, 500, 750 and 1000 rpm.

5.3.1.2 Characterization

Samples of continuous yarn and continuous composite yarn were collected on SEM stubs. Two separate tapes of aluminum sheet were laid on the surface of the circumference of the thicker disk (spool) for enabling the collection of two samples of yarns at different twist speeds.

These samples were sputter-coated with gold-palladium for 45 seconds at 18 mA using a Polaron Sc7620 sputter coater. Yarns were examined using a Hitachi S-530 scanning electron microscope at an accelerating voltage of 10 kV. Micrographs were taken at three random areas of each sample between 20,000 and 40,000 times magnification. An optical microscope (Diaplan, Germany) with soft imaging system (Altra 20, UK) was used to capture images for measuring the yarn diameter. Square holed carton frame was positioned under the yarn in the spinning zone/take up disk after seconds of electrospinning for enabling the collection of yarns for microscope optical images.

5.3.2 Results and discussion

5.3.2.1 Spinning continuous nanofibre yarn

Yarn spun from fibres with fine diameter will have a higher surface area and strength compared to another that is spun from fibres with larger diameter [29-31]. Taking into account the efforts of other researchers, we propose a mechanism to spin a yarn, based on the conventional spun yarn principle, of aligned fibres and fibre migration along the yarn forming a helix structure as shown in figure 5.4.

In this mechanism, the two disks are earthed, hence the earthed charges will attract the fibres to the disks, leading to the alignment of the fibres conically in the gap between the disks. The electric field and disk geometrical shape enable to precisely control the

deposition of the electrospun nanofibres. A controlled rotation is applied to the thin disk, which imparts twist in the fibres bundle. The twisted bundle is continuously wound on the take up thicker disk (spool) at a linear speed of 8 m/min.

In a recent patent [26], Lee et. al. have used a rotated earthed disk and an unearthen rotated roller separated by a certain distance to spin continuous yarn, but the unearthen rotated roller used in their mechanism has produced random deposition of nanofibres, as shown in the experiment in figure 5.5.

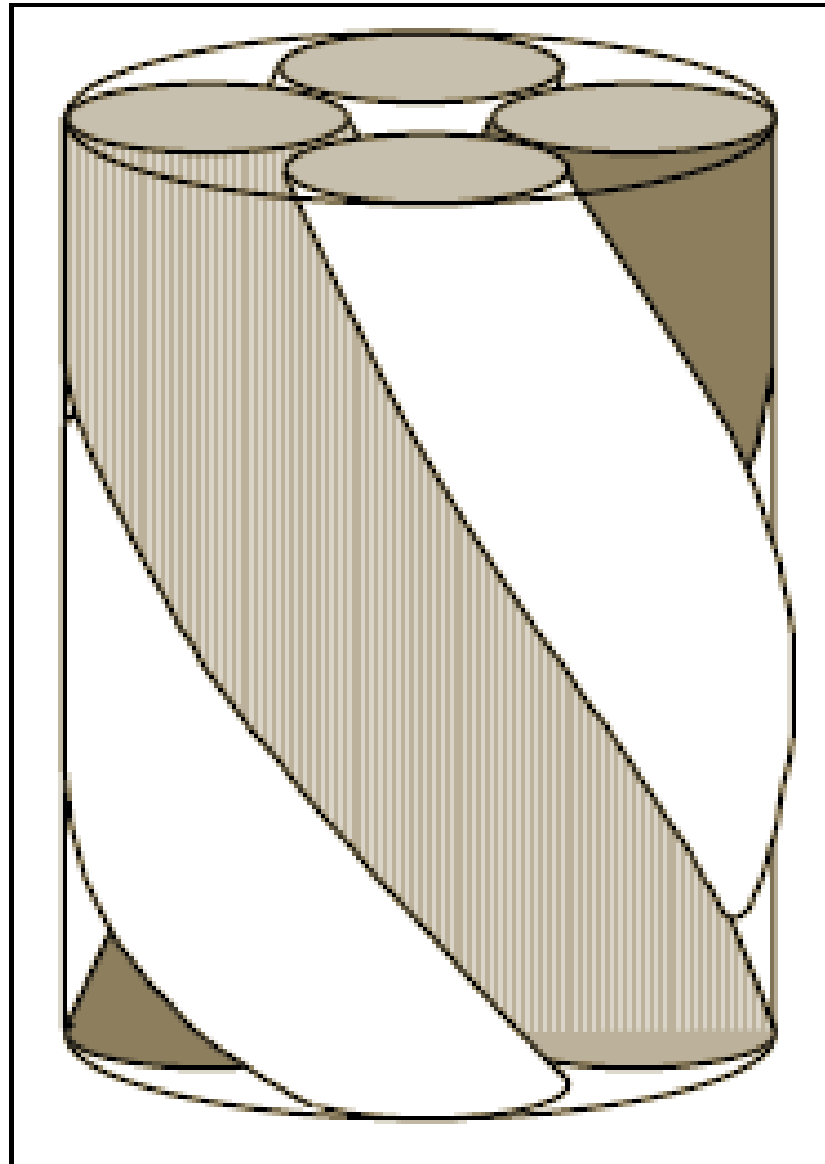


Figure 5.4. A schematic illustration of the fibres in the helical structure of the yarn; photograph was reprinted from [32].

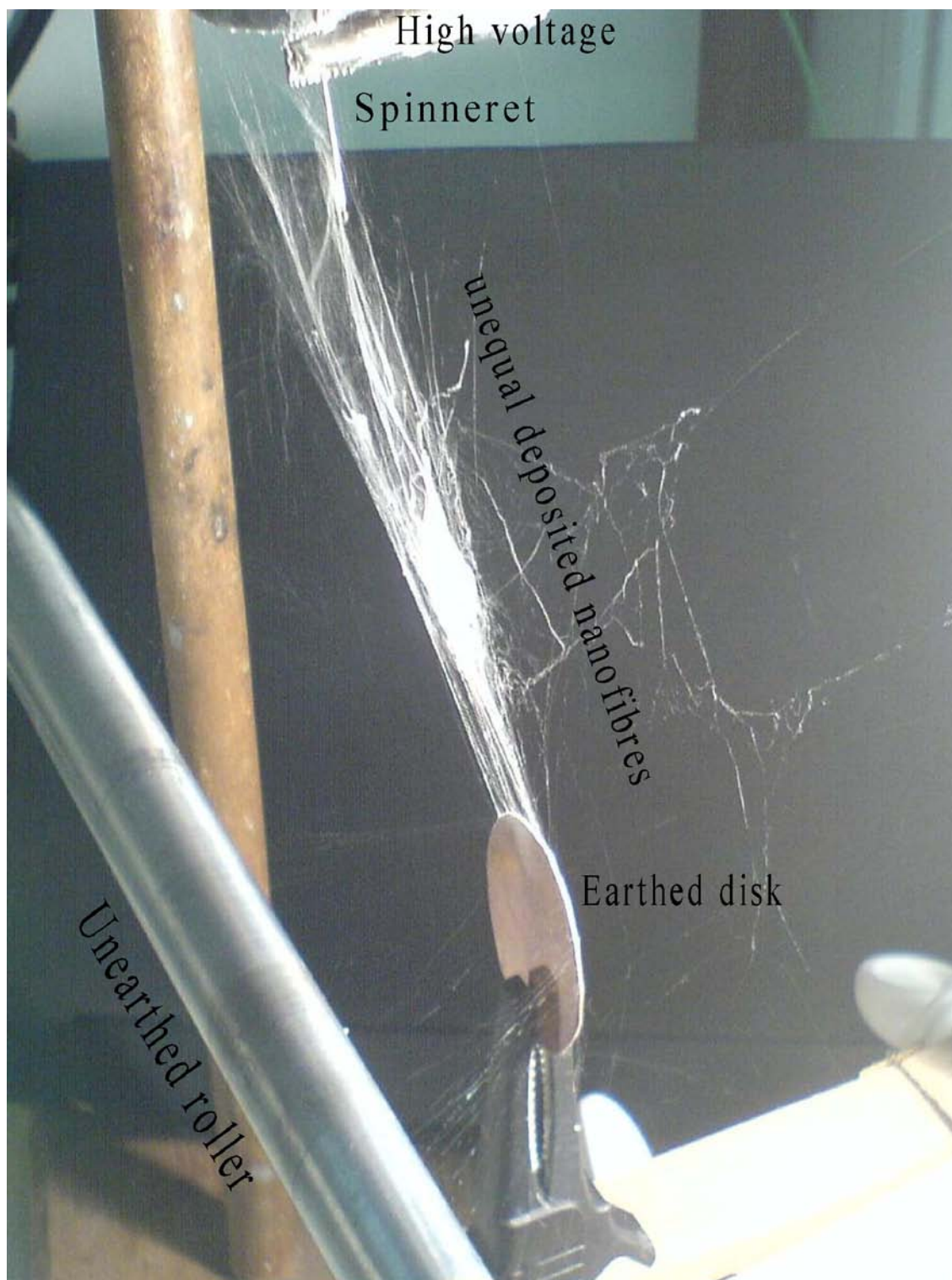


Figure 5.5. A photograph of unequal deposited nanofibres in the spinning zone between an earthed disk and an unearthed rotated roller for spinning continuous yarn.

Specifically, we produce yarn of twisted electrospun MWCNTs/ nylon 6 composite nanofibres, in diameter of 7 ± 0.5 microns which is shown in figure 5.6, [33]. Figure 5.7, shows that a spinning triangle of nanofibres was formed and the yarn was twisted during taking up. The structure of the yarn, as shown by SEM images in figure 5.9,

indicates that the fibres in the yarn are parallel, highly aligned and migrated in the direction of the yarn axis to form the required geometric helical structure. In this mechanism, the yarn linear density is affected by the number of electrospun fibres per unit time, their velocities and the take up speed.

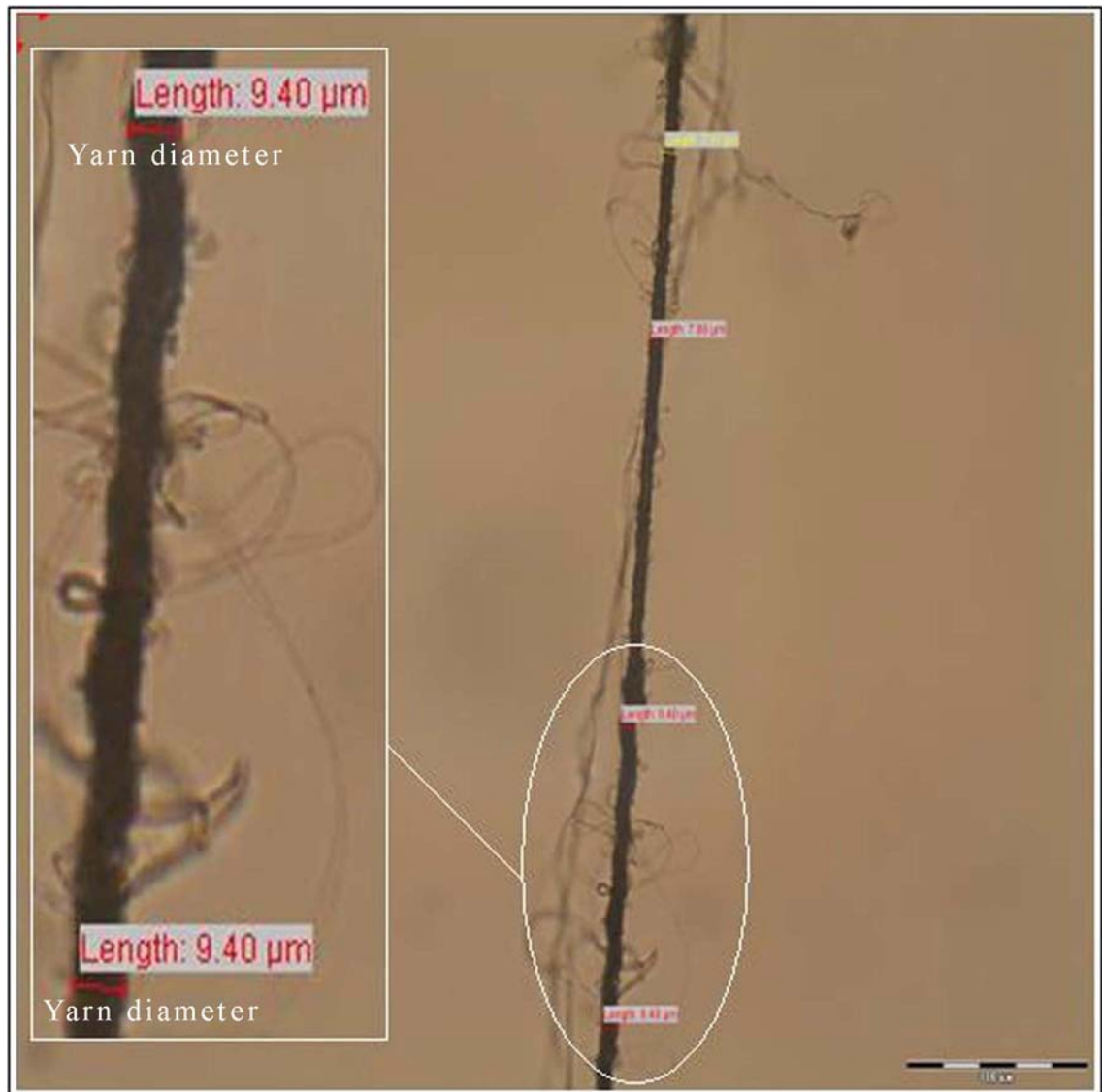


Figure 5.6, A microscopic image of continuous nanofibres yarn spun at 750 rpm twist speed and 8 m/min with diameter of 9.40 microns [33].

This work has shown that fabrication of continuous yarn can be achieved from any type of polymer or composite polymer blends under different linear density and twist level. Spinning super fine continuous yarn is of great significance for many applications, medical and industrial such as filters and sanitary pads, protective clothing and light composites for automotive and aerospace use.

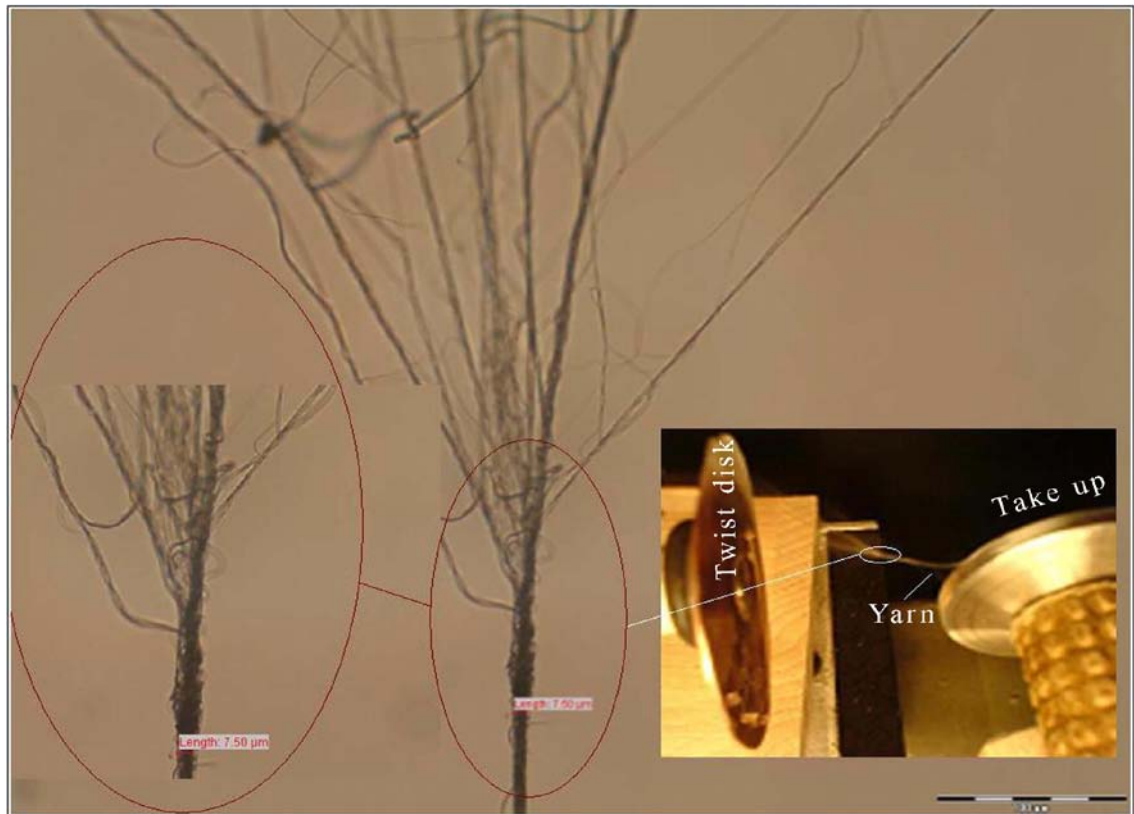


Figure 5.7, A microscopic image and photograph showing that the spinning triangle was formed and the yarn was twisted during taking up [33].

5.3.2.2 Controlling the yarn linear density and twist per unit length

Figure 5.8, shows photographs of continuous yarns produced by the mechanism. Different twist speeds at 100, 250, 500, 750 and 1000 rpm were applied to the suspended conical nanofibres bundle for providing the required inter fibre lateral cohesion interaction and friction. As can be observed from these photos, as the twist speed increases the suspended conical nanofibre are bundled together to form denser continuous yarn. Additionally, the tension applied through the drawing forces by the rotating spool straightens the fibres in the direction of the yarn axis. Figure 5.9, shows SEM images of collected continuous yarns at different twist speed, ranging from 100, 250, 500, 750 and 1000 rpm at a constant linear take up speed of 8 m/min. These images show twisted nanofibre yarns with diameters ranging from 5 to 10 microns. There seems to be unoriented (wavy) yarns at the lowest twist speed as shown in figure 5.9(a), and straight, aligned and fine yarns at the highest twist speed as shown in figure 5.9(e).

By analyzing these images, we can see that a twist speed between 500 and 750 rpm is adequate for spinning continuous yarn in relation to the operating process parameters (flow rates of 0.2 ml/hr, applied voltages of 15 KV and an electrospinning distance of 8

cm at a linear speed of 8 m/min. These operating parameters are influencing the number of nanofibres extruded from the spinneret per unit time to the yarn spinning zone and their velocity.

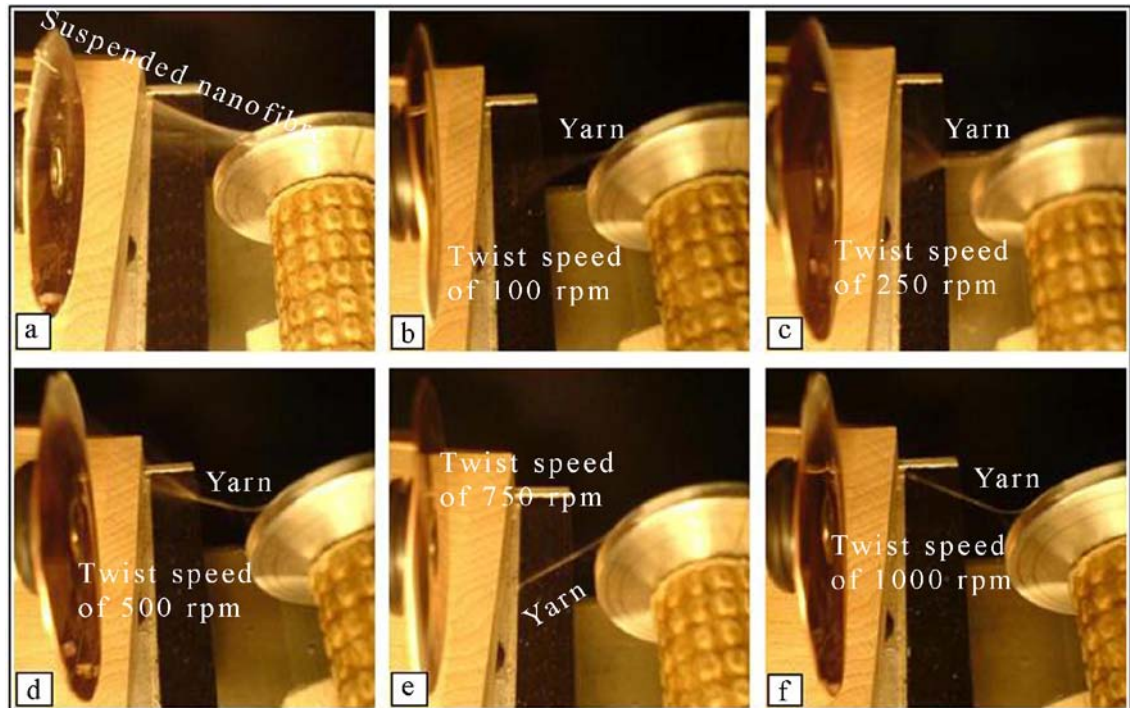


Figure 5.8, (a) A photograph of suspended aligned 1 wt. % of MWCNTs in nylon 6 nanofibres. (b-f) are photographs showing the mechanism for spinning continuous yarn at different twist speeds of 100, 250, 500, 750 and 1000 rpm respectively, and taking up the yarn at a constant linear speed of 8 m/min.

We believe that the number of nanofibres generated at the spinneret, their velocities, twist and take up speed are essential parameters to control the yarn diameter, yarn linear density and twist per unit length. Little or no information has, however, been reported on the mathematical model for predicting the number of nanofibres brunches erupted from the electrospinning jet per unit time and their velocities [34-40]. This mathematical model will be investigated in detail in the next chapter, so that the take up speed for different twist speeds and yarn linear density can be optimized.

5.3.2.3 Challenges of yarn collection for future work

Obtaining continuous twisted yarn from electrospun nanofibres is still a challenge for many researchers despite the various reported successes obtained with different nano spinning architectures [3, 5]. This is attributed to the difficulty of the electrospinning process in controlling the jet path flight and the precise deposition of nanofibres and in

the lack of evaporation of the solvent. Although, the presence of solvent as a liquid in the yarn may act as a lubricant that allows slipping of the individual fibres without breaking them and its surface tension will further compress the yarn into a tight bundle, its presence however leads to yarn sticking on the take up spool. The sticking phenomenon in spinning continuous yarn is a really a serious problem and needs further research.

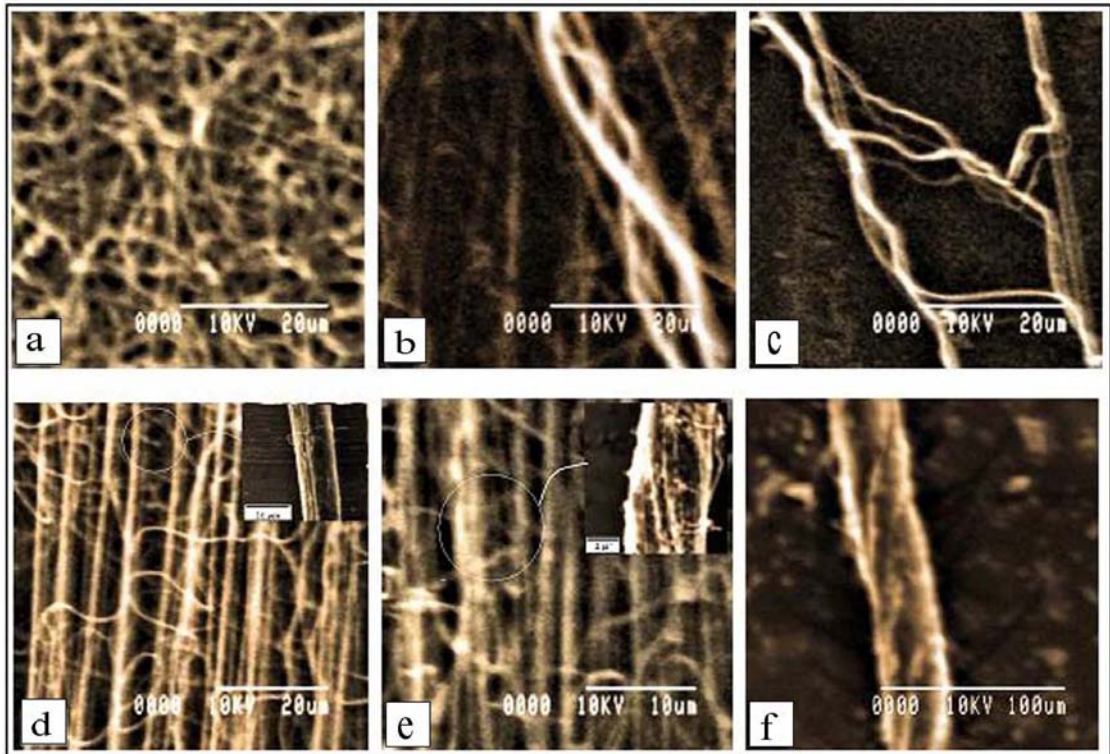


Figure 5.9, (a-e) show SEM images of electrospun continuous yarns at different twist speeds of 100, 250, 500, 750 and 1000 rpm respectively; at linear take up speed of 8 m/min. (a) represents unoriented (wavy) yarns, (e) represent straight, aligned and fine yarns. (f) shows plied yarns produced with 40 microns diameter.

From our own investigations, we can suggest that one has to find a way of completely drying the nanofibres before depositing them on the yarn zone or within the yarn zone. Consequently, we introduce changing of ‘electrospinning’ as ‘electro dry spinning’ to ‘electro melt spinning’ as it is more effective for spinning continuous yarn wound on the take up spool without sticking, provided the cooling process is investigated. Another suggestion, from the investigation, is to change the take up spool material structure by either coating the metallic spool with suitable lubricant or changing the metallic spool into another material. In order to highlight this, we replaced the grounded metallic spool by a glass one and we put a grounded needle 2 mm before the glass spool for

manipulating and directing the electrical field, as in the mechanism by Ravandi et. al. [27], as shown in figure 5.10.

Although continuous nanofibre yarn was spun and wound onto the glass spool, extracting the yarn without damage was proved difficult. Sticking of the yarn on the spool is still present and thus the glass spool did not prove advantageous. We also tried to irrigate the metallic take up spool with hot distilled water by a glass pipette during electrospinning. Hot water was used as it has lower surface tension than cold water and is suitable for consolidating of electrospun nylon 6 nanofibres and the resulting yarn. However, little or no success has been achieved by this change.

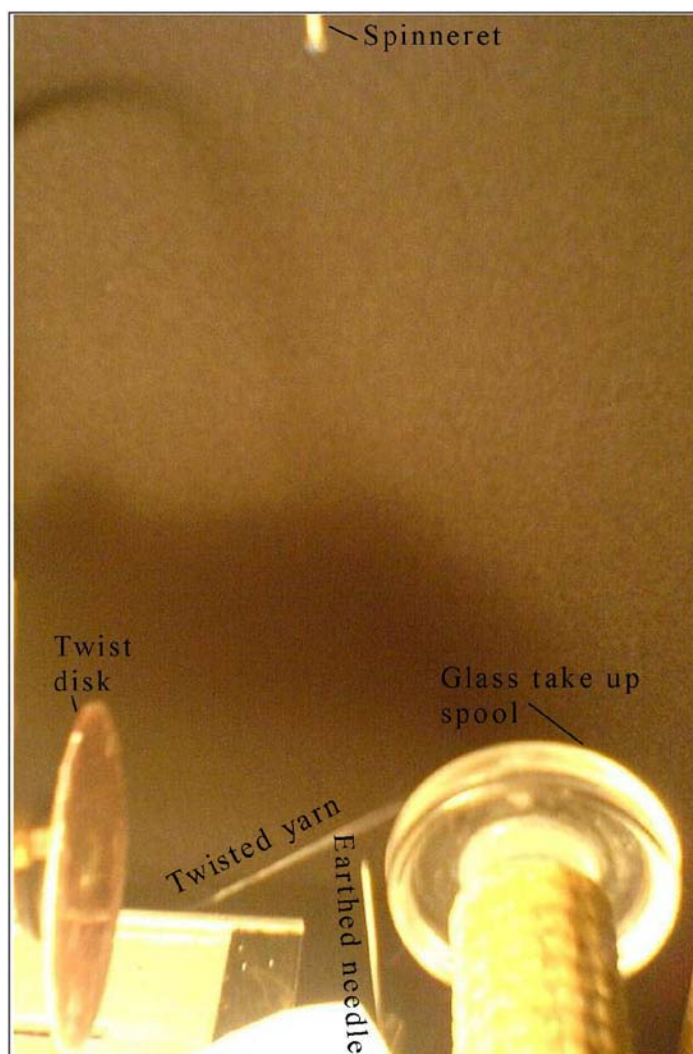


Figure 5.10, A photograph of continuous nanofibres yarn spinning zone with replacing the metallic take up spool by glass one and introducing the grounded needle.

Two further suggestions in this trial are put forward for future work. The first one is to control the evaporation rate of the solvent from the nanofibres until fully dried. The second is to coagulate the solvent during evaporation by putting the spinning zone

devices in a compatible liquid bath suitable to the polymer solution used [51], provided we can control the imparted twist in the liquid medium during nanofibre yarn formation. Controlling the yarn linear density, its uniformity and the twist per unit length are also important in nanofibre yarn formation. This can be achieved by knowing the number per unit time and velocity of the nanofibres extruded from the spinneret and deposited on the spinning yarn zone. A mathematical model is being investigated for predicting the kinetic properties of electrospun nanofibres. This will be presented in the next chapter.

Briefly, we believe that the number of nanofibres generated at the spinneret, their velocities, twist and take up speed are essential parameters to precisely control the yarn diameter, yarn linear density, twist per unit length and its mechanical properties. This will enable researchers to improve this mechanism and to increase production of nano yarns.

5.4 Core electrospun yarn

A core spun yarn is defined as ‘a structure made of a separable core constrained to be permanently at the central axis and surrounded by fibres which act as a sheath’ [41]. The mechanical behavior of such structures is governed by fibre characteristics such as length, fineness, tenacity, breaking extension and friction and by the core spun yarn characteristics such as fibre deposition and arrangement, core to sheath proportion of fibres, frequency of wraps around the core, twist angle of the fibres, packing, mass variation, etc [42]. The manufacturing process mainly consists of feeding the filament to a conventional spinning unit, where it is covered by natural or synthetic staple fibres by a suitable mechanical arrangement. Cotton spandex (elastane) yarns which are composite yarns consisting of elastane core wrapped helically by cotton staple fibres are a well known example of elastic yarns widely used in the textile industry.

The physical properties of core spun yarns depend on the sheath properties such as the fibre length, its fineness and the type of fibre. In other words, sheath constructed of small diameter fibres that must be wrapped by the same length of fibres, will result in a higher number of wrapping turns [43, 44]. This will lead to a higher surface area to volume ratio and thus more uniform morphology and usually higher yarn strength. Although, there is some prior research in which the core electrospun yarn principle is introduced, the mechanism used rendered the nanofibres to randomly cover the core without producing orderly structured yarn [14, 45].

In this study, we have designed a new mechanism and via extensive experimentation and optimization of this system we are able to produce an ordered nano yarn which can be defined as ‘a composite nano yarn structure made of a separable core in the central axis and surrounded helically by electrospun nanofibres which act as a sheath’. With this new mechanism, we were also able to analyze the effects of the nanofibre twist, the feeding angle of the core filament ‘core feed-in angles’ and the take up speeds on the structure of the resultant nano yarn.

5.4.1 Novel mechanism for continuous core electrospun yarn [52]

From continuous nanofibre yarn mechanism described in this chapter which forms as the basis of this development [4], we have designed a new mechanism for producing continuous core electrospun nano yarn. The aim is to wrap helically the deposited nanofibres on the feeding core filament, resulting in a core electrospun nano yarn with a structure similar to the core ring spun yarn shown in figure 5.11.

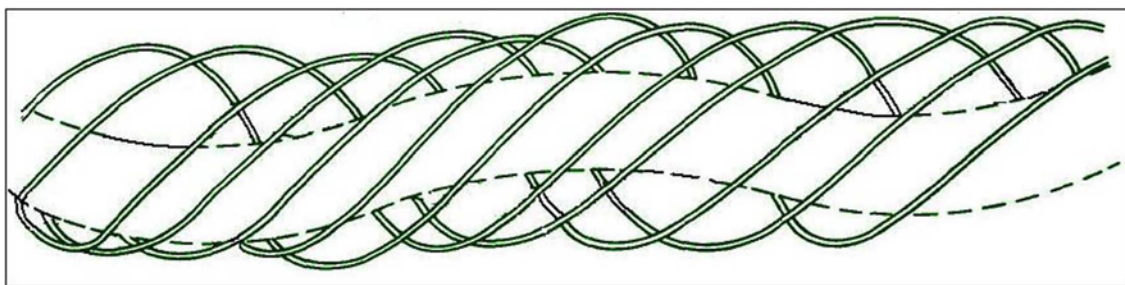


Figure 5.11, Morphological structure of the aimed core electrospun nano yarn which constructed of the man made filament core with the sheath of nanofibres, drawing was reprinted from [46].

5.4.2 Experimental work

5.4.2.1 Materials and electrospinning operation

Nylon 6 solution of 20 wt. % concentration was prepared by dissolving the polymer in 98% formic acid. The nylon 6 solution was fed through a 5 mL capacity syringe to a vertically orientated (25-gauge) blunt-ended metal needle (spinneret) via Teflon[®] tubing and the flow rate was controlled using a digitally controlled, positive displacement syringe pump Harvard Apparatus M22 PHD 2000. The needle was held by one electrode connected to a high voltage DC power supply; a Glassman MK35P 2.0-22. Typical operating regimes were applied; flow rates of 0.2 ml/hr, voltage of 15 KV and a working distance of 8 cm. These operation parameters were used for producing uniform distribution diameter nylon 6 nanofibres, based on the work in chapter two [2]. A single

polyester filament (Rhone Poulenc viscosuisse, South Africa) with count of 88 dtex and diameter of 90 microns was fed via the tension roller to the center of the holed twist disk, then to the take up disk and finally to the winder. Figure 5.12, shows a schematic drawing of the mechanism with its changeable parameters.

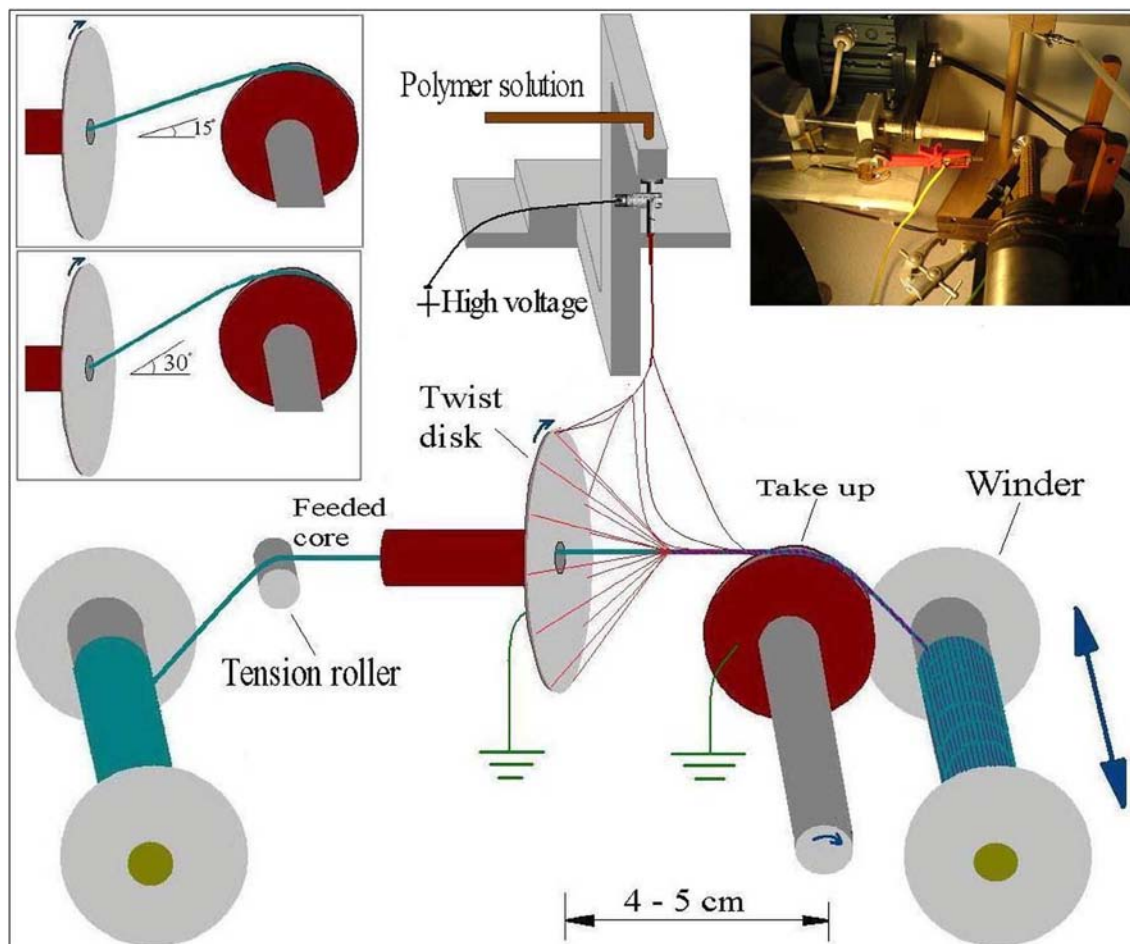


Figure 5.12, A schematic illustration of the mechanism used for spinning core electrospun nano yarn. The spinning distance between the two disks was 4 -5 cm. The twist disk was rotated around its axis and the core nano yarn was wound on the winder through the take up disk. The take up disk was placed at three different horizontal levels against the twist disk to form three core feed-in angles of 0°, 15° and 30° degrees.

5.4.2.2 The principle of the core electrospun nano yarn mechanism

The continuous core electrospun nano yarn mechanism involves feeding a tensioned single core filament through the center of a Y-Z plane holed disk, which we call 'twist disk', to a X-Z plane disk, which we call 'take up disk', to the winder. The distance between the two perpendicular set of disks at Y-Z and X-Z planes forms the spinning zone in which the nanofibres are deposited on the feeding core filament in a controllable manner, as shown in figure 5.12.

The two disks are circular; the first 60 mm in diameter and it is earthed, it has 1 mm thickness and 5 mm inside hole diameter. The second disk is a wider earthed disk, 40 mm in diameter and 4 mm thickness, separated by a distance of 4-5 cm from one another. The twist disk is rotated around its axis by means of a motorized insulated shaft/gear arrangement attached to it capable of setting the rotational speed for twisting the deposited nanofibres on the core filament. The core electrospun nano yarn was wound onto the winder through the take up disk which is also attached to a motorized insulated shaft/gear set at a given rotational speeds, as shown in figure 5.13.

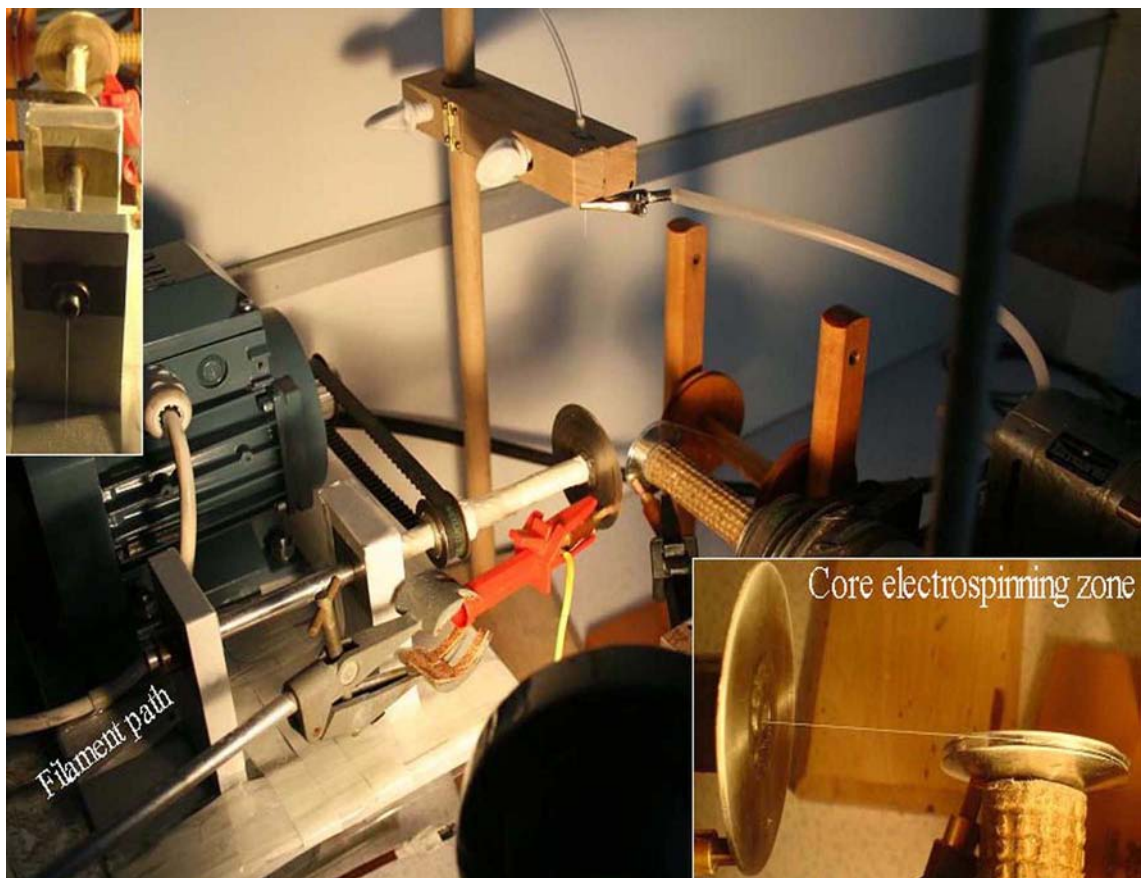


Figure 5.13, A photograph of the installed continuous core electrospun yarn mechanism used in the experiments for twisting in helical form highly aligned nylon 6 nanofibres on a feeding polyester single filament at 0° degree feed-in angle. Each disk is earthed and attached to a motorized insulated shaft to run at a controllable rotary speed.

Manufacturing parameters were altered in order to investigate the effect of the twist of the nanofibre bundle, the core filament feed-in angles and the take up speeds, on the morphological structure of the yarn. The effect of nanofibre twist angle was investigated at two rotational speeds of the twist disk, namely 500 and 750 rpm. The core polyester filament was fed into the spinning zone at three feed-in angles; 0° , 15° and 30° degrees

by placing the take up disk at three different horizontal levels against the twist disk as shown in figure 5.12. The resulting core electrospun nano yarn was wound onto the winder via the take up disk at three take up linear speeds; 1.5, 6 and 12 cm/sec. These values were based on continuous yarn mechanism, resulting work in chapter 2 and initial experimental trials of this mechanism [2, 4].

5.4.2.3 Characterization

Samples of core electrospun nano yarn were collected on SEM stubs. These samples were sputter-coated with gold-palladium for 45 seconds at 18 mA using a (Polaron Sc 7620) sputter coater. Yarns were examined using a Hitachi S-530 Scanning Electron Microscope at an accelerating voltage of 10 kV.

5.4.3 Results and discussion [52]

5.4.3.1 Observations

Figure 5.14, shows different photographs of aligned nylon 6 nanofibres deposited on the gap between the perpendicular twist disk and take up disk for continuous yarn spinning and how these nanofibres covered the feeding polyester core filament in a three dimensional conical architecture. Consequently, by rotating the twist and take up disks the incoming nanofibres deposit onto the feeding filament gradually to form a helical structure and thus forming core electrospun nano yarn.

This mechanism has been designed after careful consideration of literature and by investigating step by step the requirements for spinning continuous core electrospun nano yarn, as shown in figure 5.15.

5.4.3.2 Analytical investigation of the parameters of the mechanism on the core electrospun nano yarn morphological structure

Figure 5.16, shows three different feed-in angles of 0°, 15° and 30° degrees of the polyester filament into the spinning zone. It has been found that as the feed-in angle decreased the deposited nanofibres cover of the feeding filament per unit time increased. This resulted by electrospinning nanofibres from initially stationary disks, i.e., no twisting and by then rotating the twist disk to observe the conical twist of the nanofibres around the filament. It has therefore been confirmed that a core filament feed-in angle of 0° degree is the most suitable under this mechanism, for producing orderly nano yarn.

At an optimum core feed of 0° degree, table 5.3, shows SEM images of core electrospun nano yarn morphological structures with take up speeds of 1.5, 6 and 12 cm/sec and twists at 500 and 750 rpm.



Figure 5.14, A photograph of aligned nylon 6 nanofibres deposited in the gap between the perpendicular twist disk and take up disk for producing continuous core electrospun nano yarn. These nanofibres covered the feeding polyester filament in three dimensional conical architecture. By rotating the twist and take up disks the flying nanofibres deposited helically on the filament to form core electrospun nano yarn.

Based on a continuous nanofibre yarn mechanism described in this chapter [4], it has been found that at twists of 500 and 750 rpm, uniform and coherently tight nanofibres are wrapped around the core filament. At lower twisting speeds of 500 rpm, the deposited nanofibres move to a higher twist angle at a fixed take up speed. Therefore,

higher angular displacement leads to higher twist angles and consequently to higher twist per unit length of the core filament yarn. SEM images in table 5.3, show a twist angle of 45° – 60° degrees at 500 rpm twist (disk revolutions) and at twist angle of 30° – 45° degrees at 750 rpm twist (disk revolutions) respectively. The results obtained here are in agreement with those in the literature for conventional core spun yarn [47, 48]. One of the great advantages of this mechanism is the ability of controlling twist direction. Core yarns were electrospun with Z direction as shown in table 5.3, and in S direction as shown in figure 5.17.

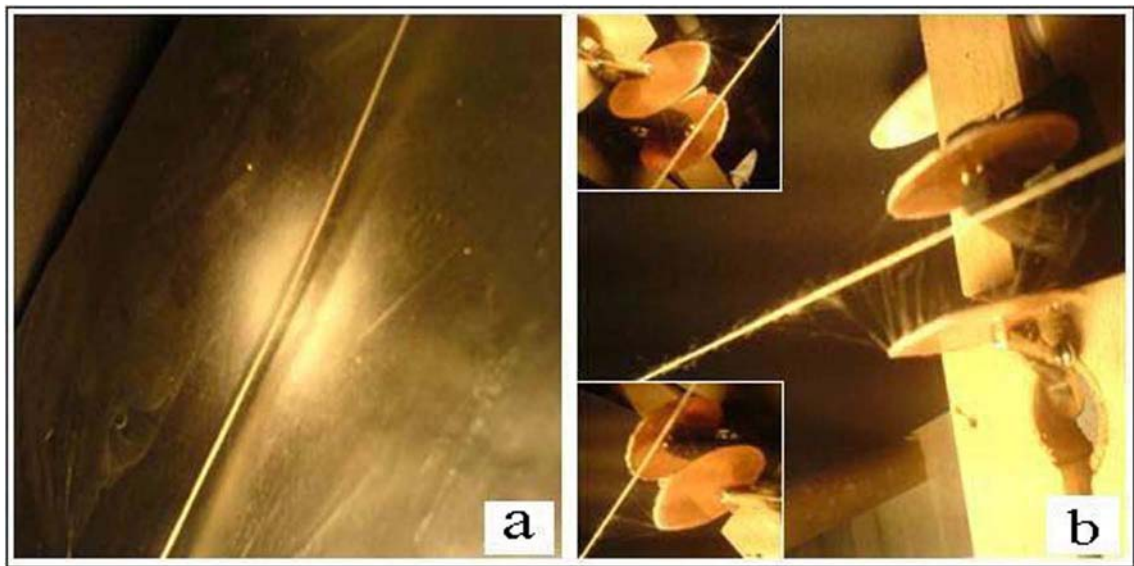


Figure 5.15, Recorded photographs showing the concept of the core electrospun nano yarn mechanism developments, (a) a filament was placed between the spinneret and the surface collector, nanofibres covered the upper part of the filament, (b) the filament was placed between two circular disks in which the nanofibres covered the upper part of the filament. From these photographs, it is necessary to think how we rotate the filament under a continuous linear motion for completing the covering of the nanofibre sheath.

In conventional core spun yarns, it is found that the critical sheath size is dependent on the fibre length, its fineness and type of fibre [49, 50]. The critical sheath size in the mechanism is dependent on the take up speed. Take up speed will affect the sheath size, sheath core ratio, adhesion, sheath number of layers and the count of the core electrospun nano yarn. The SEM images in table 5.3, show that as the sheath size increases, the sheath core ratio increases, producing best adhesion, and the highest yarn linear density, as the take up speed decreases to minimum. Moreover, at low take up speed, sheath fibres with more layers would be formed. These layers, due to their helical

configuration, generate radial pressure on the core filament and thereby restrict slippage. In fact, this is expected as with take up speed of 1.5 cm/sec there is more time for fibres to adhere and form sheath layers. On the other hand, a take up speed of 1.5 cm/sec will produce the lowest core yarn production rate. Therefore, a balance between sheath size and production rate should be found for optimization of manufacturing.

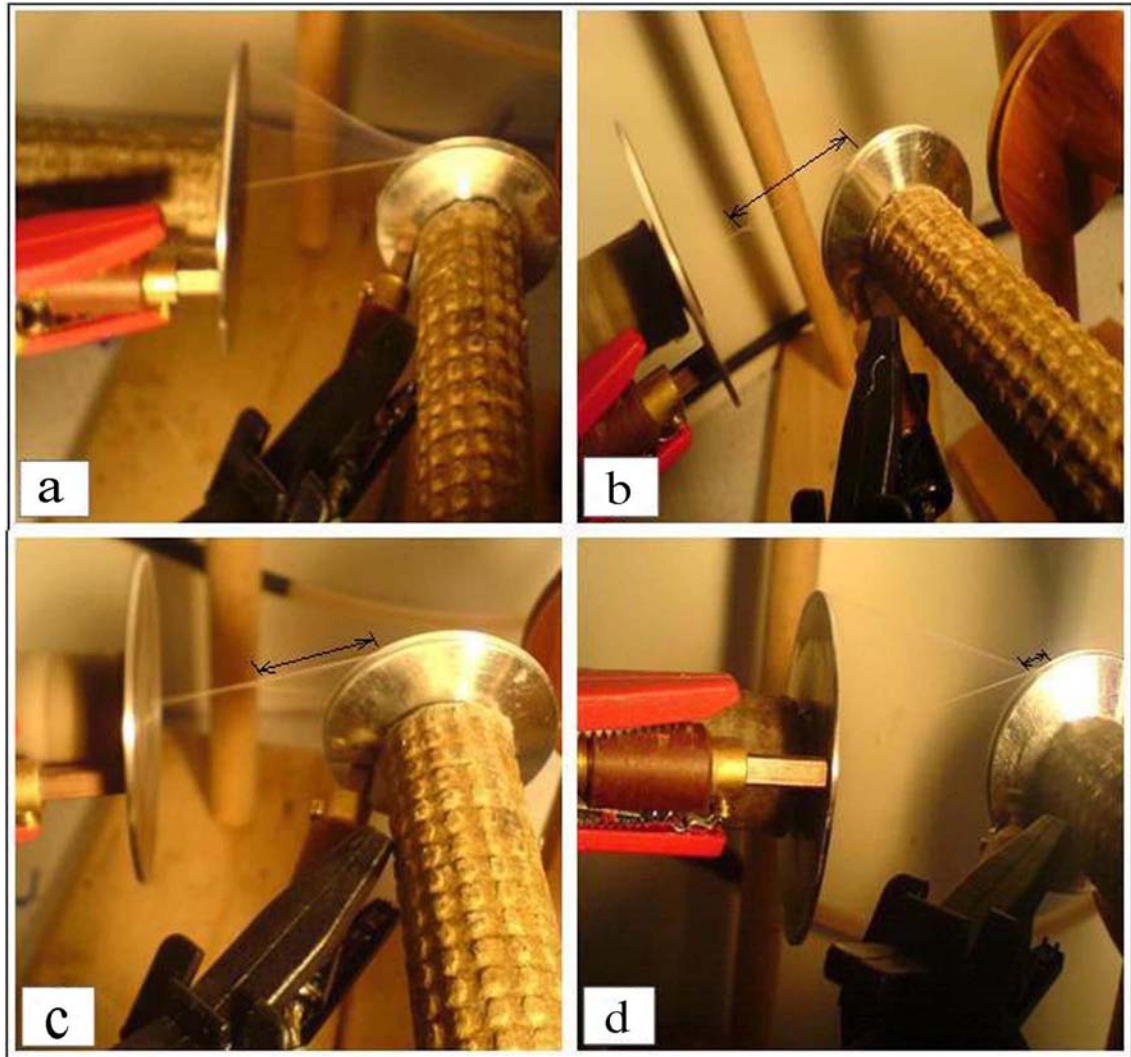
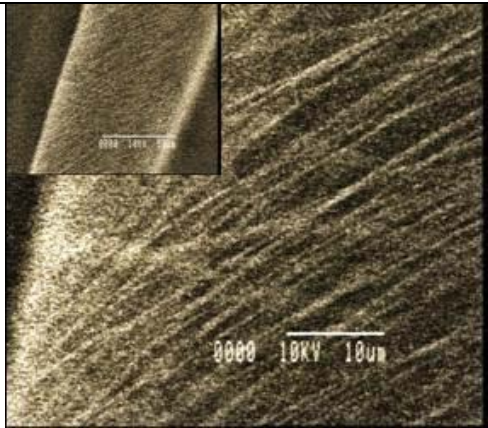
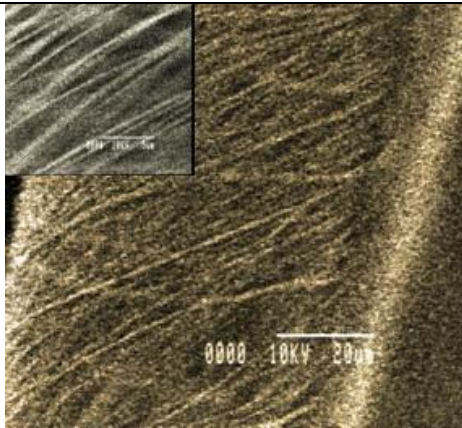
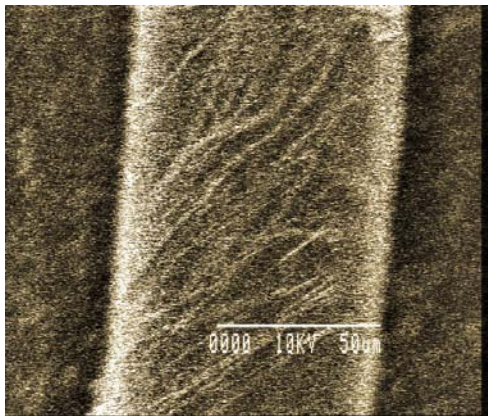

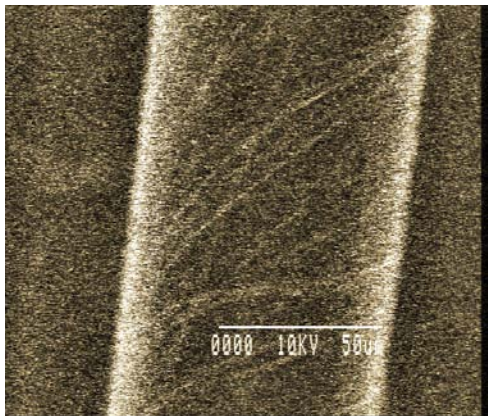
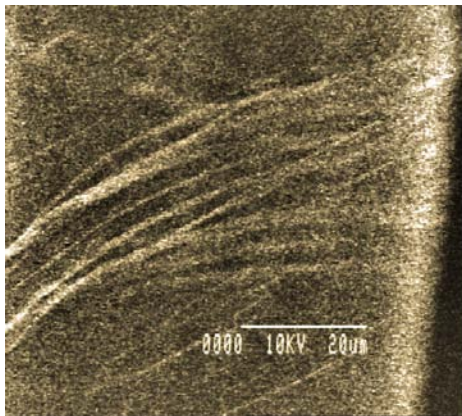


Figure 5.16, Photographs show three different feed-in angles 0° , 15° and 30° degrees, of the polyester filament into the spinning zone. (a) Deposited conical nanofibres onto the stationary twist and take up disks. (b) Applying twist to the deposited nanofibres at filament feed-in angle of 0° degree. (c) Applying twist to the deposited nanofibres at filament feed-in angle of 15° degree. (d) Applying twist to the deposited nanofibres at filament feed-in angle of 30° degree. It is easy to observe by the indicating arrows that as the feed-in angle decreases the deposited nanofibres coverage increases on the core filament.

Table 5.3, SEM images of the morphological structure of core electrospun nano yarn with different take up speed and twist speeds under 0° degree core feed- in angle.

Nylon 6 nanofibres sheath structure with core feed angle of 0° degree.		
Speed	Twist speeds of 500 rpm.	Twist speeds of 750 rpm.
Take up speed of 1.5 cm/sec.		
Take up speed of 6 cm/sec.		
Take up speed of 12 cm/sec		

Consequently, core electrospun nano yarn has been developed at core feed-in angle of 0° degree, take up speed of 1.5 cm/sec and twist at 500 rpm as shown in figure 5.18, by a new mechanical arrangement.

Optimizing these parameters further requires knowing the velocity of the deposited nanofibres and their branching out. This will be discussed in the next chapter. It can also be noted that increasing number of the spinnerets around the core filament in a circular

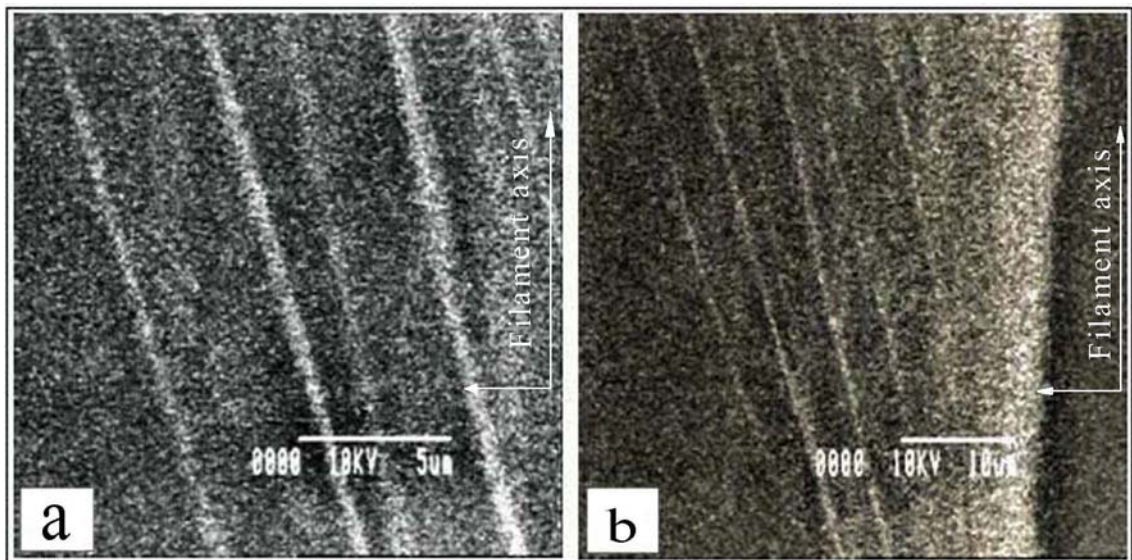


Figure 5.17, SEM images showing how electrospun nylon 6 nanofibres covered helically the polyester filament in the S direction. (a) Twist speeds of 500 rpm and take up speed of 6 cm/sec. (b) Twist speeds of 500 rpm and take up speed of 12 cm/sec.

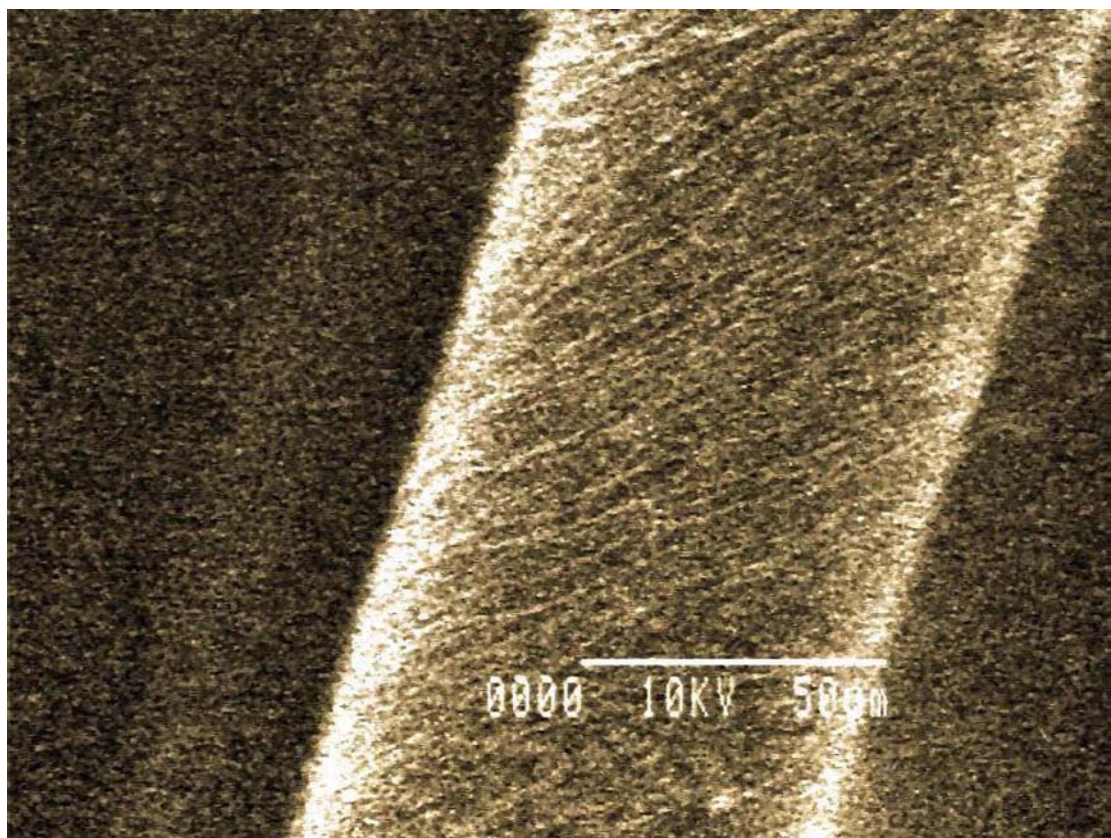


Figure 5.18, SEM image of polyester core electrospun nano yarn covered with nanofibres in a helical sheath with core feed-in angle of 0° degree, take up speed of 1.5 cm/sec and twist speed of 500 rpm.

plain geometry will provide the opportunity to increase the take up speed and thus the core yarn production rate. It should also be mentioned that to improve adhesion, pre-treatment of the synthetic core with plasma for instance will increase the adhesion and post treatment of the nanofibre sheath with hydrophilic agents will achieve greater moisture absorption and release. Adding of more spinnerets, pre-treating the filament and post treating of the core nanofibre sheath are further issues for future investigation.

5.5 Nanofibre production

5.5.1 Introduction

The critical challenge associated with electrospinning is its production rate, compared to that of conventional microfibre spinning technology. Nevertheless, improving the electrospinning design makes it possible to fabricate various nanofibre assemblies at high production rate [54, 55]. Furthermore, special electrospinning designs can provide the fabrication of complex architectures such as nonwoven and woven fabrics and fabric blends, core-shell, hollow and porous nanofibres and helical nanofibre assemblies.

Herrin, a review on the various modifications of the electrospinning designs for increasing nanofibre production rate is presented. Recent electrospinning advances regarding of industrial production, nanofibre engineering and research directions with special emphasis on mechanisms. Illustrations of mechanisms are highlighted and investigated to facilitate a better understanding of advances in this field.

5.5.2 Mechanisms of nanofibre production

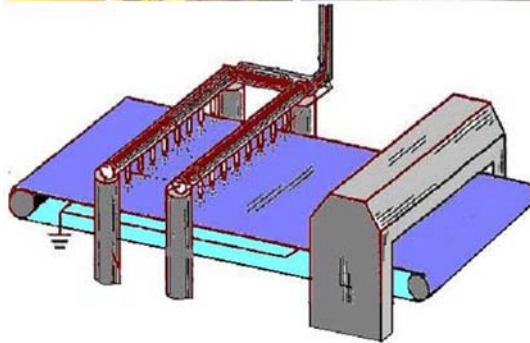
While electrospinning is an effective process for producing nanofibres, it has a well known limitation in the level of fibre production which is typically 0.1- 1.0 g/hour for a single spinneret [56]. In other words, electrospinning is a very slow process for producing nanofibres at a commercial scale compared with current microfibre spinning technology. Taking into account the polymer solution properties and the great reduction in the jet diameter which necessitates the low flow rate, the throughput of the polymer solution from the electrospinning spinneret must be in the range of 0.1 ml/hour to 10 ml/hour [57]. Therefore, to significantly increase the production rate, improvement of the electrospinning design is required. Table 5.4, shows schematic diagrams of the mechanisms developed for increasing the nanofibres production rate.

An obvious design for increasing the productivity of the electrospinning is by increasing the number of spinnerets. Multiple spinnerets have been arranged in a line [58-65], circle (concentric [64-66] or elliptic [61]) or matrix (side-by-side arrays [67-70] or regular hexagonal distribution [71]) to increase the production rate of the electrospun nanofibres. We have also constructed in our laboratory a prototype multiple jet 'spinnerets' electrospinning apparatus. In this apparatus, 32 identical spinnerets 'needles' connected to 32 identical tubes were arranged in a matrix array, as shown in figure 5.19. The distance between the individual spinnerets was 1.5 cm and their distance from the ground was 8 cm. This design demonstrated that every 3 spinnerets have been deposited as a regular triangle distribution. All spinnerets were subjected to the same applied voltage and the polymer solution 'nylon 6' was delivered to each spinneret under the same applied pressure. The electrospun fibres were collected on a large flat grounded conveyor belt. The design configuration allows the belt to move along the 'multi spinnerets array system' at two directions, back and forth. The parameters obtained from the study of the single spinneret were used as the basis for the design of this multi spinnerets system [72]. The arrangement of spinnerets requires careful design, hence a decrease in the inter spinneret distances leads to greater interference between the charged jets, resulting in an increased deposition rate over a smaller area and the onset of the electrically whipping instability is weakened which is partly responsible for the reduction of the fibre diameter to the nanometer scale. This can be overcome by increasing the spinneret to ground distance and applying a higher voltage in order to increase the collection rate of nanofibres [69]. On the other hand, to produce homogeneous nonwoven fabrics, all ejected jets and forming nanofibres need to be very closely overlapped. Figure 5.20, shows the principle of nanofibres overlapping and thus the fabric construction by this production design set-up.

For implementing a successful electrospinning process within this set-up, Zussman et. al. have experimentally investigated the arrangement of the spinnerets [69]. It has been demonstrated that not only the external applied electric field influences the jet path, but also the mutual Coulombic force interactions between the different jets. In addition, it has been found that the jets are pushed away from their neighbours by these repulsion forces, as shown in figure 5.21.

Table 5.4, Schematic diagrams of the electrospinning mechanisms for nanofibres production.

1- Electrospinning from multiple spinnerets.



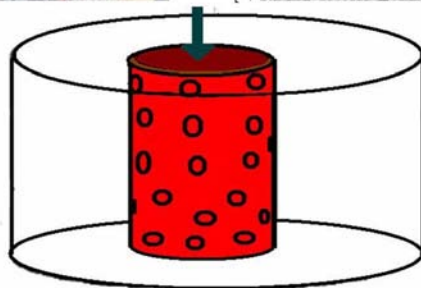
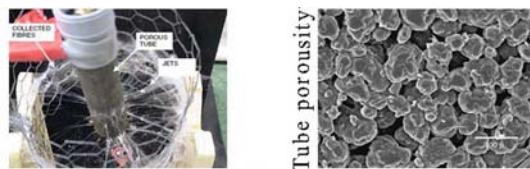
Advantages

Spinning fabric consisting of nanofibres of different materials and desired ratio.

Disadvantages

The array of spinnerets requires careful design.
 Repulsion of the neighbourhood jets.
 Blocking of some spinnerets.
 Short term operation.
 Difficulty of maintenance. [58-71].
 Right photograph was adapted from [53] and drawing was adapted from [59].

2- Electrospinning from porous tubular surface.



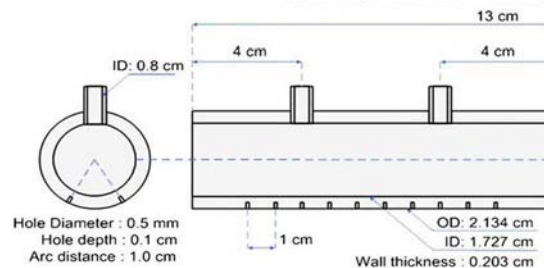
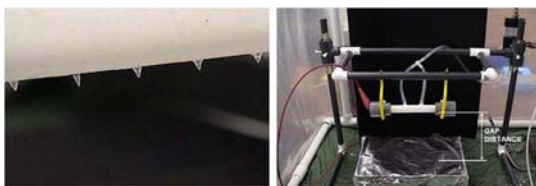
Advantages

High production of nanofibres.

Disadvantages

Large variation in nanofibre diameters.
 Difficulty in controlling the nanofibre diameters distribution uniformity.
 Investing the collected nanofibres in applications seems to be difficult. [56].
 Photographs were adapted from [56].

3- Electrospinning from a porous hollow tube with drilled holes.



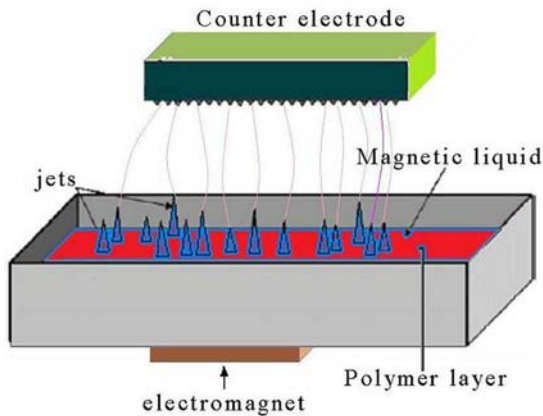
Advantages

High production of nanofibres.
 More control of jet diameter.

Disadvantages

Complicate set-up design.
 Jets repulsion and hole to hole distance are not clear.
 Difficulty in controlling the nanofibre diameters distribution uniformity. [74].
 Photographs and drawing were adapted from [74].

4- Electrospinning from polymer solution surface acted by magnetic field.



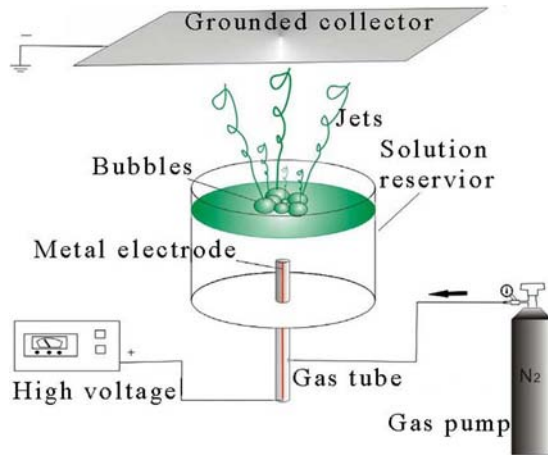
Advantages

High production rate of nanofibres.
Problem of polymer solution clogging is not existent.

Disadvantages

Complicated set-up.
Variation of nanofibre diameters is large. [75].

5- Electrospinning from polymer solution surface acted by gas pressure.



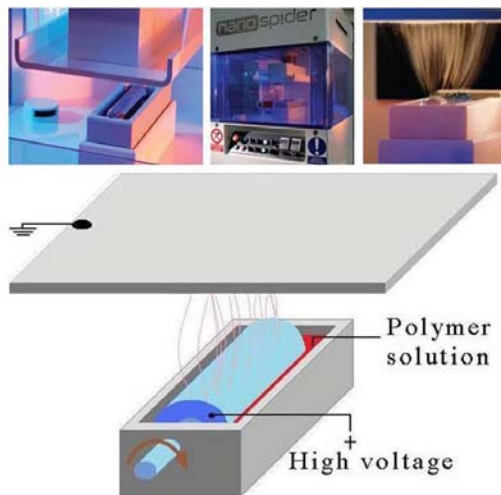
Advantages

High production rate of nanofibres.
Problem of polymer solution clogging is not existent.
Ability to control the nanofibre diameters.
Ability to produce coated fabrics.

Disadvantages

Complicated set-up.
Variation of nanofibre diameters is large. [76-79].
Drawing was adapted from [77].

6- Electrospinning from polymer solution surface acted by rotating roller.



Advantages

Simple set-up.
Easy manufacture.
Easy operation.
Low cost.
High production rate of nanofibres.
Uniform nanofibre diameters.
Problem of polymer solution clogging is not existent.
Ability to produce coated fabrics.

Disadvantages

No disadvantages. [80-83].
Photographs were adapted from [83].

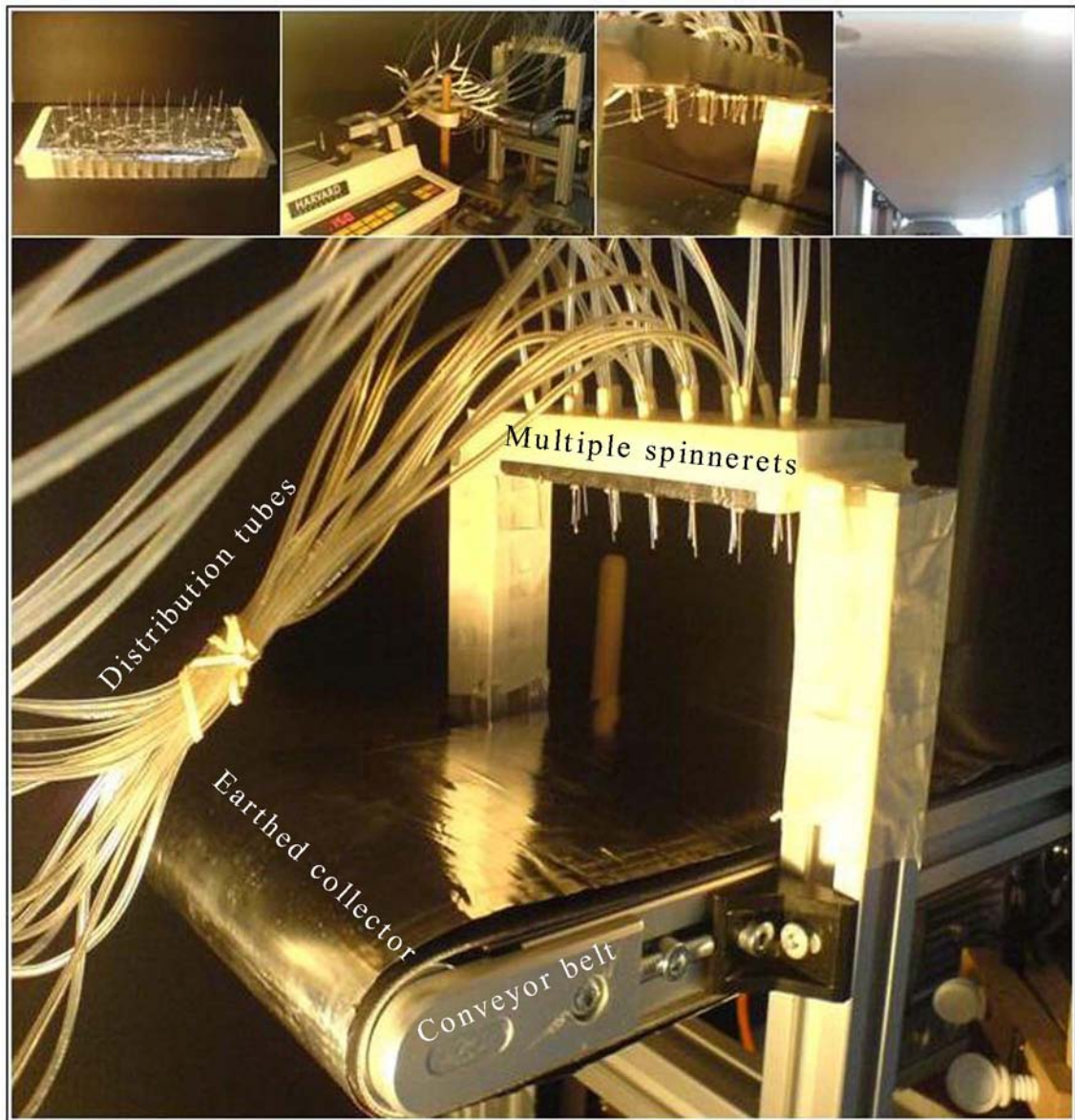


Figure 5.19, Prototype of multiple spinnerets electrospinning apparatus. (Left to right) A matrix array of spinnerets assembly, polymer solution distribution and collection of nonwoven nylon 6 fabric on the conveyor belt.

Furthermore, based on these experiments, clogging of some spinnerets during electrospinning has occurred. Hence, clogging of some spinnerets causes unevenness of the produced fabric mat and also diminishes the production rate. A possible reason for this clogging can be explained as: when the mat thickens the collected nanofibres tend to repel the coming jet thus resulting in the fluctuation and weakness of the electric field, which is responsible for withdrawing of the polymer solution, between the spinnerets and the collector. In fact, many research groups have been faced with the spinneret clogging phenomenon in their design. Larsen et. al. [73] and Hsiao et. al. [59] have used blowing gas as an enveloping current to stabilize the polymer jets during

electrospinning. In addition, a coaxial metallic ring was used as a secondary electrode around either each spinneret [64] or all spinnerets [65] in order to uniform the electrical field strength. The addition of metallic ring or applying gas jacket around the spinneret requires however, very careful design in order to ensure that the electric field distribution or the pressurized gas flow are essentially similar for each spinneret.



Figure 5.20, Photographs show collected nanofibre fabric mats electrospun from 19 spinnerets at different inter spinneret distances [71].

In summary, although this design has the possibility of increasing the production rate of spinning nonwoven fabric from different polymers at any desired ratio, its complexity and its high probability of clogging make it technologically inconvenient for industrial production.

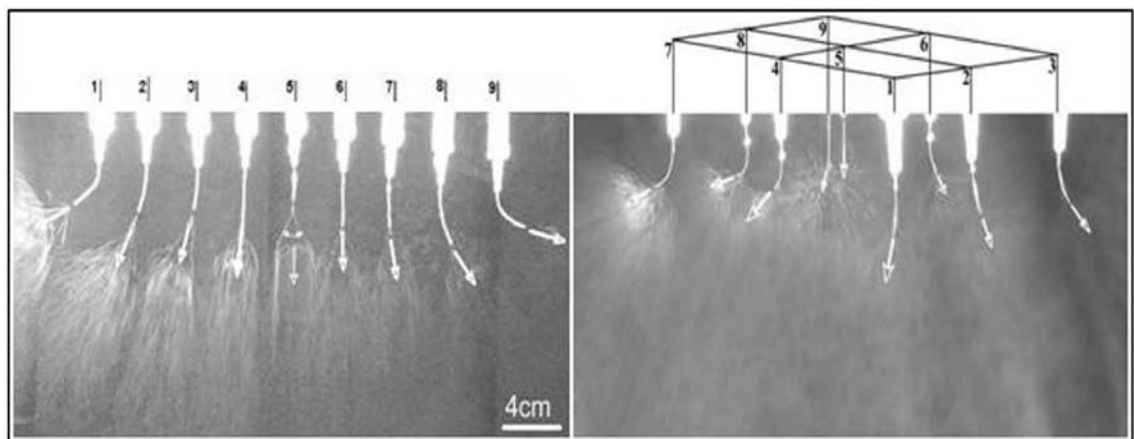


Figure 5.21, Photographs of nine spinnerets electrospinning process where the spinnerets were arranged at a 1/9 (right) and 3/3 matrix (left). It is clear how the jets are pushed away from their neighbours by the repulsion forces [69].

Chase et. al. have invented an innovative electrospinning design based on a porous tube to significantly increase the production rate, as shown in table 5.4(2) [56]. In this set-up,

a porous walled cylindrical tube with one end permanently sealed is held vertically and filled with the polymer solution. A wire electrode is inserted into the bottom of the tube to charge the polymer solution and an air pressure (0.4 - 0.8 KPa) is applied from the top of the tube. The pressurized air provides the required force to push the polymer solution through the numerous pores on the tube and thus forming drops on the outer surface of the tube. As the electric field is applied, the drops emit jets to form many electrospun nanofibres which move and deposit on the inner surface of the cylindrical collector that encloses the porous tube. Hence, tens to hundreds of jets are emitted from the porous tube surface at the same time; the mass production rate of nanofibres was found to be very large compared to the single spinneret configuration. They have demonstrated that the production rate of nanofibres of this system is about 250 times than the rate of the single spinneret. Although the porous tube is much simpler in construction and operation, the pores of the porous tube wall are highly irregular which result in unevenness of the jets mass distribution and thus different nanofibre diameter distribution. Furthermore, by this design the polymer solution passes through the porous wall tending to launch in multiple directions with little or no control; making the collected nanofibres difficult to use.

By improving this design, the same group has introduced a porous tube with wall of uniform thickness [74]. In this tube, small holes are drilled half way through the porous wall to create points of lesser resistance through which the polymer solution can preferentially electrospun to form nanofibres on a flat collector, as shown in table 5.4(3). The holes are arranged in an array and can be varied to form many hole patterns. Pressing and charging the polymer solution are similar to the previous design. The tube modification shows effective control of the locations at which drops are emitted and the collection of the electrospun nanofibres. They have noted that the production rate in this design is affected by the spaces between the drilled holes, the number of rows of holes and the collector geometry. However, although electrospinning from a porous hollow tube with drilled holes is an effective design for increasing production and is relatively simple compared to array of multiple spinnerets, it is still difficult in controlling the uniformity of the nanofibre diameter distribution.

In a trend to facilitate the spinning of multiple upward jets from a free polymer solution surface rather than the extrusion of the polymer solution through a spinneret, researchers have devised many set-ups based on the following mechanisms.

Yarin et. al. devised a set-up based on the combination of normal magnetic and electric fields acting between a ferromagnetic polymer solution layer and a metallic surface

system, as shown in table 5.4(4) [75]. Magnetic fluids were prepared by mixing Ferric-ferrous oxide black powder in silicone oil and placing the resulted fluid into a dish above a permanent magnet. A magnetic field was provided by the magnet and a metal saw with teeth oriented downward (toward the fluid surface) placed 10 cm over it. A PEO solution was carefully added onto the magnetic fluid to form a layer on the surface. It has been shown in figure 5.22, that under the influence of a magnetic field numerous conical spikes as Taylor cones were generated on the free surface of the magnetic fluid. An electrode was inserted through the bottom of the dish and a high voltage of 32 KV was applied between the magnet and the metal saw. As a result, thousands of jets were erupted from the surface of the magnetic polymer solution and nanofibres were deposited on the metal saw.

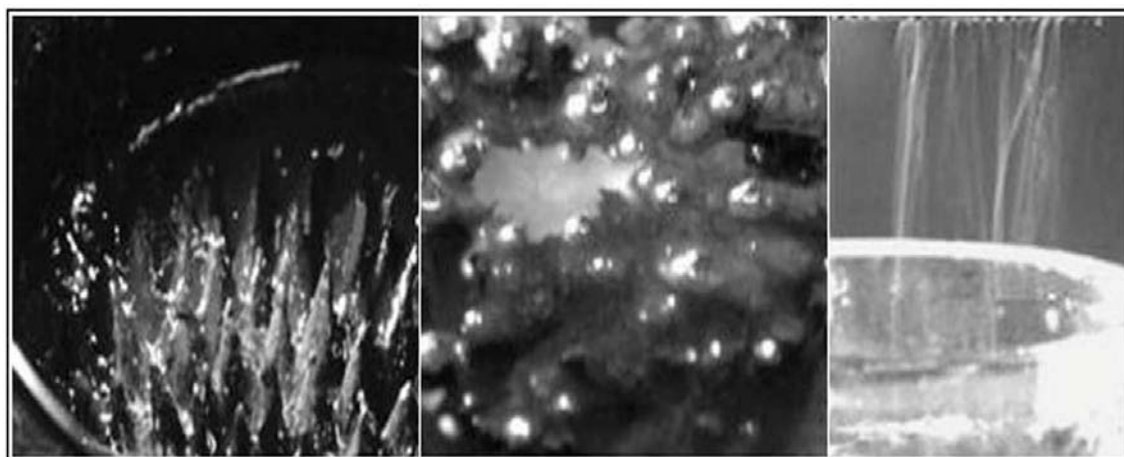


Figure 5.22. (Lift to right) conical spikes protruded from the magnetic fluid layer under normal magnetic field (there is no polymer above the magnetic fluid and no electric field is applied), protruded parts of the polymer layer located above the magnetic fluid spikes (there is still no applied electric field), nanofibres are collected on the saw teeth after applying the electric field [75].

They have reported that this mechanism leads to a 12-fold increase of the production rate over a comparable multiple spinnerets arrangement. In addition, the present mechanism eliminates the clogging problems related to the multiple spinnerets. This set-up is complicated as it is not easy to operate two layers liquids under magnetic field and variation of the nanofibre diameters is still large and not uniform.

He et. al. and their research group replaced the magnetic field by a compressed gas to reduce the surface tension of the polymer solution and thus forming bubbles and conical jets under the electric field, as shown in table 5.4(5) [76-79]. In this set-up, a thin glass

nozzle was fixed at the center of the bottom of the reservoir and then the reservoir was filled with polymer solution. A gas feeding tube was connected between the reservoir bottom and a gas pump. In addition, a metal electrode was fixed on the reservoir bottom along the centerline of the tube, and a grounded collector was placed 10 cm over the reservoir. It has been shown in figure 5.23, that many small bubbles with different sizes were generated on the polymer solution surface under the pressure of gases only. When an electric field was applied, it created a tangential stress, resulting in the deformation of the bubbles into conical uplift bubbles. The threshold value of the applied voltage and the inlet gas pressure depend on the surface tension and viscosity of the liquid [76]. Also, the number of multiple jets in this mechanism and subsequently the nanofibre production rate is related to the number and size of bubbles which can be adjusted by the pressure of the gases, the position of the tip of the gas tube, the applied voltage and the properties of the polymer solution [77]. In fact, the key advantage of this set-up in comparison to the previous one is that the average diameter of nanofibres can be controlled by controlling the set-up parameters [78].

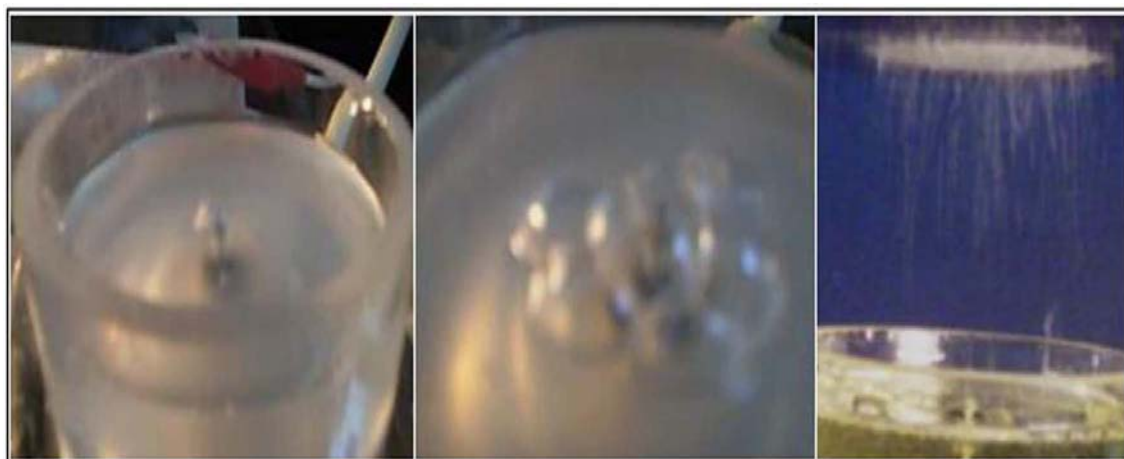


Figure 5.23, (Right to left) single conical uplift bubbles, and several uplift bubbles under different gas pressure [76], multiple jets were ejected from the bubbles to form nanofibres on the collector [78].

Jirsak et. al. (Technical University of Liberec) have invented an effective mechanism for electrospinning nanofibres from the surface of a rotating roller achieving high production rates [80, 81]. Despite that the spinning of nanofibres from the surface of a roller in a tank with circulating polymer solution has been patented by Formhals et. al. [82], Elmarco Co. effectively modified it to introduce the world's first industrial

nanofibre production machine 'NanospiderTM' [83]. In this set-up, a roller is submerged half way in the polymer solution tank and by rotating the roller a thin layer of the polymer solution is carried to the roller's peak. When a high voltage electric field is applied between the roller and a flat surface over it, this layer generates up lift Taylor cones to be electrospun into nanofibres deposited upwards and on the flat surface as shown in table 5.4(6). Practically in this mechanism, the nanofibres production rate depends on the applicable roller working width, the linear speed of the roller and the number of rollers 'spinning heads' placed in series. For instance, Elmarco claimed that the NanospiderTM machine can produce nanofibrous nonwoven mats of 50 - 500 nm nanofibre diameter and at production rate of 1.5 g/min per one meter roller length covering area and weight of 0.1 - 10 g/m². In fact, with this mechanism, optimizing nanofibre production rates versus nanofibre diameter and nanofibre diameter distribution uniformity requires investigating the roller linear speed with the polymer solution properties (viscosity, surface tension, etc.) and electrospinning parameters (applied electric field, etc.) for each polymer used.

However, this high productivity electrospinning mechanism provides many advantages, such as high production rate and lowest cost per square meter among all nanofibre production mechanisms [83], easy operation and maintenance and its ability to coat nonwoven fabrics effectively. Furthermore, a variety of organic, inorganic and biopolymers can be electrospun by the same mechanism.

In summary, while the electrospinning mechanisms working with sets of spinnerets, porous tube and hollow tube with drilled holes show some difficulties in continuous nanofibre production and operation difficulties, the electrospinning from the surface of the polymer solution acted by a rotating roller provides high production rate and uniform nanofibres at an acceptable nanofibre diameters distribution.

5.6 References

- [5.1] D. Li, Y. Wang, Y.N. Xia, *Electrospinning of polymeric and ceramic nanofibres as uniaxially aligned arrays*, Nano Letters, **3**, 1167-1171 (2003)
- [5.2] M.B. Bazbouz, G.K. Stylios, *Alignment and optimization of nylon 6 nanofibres by electrospinning*, Journal of Applied Polymer Science, **107**, 3023-3032 (2008)
- [5.3] W.E. Teo, S. Ramakrishna, *A review on design and nanofibre assemblies*, Nanotechnology, **17**, R89-R106 (2006)
- [5.4] M.B. Bazbouz, G.K. Stylios, *Novel mechanism for spinning continuous twisted composite nanofibre yarns*, European Polymer Journal, **44**, 1-12 (2008)

- [5.5] F.L. Zhou, R.H. Gong, Manufacturing technologies of polymeric nanofibres and nanofibre yarns, *Polymer International*, **57**, 837-845 (2007)
- [5.6] E. Smit, U. Büttner, R.D. Sanderson, *Continuous yarns from electrospun fibres*, *Polymer*, **46**, 2419-2423 (2005)
- [5.7] M.S. Khil, S.R. Bhattarai, H.Y. Kim, S.Z. Kim, K.H. Lee, *Novel fabricated matrix via electrospinning for tissue engineering*, *Journal of Biomedical Materials Research part B*, **72**, 117- 124 (2005)
- [5.8] K.H. Yong, P.J. Cheol, *A process of preparing a continuous filament or yarn composed of nanofibres*, World Intellectual Property Organization Patent, **WO052039** (2006)
- [5.9] W. Kataphinan, S. Dabney, D. Smith, D.H. Reneker, *Fabrication of electrospun and encapsulation into polymer nanofibres*, Book of Abstracts, The Fibre Society, 23-25 (2001)
- [5.10] H. Berghmans, R.D. Cooman, J.D. Rudder, R. Koningsveld, *Structure formation in polymer solutions*, *Polymer*, **39**, 4621-4629 (1998)
- [5.11] K.H. Yong, *A process of preparing continuous filament composed of nanofibre*, World Intellectual Property Organization Patent, **WO073442** (2005)
- [5.12] W.E Teo, K. Fujihara, S. Ramakrishna, *Method and apparatus for producing fibre yarn*, World Intellectual Property Organization Patent, **WO013858** (2007)
- [5.13] W.E. Teo, R. Gopal, R. Ramaseshan, K. Fujihara, S. Ramakrishna, *A dynamic liquid support system for continuous electrospun yarn fabrication*, *Polymer*, **48**, 3400-3405 (2007)
- [5.14] F.L. Scardino, R.J. Balonis, *Fibrous structures containing nanofibrils and other textile fibres*, US Patent, **6308509** (2001)
- [5.15] S.F. Fennessey, R.J. Farris, *Fabrication of aligned and molecularly oriented electrospun polyacrylonitrile nanofibres and the mechanical behavior of their twisted yarns*, *Polymer*, **45**, 4217-4225 (2004)
- [5.16] S.Y. Jee, J.R. Lee, H.J. Kim, Y.T. Hong, S. Kim, S.J. Park, *Filament bundle type nanofibre and manufacturing method thereof*, World Intellectual Property Organization Patent, **WO123995** (2005)
- [5.17] F. Ko, Y. Gogotsi, A. Ali, N. Naguib, H. Ye, G. Yang, C. Li, P. Willis, *Electrospinning of continuous carbon nanotube-filled nanofibre yarns*, *Advanced Materials*, **15**, 1161-1165 (2003)
- [5.18] H.L. Lam, *Electrospinning of single wall carbon nanotube reinforced aligned fibrils and yarns*, PhD Thesis, Drexel University (2004)

- [5.19] A. Formhals, *Artificial thread and method of producing same filed*, US Patent, **2187306** (1940)
- [5.20] A. Formhals, *Producing of artificial fibres from fibre forming liquids*, US Patent, **2323025** (1943)
- [5.21] A. Formhals, *Method and apparatus for spinning*, US Patent, **2349950** (1944)
- [5.22] P.D. Dalton, D. Klee, M. Möller, *Electrospinning with dual collection rings*, *Polymer*, **46**, 611-614 (2005)
- [5.23] L.Q. Liu, M. Eder, I. Burgert , D. Tasis , H.M. Prato, D. Wagner, *One-step electrospun nanofibre-based composite ropes*, *Applied Physics Letters*, **90**, 083108-083110 (2007)
- [5.24] H. Pan, L. Li, L. Hu, X. Cui, *Continuous aligned polymer fibres produced by a modified electrospinning method*, *Polymer*, **47**, 4901-4904 (2006)
- [5.25] B.K. Gu, M.K. Shin, K.W. Sohn, S.I. Kim, S.J. Kim , S.K. Kim, H. Lee, J.S. Park, *Direct fabrication of twisted nanofibres by electrospinning*, *Applied Physics Letters*, **90**, 3902-3904 (2007)
- [5.26] S.Y. Jee, J.R. Lee, H.J. Kim, Y.T. Hong, S. Kim, S.J. Park, *Filament bundle type nano fibre and manufacturing method thereof*, World Intellectual Property Organization Patent, **WO123995** (2005)
- [5.27] F. Dabirian, Y. Hosseini, S.A.H. Ravandi, *Manipulation of the electric field of electrospinning system to produce polyacrylonitrile nanofibre yarn*, *Journal of the Textile Institute*, **98**, 237-241 (2007)
- [5.28] X. Wang, K. Zhang, M. Zhu, H. Yu, Z. Zhou, Y. Chen, B.S. Hsiao, *Continuous polymer nanofibre yarns prepared by self-bundling electrospinning method*, *Polymer*, **49**, 2755–2761 (2008)
- [5.29] A.R. Horrocks, S. Anand, *Handbook of technical textiles*, Woodhead Publishing Ltd, Cambridge (2000)
- [5.30] P.R. Lord, *Handbook of yarn production: technology, science and economics*, Woodhead Publishing LTD, Cambridge (2003)
- [5.31] C. A. Lawrence, *Fundamentals of spun yarn technology*, CRC Press, London (2003)
- [5.32] F.K. Ko, *Nanofibre technology: bridging the gap between nano and macro world*, In NATO ASI on Nanoengineered Nanofibrous Materials Book, Edited by S. Guceri, Y. Gogotsi, Kluwer Academic Publishers (2004)
- [5.33] M.B. Bazbouz, G.K. Stylios, *A spinning concept for ultrafine composite nanofibre yarns*, Presented at Green chemistry & engineering, The first international

conference on process intensification & nanotechnology, Albany, New York state, USA, ISBN: 978 1 85598 101 0, 145-160 (15th -18th September 2008)

[5.34] D.H. Reneker, A.L. Yarin, H. Fong, S. Koombhongse, *Bending instability of electrically charged liquid jets of polymer solutions in electrospinning*, Journal of Applied Physics, **87**, 4531-4547 (2000)

[5.35] J.H. He, Y. Wu, W.W. Zuo, *Critical length of straight jet in electrospinning*, Polymer, **46**, 637-640 (2005)

[5.36] D.H. Reneker, A.L. Yarin, S. Koombhongse, *Bending instability in electrospinning of nanofibres*, Journal of Applied Physics, **89**, 3018-3026 (2001)

[5.37] S.V. Fridrikh, J.H. Yu, M.P. Brenner, G.C. Rutledge, *Controlling the fibre diameter during electrospinning*, Physical Review Letters, **90**, 144502-1 – 144502-4 (2003)

[5.38] E. Zussman, D. Rittel, A.L. Yarin, *Failure modes of electrospun nanofibres*, Applied Physics Letters, **82**, 3958-3960 (2003)

[5.39] D.H. Reneker, I. Chun, *Nanometre diameter fibres of polymer produced by electrospinning*, Nanotechnology, **7**, 216–223 (1996)

[5.40] M.E. Helgeson, K.N. Grammatikos, J.M. Deitzel, N.J. Wagner, *Theory and kinematics measurements of the mechanics of stable electrospun polymer jets*, Polymer, **49**, 2924-2936 (2008)

[5.41] DuPont Bulletin, *Producing core-spun yarns containing Lycra*, Bulletin, **L519**, 6-7 (1997)

[5.42] W.E. Morton, J.W.S. Hearle, *Physics properties of textile fibres*, 2nd Edition, Textile Institute and Butterworth & Co, 322-340 (1975)

[5.43] P. Radhakrishnaiah, T. Sukasem, A.P.S. Sawhney, *Handle and comfort properties of fabrics made from random blend cotton covered polyester yarns*, Textile Research Journal, **63**, 573-579 (1993)

[5.44] M. Miao, Y.L. How, S.Y. Ho, *Influence of spinning parameters on core yarn sheath slippage and other properties*, Textile Research Journal, **66**, 676-684 (1996)

[5.45] W.E. Teo, M. Kotaki, X.M. Mo, S. Ramakrishna, *Porous tubular structures with controlled fibre orientation using a modified electrospinning method*, Nanotechnology, **16**, 918-924, (2005)

[5.46] A. Parker, P.J. Dickinson, *Composite yarn*. US Patent, **4411129** (1983)

[5.47] O. Babaarslan, *Method of producing a polyester viscose core-spun yarn containing spandex using a modified ring spinning frame*, Textile Research Journal, **71**, 367-371 (2001)

- [5.48] A.P.S. Sawhney, L.B. Kimmel, G.F. Ruppenicker, D.P. Thibodeaux, *A unique polyester staple core/ cotton-warp yarn made on a tandem spinning system*, Textile Research Journal, **63**, 764-769 (1993)
- [5.49] A.P.S. Sawhney, R.J. Harper, G.F. Ruppenicker, K.Q. Robert, *Comparison of greige fabrics made with cotton covered polyester staple-core yarn and 100% cotton yarn*, Textile Research Journal, **61**, 71-74 (1991)
- [5.50] A.P.S. Sawhney, R.J. Harper, G.F. Ruppenicker, K.Q. Robert, *Cotton covered nylon core yarns and greige fabrics*, Textile Research Journal, **59**, 185-190 (1989)
- [5.51] M. Gorantla, S.E. Boone, M. El-Ashry, D. Young, *Continuous polymer nanofibres by extrusion into a viscous medium: a modified wet-spinning technique*, Applied Physics Letters, **88**, 073115-1 – 073115-3 (2006)
- [5.52] M.B. Bazbouz, G.K. Stylios, *A new mechanism for the electrospinning of nano yarns*, Journal of Applied Polymer Science, Submitted for publication, WILEY InterScience (2009)
- [5.53] C. Burger, B.S. Hsiao, B. Chu, *Nanofibrous materials and their applications*, Annual Review Materials Research, **36**, 333-368 (2006)
- [5.54] W.E. Teo, S. Ramakrishna, *A review on electrospinning design and nanofibre assemblies*, Nanotechnology, **17**, R89-R106 (2006)
- [5.55] F.L. Zhou, R.H. Gong, I. Porat, *Mass production of nanofibre assemblies by electrostatic spinning*, Polymer International, Early View (2009)
- [5.56] O.O. Dosunmu, G.G. Chase, W. Kataphinan, D.H. Reneker, *Electrospinning of polymer nanofibres from multiple jets on a porous tubular surface*, Nanotechnology, **17**, 1123-1127 (2006)
- [5.57] H. Reneker, A.L. Yarin, H. Fong, S. Koombhongse, *Bending instability of electrically charged liquid jets of polymer solutions in electrospinning*, Journal of Applied Physics, **87**, 4531-4547 (2000)
- [5.58] S. Madhugiri, A. Dalton, J. Gutierrez, J.P. Ferraris, K.J. Balkus, Jr., *Electrospun MEH-PPV/SBA-15 composite nanofibres using a dual syringe method*, Journal of American Ceramic Society, **125**, 14531-14538 (2003)
- [5.59] B. Chu, B.S. Hsiao, D. Fang, *Apparatus and methods for electrospinning polymeric fibres and membranes*, US Patent, **6713011** (2004)
- [5.60] B. Ding, E. Kimura, T. Sato, S. Fujita, S. Shiratori, *Fabrication of blend biodegradable nanofibrous nonwoven mats via multi-jet electrospinning*, Polymer, **45**, 1895-1902 (2004)

- [5.61] W. Tomaszewski, M. Szadkowski, *Investigation of electrospinning with the use of a multi-jet electrospinning head*, *Fibres & Textiles in Eastern Europe*, **13**, 22-26 (2005)
- [5.62] H.Y. Kim, N.Y. Kim, J.C. Park, *Electronic spinning apparatus*, US Patent, **6991702** (2006)
- [5.63] M. Li, Y. He, C. Xin, X. Wei, Q. Li, C. Lu, *Dual electrode mode electrospinning of biodegradable polymers*, *Applied Physics Letters*, **92**, 213114 -1 – 213114-3 (2008)
- [5.64] W.S. Lee, S.M. Jo, S.G. Go, S.W. Chun, *Apparatus of polymer web by electrospinning process*, US Patent, **6616435** (2003)
- [5.65] G.H. Kim, Y. Cho, W. Kim, *Stability analysis for multi-jets electrospinning process modified with a cylindrical electrode*, *European Polymer Journal*, **42**, 2031-2038 (2006)
- [5.66] Y. Yang, Z. Jia, Q. Li, L. Hou, H. Gao, L. Wang, Z. Guan, *Multiple jets in electrospinning*, 8th International Conference on Properties and Applications of Dielectric Materials, 940-943 (2006)
- [5.67] D.J. Smith , D.H. Reneker, A.T. McManus, A.L.S. Gibson, C. Mello, M.S. Sennett, *Electrospun fibres and an apparatus therefore*, US Patent, **6753454** (2004)
- [5.68] H.Y. Chung, J.R.B. Hall, M.A. Gogins, D.G. Crofoot, T.M. Weik, *Polymer, polymer microfibre, polymer nanofibre and applications including filter structures*, US Patent, **6743273** (2004)
- [5.69] S.A. Theron, A.L. Yarin, E. Zussman, E. Kroll, *Multiple jets in electrospinning: experiment and modeling*, *Polymer*, **46**, 2889-2899 (2005)
- [5.70] T. Matsuo, *Fibre materials for advanced technical textiles*, *Textile progress*, **40** (2), PP. 110 (2008)
- [5.71] Y. Yang, Z. Jia, Q. Li, L. Hou, Z. Guan, *Electrospun uniform fibres with a special regular hexagon distributed multi-needles system*, *Electrostatics Conference*, **142**, 012027-1 – 012027-6 (2008)
- [5.72] M.B. Bazbouz, G.K. Stylios, *Alignment and optimization of nylon 6 nanofibres by electrospinning*, *Journal of Applied Polymer Science*, **107**, 3023-3032 (2008)
- [5.73] R. Spretz, R.V. Ortiz, G. Larsen, *Use of coaxial gas jackets to stabilize Taylor cones of volatile solutions and to induce particle-to-fibre transitions*, *Advanced Materials*, **16**, 166-169 (2004)
- [5.74] J.S. Varabhas, G.G. Chase, D.H. Reneker, *Electrospun nanofibres from a porous hollow tube*, *Polymer*, **49**, 4226-4229 (2008)

- [5.75] A.L. Yarin, E. Zussman, *Upward needleless electrospinning of multiple nanofibres*, *Polymer*, **45**, 2977-2980 (2004)
- [5.76] Y. Liu, J. He, *Bubble electrospinning for mass production of nanofibres*, *International Journal of Nonlinear Sciences and Numerical Simulation*, **8**, 393-396 (2007)
- [5.77] J.H. He , Y. Liu, L. Xu, J.Y. Yu, G. Sun, *Biomimic fabrication of electrospun nanofibres with high-throughput*, *Chaos, Solitons and Fractals*, **37**, 643-651 (2008)
- [5.78] Y. Liu, J.H. He, J.Y. Yu, *Bubble-electrospinning: a novel method for making nanofibres*, *International Symposium on Nonlinear Dynamics Conference*, **96**, 012001-1 – 012001-4 (2008)
- [5.79] Y. Liu, J.H. He, J.Y. Yu, L. Xu, L.F. Liu, *A novel electrospinning apparatus for mass production of nanofibres using aerated solutions*, *Chinese Patent*, **10036447.4** (2007)
- [5.80] O. Jirsak, F. Sanetnik, D. Lukas, V. Kotek, L. Martinova, J. Chaloupek, *A method of nanofibres production from a polymer solution using electrostatic spinning and a device for carrying out the method*, *World Intellectual Property Organization Patent*, **WO024101** (2005)
- [5.81] O. Jirsak, K. Kalinova, D. Stranska, *Nanofibre technologies and nanospider applications*, *VDI-Berichte*, **1940**, 41-44 (2006)
- [5.82] A. Formhals, *Process and apparatus for preparing artificial threads*, *US Patent*, **1975504** (1934)
- [5.83] Elmarco company, www.elmarco.com, accessed 18/02/2009

CHAPTER 6: MODELLING THE ELECTROSPINNING OF NANOFIBRES

6.1 Introduction

Electrospinning involves the application of electrical force instead of the mechanical force to charge polymer solutions into a string of charged nanofibres. Electrospinning typically consists of four operational stages. In the first stage, a charged cone jet is initiated by applying electric field on the droplet of the polymer solution at the tip of the spinneret. In the second stage, a staple jet is accelerated and stretched smoothly in a straight line away from the spinneret. In the third stage, the jet becomes unstable; it splits, whips and bends violently with chaotic instabilities. In the fourth stage, charged nanofibres are formed to be collected as aligned fibres or mats [1, 2].

Controlling the electrospinning requires an electrohydrodynamic mathematical model by which the electrified fluid jet can be quantified. Moreover, in order to control the dynamic properties, geometry, and mass production of the nanofibres produced, it is necessary to model quantitatively each of these stages of electrospinning.

Hereinafter, we provide a mathematical model for quantifying the process, for developing a better understanding of electrospinning and for achieving better process control and process optimization. The mathematical equations can define the kinematics properties of the electrospinning of nanofibres which is important in the process control.

6.2 Review of mathematical models of the electrospinning process

6.2.1 Mathematical models for the initiation of the jet

In electrospinning, the jet initiation from a droplet of polymer solution is a self accelerating process [3]. Once an electric field is applied on the droplet of the polymer solution at the tip of the spinneret, the surface of the liquid becomes electrically charged. If the electric potential of the surface charge exceeds a critical value, the electrical forces overcome the polymer solution surface tension and thus expanding and contracting the charged droplet in conic shape [4]. The balance between the surface tension and the applied electric forces is critical to determine the initial cone shape of the polymer solution at the tip of the spinneret [5]. This conical shape is scientifically known as “Taylor cone” [5-7]. A straight and electrically charged jet of polymer solution will erupt from the surface of the cone and travel toward the collector. Much of the literature on electrically driven jets has concentrated on the initiation processes that transform a polymer solution liquid surface into a jet.

Taylor et. al. have shown that a viscous fluid existed in equilibrium in an electric field has the form of a cone with a semi-vertical angle, $\Theta = 49.3^\circ$ [7]. Another issue related to the initiation of the jet is the required strength of the electric field. They have indicated that the critical voltage V (expressed in kilovolts) at which the jet fluid is initiated is given by the following equation:

$$V^2 = 4 \frac{H^2}{L^2} \left(\ln \frac{2L}{R} - 1.5 \right) (0.117 \pi R \gamma) \quad (6.1)$$

Where H is the electrospinning distance, L is the length of the capillary tube, R is the radius of the tube and γ is the surface tension of the fluid (units: H , L , and R are in cm, γ is in dyn/cm).

Hendricks et. al. [8] have also calculated the minimum spraying applied electric field 'voltage potential' of a suspended hemispherical conducting droplet in the air as the following equation:

$$V = 300 \sqrt{20 \pi r_j \gamma} \quad (6.2)$$

Where r_j is the jet radius and γ is the surface tension of the fluid.

Cloupeau et. al. have investigated several functioning modes of operation for electrohydrodynamic droplets leading ultimately to the formation of charged droplets, jets or aerosol [9]. However, although they described the electrospinning cone-jet as a particular case of electrospraying, multiple jetting from the spinneret at high voltage is not discussed further [38].

Ganan Calvo et. al. have achieved an asymptotic solution for the cone jet configuration in electrospinning which expresses the charge distribution within the jet, the cone jet shape and the electric current across the jet [10].

Yarin et. al. and co workers [3] established the droplet configuration nature of the polymer solution corresponding to the Taylor cone. They have considered an axisymmetrical liquid body kept at constant electric field with its tip at a distance 'a' from an equipotential plane, as shown in figure 6.1. They have obtained the equation for 'a' as the following:

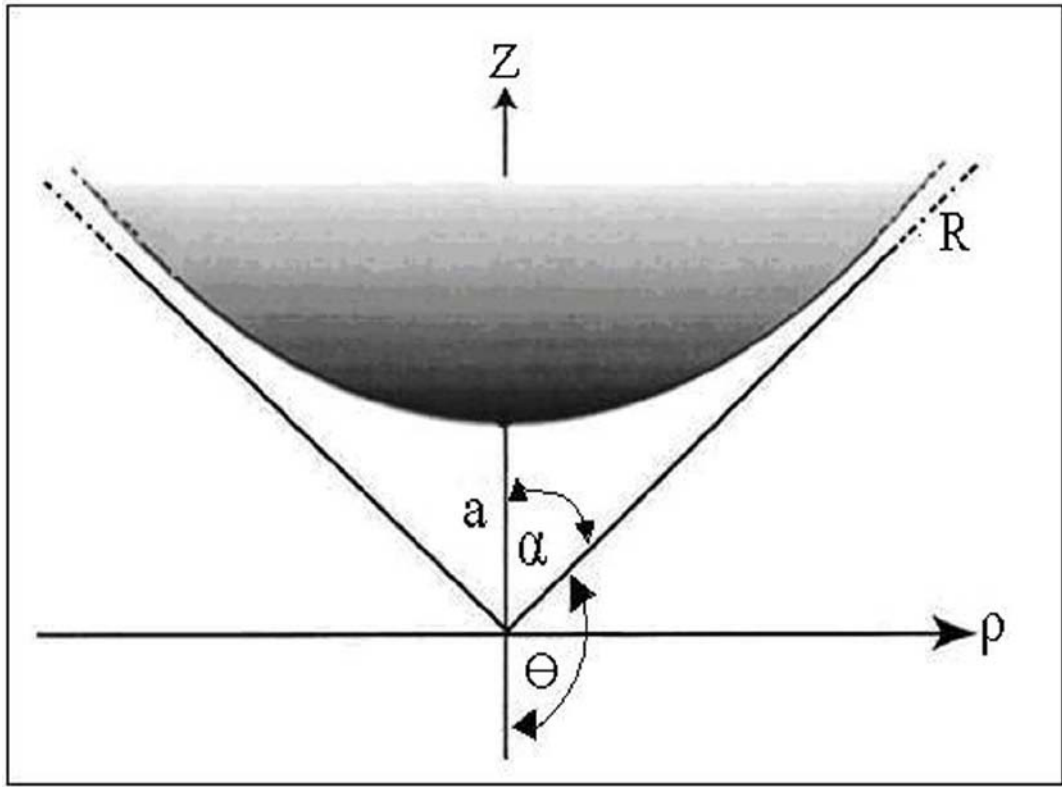


Figure 6.1, Axisymmetrical fluid body kept at constant electric field at a distance ‘a’ from an equipotential plane [3].

$$a = \frac{1}{2} \left(\frac{1}{\beta^2} - 2h \right) \left[\frac{1}{4} \left(\frac{1}{\beta^2} - 2h \right)^2 - h^2 \right]^{1/2} \quad (6.3)$$

$$\beta = \frac{\Phi}{H (4\pi\gamma)^{1/2} \ln[(1+\xi)/(1-\xi)] (1-\xi^2)^{1/2}} \quad (6.4)$$

Whereas ξ is a constant representing hyperboloids, h is the height of the droplet, Φ is the critical electric field, H is the electrospinning distance and γ is the surface tension coefficient.

An interesting theory of stable shapes of droplets affected by an electric field is proposed and compared with data acquired in their experimental work on electrospinning of nanofibres from polymer solutions and melts. Once the jet initiation model has been shown to be applicable in predicting the initial jets formed in electrospinning, the model results can then be invested as a basis for the analysis of the subsequent emergence of the jet and propagation of its instability.

6.2.2 Mathematical models for the straight jet

Upon initiation, a charged jet of polymer solution is rapidly stretched and accelerated away from the conical droplet at the spinneret toward the grounded collector by electrical forces. It has been assumed in this case that the electrospinning jet is a string of charged elements connected by a viscoelastic medium, one end is fixed at the point of origin and the other end is free [1]. Numerous models have been made using conventional electrohydrodynamic equations for mathematical description of the stretched liquid jet [11]. These useful descriptions were either based on slender body theory or allometric scaling laws.

6.2.2.1 Mathematical models for the straight jet based on slender body theory

In electrospinning, elongation of the jet is governed by electric field pulling forces, surface charge density, gravity, surface tension and viscosity. It has been assumed in this theory that the jet liquid is weakly conducting ‘leaky dielectric’, so that sustaining the electric field will be tangential to the jet surface [12]. Additionally, the jet carries electric charges only on its surface, the jet radius decreases slowly along the axial direction z and the axial velocity is uniform in the cross section of the jet [10-12]. Models with one dimensional problem are modified based on governing jet liquid equations which are: conservation of mass (for an incompressible fluid), conservation of charge, linear momentum conservation and Coulomb’s equation for the electric field [13-25].

Mass conservation is written as:

$$\pi r_j^2 \rho u = Q \quad (6.5)$$

Where r_j is the radius of the jet at z cross section, Q is the mass flow rate, ρ is the specific mass of the liquid and u is the velocity at z direction.

Charge conservation is written as:

$$\pi r_j^2 kE + 2\pi r_j u \sigma = I \quad (6.6)$$

Where E is the z component of the electric field, K is the conductivity of the liquid, σ is the surface charge density and I is the total current in the jet.

We can note from this equation that the current carried by the jet consists of two components: charges convected within the jet and charges convected on the surface of

the jet. The differential momentum balance equation is written by considering the forces on a short segment of the jet, as shown in figure 6.2, [17, 18].

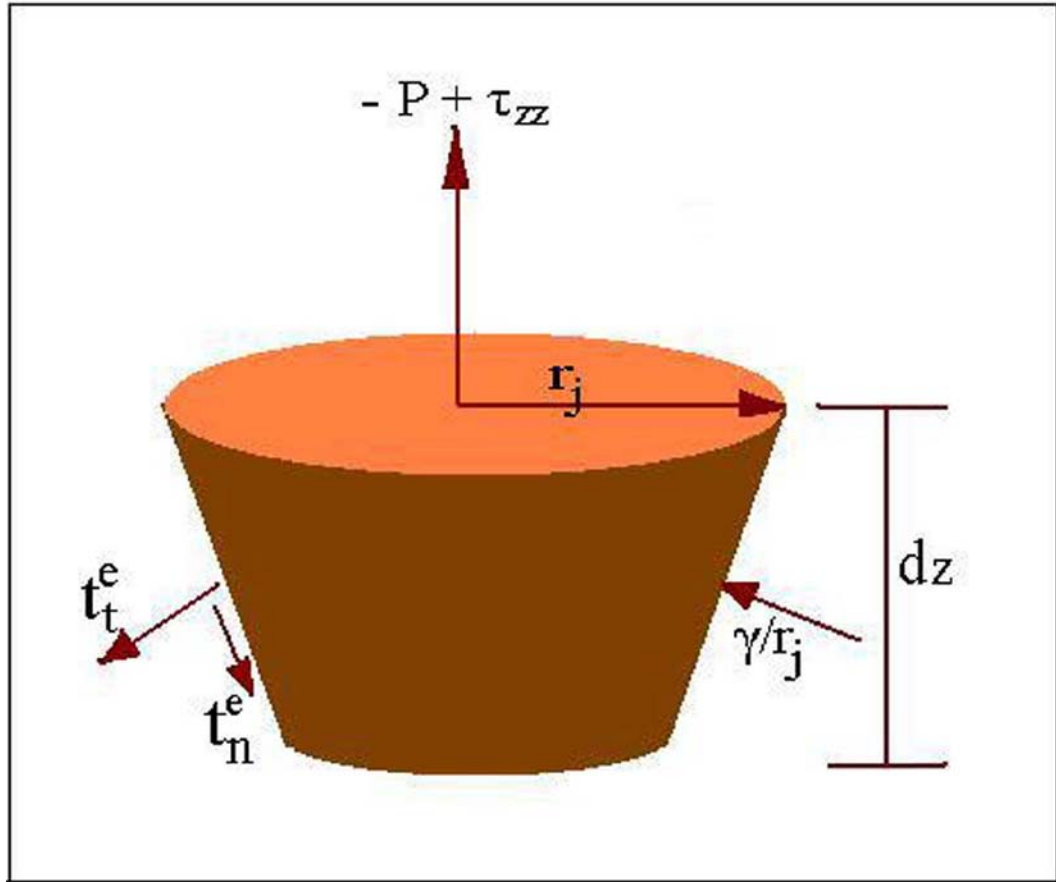


Figure 6.2, Momentum balance on a unit section of the jet [18].

$$\frac{d}{dz} (\pi r_j^2 \rho u^2) = \pi r_j^2 \rho g + \frac{d}{dz} [\pi r_j^2 (-P + \tau_{zz})] + \frac{\gamma}{r_j} 2 \pi r_j r_j' + 2 \pi r_j (t_t^e - t_n^e r_j') \quad (6.7)$$

Where τ_{zz} is the axial viscous stress, P is the pressure, γ is the surface tension, t_t^e , t_n^e are the tangential and normal electric traction forces on the surface of the jet and r_j' is the slope of the jet surface.

Equation (6.7) can be simplified by dividing the equation of $(\pi r_j^2 \rho)$ to be:

$$\frac{d}{dz} \left(\frac{u^2}{2} \right) = -\frac{1}{\rho} \frac{dp}{dz} + g + \frac{2 \sigma E}{\rho r_j} + \frac{1}{r^2} \frac{\partial}{\partial z} \tau \quad (6.8)$$

Where p is the internal pressure of the fluid and τ is the viscous force.

The tangential and normal electric traction forces on the surface of the jet are determined by the surface charge density and the electric field as:

$$t_n^e = \left\| \frac{\epsilon}{2} (E_n^2 - E_t^2) \right\| \approx \frac{\sigma^2}{2\epsilon} - \frac{\epsilon' - \epsilon}{2} E^2 \quad (6.9)$$

$$t_t^e = \sigma E_t \approx \sigma E \quad (6.10)$$

Where ϵ and ϵ' are the dielectric constants of the jet and the ambient air, respectively, E_n and E_t are the normal and tangential components of the electric field at the surface of the jet [17].

These equations are then simplified to a relatively simple 1D model for the slender thinning jet. Hohman et. al. used the slender body equations for Newtonian jets to write relationships in the aspect ratio of the jet for the relevant jet characteristics such as; diameter, velocity, surface charge density and local electric field strength in terms of radial and axial coordinates [13-16].

Feng et. al. subsequently reformulated the slender body equations of Newtonian jets into non Newtonian jets by nondimensionalization of the governing equations for approximation of the electric field equations [17-18]. They have found that the electric potential inside the jet is governed by the free and induced charges on the surface of the jet. However, it has been indicated by their equations that the profile of the cone thinning jet is strongly related to the surface charge density and the applied electric field, as shown in figure 6.3.

More recently, Carroll et. al. [19] have extended the slender jet model further, to include viscoelastic effects and Wan et. al. have taken the thermal effect into account [20].

Spivak et. al. have modified nonlinear rheological equations based on slender body theory for the variation of the jet radius with axial coordinate [21, 22]. They have considered the power law asymptotic approximation of the jet radius $r \sim Z^{-\alpha}$ where the exponent α is a positive constant. Their analysis showed that the power law asymptote for Newtonian fluids with the exponent of 1/4 holds satisfactorily for more general types of fluid.

In addition to the classic equations, Ko et. al. have employed numerical simulation to match the slender thinning jet [23].

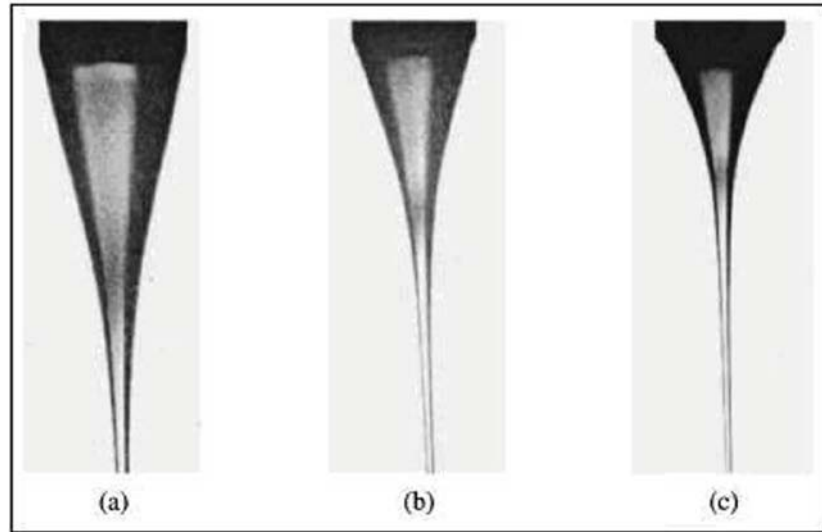


Figure 6.3, (a-c) Experimental pictures producing different cone thinning jet profiles [13].

6.2.2.2 Mathematical models for the straight jet based on allometric scaling laws

The allometric scaling for electrospinning has been proposed by theoretical considerations of the previous governing jet electrohydrodynamic equations which took into account that the viscous jet is a weakly electrical conductive in an external electric field [12]. In this asymptotic regime, the scaling relations between jet radius, other operating parameters and the axial distance z from the spinneret have been investigated [26-38]. These allometric scaling relations were either derived in case of full surface charges or part surface charges of the jet.

Allometric scaling relations in case of full surface charges were processed based on the assumed theory: as the jet is a steady stream at the beginning of electrospinning, the electrical force is dominant over other forces acting on the jet [26-29]. In such a case, equation (6.8) can be approximately expressed as:

$$\frac{d}{dz} \left(\frac{u^2}{2} \right) = \frac{2\sigma E}{\rho r_j} \quad (6.11)$$

It has been allometrically derived from equations (6.5) and (6.6) the following:

$$u \sim r_j^{-2} \quad (6.12)$$

$$\sigma \sim r \quad (6.13)$$

$$E \sim r_j^{-2} \quad (6.14)$$

By substituting equations (6.12), (6.13) and (6.14) into (6.11), we have:

$$\frac{d}{dz} (r^{-4}) = r^{-2} \quad (6.15)$$

This led to the following scaling equation:

$$r \sim z^{-1/2} \quad (6.16)$$

This scaling equation is valid only in the case when the electrical force acting on the jet dominates over the viscous force and the internal pressure of the fluid [28]. Contrary to this, other researchers combined electric field and viscous forces and obtained the following scaling equation with an exponent of -1/4 for the jet radius [21, 22, 30-32]:

$$r \sim z^{-1/4} \quad (6.17)$$

Particularly, it has been expressed that when z distance comes to ∞ , acceleration of the jet in the z direction will vanish completely to lead to the following scaling [28]:

$$r \sim z^0 \quad (6.18)$$

Generally, the relationship between r and z can be expressed as an allometric equation in the form of:

$$r \sim z^b \quad (6.19)$$

Where b is the power exponent.

When $b = 1$ the relationship is isometric and when $b \neq 1$ the relationship is allometric.

In case of part surface charge in the jet, equation (6.6) has been modified to be as the following [26, 33]:

$$\pi_j^2 kE + 2\pi_j u \sigma^\alpha = I \quad (6.20)$$

Where α is a surface charge parameter, when $\alpha = 0$ there is no charge in the jet surface, and when $\alpha = 1$, equation (6.20) becomes the traditional equation for full surface charge, the value of α depends upon the surface charge in the jet.

Similarly, Qin et. al. have obtained the scaling equation for jet radius to be written as [33]:

$$r \sim z^{-\alpha/(1+\alpha)} \quad (6.21)$$

According to the previous study, for equations (6.19) and (6.21), $b = -1/2$ corresponds to a full surface charge and $b > -1/2$ corresponds to a part surface charge. However, it has been found that adding salt to the polymer solution, the power exponent 'b' can be changed [34, 35]. Under a similar scaling laws derivation, allometric scaling relationships between current and solution flow rate, current and electric field and surface charge density and electric field have been reported [36-38].

Briefly, although allometric equations nearly approximate, nonetheless they lead to describe and simplify the complex phenomena in electrospinning from traditional modeling equations.

6.2.3 Mathematical models for the instability and splitting of the jet

Hence an electrified liquid jet travels toward the grounded collector in a straight line, it accelerates and stretches in the presence of the electric field. As it does so, the jet will experience a number of instabilities which are the result of interactions between the charges in the jet and the external electric field. These instabilities which are convected downstream and grow at different rates depend on numerous complicated interactions of variables, such as; the physical properties of the liquid jet, the geometrical shape and strength of the electric field, the air friction and the gravity [1]. The whipping instability 'nonaxisymmetric of the growing perturbations of the jet' is one of several possible instabilities that may occur in an electrified liquid jet [14-16]. Additional types of instabilities may lead, for example, to breakup of the jet into droplets [39-41].

Once the whipping instability starts, it generates a splitting of the jet into a bunch of secondary liquid jets due to the radial charge repulsion forces [42, 43], and each secondary jet generates a sequence of spiral and helical loops [44]. The cycles of whipping instability repeats itself in a similar way until the solvent evaporates, and hence any fibres formed will be resisted from any further elongation [1].

It is currently fully understood that the rapid growth of the whipping instability during electrospinning is the reason for massive stretching of the fluid jet and the continuous decrease of fibre diameter [45]. This reduction in diameter implies increasing of the contact area with the surrounding air and provides greater opportunity for the solvent evaporation and jet solidification during whipping instability. Controlling the

electrospinning therefore requires a mathematical model by which liquid jet instabilities can be quantified.

Recently, many researchers have modeled the dynamics of instability based on the Newton's second law of motion that describes the balance of surface tension forces, viscoelastic forces and applied electrical forces [1, 2, 14-16, 30, 31, 46-55].

Hohman et. al. and co researchers have identified the instabilities for the droplet break up and the whipping of viscous charged liquid jet in a finite electric field [14, 16, 30]. Three different instabilities were identified as: the classical axisymmetric 'Rayleigh', electric field induced axisymmetric and whipping instabilities. They have reported that as the electric field strength increased, the electrical instabilities were enhanced whereas the Rayleigh instability was suppressed. In addition, they have demonstrated that an essential part of the electrospinning mechanism is the rapid whipping liquid jet. In addition, increasing of the electric field strength and dominating of the instabilities depends strongly on the surface charge density and the radius of the jet. In their later work [15], they have used the stability theory to develop a quantitative way for predicting the time when electrospinning occurs, scaling laws for the jet behavior and how electrospinning changes as a function of the liquid jet conductivity and viscosity. Moreover, analyzing of the instabilities has enabled them in producing operating diagrams of electrospinning instabilities that illustrate the combinations of controllable parameters under which a particular liquid is electrospun in whipping way rather than spraying way 'droplet break up'.

Fridrikh et. al. [31, 49] have subsequently analyzed the dynamic equations of Hohman et. al. for the viscoelastic fluid jet in a nonlinear way. The term of these equations are due to acceleration of the charged jet under the influence of the applied electric field, normal stresses due to surface tension and bending of electric field lines and charge to charge repulsion.

Reneker et. al. were the first in establishing a viscoelastic model of a rectilinear electrified liquid jet [1, 54]. The trajectory of the fibre is calculated in accordance with Newton's second law of motion, assuming that the fibre jet consists of a strand of charged beads which are springs and dashpots connected by viscoelastic dumbbells. In their mathematical model description, they have used the Gaussian electrostatic system of units. The model showed that both the viscoelastic force along the fibre jet and the surface tension tend to stabilize the charged fibre jet. In addition, a nearly linear increase of the straight segment with the applied voltage and the whipping frequency is so fast that the jet appears to be splitting into multiple secondary fibre jets.

Aerodynamic forces and gravity effect were neglected as well as solvent evaporation. This was taken into account in a later study [2], in which it has been found that the initial angle of the looping envelope strongly depends on evaporation and solidification rates for the polymer solutions. Nevertheless, the expected tendency is a decrease of the loop radius and the envelope angle with increasing electric field.

Dayal et. al. have extended the bead model developed by Reneker et. al. to multiple virtual strands of beads because of its capability in capturing the fibre wiggling or whipping dynamics [55]. It has been taken into account that the solvent evaporation plays a pivotal role in determining the internal fibre morphology and describing the real time evolution of microstructure for providing guidance to the actual electrospinning process.

6.2.4 Mathematical models for nanofibres collection

As it has been described above, electrospun nanofibres fly downwards until they impact with the collector, resulting in a nonwoven membrane of unoriented fibres. However, the bending, winding, spiraling and looping path of the jet strongly influences the extent of crossing nanofibres, which affects the structural (pore size distribution, pore porosity) and the permeability properties of the electrospun nanofibre mat during collection. Moreover, if the collected electrospun nanofibres still contain a small amount of solvent, welding at contact points between overlapping fibres may occur. Therefore the structure of the collected nanofibres web is usually very irregular and a theoretical model is necessary to describe the structure of the types of fibrous network produced by electrospinning.

Eichhorn et. al. have recently modeled the electrospun nanofibrous web by investigating the network mass per unit area and porosity [56]. It has been shown by their model that the electrospun nanofibre diameter is a dominant factor in controlling the pore diameter of the nanofibres network. However, little information on the mathematical models for predicting the distribution of mass, inter fibre contacts, fibre contact distributions for integrity of the networks and the porosity and pore size distributions has been reported in the literature.

6.3 Electrospinning jet/ nanofibres velocity

The above review has showed that the movement of the electrospinning jet is a complicated electrohydrodynamic problem. The objective here is twofold. Firstly, we wish to clarify the modes theory related to the thinning and splitting of the jet and secondly to review the methods used for finding practically the jet velocity.

6.3.1 Electrospinning modes theory

Recently, researchers have published two different modes theory for the electrospinning process. The first mode has been clarified as; after Taylor cone is elongated to a straight line jet, there would be a sudden whipping instability which will curve the elongated jet along its axis to form a series of spiral loops and the diameter of the curved jet becomes thinner as the loop circumference increases as shown in figure 6.4, [1, 2]. Splitting of the jet into secondary jets does not occur according to this mode. In other words, the deposited fibre is single and it is obtained in nano scale because of evaporation of the solvent, elongation and whipping instability of the jet.

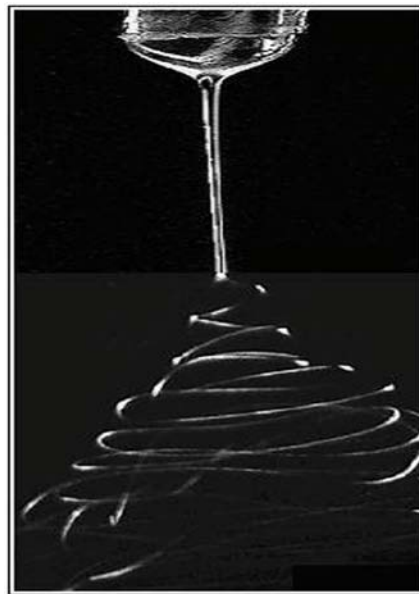


Figure 6.4, Mode of single jet thinning [1, 2].

In another mode theory [57-61], the single jet elongates and thins for a small spinning distance and then it splits into multiple jets by the radial electric repelling forces as shown in figure 6.5.

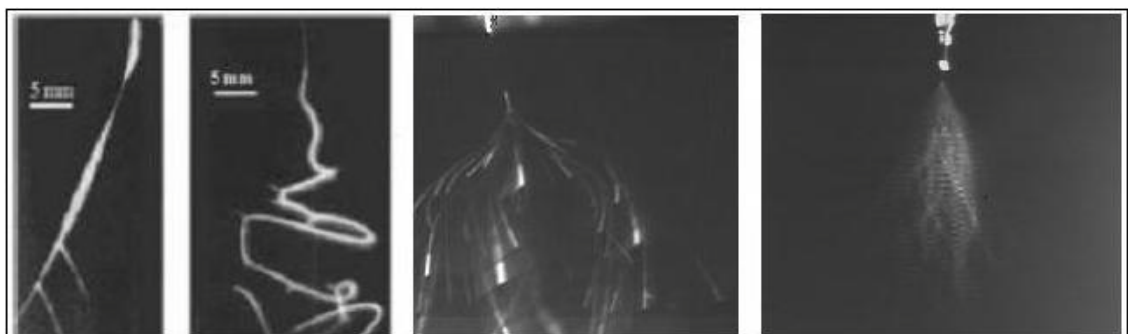


Figure 6.5, Literature photos for the second mode of splitting single jet into multiple jet nanofibres [60, 61].

Technically, both modes can occur by controlling the liquid jet viscosity, surface tension and conductivity and the applied electric field [19]. However, the single thinning jet mode may only occur with high viscous liquid jet and low applied electric field [19].

The analysis can prove the values of jet and its collected nanofibres velocity, strain, draw ratio and nanofibres area reduction of a complicated jet movement. For the first mode, the velocity of the electrospun single nanofibre can be calculated by relating the mass flow rate of polymer solution from the spinneret and the rate at which the polymer mass is being collected [43]. The theoretical calculation results by Yarin et. al. have indicated a draw ratio of the collected single nanofibre due to elongation is equal to 34815 for PEO and water at 6 wt. % concentration [2, 62]. In this case, if the jet was drawn in a straight line at a velocity of around 1.0 m/sec, and then elongated to a draw ratio of 34815, the velocity achieved at the nanofibre end of the jet would be about 35000 m/sec, thus it is 100 times faster than the speed of sound in the air. The high value of the nanofibre velocity and the associated high area reduction ratio and longitudinal strain rate imply that the macromolecules in the nanofibre should be stretched and axially oriented. It has been reported later, by the same author, that the mode was failed by collecting the electrospun polymer nanofibre on a rotating wheel with linear speed on the edge of the wheel of 5.3 m/sec [63]. SEM examinations of nanofibres collected on the rotating wheel revealed multiple necking patterns at certain places along the nanofibre length, as shown in figure 6.6. They have also indicated clearly that the source of necking is the strong stretching of solidified nanofibres by the tapered wheel, concluding that the velocity of the collected nanofibres ‘not only one nanofibre’ is in excess of 5 m/sec. This conclusion is supported by the fact that necking was not observed in nonwoven nanofibre mats collected on a grounded plate.

Therefore, to achieve the correct velocity, many successive splits into many fibres ‘final number of branches’ would be accounted for the observed velocity and reduction in diameter. Typically, the velocity of the electrospun nanofibres can be calculated by relating the mass flow rate of polymer solution from the spinneret and the rate at which the polymer mass is being collected with its associated number of branches as will be considered later in equation (6.28).

On the grounds of the analysis above, the mode of continuous single collected nanofibre cannot exist, unless the jet is highly viscous [19]. So that, alternatively, the possibility

of the jet splitting mode has to be assumed and further discussed. In addition, starting from this mode, we will derive simple mathematical equations for calculating the velocity of the jet and the collected nanofibres and their branch numbers and then measure practically the velocity of the collected nanofibres for actual comparison.

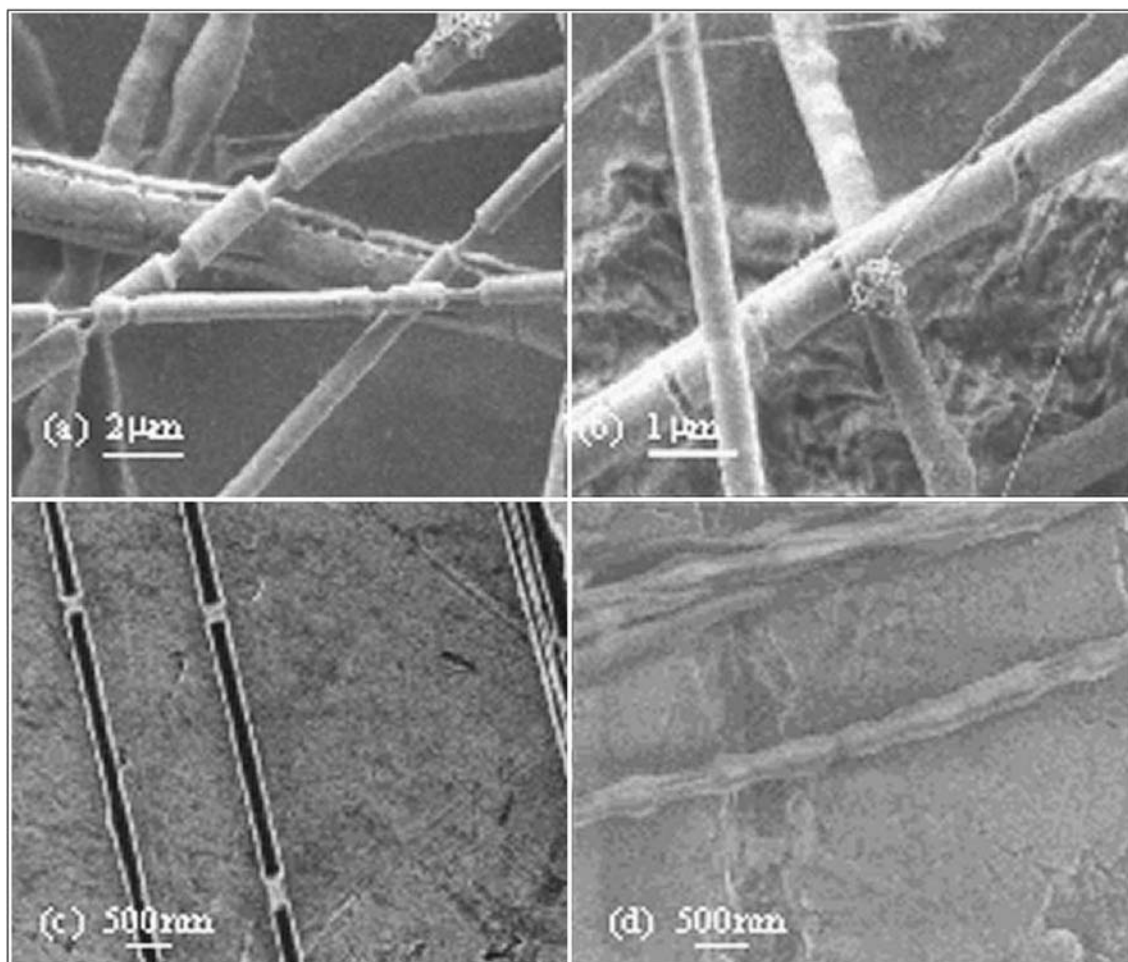


Figure 6.6, (a-d) SEM images of multiple neck formation in PEO electrospun nanofibres collected on rotating wheel at linear speed of 5.3 m/sec [63].

6.3.2 Practical methods for determining the jet velocity

Recently, researchers have used different tools and methods for determining the jet velocity [1, 2, 64-66]. Reneker et. al. analyzed the movement of the jet by observing particular sequential images of the growing whipping instability and the length of the straight segment change per unit time for schematically calculating the velocity of the flying nanofibres [1, 2]. Warner et. al. measured the velocities along the straight segment of the jet with a laser Doppler velocimeter and reported a velocity of 1 to 15 m/sec [64]. In fact, Doppler velocimetry is more applicable for monitoring the longitudinal strain rate, particularly where the jet diameter is large. However, the

Doppler velocimetry data become more difficult when whipping instability is encountered [1].

Xu et. al. [65] incorporated tracer particles ‘glass beads’ into the polymer solution for electrospinning and the particles speed was measured by observing the particle movement using a high speed video camera, as shown in figure 6.7.

Bellan et. al. used fluorescence microscopy to track individual fluorescent particles in the Taylor cone and in the fluid jet [66].

However, the optical system used to observe the moving particles within the jet consisted of several complicated parts. Hence, the field of view must be of dimensions similar to those in the jet and high velocity particles will only appear to the imaging system for a short period of time necessitating a high speed video camera.

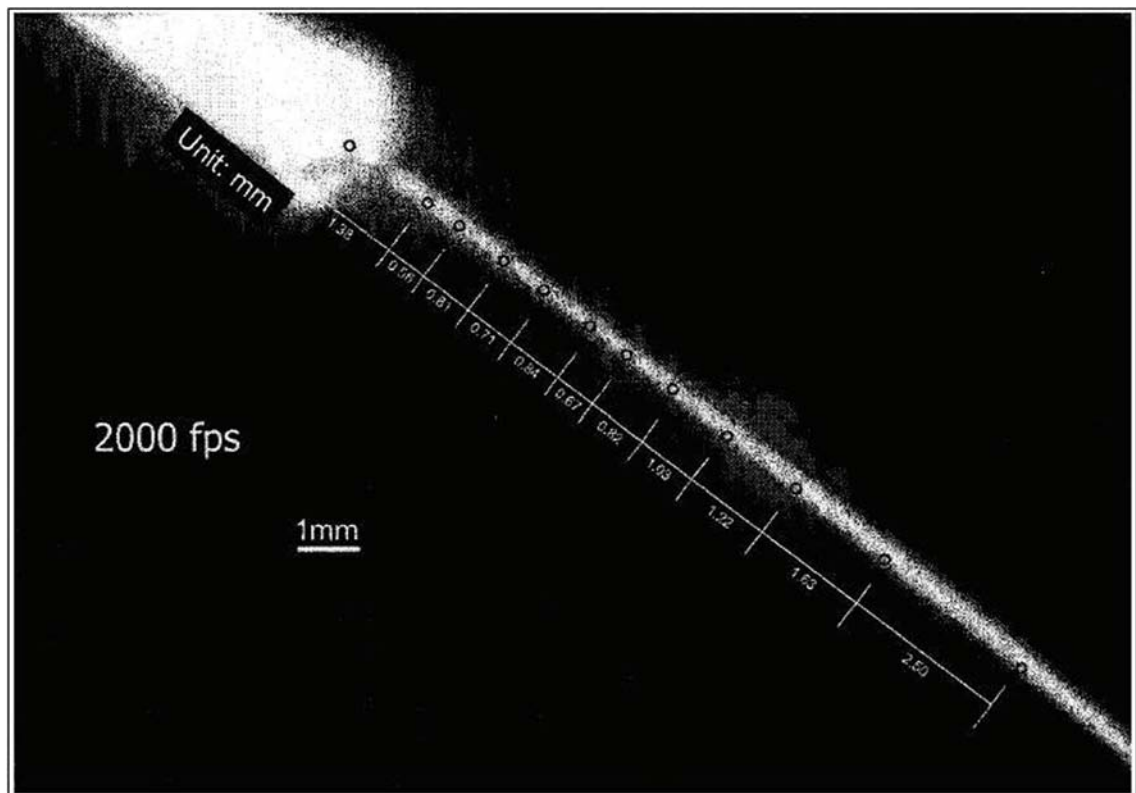


Figure 6.7. Jet speed measurement by particle tracing [65].

6.4 Novel mathematical model for determining the kinematics of the electrospinning nanofibres [67]

The real movement of the electrically charged jet which is ejected out of the spinneret towards the collector, consists of three stages. The first stage is the formation of Taylor cone, the second is acceleration and thinning elongation of the jet and the third is splitting and whipping instability of the jet. Here, let us examine the second stage and

its contribution to the onset of the splitting and whipping instability. Subsequently, we will derive, based on the second mode, simple mathematical equations for calculating **Table 6.1**, Definitions and units of measurement for deriving of the jet/ nanofibres velocity equations.

Symbol	Meaning	SI Unit of Measure
r_j	Radius of the jet at any point of its length	Meter
r_{jMin}	Minimum radius of the jet at which splits	Meter
r_o	Initial radius of the jet	Meter
u_j	Velocity of the jet at any point of its line	Meter per second
u_{jMax}	Maximum velocity of the jet corresponded to (r_{jMin}) at which the jet splits	Meter per second
u_f	Velocity of the collected nanofibres	Meter per second
ρ	Specific mass of the jet liquid	Kilogram per cubic meter
Q	Mass flow rate of the jet	Kilogram per second
σ	Surface charge density of the liquid jet	Coulombs per square meter
k	Electrical conductivity of the liquid jet	Siemens per meter
E	Unit electric field	Volt per meter
I	Total electric current along the fibres jet between the spinneret and collector	Ampere or volt per ohm or coulombs per second
τ	Viscous stress in the liquid jet	Newton per square meter
p	Internal pressure in the liquid jet	Newton per square meter
Z	Spinneret- collector distance	Meter
g	Gravity	Meter per square meter
a_j	Cross section of the jet at which splits	Square meter
a_f	Cross section of one nanofibre	Square meter
c_p	Concentration of the polymer in the solution	
L_j	Length of the total jet before splitting	Meter
L_f	Length of collected one nanofibre	Meter
$L_{\Sigma f}$	Sum of lengths of the collected nanofibres	Meter
N_b	Final number of branches at collection	
E_v	Evaporation percentage of the solution	%
Mf_w	Mass of collected wet fibres per unit time	Kilogram per second
Mf_d	Mass of collected dry fibres per unit time	Kilogram per second

the velocity of the jet and thus the collected nanofibres and their branch numbers. These equations will form an analytical basis of jet formation and nanofibres kinematics in electrospinning. These predictions will be verified with experimental measurements. Before we start deriving the theoretical equations, table 6.1, provides the meaning of each symbol and the SI 'International System' or 'metric system' units of measurement. We assume that the jet splits uniformly in area into secondary jets and so on as shown schematically in figure 6.8. At the beginning, we consider the conservation of mass equation without evaporation of the solvent i.e. the mass is constant across the spinning line, we mention loss of mass later.

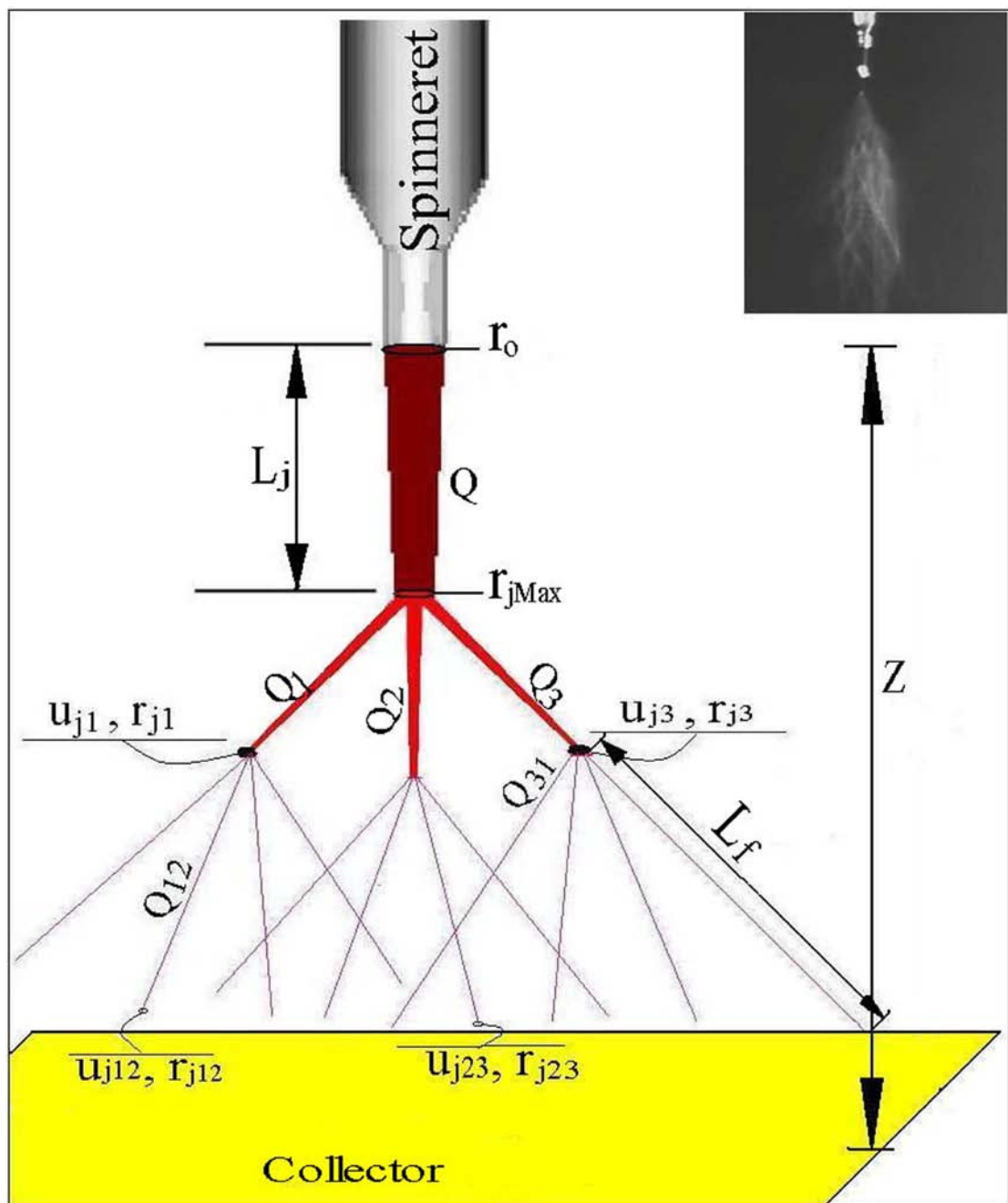


Figure 6.8, Schematic drawing of the jet stretching and splitting into uniform branches.

The relation between the mass flow rate and polymer solution density, velocity and cross section area in equation (6.5), neglecting the evaporation of the solvent to produce:

$$a_o = a_j = a_1 + a_2 + a_3 + \dots + a_n = \dots \quad (6.22)$$

When evaporation of the solvent ‘solidification effect’ is accounted for, the mass flow rate equation can be written as:

$$\begin{aligned} Q &= \rho_o u_o a_o = E_{vj} \rho_j u_j a_j = E_{v1} [\rho_1 u_1 a_1 + \rho_1 u_2 a_2 + \rho_1 u_3 a_3 + \dots + \rho_1 u_n a_n] \\ &= E_{v2} [\dots] = \dots = E_{vn} [\dots] \end{aligned} \quad (6.23)$$

Here, the symbol E_v represents the total evaporation of the solvent during the electrospinning process or in other words the ‘concentration of the polymer in the solution’; E_{vj} , E_{v1} , E_{v2} , and E_{vn} represent the partial evaporation of solvent or solidification. Thus, we can express the following expression as:

$$E_v = E_{vj} \cdot E_{v1} \cdot E_{v2} \dots E_{vn} \quad (6.24)$$

Typically, equation (6.23) represents the real dynamic path and mass change during electrospinning. For instance, let us take a part of the equation as $\rho_o u_o a_o = E_{vj} \rho_j u_j a_j$. As in electrospinning the electrical forces stretch the jet causing an area reduction and thus velocity increase and solvent evaporation causing a change of the density, the components of the equations will balance each other to be correct. In other words, as $E_{vj} \ll 1$, $\rho_o \leq \rho_j$ and $a_j < a_o$ the u_j must be bigger than u_o in number of times at which the equation $\rho_o u_o a_o = E_{vj} \rho_j u_j a_j$ balances out.

Electrospinning is a dynamic process in which the electrical and viscoelastic forces control the nanofibres velocity and the solvent evaporation from the jet during its flight from the spinneret to the collector. Here by manipulating equation (6.23) and the schematic drawing of the jet stretching and splitting in figure 6.8, we can write the fundamental equations for theoretically calculating the velocity of jet and collected nanofibres and their length and branch numbers as following:

Velocity of the collected nanofibres:

$$\boxed{u_f = \frac{u_{jMax}}{N_b} \left(\frac{a_j}{a_f} \right)^2 c_p} \quad (6.25)$$

And the final number of the branches at collection:

$$\boxed{N_b = \frac{L_j}{L_f} \left(\frac{a_j}{a_f} \right)^2 c_p} \quad (6.26)$$

And the sum of the lengths of the collected nanofibres:

$$\boxed{L_{\sum f} = L_j \left(\frac{a_j}{a_f} \right)^2 c_p} \quad (6.27)$$

And

$$\boxed{L_{\sum f} = N_b \cdot L_f} \quad (6.28)$$

Additionally, the evaporation percentage of the solution during electrospinning process can be calculated as:

$$\boxed{E_v = \frac{(Q - Mf_w)}{(Q - Mf_d)} \times 100} \quad (6.29)$$

The above equations represent the fundamentals for calculating the kinematics of the nanofibres. The key component, based on these equations, is the u_{jMax} which is going to be mathematically derived hereinafter for finding the actual values of these equations.

Based on slender body theory, mass conservation and charge conservation (Maxwell) equations (above) can be written as:

$$\pi r_j^2 \rho u_j = Q$$

In SI meaning: $\text{meter}^2 \cdot \text{kg/meter}^3 \cdot \text{meter/sec} = \text{kg/sec}$ (6.30)

$$2\pi r_j \sigma u_j + k\pi r_j^2 E = I$$

In SI meaning:

$$\text{meter} \cdot \text{coulombs/meter}^2 \cdot \text{meter/sec} + (1/\text{ohm} \cdot \text{meter}) \cdot \text{meter}^2 \cdot \text{volt/meter} = \text{Ampere} = \text{coulombs/sec} = \text{volt/ohm}$$
 (6.31)

As has already been discussed, at the initial stage of the electrospinning, the electrical forces are dominant over other forces such as surface tension and internal viscosity [26-29, 43, 54]. Otherwise, no fine charged jet will eject. Additionally, the drag force and the gravity force acting on the jet are very small in magnitudes and can be easily neglected [1]. Thus equation (6.8) can be simplified to equation (6.11).

$$\frac{d}{dz} \left(\frac{u_j^2}{2} \right) = -\frac{1}{\rho} \frac{dp}{dz} + \frac{2\sigma E}{\rho r_j} + \frac{1}{\rho} \frac{d\tau}{dz} + g \quad \text{to be} \quad \frac{d}{dz} \left(\frac{u_j^2}{2} \right) = \frac{2\sigma E}{\rho r_j}$$

By using the Cauchy's inequality and similarly applying it on the equations (6.6) and (6.11) similar to He et. al. [68], to derive the velocity of the straight jet in the point at which the splitting of the jet into secondary jets occurs.

Cauchy's inequality can be written as:

$$ab \leq \frac{1}{4}(a+b)^2, a > 0, b > 0$$
 (6.32)

For example: $2 * 3 < \frac{1}{4}(2+3)^2$ and $2 * 2 = \frac{1}{4}(2+2)^2$

Now by multiplying the numerator and denominator in the fraction of equation (6.11) by $(\pi^2 \cdot k \cdot r_j^3 \cdot u_j)$, we can obtain the following equation:

$$\frac{d}{dz} \left(\frac{u_j^2}{2} \right) = \frac{2\pi r_j \sigma u_j \times k\pi r_j^2 E}{\pi^2 \rho k r_j^4 u_j} \quad (6.33)$$

Using the Cauchy's inequality in view of equation (6.33), we can obtain the following inequality:

$$\frac{d}{dz} \left(\frac{u_j^2}{2} \right) \leq \frac{(2\pi r_j \sigma u_j + k\pi r_j^2 E)^2}{4\pi^2 \rho k r_j^4 u_j} \quad (6.34)$$

And

$$\frac{d}{dz} \left(\frac{u_j^2}{2} \right) \leq \frac{(2\pi r_j \sigma u_j + \pi k r_j^2 E)^2}{4\pi k r_j^2 (\pi r_j^2 \rho u_j)} \quad (6.35)$$

In view of mass conservation and Maxwell's equation of charges in equations (6.5) and (6.6), we can immediately obtain:

$$\frac{d}{dz} \left(\frac{u_j^2}{2} \right) \leq \frac{I^2}{4\pi k Q r_j^2} \quad (6.36)$$

We have also from equation (6.5):

$$u_j^2 = \frac{Q^2}{\pi^2 \rho^2 r_j^4} \quad (6.37)$$

Putting equation (6.37) into equation (6.36) will give us the following inequality:

$$\frac{d}{dz} \left(\frac{Q^2}{2\pi^2 \rho^2 r_j^4} \right) \leq \frac{I^2}{4\pi k Q r_j^2} \quad (6.38)$$

So the inequality of jet radius can be written as:

$$\frac{d}{dz} (r_j^{-2}) \leq \frac{\pi \rho^2 I^2}{2kQ^3} \quad (6.39)$$

Now by integrating equation (6.39) for z we can immediately obtain:

$$r_j^{-2} \leq \frac{\pi \rho^2 I^2}{2kQ^3} z + r_o^{-2} \quad (6.40)$$

Hence we have $r_j = r_o$, when $z = 0$

Let us define δ as:

$$\delta = \frac{\pi \rho^2 I^2}{2kQ^3} \quad (6.41)$$

Now in view of equations (6.40) and (6.41) we can write:

$$r_j \geq \frac{1}{\sqrt{\delta z + r_o^{-2}}} \quad (6.42)$$

As we have already seen, based on slender body theory, the jet radius decreases along its straight line up to the point of splitting. On this point of view, ($r_j = r_{j\text{Min}}$) if z reached to L_j , equation (6.42) can be written as:

$$r_{j\text{Min}} = \frac{1}{\sqrt{\delta L_j + r_o^{-2}}} \quad (6.43)$$

Subsequently, the minimum value of r_j in the initial stage of the jet can be written as:

$$r_{j\text{Min}} = \frac{r_o}{\sqrt{\delta r_o^2 L_j + 1}} \quad (6.44)$$

And

$$r_{jMin}^2 = \frac{r_o^2}{\delta r_o^2 L_{j+1}} \quad (6.45)$$

From the mass conservation equation we can obtain the following relationship:

$$u_{jMax} = \frac{Q}{\pi \rho r_{jMin}^2} \quad (6.46)$$

Now from equations (6.45) and (6.46), we can calculate the maximum velocity of the straight jet of the electrospinning at the point where instability and splitting occur as:

$$u_{jMax} = \frac{Q(\delta r_o^2 L_{j+1})}{\pi \rho r_o^2} \quad (6.47)$$

Where δ is defined as: $\delta = \frac{\pi \rho^2 I^2}{2kQ^3}$ and all other symbols are defined in the above table and measured in SI units.

By exchanging the symbols by their SI units as the following:

$$\delta = \frac{\left(\frac{\text{kg}}{\text{m}^3}\right)^2 \times \left(\frac{\text{volt}}{\text{Ohm}}\right)^2}{\left(\frac{1}{\text{Ohm.m}}\right) \times \left(\frac{\text{kg}}{\text{sec}}\right)^3} = \frac{\text{sec}^3 \times \text{volt}^2}{\text{m}^5 \times \text{Ohm} \times \text{kg}} = \frac{\text{sec}^3 \times \text{Watt}}{\text{m}^5 \times \text{kg}} = \frac{\text{sec}^3 \times \left(\frac{\text{N} \times \text{m}}{\text{sec}}\right)}{\text{m}^5 \times \text{kg}} = \frac{1}{\text{m}^3} \quad (6.48)$$

$$\text{Where: } I = \text{Ampere} = \frac{\text{volt}}{\text{Ohm}},$$

$$k = \frac{\text{Siemens}}{\text{m}} = \frac{1}{\text{Ohm} \times \text{m}},$$

$$\frac{\text{volt}^2}{\text{Ohm}} = \frac{\text{volt}}{\text{Ohm}} \times \text{volt} = \text{Ampere} \times \text{volt} = \text{Watt} \quad ,$$

$$\text{Watt} = \frac{\text{N} \times \text{m}}{\text{sec}} \quad ,$$

$$\text{N} = \frac{\text{kg} \times \text{m}}{\text{sec}^2}$$

$$u_{j\text{Max}} = \frac{\frac{\text{kg}}{\text{sec}} \left(\frac{1}{\text{m}^3} \times \text{m}^2 \times \text{m} + 1 \right)}{\frac{\text{kg}}{\text{m}^3} \times \text{m}^2} = \frac{\text{m}}{\text{sec}} \quad (6.49)$$

The operational parameters of the electrospinning process, in accordance with this model are; flow rate (Q), electric current (I), and the jet geometrical dimensions L_j and r_o and its physical properties of density ρ and conductivity k .

It is necessary to mention that the best calculation of the jet velocity can be from measurements of the mass of the collected nanofibres over a known time interval the cross section area of the jet and the density of the polymer solution [43].

6.5 Experimental work [67]

6.5.1 Polymer solution preparation, electrospinning and characterization

Polyethylene oxide (PEO) with molecular weight of 400.000 gram/mole and zero shear viscosity of 5 Pascal.sec in 6 % wt. water was purchased from Sigma-Aldrich (Gillingham, UK). The density of 6 % wt. PEO dissolved in water is $1.075 \times 10^{+3} \text{ kg/m}^3$, and the electrical conductivity is 0.0125 Siemens/m measured by using four probes method. The polymer solution was placed in a 5 mL capacity syringe (Fisher Co., Leicestershire, UK) and fed through a vertically orientated (17 gauge) blunt ended metal needle ‘spinneret’ with 1 mm inner diameter. The needle was connected to one electrode of a high voltage direct current power supply (MK35P2.0-22, Glassman, New Jersey, USA) which will supply a voltage of 9 KV. An earthed aluminium collector plate measuring 15 cm \times 15 cm was set 18.5 cm ‘spinning distance’ below the

spinneret. We note that, operation parameters such as needle gauge, applied voltage, electrospinning distance, polymer type and its molecular weight and PEO/water concentration were based on Xu et. al. research work and fully imitated [65]. In their experimental research, a novel method was developed to characterize the micron scale jet diameter and length. In this work, we will use their results in measuring the minimum jet diameter and its length before going into splitting and whipping instability stage. The collector plate was insulated from the ground, and the electrical jet current was obtained by measuring the voltage drop across a resistor. The current measurement was taken through a digital reading and converted using Ohm's law. The experiment was run for 12 minutes and the polymer solution flow rate was measured during this time. The collector mass was weighted before and after the collection of nanofibres using a micro balance (Mettler TG 50 thermobalance, KPS Calibrations, Zurich, Switzerland) at 1 microgram weight resolution. The mass difference was considered as the amount of the depositing wet nanofibres within 12 minutes. Then, in order to fully drying and weighting the collected nanofibres, the collector was placed inside the oven under the temperature of 40° C for 24 hours.

For practical determination of the nanofibres velocity, the electrospun nanofibres were collected on the edge of a collector disk rotating around a horizontal axis. The edge of the disk was placed at a distance of 18.5 cm below the spinneret. An electric field of 9 kV was created between the surface of the liquid drop 'spinneret' and the rotating disk collector. During the spinning process, the disk was rotated at different controlled linear speeds of 0 m/sec 'constant collector speed'; 1 m/sec; 2 m/sec; 3 m/sec; 4 m/sec; 4.8 m/sec; 5 m/sec; 6 m/sec; 7 m/sec; 8 m/sec and 9 m/sec. As the nanofibres reach the disk, they are wound onto the edge of the rotating disk, as shown in figure 6.9.

For characterizing the deposited nanofibres, two separate tapes of aluminum sheets were laid on the surface of the circumference of the rotating disk, for enabling the collection of two samples of nanofibres. These samples were sputter coated with gold-palladium for 45 sec at 18 mA using a sputter coater. Nanofibres were examined using a JEOL JSM 5600 scanning electron microscope at an accelerating voltage of 5 kV. The experiments were conducted under ambient condition at room temperature and 25 % RH humidity. For measuring the average diameters of the fibres viewed on a photograph, a transect line was drawn from the bottom right to the top left of the SEM image and fibre diameters were measured at the point the line transected, perpendicular

to the fibre length. These results were used to compile fibre diameters distribution profiles.

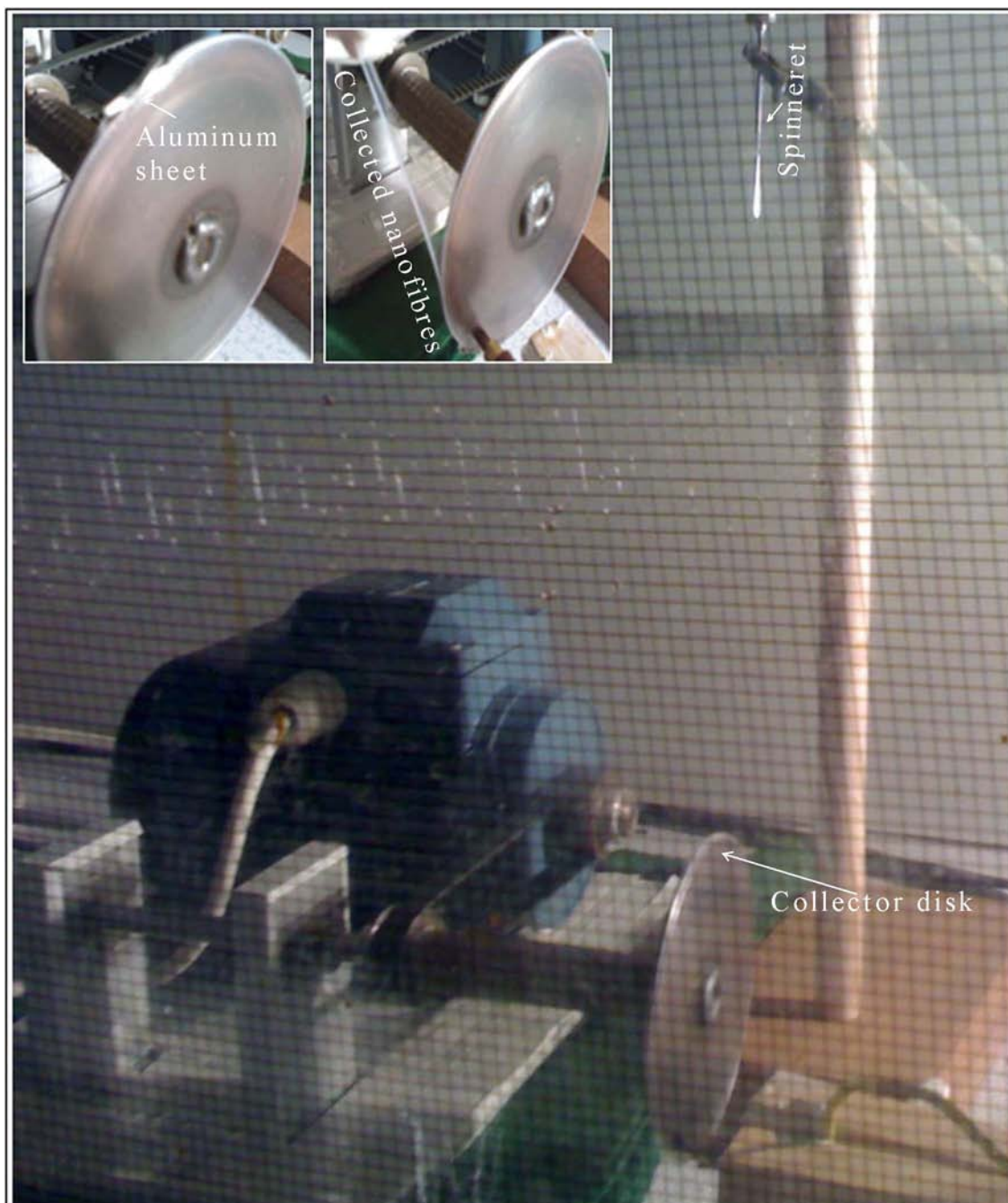


Figure 6.9, Photograph for the electrospinning process with operation parameters similar to Xu's et. al. electrospinning operation parameters [65]. The disk was rotated at different controlled linear speeds of stationary collector; then 1 m/sec; 2 m/sec; 3 m/sec; 4 m/sec; 4.8 m/sec; 5 m/sec; 6 m/sec; 7 m/sec; 8 m/sec and 9 m/sec. The electrospun nanofibres were collected on the edge of a collector rotating disk around its horizontal axis. Two separate tapes of aluminum sheet were laid on the surface of the circumference of the rotating disk, for enabling the collection of two nanofibre samples.

6.5.2 Theoretical and practical calculation of the jet velocity

To get the theoretical values of the jet/ nanofibres velocity, number of branches and dynamics of evaporation, we will present the measured values of the electrospinning process parameters. The polymer solution was spun at flow rate of 0.12 mL during 12 minutes of electrospinning, and thus it is equivalent to 0.6 mL/hour. By taking into account the density of the polymer solution ($1.075 \times 10^3 \text{ kg/m}^3$), the flow rate of the polymer solution is $Q = 1.792 \times 10^{-7} \text{ kg/sec}$. Collected nanofibres during the electrospinning period of 12 minutes, were weighted (0.0109 grams) i.e. the mass of collected wet nanofibres $Mf_w = 1.516 \times 10^{-8} \text{ kg/sec}$. Then, these nanofibres were fully dried for 24 hours and weighted again (0.0077 grams) i.e. the mass of collected dry nanofibres $Mf_d = 1.07 \times 10^{-8} \text{ kg/sec}$. When compared, the measured mass of the collected dry nanofibres agrees fully with the theoretical equation of mass of the collected dry nanofibres such as:

Mass of the collected dry nanofibres = Mass flow rate of the jet \times Concentration of the polymer in the solution

In the unit's expression:

$$Mf_d = Q \cdot c_p \quad (6.50)$$

The electrical jet current was 10 nanoamperes. In fact, the value of the current is so small which was expected due to low applied voltage, low flow rate, low polymer concentration and high electrospinning distance. This value is also in agreement with other research literature [69].

As we mentioned above, Xu et. al. used two different optical methods which are light diffraction and interference colour for measuring of the minimum straight jet diameter and its length based on the same parameters that we used. Figure 6.10, shows the jet profile i.e. diameter of the jet path with travelling distance produced by Xu et. al. research work [62, 65]. A minimum jet diameter of 2 microns and length of 36 mm was analyzed and concluded in their work. At present, we will put these values in the following equations for calculating the theoretical value of the maximum jet velocity. Theoretical value of the maximum jet velocity can be calculated from equation (6.47) as:

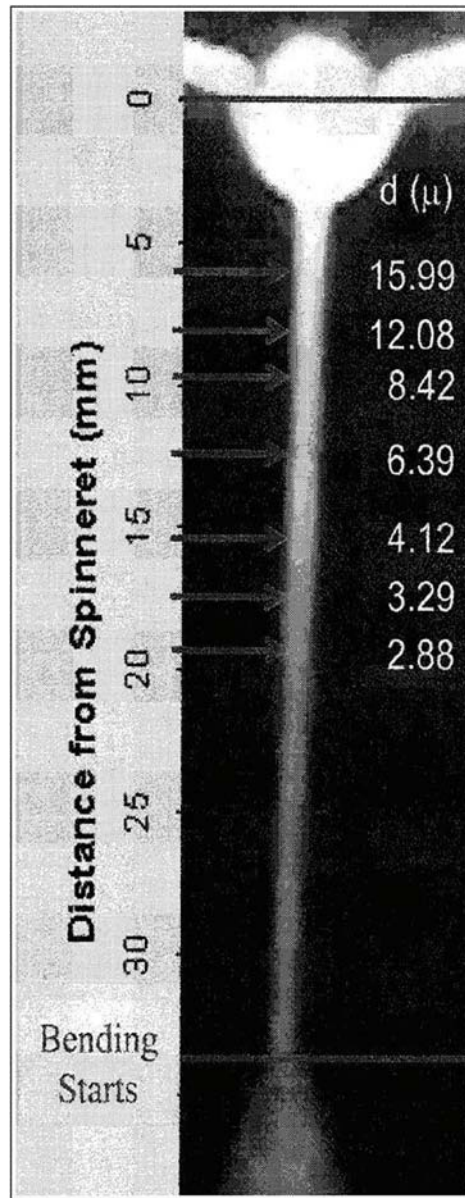


Figure 6.10, This photograph shows a diameter change of the straight segment of the jet as a function of position along the jet, measured by the diffraction of a laser beam. This jet profile was produced by Xu et. al. under the following electrospinning parameters; Polyethylene oxide (PEO) with molecular weight of 400.000 gram/mole in 6 % wt. water and fed through a vertically orientated (17 gauge) blunt ended metal needle ‘spinneret’ with 1 mm inner diameter. The needle was connected to a voltage of 9 KV and delivered by a collector set at 18.5 cm ‘spinning distance’ below the spinneret [62, 65].

$$u_{j\text{Max}} = \frac{Q(\delta r_o^2 L_j + 1)}{\pi \rho r_o^2} \quad \text{and} \quad \delta = \frac{\pi \rho^2 I^2}{2 k Q^3}$$

$$\delta = \frac{\pi \cdot (1.075 \cdot 10^3)^2 \cdot (10 \cdot 10^{-9})^2}{2 \times 0.0125 \times (0.1792 \cdot 10^{-6})^3} = 2.523555 \cdot 10^{12}$$

$$u_{jMax} = \frac{0.1792 \cdot 10^{-6} \cdot \left[2.523555 \cdot 10^{12} \times (1 \cdot 10^{-3})^2 \times (36 \cdot 10^{-3}) + 1 \right]}{\pi \times 1.075 \cdot 10^3 \times (1 \cdot 10^{-3})^2}$$

$$u_{jMax} = 4.82 \text{ [m/sec]}$$

It is also possible as mentioned that the practical velocity of the jet can be calculated by knowing the mass of the collected 'wet' nanofibres in a known time, the cross section area of the jet and the density of the polymer solution, assuming it stays constant across the jet length. Subsequently, the velocity of the jet at any point of its z axis can be written as:

$$u_j = \frac{4 \times Mf_w}{\rho \pi r_j^2} \quad (6.51)$$

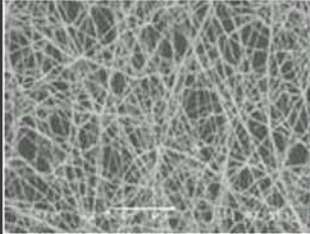
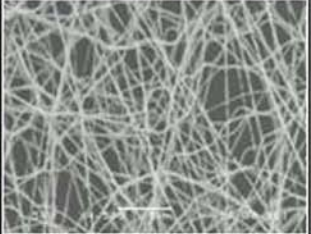
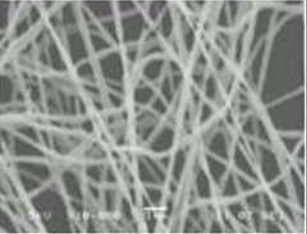
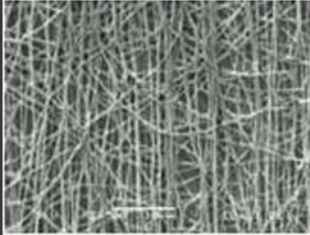
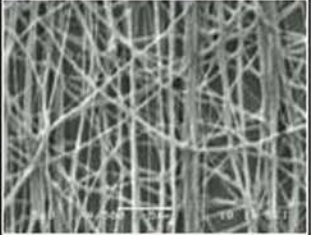
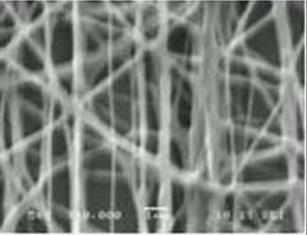
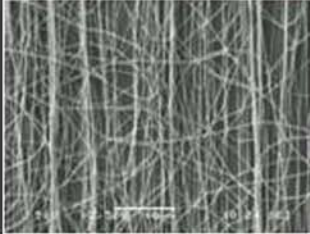
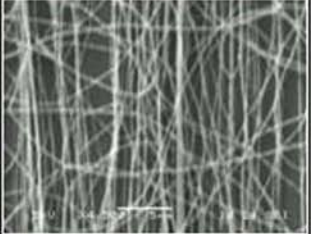
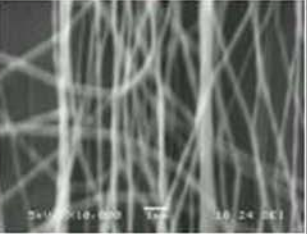
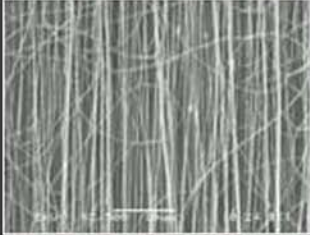
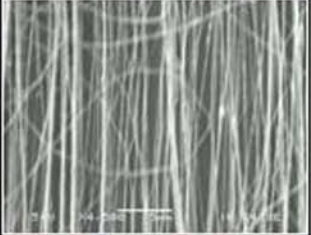
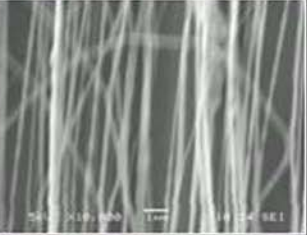
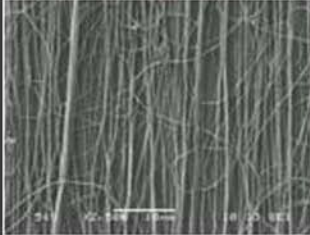
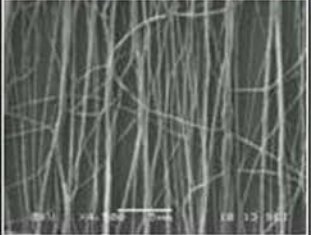
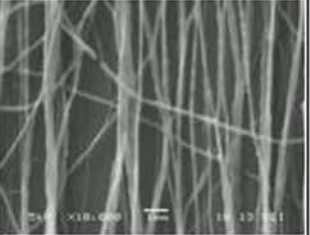
$$u_{jMax} = \frac{4 \cdot (1.516 \times 10^{-8})}{\pi \cdot (1.075 \times 10^3) \cdot (2 \times 10^{-6})^2}$$

$$u_{jMax} = 4.49 \text{ [m/sec]}$$

6.5.3 Practical determination of the collected nanofibres velocity

The work for measuring the velocity of the collected nanofibres was based on Yarin et. al. method by collecting the nanofibres on a rotating grounded disk [63]. Changing the linear speed of the rotating disk and observing the speed value at which the diameter of the collected nanofibres start to reduce will define the velocity of the nanofibres. Ten different linear speeds of the disk collector (1 m/sec and 9 m/sec) are taken to match the velocity of the nanofibres. Figure 6.11, shows SEM images of the electrospun polyethylene oxide nanofibres prepared by using different disk collector linear speeds. When the disk was constant during the spinning process, the electrospun nanofibres

were randomly distributed in the mat and were cylindrical with diameters of 288 ± 70 nm, as shown in figures 6.11, and 6.12. It has been believed that, based on theoretical equations, the velocity of the collected nanofibres is higher than 4.8 m/sec, hence the theoretical value of the jet velocity is 4.82 m/sec and the practical value is 4.49 m/sec. Figure 6.11, shows that as the linear speed of the disk increases to 5 m/sec and 6 m/sec, the alignment of the electrospun nanofibres increases but still has some randomly distributed nanofibres. This is because when the velocity of the electrospun nanofibres is higher than the linear speed of the disk collector, the nanofibres could not be taken up at a matching velocity by the disk due to higher nanofibre velocity. When the linear speed of the disk was 7 m/sec and 8 m/sec, most of the electrospun nanofibres were aligned along one direction without being stretched, as shown in figure 6.11.

Speed	Scale bar of 10 μm	Scale bar of 5 μm	Scale bar of 1 μm
Constant collector speed			
Collector linear speed of 1 [m/sec]			
Collector linear speed of 2 [m/sec]			
Collector linear speed of 3 [m/sec]			
Collector linear speed of 4 [m/sec]			

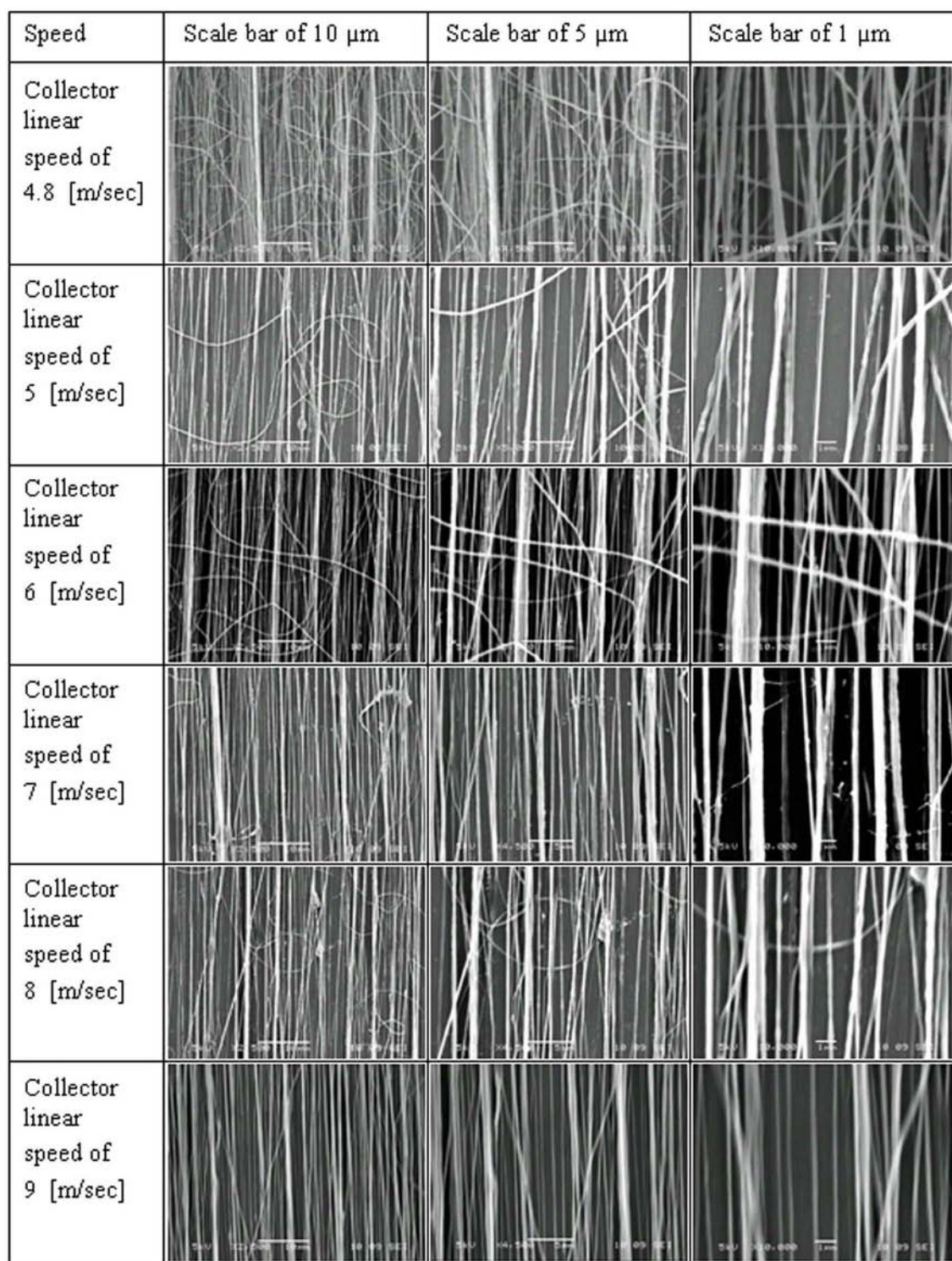


Figure 6.11, SEM images of PEO mats collected using a grounded disk collector at different linear speed: 0 m/sec ‘constant collector speed’; 1 m/sec; 2 m/sec; 3 m/sec; 4 m/sec; 4.8 m/sec; 5 m/sec; 6 m/sec; 7 m/sec; 8 m/sec and 9 m/sec. The SEM images are shown at different scale bar: 10 μm ; 5 μm and 1 μm .

In fact, this proves that the velocity of the electrospun nanofibres was very close to the linear speed of the disk. As the linear speed of the disk was increased to 9 m/sec, the electrospun nanofibres were collected onto the disk with full alignment but were

stretched and thinned as shown in figures 6.11 and 6.13. This is because the linear speed of the disk collector was higher than the velocity of the electrospun nanofibres. It can be concluded from the SEM images that the linear speed of the disk at 8 m/sec was an appropriate take up speed for the electrospun PEO nanofibres without stretching and thinning of nanofibres. In other words, electrospun PEO nanofibres under the above electrospinning operation parameters accept 8 m/sec as a deposited ‘collected’ nanofibre velocity.

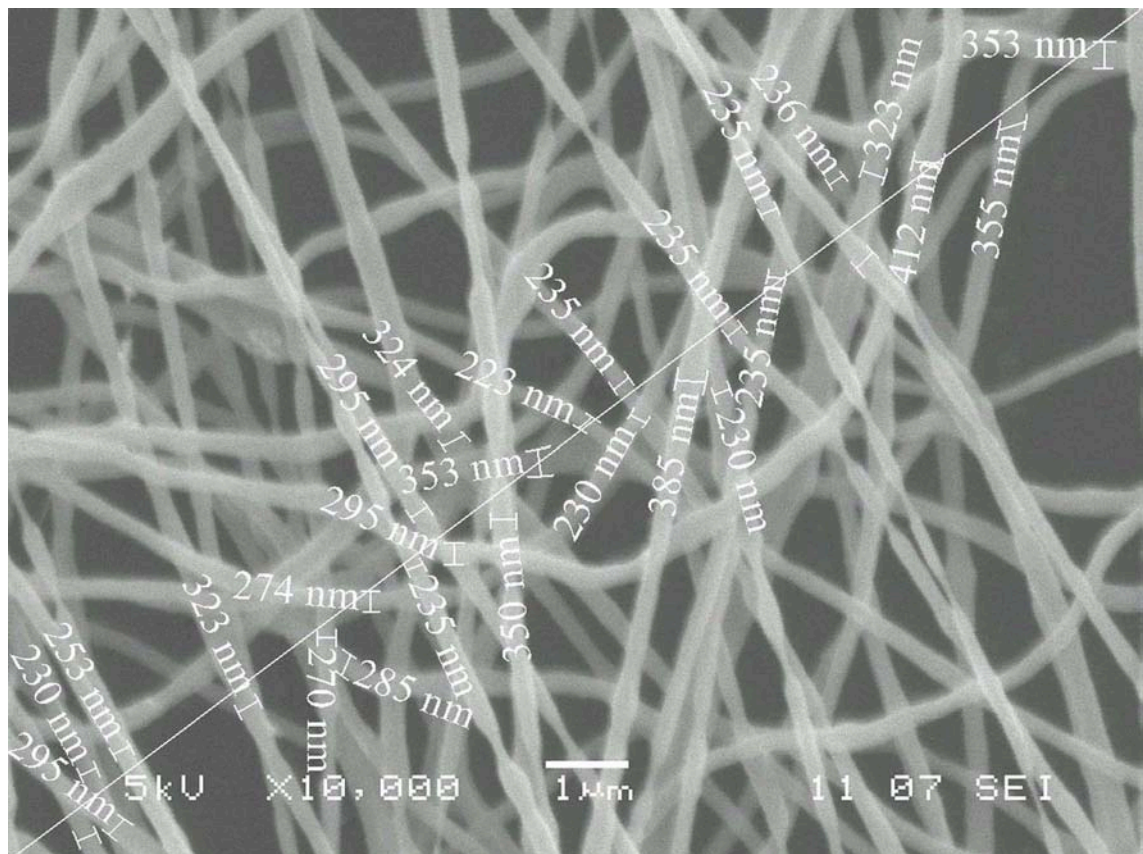


Figure 6.12, SEM image of PEO mat collected using a constant disk collector and scale bar of 1 μm . The electrospun nanofibres were randomly distributed in the mat with nanofibre diameters distribution of 288 ± 70 nm.

6.6 Discussion [67]

The mathematical model for deriving the equation of the velocity of the jet at the splitting point offers the basic stepping stone for establishing the equations of collected nanofibres velocity, their length and number of branches. Equation (6.47) dictates that the maximum velocity of the jet is controlled by the flow rate, electric current, electrical conductivity and density of the polymer solution and the jet dimensions. The theoretical

value of the jet velocity at the splitting point of 4.82 m/sec is with convenient agreement of the practical value of 4.49 m/sec, based on the conservation mass law. Further support for velocity prediction of the model is needed for other polymers under different conditions.

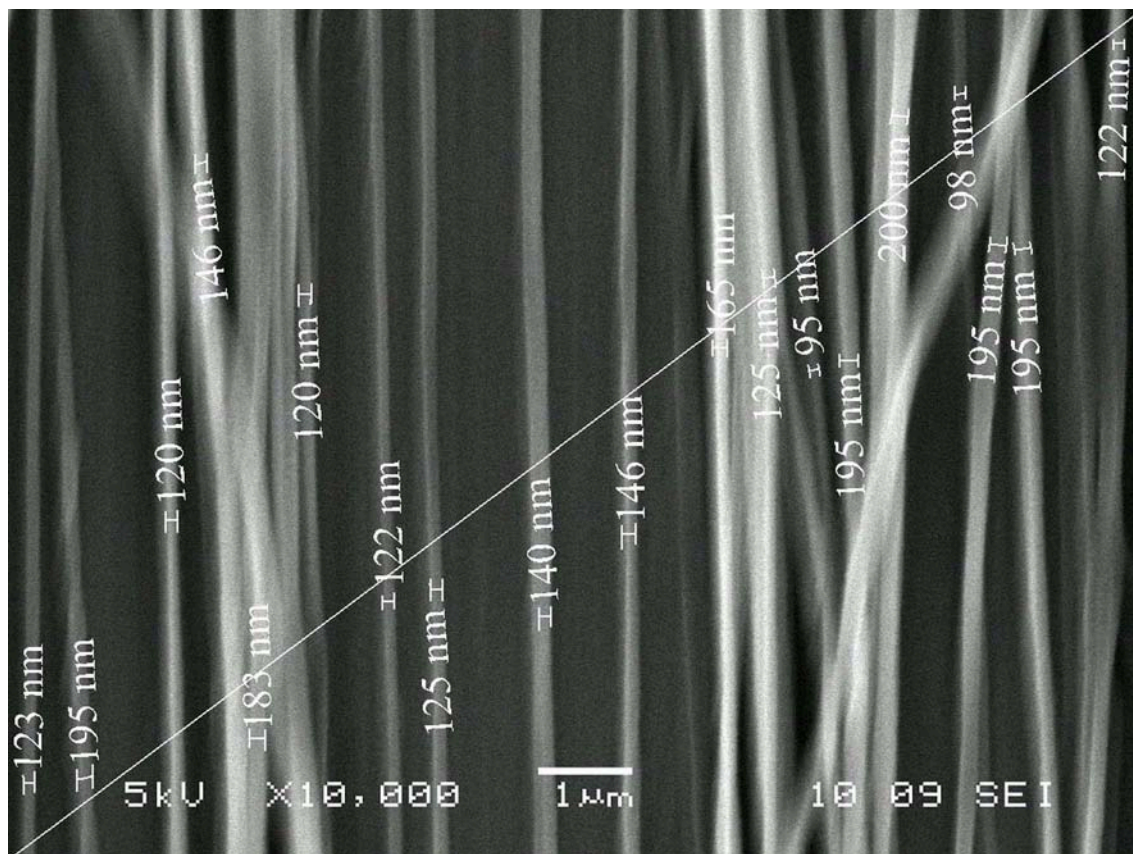


Figure 6.13, SEM image of PEO mat collected using an earthed disk collector rotated at linear speed of 9 m/sec and scale bar of 1 μm. The electrospun nanofibres were aligned, stretched and thinned in the mat with nanofibre diameters distribution of 150 ± 50 nm.

Equation (6.25) requires knowing N_b and c_p ‘number of branches and concentration of the polymer in the solution’ for finding theoretically the value of the nanofibre velocity at the collection position. Please note that the c_p value changes along the path of the jet due to solvent evaporation. However, based on the experimental measurements, evaporation percentage of the solution E_v can be calculated by equation (6.29), to be 97.3 %. It is interesting to note that the velocity of jet reaches a value of 4.49 m/sec within 36 mm travelling length according to the mass of the collected nanofibres used and the jet cross section area at the splitting point, figure 6.10. In comparison with the polymer solution velocity of 0.21 mm/sec in the needle, it is rather intriguing to note the high acceleration of jet velocity due to the driving force associated with the applied

electric voltage. Based upon the experimental results of collecting PEO nanofibres on a rotating disk, it is appropriate to find out the velocity of the nanofibre at collection point. The actual values of nanofibre velocity of 8 m/sec, the jet velocity of 4.49 m/sec and the jet to nanofibre area reduction 'from 2 μm to 0.288 μm ' prove the second electrospinning mode theory 'the single ejected jet elongates and thins for a short electrospinning distance and then it splits into multiple jets by the radial electric repelling forces'. In other words, by analyzing the values of jet and collected nanofibres velocity, strain, draw ratio and nanofibres area reduction, the nanofibres were not just single jet.

We believe that the jet velocity, number of nanofibres generated from the jet and their velocities are essential parameters to precisely control the engineering architecture of nanofibres such as; nanofibres alignment, nonwoven mat geometry and yarn manufacturing. In other words, this study will enable us to control and optimize the geometric properties 'linear density, twist per unit length and uniformity' of the continuous yarn and core electrospun yarn produced in the previous chapter. Moreover, this will enable researchers to further improve their nano engineering research and increase nanofibre productivity for end uses.

6.7 References

- [6.1] H. Reneker, A.L. Yarin, H. Fong, S. Koombhongse, *Bending instability of electrically charged liquid jets of polymer solutions in electrospinning*, Journal of Applied Physics, **87**, 4531-4547 (2000)
- [6.2] A.L. Yarin, S. Koombhongse, D.H. Reneker, *Bending instability in electrospinning of nanofibres*, Journal of Applied Physics, **89**, 3018-3026, (2001)
- [6.3] D.H. Reneker, A.L. Yarin, S. Koombhongse, *Taylor cone and jetting from liquid droplets in electrospinning of nanofibres*, Journal of applied Physics, **90**, 4836-4846 (2001)
- [6.4] C. Mit-uppatham, M. Nithitanakul, P. Supaphol, *Ultrafine electrospun polyamide-6 fibres: effect of solution conditions on morphology and average fibre diameter*, Macromolecular Chemistry and Physics, **205**, 2327-2338 (2004)
- [6.5] G.I. Taylor, *Disintegration of water drops in an electric field*, Proceedings of the Royal Society of London Series A, **280**, 383-397 (1964)
- [6.6] G.I. Taylor, *The circulation produced in a drop by an electric field*, Proceedings of the Royal Society of London Series A, **291**, 159-166 (1966)

- [6.7] G.I. Taylor, *Electrically driven jets*, Proceedings of the Royal Society of London Series A, **313**, 453-475 (1969)
- [6.8] C.D Hendricks Jr, R.S. Carson, J.J. Hogan, J.M. Schneider, *Photomicrography of electrically sprayed heavy particles*, The American Institute of Aeronautics and Astronautics Journal (AIAAJ), **24**, 733-737 (1964)
- [6.9] M. Cloupeau, B. Prunetfoch, *Electrohydrodynamic spraying functioning modes-a critical review*, Journal of Aerosol Science, **25**, 1021-1036 (1994)
- [6.10] A.M. Ganan-Calvo, *On the theory of electrohydrodynamic driven capillary jets*, Journal of fluid mechanics, **335**, 165-188 (1997)
- [6.11] A.M. Ganan-Calvo, *Cone-jet analytical extension of Taylor's electrostatic solution and the asymptotic universal scaling laws in electrospraying*, Physical Review Letters, **79**, 217-220 (1997)
- [6.12] D.A. Saville, *Electrohydrodynamics: the Taylor-Melcher leaky dielectric model*, Annual Review-Fluid Mechanics, **29**, 27-64 (1997)
- [6.13] M.M. Hohman, *A physical theory of the instabilities of electrically driven jets by*, Ph.D Thesis, The University of Chicago (2000)
- [6.14] M.M. Hohman, M.Y. Shin, G.C. Rutledge, M. Brenner, *Electrospinning and electrically forced jets I stability theory*, Physics of Fluids, **13**, 2201-2220 (2001)
- [6.15] M.Y. Shin, M.M. Hohman, M. Brenner, G.C. Rutledge, *Electrospinning and electrically forced jet II application*, Physics of fluids, **13**, 2221-2236 (2001)
- [6.16] M.Y. Shin, M.M. Hohman, M. Brenner, G.C. Rutledge, *Electrospinning: a whipping fluid jet generates submicron polymer fibres*, Applied Physics Letters, **78**, 1149-1151 (2001)
- [6.17] J.J. Feng, *The stretching of an electrified non-Newtonian jet: a model for electrospinning*, Physics of Fluids, **14**, 3912-3926 (2002)
- [6.18] J.J. Feng, *Stretching of a straight electrically charged viscoelastic jet*, Journal of Non-Newtonian Fluid Mechanics, **116**, 55-70 (2003)
- [6.19] C.P. Carroll, Y.L. Joo, *Electrospinning of viscoelastic Boger fluids: modeling and experiments*, Physics of Fluids, **18**, 053102-1 - 053102-14 (2006)
- [6.20] Y.Q. Wan, Q. Guo, N. Pan, *Thermo-electro-hydro-dynamic model for electrospinning process*, International Journal Nonlinear Science and Numerical Simulation, **5**, 5-8 (2004)
- [6.21] A.F. Spivak, Y.A. Dzenis, *Asymptotic decay of radius of a weakly conductive viscous jet in an external electric*, Applied Physics Letters, **73**, 3067-3069 (1998)

- [6.22] A.F. Spivak, Y.A. Dzenis, D.H. Reneker, *A model of steady state jet in the electrospinning process*, Mechanics Research Communications, **27**, 37-42 (2000)
- [6.23] F. Yan, B. Farouk, F. Ko, *Numerical modeling of an electrostatically driven liquid meniscus in the cone-jet mode*, Journal of Aerosol Science, **34**, 99-116 (2003)
- [6.24] R.P.A. Hartman, D.J. Brunner, D.M.A. Camelot, J.C.M. Marijnissen, B. Scarlett, *Electrohydrodynamic atomization in the cone-jet mode physical modeling of the liquid cone and jet*, International Journal of Aerosol Science, **30**, 823-849 (1999)
- [6.25] M.M. Denn, C.J.S. Petrie, P. Avenas, *Mechanics of steady spinning of a viscoelastic liquid*, The American Institute of Chemical Engineers Journal (AIChEJ), **21**, 791-799 (1975)
- [6.26] J.H. He, H.M. Liu, *Variational approach to nonlinear problems and a review on mathematical model of electrospinning*, Nonlinear Analysis, **63**, e919-e929 (2005)
- [6.27] J.H. He, Y.Q. Wan, J.Y. Yu, *Application of vibration technology to polymer electrospinning*, International Journal Nonlinear Science and Numerical Simulation, **5**, 253-261 (2004)
- [6.28] J.H. He, Y.Q. Wan, J.Y. Yu, *Allometric scaling and instability in electrospinning*, International Journal Nonlinear Science and Numerical Simulation, **5**, 243-252 (2004)
- [6.29] C. Wang, C.H. Hsu, J.H. Lin, *Scaling laws in electrospinning of polystyrene solutions*, Macromolecules, **39**, 7662-7672 (2006)
- [6.30] Y.M. Shin, M.M. Hohman, M.P. Brenner, G.C. Rutledge, *Experimental characterization of electrospinning: the electrically forced jet and instabilities*, Polymer, **42**, 9955-9967 (2001)
- [6.31] S.V. Fridrikh, J.H. Yu, M.P. Brenner, G.C. Rutledge, *Controlling the fibre diameter during electrospinning*, Physical Review Letters, **90**, 144502-1 - 144502-5 (2003)
- [6.32] V.N. Kirichenko, I.V. Petryanov-Sokolov, N.N. Suprun, A.A. Shutov, *Asymptotic radius of a slightly conducting liquid jet in an electric field*, Doklady Physics, **31**, 611-614 (1986)
- [6.33] J.H. He, Y.Q. Wan, *Allometric scaling for voltage and current in electrospinning*, Polymer, **45**, 6731-6734 (2004)
- [6.34] X.H. Qin, S.Y. Wang, T. Sandra, D. Lukas, *Effect of LiCl on the stability length of electrospinning jet by PAN polymer solution*, Materials Letters, **59**, 3102-3105 (2005)

- [6.35] X.H. Qin, Y.Q. Wan, J.H. He, *Effect of LiCl on electrospinning of PAN polymer solution: theoretical analysis and experimental verification*, *Polymer*, **45**, 6409-6413 (2004)
- [6.36] J.H. Hea, Y.Q. Wanc, J.Y. Yu, *Scaling law in electrospinning: relationship between electric current and solution flow rate*, *Polymer*, **46**, 2799-2801 (2005)
- [6.37] S.A. Theron, E. Zussmana, A.L. Yarin, *Experimental investigation of the governing parameters in the electrospinning of polymer solutions*, *Polymer*, **45**, 2017-2030 (2004)
- [6.38] M.M. Demir, I. Yilgor, E. Yilgor, B. Erman, *Electrospinning of polyurethane fibres*, *Polymer*, **43**, 3303-3309 (2002)
- [6.39] D.A. Saville, *Electrohydrodynamic stability: effects of charge relaxation at the interface of a liquid jet*, *Journal of Fluid Mechanics*, **48**, 815-827 (1971)
- [6.40] A.L. Yarin, *Free liquid jets and films: hydrodynamics and rheology*, Longman Harlow & Wiley, New York (1993)
- [6.41] A.L. Yarin, *Strong flows of polymeric liquids: Part (1) rheological behavior*, *Journal of Non-Newtonian Fluid Mechanics*, **37**, 113-138 (1990)
- [6.42] J. Doshi, D.H. Reneker, *Electrospinning process and applications of electrospun fibres*, *Journal of Electrostatics*, **35**, 151-160 (1995)
- [6.43] D.H. Reneker, I. Chun, *Nanometer diameter fibres of polymer produced by electrospinning*, *Nanotechnology*, **7**, 216-223 (1996)
- [6.44] D.H. Reneker, W. Kataphinan, A. Theron, E. Zussman, A.L. Yarin, *Nanofibre garlands of polycaprolactone by electrospinning*, *Polymer*, **43**, 6785-6794 (2002)
- [6.45] A. Frenot, I.S. Chronakis, *Polymer nanofibres assembled by electrospinning*, *Current Opinion in Colloid & Interface Science*, **8**, 64-75 (2003)
- [6.46] J.M. Deitzel, D. Kleinmeyer, J.K. Hirvanen, N.C.B. Tan, *Controlled deposition of electrospun poly (ethylene oxide) fibres*, *Polymers*, **42**, 8163-8170 (2001)
- [6.47] V.V. Soongnorn, W.L. Mattice, *Dynamic properties of an amorphous polyethylene nanofibre*, *Langmuir*, **16**, 6757-6758 (2000)
- [6.48] V. Vao-Soongnorn, P. Doruker, W.L. Mattice, *Simulation of an amorphous polyethylene nanofibre on a high coordination lattice*, *Macromolecular Theory and Simulations*, **9**, 1-13 (2000)
- [6.49] S.V. Fridrikh, J.H. Yu, M.P. Brenner, G.C. Rutledge, H. Fong, D.H. Reneker, *Polymer nanofibres*, American Chemical Society Symposium Series, American Chemical Society, **918**, Washington DC (2006)

- [6.50] M.M. Bergshoef, G.J. Vancso, *Transparent nanocomposites with ultrathin electrospun nylon-4.6 fibre reinforcement*, *Advanced Materials*, **11**, 1362-1365 (1999)
- [6.51] Z. Sun, E. Zussman, A.L. Yarin, J.H. Wendorff, A. Greiner, *Compound core-shell polymer nanofibres by co-electrospinning*, *Advanced Materials*, **15**, 1929-1932 (2003)
- [6.52] H. Fong, D.H. Reneker, *Electrospinning and formation of nanofibres*, In *structure formation in polymer fibres*, D. R. Salem & M. V. Sussman, Munich, 225-246 (2000)
- [6.53] A.E. Tonelli, R. Kotek, D.W. Jung, N.J. Vasanthan, *Novel methods for obtaining high modulus aliphatic polyamide fibres*, *Macromolecular Science Polymer Reviews*, **45**, 201-230 (2005)
- [6.54] D.H. Reneker, A.L. Yarin, *Electrospinning jets and polymer nanofibres*, *Polymer*, **49**, 2387-2425 (2008)
- [6.55] P. Dayal, J. Liu, S. Kumar, T. Kyu, *Experimental and theoretical investigations of porous structure formation in electrospun fibres*, *Macromolecules*, **40**, 7689-7694 (2007)
- [6.56] S.J. Eichhorn, W.W. Sampson, *Statistical geometry of pores and statistics of porous nanofibrous assemblies*, *Journal of the Royal Society*, **2**, 309-318 (2005)
- [6.57] X. Wang, Jin Cao, Z. Hu, W. Pan, Z. Liu, *Jet shaping nanofibres and the collection of nanofibre mats in electrospinning*, *Journal of Material Science Technology*, **22**, 536-540 (2006)
- [6.58] S.C. Moon, R.J. Farris, *How is it possible to produce highly oriented yarns of electrospun fibres*, *Polymer Engineering and Science*, **47**, 1530-1535 (2007)
- [6.59] D. Berdy, H. Chong, S. Paruchuri, J. Yu, K. Hollar, D. Weitz, H. Stone, M. Brenner, R. Hulman, *Bifurcations in electrospinning: splitting a polymer jet*, *Harvard Research Experience for Undergraduates*, Harvard University (2005)
- [6.60] T.A. Kowalewski, S. Blon, S. Barral, *Experiments and modelling of electrospinning process*, *Bulletin of the Polish Academy of Sciences-Technical Sciences*, **53**, 385-394 (2005)
- [6.61] D.H. Reneker, A.L. Yarin, W. Kataphinan, *Branching in electrospinning of nanofibres*, *Journal of applied physics*, **98**, 064501-0645012 (2005)
- [6.62] D.H. Reneker, A.L. Yarin, E. Zussman, H. Xu, *Electrospinning of nanofibres from polymer solutions and melts*, *Advances in Applied Mechanics*, **41**, 44-195 (2007)
- [6.63] E. Zussman, D. Rittel, A.L. Yarin, *Failure modes of electrospun nanofibres*, *Applied Physics Letters*, **82**, 3958-3960 (2003)

- [6.64] S.B. Warner, A. Buer, S.C. Ugbolue, G.C. Rutledge, M.Y. Shin, *A fundamental investigation of the formation and properties of electrospun fibres*, In National Textile Center Annual Report, 83-90 (1998)
- [6.65] H. Xu, *Formation and characterization of polymer jets in electrospinning*, PhD Thesis, University of Akron, USA (2003)
- [6.66] L.M. Bellan, H.G. Craighead, J.P. Hinstroza, *Direct measurement of fluid velocity in an electrospinning jet using particle image velocimetry*, Journal of Applied Physics, **102**, 094308-1 – 094308-5 (2007)
- [6.67] M.B. Bazbouz, G.K. Stylios, *Modeling the effect of jet kinematics in electrospinning of nanofibres*, Journal of Non-Newtonian Fluid Mechanics, Submitted for publication, Elsevier (2009)
- [6.68] J.H. He, Y. Wu, W.W. Zuo, *Critical length of straight jet in electrospinning*, Polymer, **46**, 637-640 (2005)
- [6.69] Y. Ying, J. Zhidong, L. Qiang, G. Zhicheng, *Controlling the electrospinning process by jet current and Taylor cone*, Annual Report Conference on Electrical Insulation and Dielectric Phenomena, China, 453-456 (2005)

CHAPTER 7: MECHANICAL CHARACTERIZATION OF NYLON 6 NANOFIBRES

7.1 Introduction

Recent advances in nanoengineering of materials have enabled researchers and engineers to fabricate fibres at the nanoscale for a wide range of applications. In fact, during nanofibre processing, the loaded forces on the fibres can cause temporary or permanent deformation or even mechanical failure. Mechanical properties of individual nanofibres dominate their dynamic and static response, contact and friction and final deformation in the nanofibre network. Therefore, it is essential to know if individual nanofibres are strong enough to withstand the external and internal forces exerted for performing further processing during application. Furthermore, mechanical characterization provides benchmarking and comparison of optimization of performance requirements and specification.

So far, several experimental techniques have been developed to characterize the mechanical properties of either individual electrospun nanofibres or entangled in the form of three dimensional nonwoven mats. Among those, a universal testing machine is the simplest experimental technique for measuring the tensile properties on a nanofibrous mat. While, single electrospun nanofibres has been mechanically characterized by the nano tensile test or by bending test or by indentation tests conducted at the nanoscale [1]. Due to the nanoscale diameters of the nanofibres, manipulating these fibres without breaking can be very time consuming. In practice, four main challenges have to be overcome. The first is to precisely isolate, align and grip the single nanofibre on the test frame without slipping or breaking. The second is to accurately measure the nanofibre diameter making sure that it is not damaged by SEM or TEM characterization instruments. It is common practice to measure the nanofibre diameter after conducting the mechanical test [2]. The third is to find a sensitive force transducer which can measure the applied force in the nano/micro Newton range and has a low nano/micro Newton resolution. The fourth is to find a precise actuator which can load the nanofibre till failure in the micro Newton range.

In this chapter, a review of the mechanical characterization testing methods that have been developed for nanofibres is investigated. The tensile - strain curves of the electrospun nylon 6 and nylon 6/MWCNTs nanofibre mats are plotted and investigated using a universal tensile test machine. A novel simple laboratory set-up for performing the tensile test on single nanofibre and nanofibre bundles has been designed and

implemented. Tensile strength, axial tensile modulus and ultimate strain of electrospun single nylon 6 nanofibres have been obtained by defining the stress - strain curve of the material. Consequently, optimizing the mechanical properties of nylon 6 nanofibre and specific challenges of tensile testing are further discussed.

7.2 Review of the mechanical testing methods of single nanofibres

Mechanical testing of nanofibres have been classified into three basic methods namely; tensile test methods by using commercial nano tensile testing or the atomic force microscope cantilever or other novel techniques, bending test methods and nanoindentation methods [1]. Hereinafter, a comprehensive review of these methods and their techniques is presented and discussed.

7.2.1 Tensile test method

Tensile test is a well known as the most effective method used for establishing the tensile properties of the fibres ‘tensile strength, yield stress, Young’s modulus, strain at break, etc.’ which involves measuring the applied load and elongation of the fibre under a known cross-sectional area [3]. Specifically, to perform a direct tension test on a single nanofibre, the tensile tester must be able to measure the micro Newton load required to deform the fibre. Recently, researchers have used either a tensile testing machine or atomic force microscope ‘‘cantilever’’ or even other novel techniques for finding the mechanical characteristics of the electrospun nanofibre.

The smallest load cell that can be obtained commercially for testing is of a load resolution of 0.1 mN [4], which is insufficient for the tensile testing of single nanofibre. Where, the force required to break the nanofibre can be in the nano/micro Newton range ‘e.g. approximately 66 micro Newtons for polycaprolactone (PCL) single nanofibre with 1.03 μm diameter [5]’. Recently, the American system corporation MTS, the world’s leader in mechanical and material testing and simulation, has engineered a nano tensile tester called ‘NanoBionix tensile tester’. This highly accurate tester is said to be ideal for low-force static and dynamic mechanical testing of single nanofibre. It has a load test capability at a nano Newton range with 50 nano Newton load resolution, an extension resolution of 35 nanometers and a frequency of up to 50 Hz [6]. Nevertheless, the testing process requires preparation of the tensile test samples properly, it involves loading of the nanofibres vertically on the testing frame, then removing the non required nanofibres by ensuring that only one nanofibre is obtained, mounting the frame into the clamps of the tensile tester, cutting the ‘rib’ of the frame and applying the load. Figure

7.1, shows nano tensile tester (NanoBionix, MTS, USA) with a single nanofibre being mounted on a cardboard frame [2, 5]. Electrospun a polycaprolacton (PCL) [5, 7, 8], a poly (L-lactic acid) (PLLA) [9, 10] and a precursor polyamic acid (BPDA/PPA) [2] single nanofibre have been tested using this tensile tester.

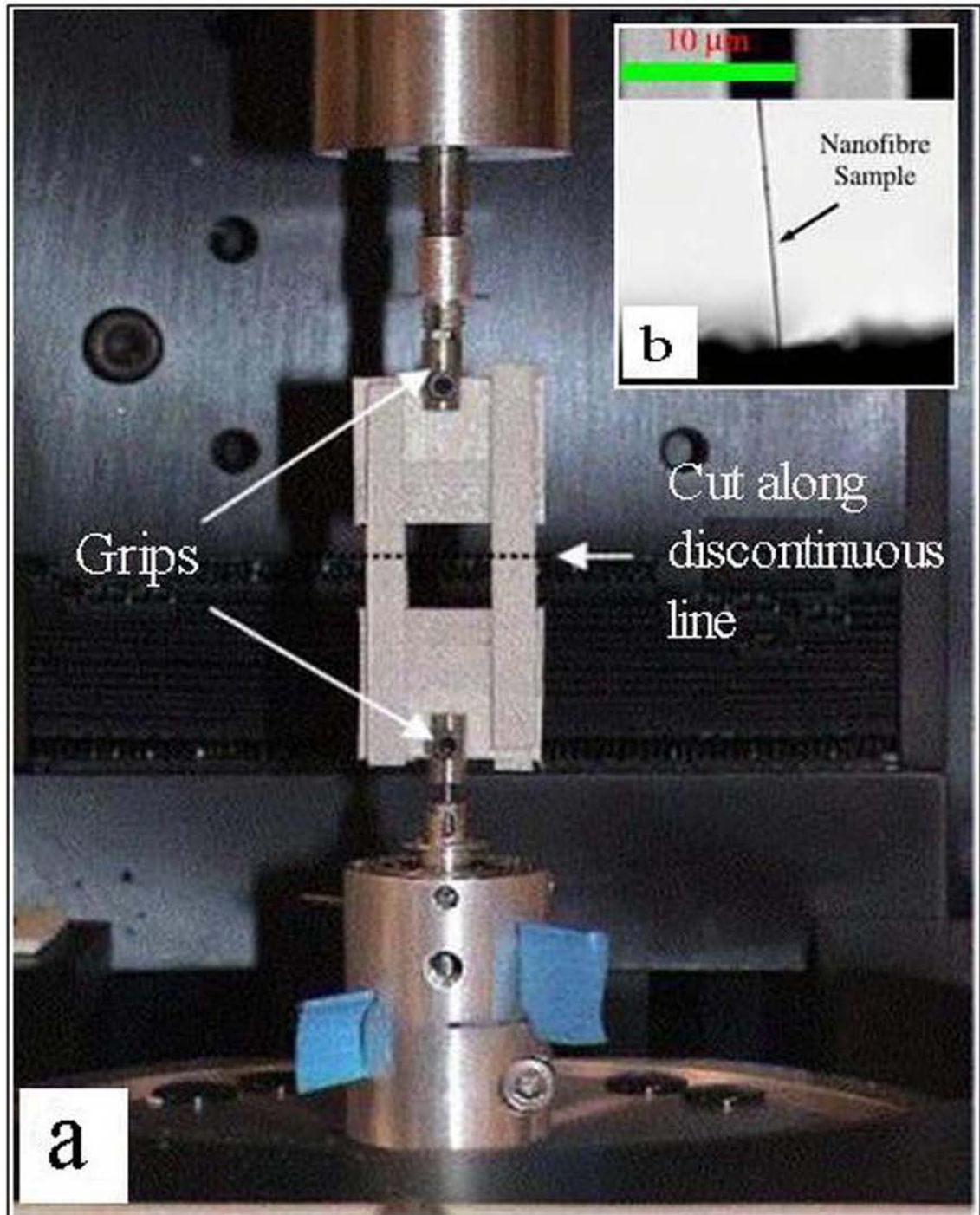


Figure 7.1, (a) A photograph shows the nano tensile tester (NanoBionix, MTS, USA) for nano tensile testing of a single polymer nanofibre [5], (b) An optical image shows the tensile stretching of the single nanofibre mounted vertically on the edges of a cardboard frame [2].

The mechanical properties ‘stress - strain curve’ for these nanofibres were observed to vary with the fibre diameter and the physical structure of the fibre. This indicates that the mechanical properties are influenced by the structure of the electrospun nanofibre which is the result of the draw ratio applied during the electrospinning process [8]. However, one disadvantage of this technique is that it is a very costly machine and complex to construct and still may not be appropriate for fibres with diameters in the range of tens of nanometers [1]. Subsequently, as current nano tensile testers are very costly, researchers designed laboratory set-ups for tensile testing [11] or they used a universal tensile tester [12-14] for testing a bundle ‘rope’ of nanofibres.

Atomic force microscope cantilever has been utilized to characterize the mechanical properties of individual electrospun fibres as an alternative technique. The superior displacement resolution of the AFM cantilever is in Angstrom level and its super low stiffness is ranging from 0.1 to 0.01 N/m [15, 16]. Thus, an AFM cantilever has been rendered as a very useful system for tensile requirements. In this technique, an individual electrospun nanofibre is removed from the fibre holder. One end is tethered to the tip of an AFM cantilever which serves as a force sensing element and the other end is fastened on the surface of a movable body by adhesive which serves as a pulling element. The initial positions of the cantilever tip and the pulling element must be noted for the calculation of the gauge length of the fibre, as shown in figure 7.2.

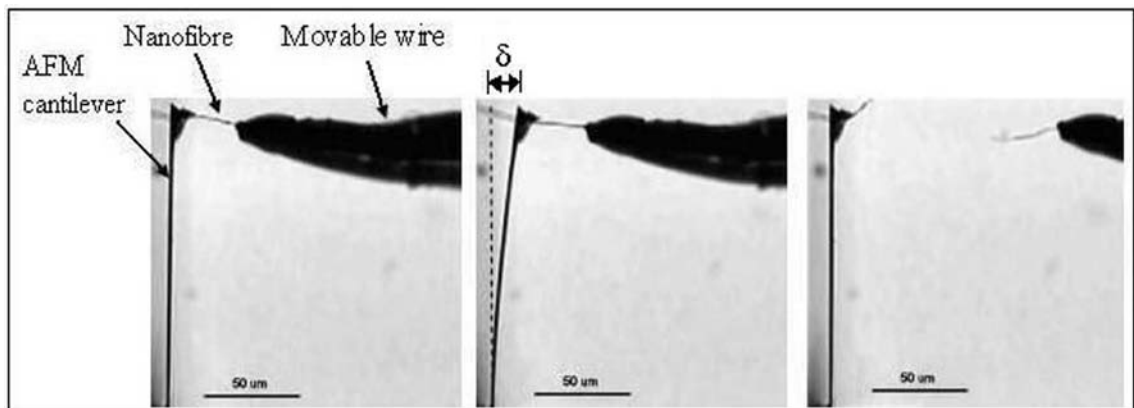


Figure 7.2, A series of images for breaking an electrospun nanofibre during the tensile test. The fibre was attached to the tip of an AFM cantilever and pulled transversally by a wire. The deflection of the cantilever, δ , is proportional to the applied force and has to be measured at the time of breaking throughout the tensile test [17].

At the start of the tensile test, the deflection of the AFM cantilever is observed using a microscope equipped with a CCD camera. As the elastic constant of the cantilever can

be mathematically calculated or is already known, the tensile load acting on a single nanofibre can be easily determined [17]. Or for more accuracy, the induced force on the single nanofibre can be measured by integrating a resistive strain gauge into the cantilever flexible arm. Consequently, deflection of the cantilever tip results in a linear change in resistance which can be easily converted to load readings by connecting the cantilever tip to a multimeter [18]. The pulling element is linearly moved at step intervals of micrometer range to stretch the fibre with the cantilever deflection reading taken at each step. As a result, based on these measuring steps, the stress - strain curve of a single nanofibre can be plotted and the mechanical properties of the fibre can be determined. At a similar principle but different manner, Turner et. al. have obtained the Young's modulus of a nanofibre by using two atomic force microscope cantilevers which are cantilevered at one end and coupled with a nanofibre at the other end, as shown in figure 7.3 (b), [19]. This measuring method is based on the dynamic relation between the fibre stiffness 'spring constant' and the resonant frequencies of the cantilevers vibration mode [20, 21].

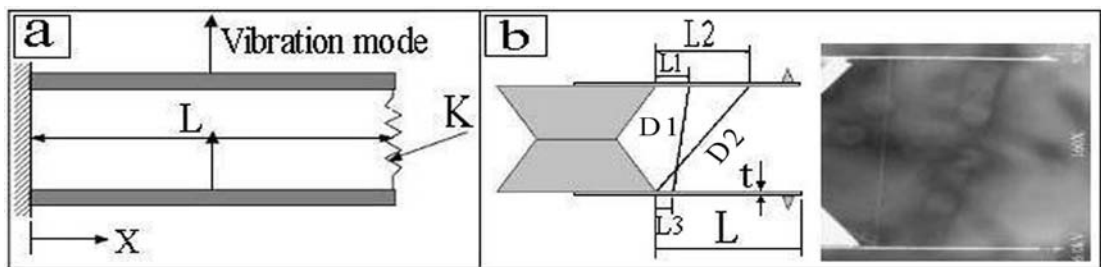


Figure 7.3, Mechanical properties of nanofibres are measured by AFM cantilever probes. (a) A schematic of the theory of conventional beam dynamics, shows two prismatic beams of length L cantilevered at one end and coupled with a spring of stiffness K . (b) A schematic and scanning electron microscopic image that shows how the nanofibres are attached to the cantilevers at distances: $L = 450 \mu\text{m}$, $t = 2 \mu\text{m}$, $K = 0.1 \text{ N/m}$, $L_1 = 94.5 \mu\text{m}$, $D_1 = 606.67 \mu\text{m}$ and $D_2 = 691.02 \mu\text{m}$ represent the lengths of the nanofibres, $L_2 = 342.8 \mu\text{m}$ and $L_3 = 47.8 \mu\text{m}$ [19].

Applying the cantilever technique for nanofibre tensile test requires selecting the appropriate spring constant of the cantilever and the micrometer displacement range of the pulling element or the frequency 'kilohertz' of the vibration mode for succeeding the test.

Nevertheless, due to the high load and displacement resolution of the AFM cantilevers, using the cantilever system for tensile test of finer nanofibres is proven to be more

feasible than using commercial nano tensile testers. On the other hand, this technique consumes even more time and effort than commercial nano tensile testers, and it needs familiarity in choosing and manipulating the appropriate cantilevers when different samples are tested [18].

Other novel techniques have been also utilized for performing tensile tests of nanofibres, based on either a developed precise load cell [22] or an AFM cantilever mode system [4]. In the second technique, and based on vibration fundamentals, an AFM system which involves a stepper motor and a transducer spring have been used to provide the force required for stretching the fibre. The applied load and elongation of the fibre were measured by the transducer spring and by subtracting the elongation of the transducer spring from the total elongation of the stepper motor respectively. Consequently, the stress - strain curve of the fibre is obtained by dividing the measured tensile load over the cross sectional area of the fibre and by dividing the elongation over the gauge length respectively. Generally, this technique has many advantages, it can be custom made, it is able to provide a high load and displacement resolution and it is not costly to construct.

7.2.2 Bending test method

Based on the atomic force microscope AFM principle, the topology of the fibre surface is imaged by scanning a long, small and thin cantilever across the whole surface and thus measuring the cantilever deflection with respect to the scan position [23-25]. Based on this principle, the indentation of the AFM cantilever probe into a fibre surface has offered researchers a direct determination of the applied force as a function of displacement. Therefore, a wide range of electrospun polymer nanofibres has been tested using this method for calculating both the elastic bending modulus and the shear modulus. Here, we review the two techniques of using the AFM cantilever to conduct either two-point or three-point bending test of electrospun nanofibres.

In the two-point bending test, the electrospun nanofibres must be aligned on two grounded edges [26], isolated into a single nanofibre, cut and attached to a cantilever as shown and described in figure 7.4 (a), [27-29]. Consequently, the nanofibre is bent by pushing the AFM cantilever in the z direction at a movement range of microns while the other edge is kept constant, or the vice versa. The displacement of fibre during the test is measured usually by an optical microscope. The applied force is calculated from the results of displacement and the spring constant of the cantilever.

Subsequently, the Young's modulus of the fibre is calculated according to equation (7.1) [29, 30]:

$$E = \frac{4}{3\pi} \times \frac{F}{\delta} \times \frac{L^3}{r^4} \quad (7.1)$$

Where L is the length of the fibre, r is the radius of the fibre, F is the force exerted and δ is the z direction displacement of the fibre.

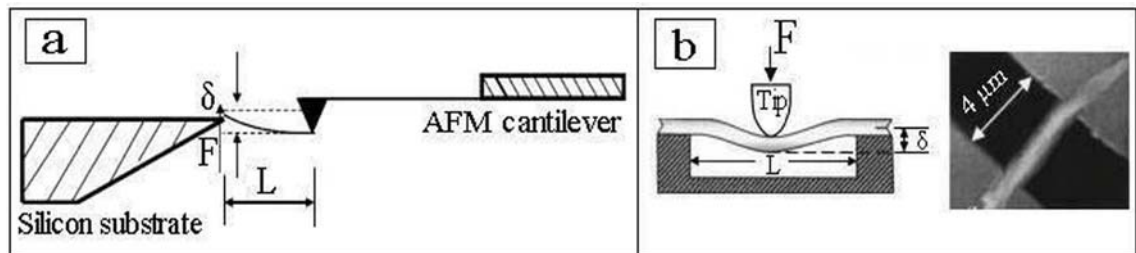


Figure 7.4. (a) A schematic drawing shows one end of single nanofibre attached to a contact mode AFM cantilever and the other end free to be loaded by a substrate edge to form the two-point bending test [29]. (b) A schematic drawing shows a single nanofibre deflected by the AFM cantilever tip to form the three-point bending test and a SEM image of PLLA single nanofibre which is deposited onto an etched groove of silicon wafer with a span length of 4 μm [35].

In the three-point bending test, a well aligned single nanofibre must be suspended over an empty space between two parallel metal strips points. An AFM cantilever tip with spring constant of milli Newtons per meter is used to apply the nano Newton vertical force at the mid point of the suspended length of the nanofibre, as shown in figure 7.4 (b) [10, 31-37, 57]. As this technique is for calculating only the elastic property of the fibre, the loading force must be precisely determined to prevent permanent deformation or even break to failure. For instance, an example case reported in the literature is: a maximum force of 2.7 nano Newton with loading rate of 0.2 $\mu\text{m}/\text{sec}$ was applied at the mid point of poly (2-acrylamido-2-methyl-1-propanesulfonic acid) (PAMPS) nanofibre with span length of 1.5 μm and nanofibre diameter of 116 nm [31]. In this testing technique, the nanofibre must be aligned perfectly perpendicular to the parallel strips without any additional initial tension, the fibre must be assumed to be linearly elastic and that its cross section must be circular. In addition, it has been recommended that to minimize the deformation of nanofibre by the shear stress generating during the three-

point bending test, the span length to diameter ratio of the measured nanofibre must be < 10 [31, 38]. The elastic modulus of nanofibre is calculated from the beam bending theory given by equation (7.2) [38] as:

$$E = \frac{FL^3}{192\delta I} \quad (7.2)$$

$$I = \frac{\pi d^4}{64} \quad (7.3)$$

Where L is the length of the span ‘suspended’ fibre, d is the diameter of the fibre, F is the force exerted, δ is the z direction displacement of the fibre and I is the second moment area of the fibre.

The calculation of the elastic modulus using the bending test method requires an accurate measurement of the dimensions of the nanofibre because the elastic modulus is related to diameter to the fourth power (d^4) and length to the third power (L^3). Furthermore, measurement errors can occur easily and for not affecting the calculated value of the elastic property, many measurements must be conducted and averaged.

7.2.3 The nanoindentation method

Nanoindentation has been recently utilized for calculating the elastic modulus of nanofibres by determining the applied force, the depth and the contact area between the nanofibre and the indenter [39-42]. In this method, the sample is prepared for testing by depositing the nanofibres on a hard and flat substrate, with sufficient sticking between the substrate and the nanofibres. Then, the nanofibres are inspected by the AFM tapping mode ‘as a most effective indenter’ in the radial direction of the fibres. Using the AFM tip to perform nanoindentation on the nanofibre requires a tip radius at a low nanometer range ‘say 5 nm [39]’ for ignoring the curvature of the nanofibre [1]. However, as the method deals with resonance frequency measurements, many factors must be considered carefully such as; effect of the underlying substrate, the tip shape and the cantilever spring constant, the fibre surface roughness, the curvature of fibre surface, the non-perpendicular loading and the adhesion force [42]. Therefore, for calculating the value of the elastic modulus a model estimation may be used.

Briefly, the method deals with a sophisticated instrument for only one measured mechanical property leading to a limited use of this method in practice.

Finally, table 7.1 shows a summary of all the up-to-date mechanical characterization methods for single nanofibres of various types of polymers.

Table 7.1, Mechanical characterization of single nanofibres.

Test methods	Technique and instruments	Materials	Ref.
Tensile test	1- Nano tensile tester	Polycaprolacton (PCL)	[5, 7, 8]
		Poly (L-lactic acid) (PLLA)	[9, 10]
		Polyamic acid (BPDA/PPA)	[2]
		CNTs rope	[11]
	2- Commercial tensile tester	Polyacrylonitrile (PAN)	[12-14]
		3- Test based on AFM cantilever	Nylon 6,6
	4- AFM cantilevers system	Polyethylene oxide (PEO)	[18]
		Poly lactide/ polyglycolide	[4]
		Polyacrylonitrile (PAN)	[19]
		Polyacrylonitrile (PAN)	[19]
Bending test	1- Two-point bending test	PEO, PAN	[27]
		Collagen type I	[28]
		Polyacrylonitrile (PAN)	[29]
	2- Three-point bending test	Poly (L-lactic acid) (PLLA)	[10]
		PAMPS hydrgel	[31]
		PEO, glass	[32]
		PVP/TiO ₂ , TiO ₂ nanofibres	[33]
		Nylon6/SiO ₂ composites	[34]
		Poly (L-lactic acid) (PLLA)	[35]
		Polycarbonate, polypyrrole	[36]
		Nylon 6	[37]
		Fibrinogen	[57]
		Nanoindentation	Indentation using AFM cantilever
Polyacrylonitrile (PAN)	[40, 41]		
Poly (L-lactic acid) (PLLA)	[42]		

7.3 Tensile test of nonwoven nylon 6 nanofibre mats [58]

The formation of an electrospun fibrous structure depends on the construction and geometrical shape of the electrospinning machine set-up. Number of crossings per nanofibre, number of intersections per unit area, total nanofibre crossings in the mat and three dimensional joints morphology play an important role in the mechanical properties of the nonwoven nanofibres mat [43]. However, the nanofibre molecular structure and orientation play even more important critical role in these properties [8]. In order to gain a better understanding of how the electrospun fibres behave, a preliminary tensile test has been performed on nylon 6 and composite nylon 6/ MWCNTs nanofibre mats described in this section and on a single nylon 6 nanofibre described in section 7.4.

7.3.1 Experimental; electrospinning of nylon 6 nanofibres, samples preparation and nano tensile testing

Polymer solutions of nylon 6 and formic acid at concentration of 20 wt. % and composite nylon 6/ MWCNTs of 1 % wt. were spun with electrospinning parameters; a volume feed rate of 0.2 ml/h, an applied voltage of 15 KV and an electrospinning distance of 8 cm for producing nanofibre mats. These mats were carefully cut into strip-shaped specimens with rectangular dimensions of 12 mm width and 30 mm length. The thickness of the nanofibre mat samples is 0.011 mm, calculated through the samples weight (Mettler TG 50 thermobalance) and dimensions, and the densities of nylon 6 and MWCNTs using an assumed porosity of 20 %, based on published mercury intrusion porosimetry measurements [44]. The density of nylon 6 is 1.084 g/cm³ [45], and that of MWCNTs is 1.8 g/cm³ [46]. A tabletop 'purpose built' tensile tester (Ernest. F. Fulham, 100 lb) was used to stretch the mats. Stretching was carried out at room temperature with a crosshead speed of 12.7 mm/min and a gauge length of 20 mm for both mat samples, as shown in the attached photos in figure 7.5. The results of the experiments were computed in a load (pounds force) vs. time (seconds). Stress - strain curves were regenerated by dividing the load by the cross sectional area and the displacement by the gauge length with their conversion factors respectively. The mechanical properties of the mats 'tensile strength, Young's modulus, strain at break as well as yield stress and strain' were determined from the plotted tensile stress - strain curves.

7.3.2 Results and discussion

The tensile testing of nanofibre mats provides an assessment of the average mechanical properties of the nanofibres rather than measuring an individual nanofibre. Figure 7.5,

shows the plotted stress - strain curves of the mats. It can be seen from the attached photos that the mat was stretched up to around 125-150 % strain without visible rupture. The initial part of these curves shows a linear elasticity within a small range of strain followed by nonlinear elasticity and a high resistance to deformation. In fact, the possible reasons for such high resistance are the high entanglement of fibre-to-fibre and the cohesive forces in the fibres assembly which lead to resisting slippage and deformation under loading.

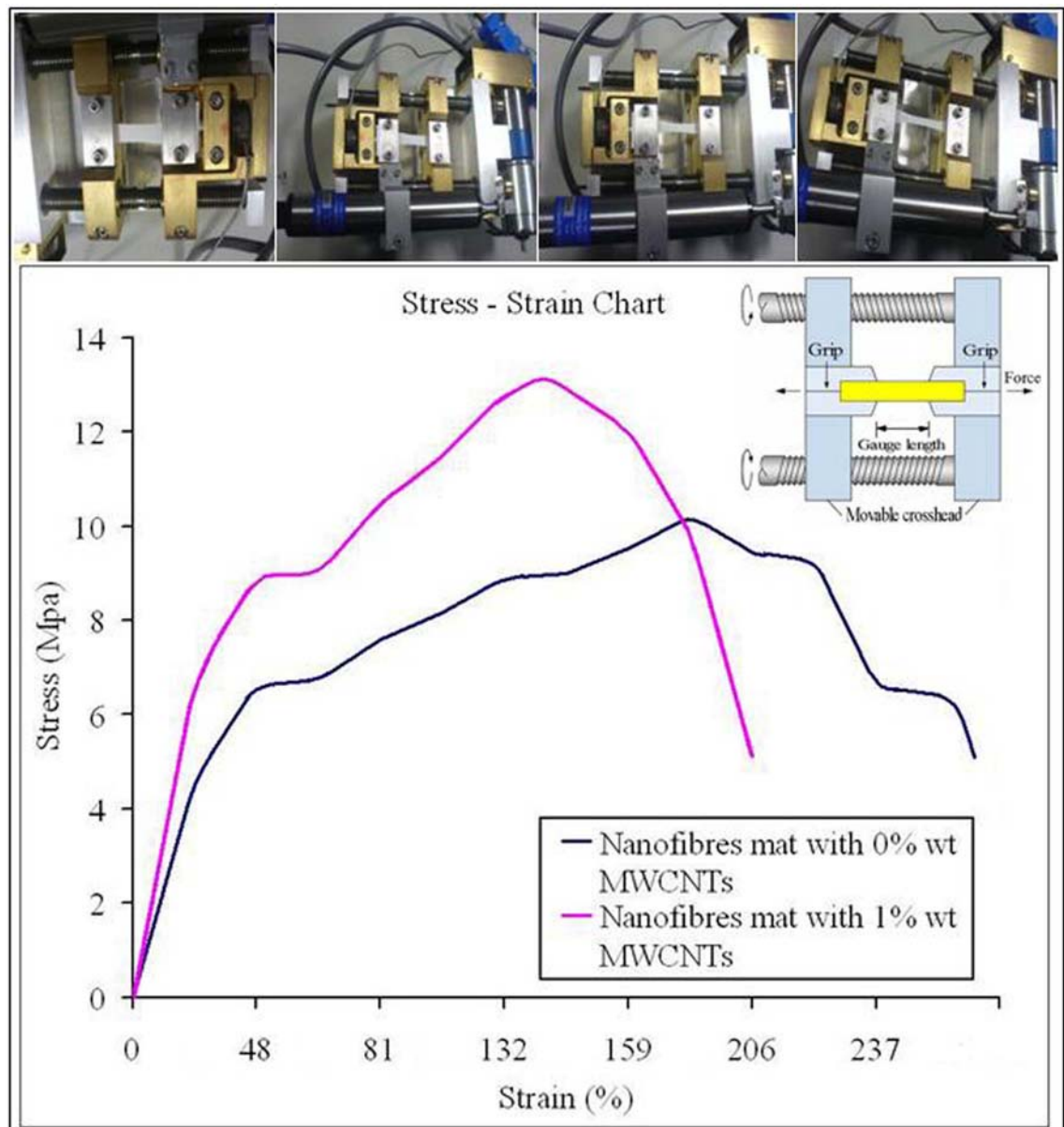


Figure 7.5, Typical stress - strain curves of nylon 6/MWCNTs composite nanofibre mats. The curves were correlated to samples containing MWCNTs of 0 and 1 wt. % in the composite nanofibres respectively. The attached photos show clearly how the mat was stretched and a schematic drawing of the tensile tester principle.

A yield stress point can also be observed after the initial part of the stress - strain curves followed by a gradual reduction in the Young's modulus caused by the initiation of the fibre slippage. As a result, fibre slippage has led to a slight fibre alignment along the tensile axis which made a slow increase in stresses being generated [47]. Further increase in stretching has led to a decrease in the cross sectional area of the mats up to 45 %, resulting in a subsequent failure of the fibres assembly.

Electrospun nylon 6 nanofibre mats are found to exhibit a tensile strength of 10.45 MPa, strain at break of 250 %, a 2 % offset yield stress of 6.7 MPa and yield strain of 48 %. The young's modulus of the electrospun nylon 6 mat was 19.4 MPa calculated from the linear portion of the stress - strain curve. However, the Young's modulus of the nylon 6 nanofibre mat is about 56 times lower than that of an undrawn single nylon 6 filament [48], 770 times lower than that of a conventional nylon 6 fibre and 1540 times lower than that of a single nylon 6 nanofibre at diameter of 85 nm [37]. The possible reasons for these low mechanical properties are because the molecular chains inside the electrospun fibre are not in good orientation along the fibre axis and due to the weak entanglements inside the nanofibrous mat.

Compared to the nylon 6 mat, the tensile strength of the nylon 6/MWCNTs mat containing only 1.0 wt. % of multiwall carbon nanotubes was increased by 25 % from 10.45 to 13.05 MPa, the strain at break was decreased by 18 % from 250 % to 205 %, the yield stress was increased by 34 % from 6.7 MPa to 9 MPa and the Young's modulus was increased by 46 %, from 19.4 MPa to 28.34 MPa. Thus the composite nanofibre mat has a higher stiffness and strength but lower ductility. In general, the improvement of the strength property by incorporating carbon nanotubes into the nanofibres was expected and fully agreed with the reported literature [46, 49-51].

Further alignment of nylon 6 nanofibres and proper drawing of the aligned fibre assembly are necessary in order to attain the required mechanical properties of the nanofibre mat. It has been found by Dean et. al. [52] that an improvement of molecular orientation of the nanofibre and thus Young's modulus of the mat can be achieved by collecting the nanofibres on a rotating collector. They have reported increases in Herman's orientation factor [53] from 0.149 to 0.204 and young's modulus from 58 MPa to 202 MPa with increasing the collector take up speed from 3000 rpm to 6000 rpm.

However, the tensile test of nonwoven mat is not suitable for characterizing the mechanical properties of nanofibres, because the fibre orientation is changed during the tensile test and also the nanofibre mat includes friction between the fibres which

influence the fibre property results. A more accurate analysis can be achieved by conducting the tensile test on a single nanofibre or on aligned nanofibre bundles.

7.4 Novel approach for tensile testing of single nanofibre [58]

A direct tension test of single nanofibre is a better way to characterize the mechanical properties of electrospun nanofibres. We designed a laboratory test rig set-up to conduct tensile tests on single nanofibres. The proposed set-up of load and elongation measurements is based on two linear springs in series principle and in accordance with the vibrations fundamentals [1, 4, 55], as shown in figure 7.6. In this principle, a spring with stiffness constant (K_s) and a single nanofibre 'representing a spring' with stiffness constant (K_f) are configured in series. Provided we apply a force F on this series, the force itself will transfer to the spring and the fibre at the same time i.e. $F = F_s = F_f$.

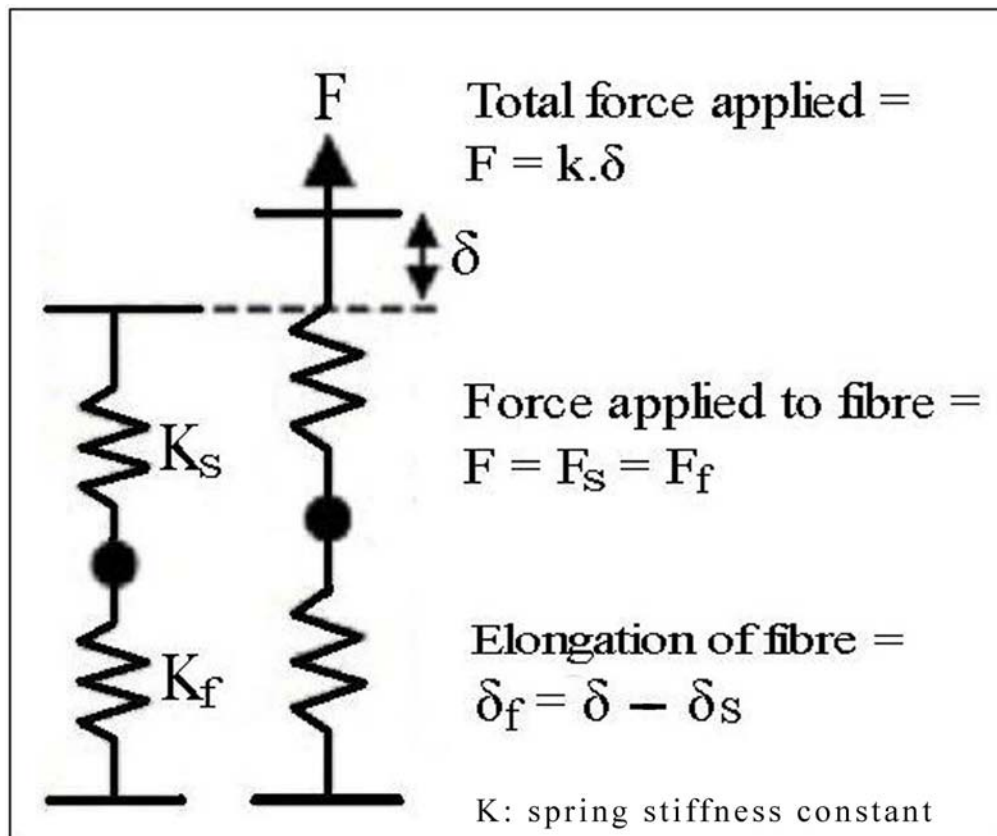


Figure 7.6, Schematic drawing of the spring 'transducer'- fibre series configuration [1, 4].

Elongation of the nanofibre can be calculated by subtracting displacement 'elongation' of the spring from elongation of the moving head 'the movable clamp' i.e. $\delta_f = \delta - \delta_s$. It must be noted that the applied force 'load' F and the elongation of the moving head are

known by the spring stiffness constant (K_S) and its elongation (δ_S) and the moving head velocity. We also note, in this set-up, that the elongation resolution is dependent from both the movable head velocity and the spring stiffness constant (K_S), while the force resolution is dependent only on the spring stiffness constant (K_S).

The tensile test set-up contains different parts. The first part is a movable head as in the case of an actuator, moved by attaching it to a digital pump. The head movement velocity can be controlled by the pump software being from several nanometers per second to several millimeters per second [54]. The second part is a spring acting as a transducer for measuring the tensile load. The load resolution is determined by the spring stiffness constant, this constant must be small in order to increase the load resolution. A cardboard frame with adhesive for holding vertically the nanofibre, a fixed head 'clamp' for holding the nanofibre frame, two grips for holding the frame - spring - movable head altogether in series, a ruler for reading the spring displacement and a vario illuminated stand magnifier are the other parts of this set-up. Figure 7.7, shows a schematic drawing of the designed tensile test set-up and a photograph of the set-up during experiment.

7.4.1 Experimental; electrospinning, samples preparation and nano tensile testing

A polymer solution of nylon 6 and formic acid at concentration of 20 wt. % was spun with electrospinning parameters; a volume feed rate of 0.2 ml/h, an applied voltage of 15 KV and a spinning distance of 8 cm. Aligned nanofibres were deposited over two circular electrically grounded disks separated by 4 cm space distance and collected over 2 minutes time. These operational parameters were used for producing aligned and uniform distribution diameter nylon 6 nanofibres, as described in chapters two and three [26]. To determine the tensile load acting on a single nanofibre, a typical micro spring with stiffness constant of 3.75 mg(wt)/mm '0.03823 N/m' and wire diameter of 100 μm supplied by (Skegness Springs Ltd, Lincs, UK) was used to measure the micro Newton force applied on the fibre. Tensile tests on a number of 12 samples were carried out as the following; double-sided adhesive tapes were placed on the cardboard frame to attach the nanofibres on the frame. By using the alignment mechanism of nylon 6 nanofibres (see figure 3.2), the cardboard frame was located beneath the collection disks and moved upwards to the targeted nanofibres until a bundle of aligned nanofibres was collected onto the two pieces of the adhesive tapes on the cardboard frame. Then the frame was held by the fixed head and gripped on the spring and then the 'rib' of the cardboard frame was cut carefully, leaving the two ends gripped between the spring and

the fixed head. With the aid of an intense bright light source and a dark background, individual nanofibres on the cardboard frame were visible due to light scattering through the nanofibres [2].

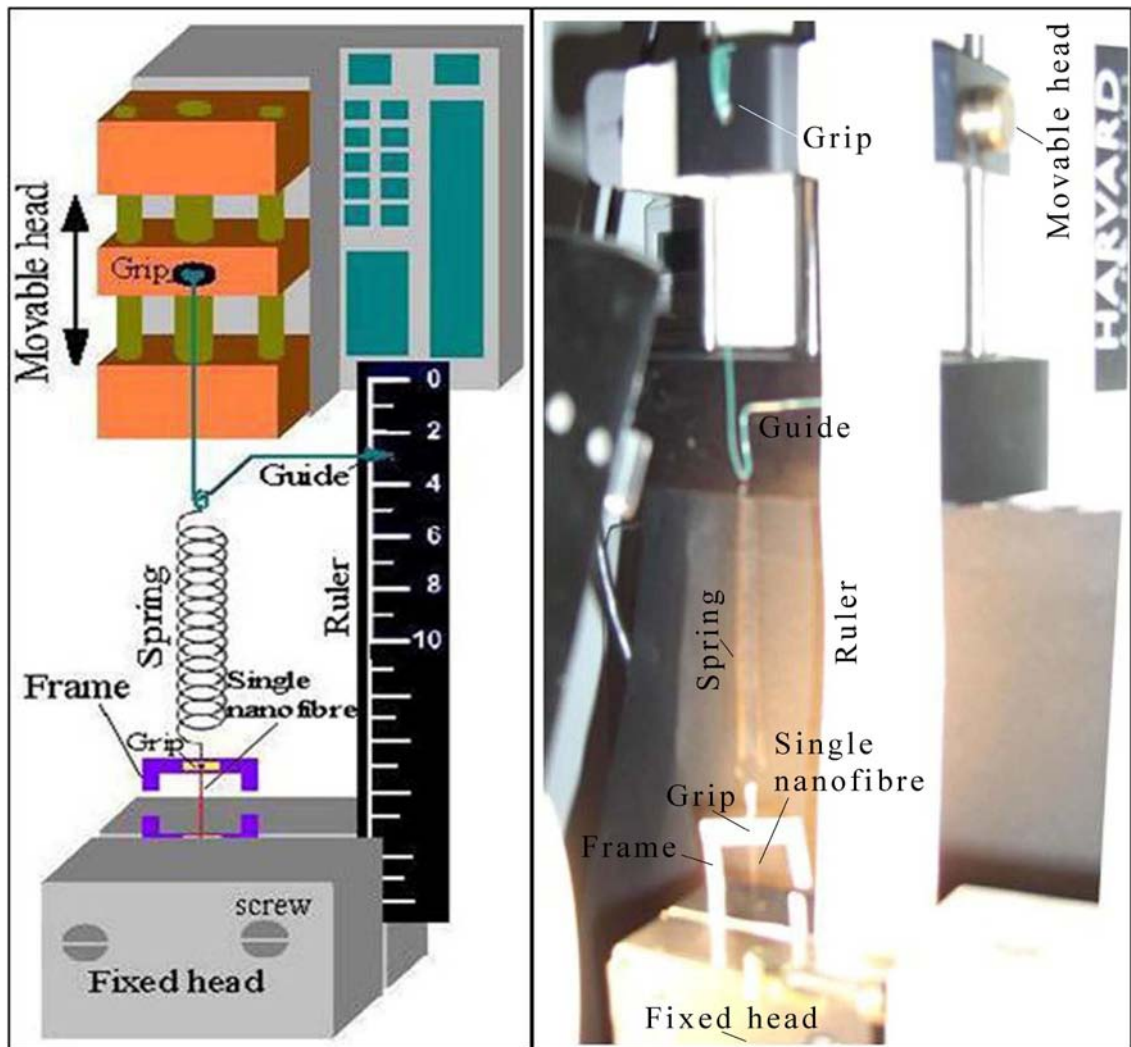


Figure 7.7, (Left) a schematic drawing shows the tensile testing set-up. It contains a single nanofibre held by a cardboard frame, the frame is held by a fixed head ‘clamp’ and gripped to a spring and the spring is gripped to a movable head by a rigid wire which does not significantly influence the actual tensile test of the nanofibre. A ruler is also held by the fixed head for reading the spring displacement. (Right) a photograph of the tensile testing set-up during on experiment.

Consequently, an electrospun single nanofibre or known number of individual nanofibres is obtained by removing the non-required nanofibres as shown in figure 7.8. An electrospun single nanofibre on the cardboard frame of a 20 mm gauge length was used as the tensile test sample. The velocity of the moving head was adjusted at 7.2 mm/min to allow the stretching of the nanofibre at constant loading rate.

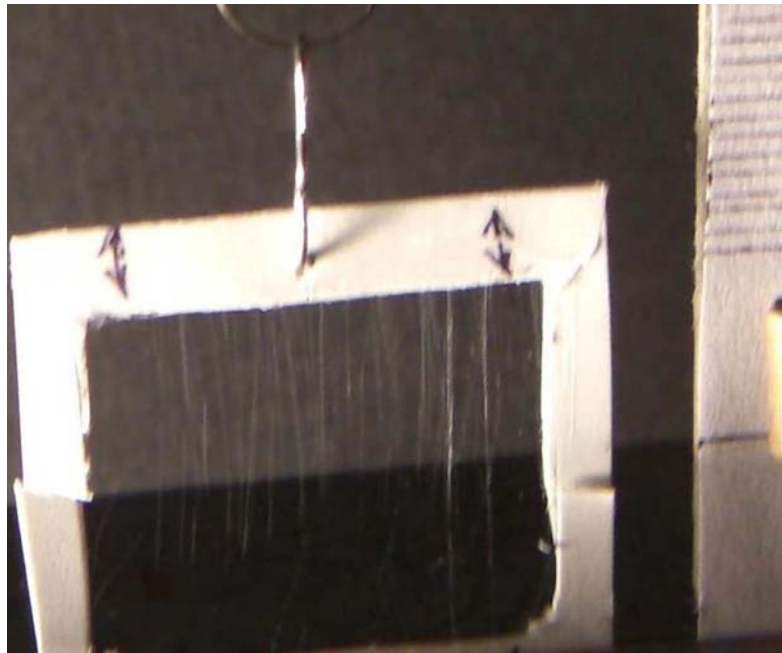


Figure 7.8, Individually aligned nanofibres are visible by light scattering. They are gripped between the spring and the fixed head through the cut cardboard frame.

Figure 7.9, shows different stages of the tensile testing for each sample. Proper sample gripping is necessary to prevent fibre slipping from the grips or breaking at the grips. Care was taken so that the single nanofibre appeared always vertical before the tensile test. Twelve samples were prepared under the same processing conditions for each tensile test and stretched to failure. After every tensile test, the broken fibre segments were coated and characterized by the SEM for measuring the nanofibre diameter.

The cross sectional area of the fibre is calculated from the diameter of the fibre, assuming circular cross section, measured by the SEM image as shown in figure 7.10. The initial and final X-position of the spring was noted for the calculation of the nanofibre elongation after the tensile test is conducted. The force was divided by the cross-sectional area and the linear density ‘tex’ of the single nanofibre to obtain the stress applied in different units ‘g (wt)/tex and MPa’. The single nanofibre strain was obtained by dividing the elongation by the gauge length.

7.4.2 Results and discussion

Good care, skillful manipulation, familiarity and time are required to conduct the tensile test for each sample. Nevertheless, the set-up is capable of providing data of the mechanical response of the spring and the nanofibre subjected to a tensile load. The data obtained is displacement of the spring over time, and hence the applied load and the nanofibre elongation. The average plots of the moving head velocity, the spring

displacement and the fibre elongation over time are shown in figure 7.11. Due to the resolution of the applied load, the nanofibre elongation is determined by the number of



Figure 7.9, Recorded photographs show the tensile test set-up is conducted step by step. (a) Shows the spring ‘transducer’ loaded by its weight only. (b) A cardboard frame containing aligned nanofibres was gripped to the spring, it is clear to see the spring displacement under the frame and nanofibres weight. (c) The cardboard frame was laid on and suspended between the fixed head jaws. (d) The cardboard frame was gripped by the fixed head jaws and its rib was clipped. (e) The cut rib of the cardboard frame (f) Non- required aligned nanofibres were carefully removed and thus a single nanofibre gripped between the fixed head and the spring with a 20 mm gauge length is ready for tensile test. (g) The tensile test process is utilized under a constant loading rate. (h) Tension is still applied on the nanofibre without nanofibre breaking. (i) Breaking ‘failure’ of the tensioned nanofibre has occurred, and the bounce of the upper end of the frame is clear as a result of nanofibre breaking.

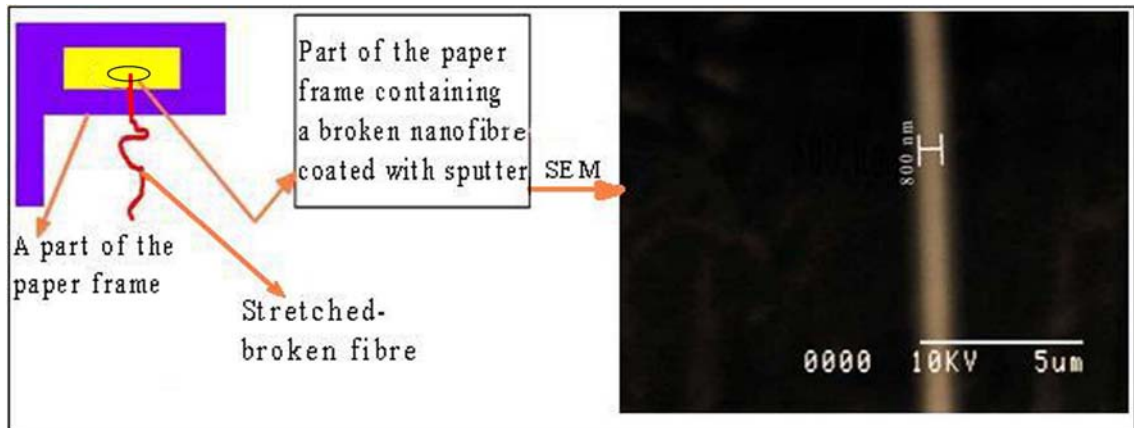


Figure 7.10, A schematic of the steps for determining the diameter of the broken single nanofibre, SEM image used to determine the diameter of the broken single nylon 6 nanofibre after the tensile test has been conducted.

readings in unit time, hence the higher the number of readings the higher the accuracy.

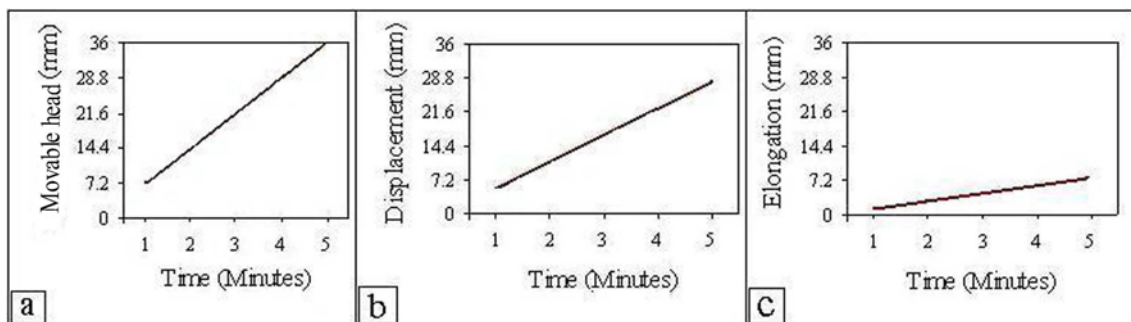


Figure 7.11, Method of calculating the fibre elongation over time. (a) Plot of the loading head movement versus time. (b) Average plot of the transducer spring displacement versus time. (c) Average plot of the nanofibre elongation versus time which indicates an approximately strain rate of 8 %/min.

The applied load on the nanofibre and the elongation over time were calculated from the equations mentioned in figure 7.6, above. Subsequently, the average stress - strain curve of a single nylon 6 nanofibre with diameter of 800 nm is plotted in figure 7.12. Based on this curve, when the nanofibre is loaded it goes through a linear elastic deformation followed by linearly strain - plastic deformation till the final breakage point is reached at the ultimate strain. It can be seen that the mechanical properties of single nylon 6 nanofibre are: Young's modulus of 901.65 MPa, tensile strength of 304 MPa, yield stress of 136.9 MPa and yield strain of 15 % and strain at break of 40 %.

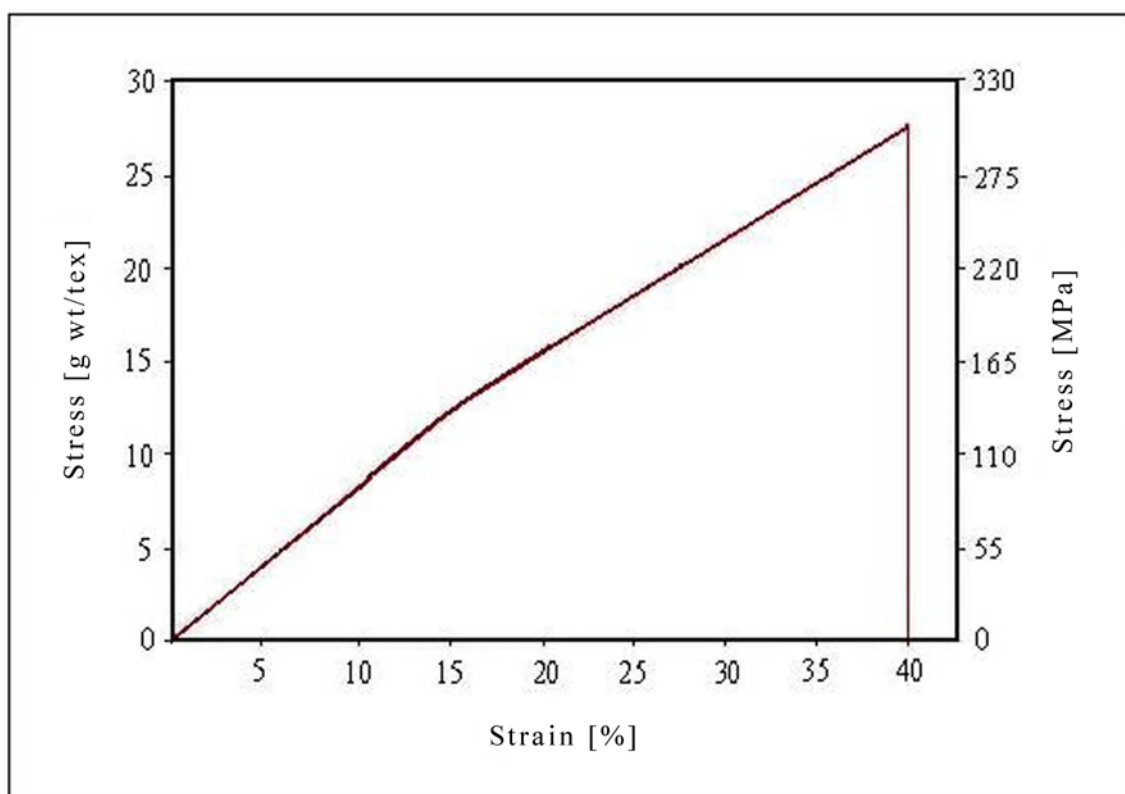


Figure 7.12, Average stress - strain curve of single electrospun nylon 6 nanofibre.

It has been shown that the ultimate tensile strength and the Young's modulus of single nylon 6 nanofibre were improved up to 30 times and 47 times respectively, than that of nonwoven nylon 6 nanofibre mat. This improvement is partly due to the orientation of the internal molecular structure of nylon 6 nanofibre induced by the alignment mechanism. On the other hand, the highest Young's modulus obtained for the electrospun nylon 6 single nanofibre with 85 nm diameter was about 30 GPa by using bending test method [37]. Moreover, conventional nylon 6 microfibre has a stiffer microstructure than the nylon 6 nanofibre and thus higher mechanical properties, such as; ultimate tensile strength up to 490 Mpa and strain at break of 25 % [56]. Little or no information has been reported on tensile testing of single nylon 6 nanofibre, and hence no comparison of results can be made.

It is expected that the orientation of nylon 6 molecules along the nanofibre axis is completely formed due to the extra 'drawing' effect during electrospinning and the alignment mechanism which in additionally orientates the molecules along the fibre axis. In this study, we evaluated the mechanical properties of single nylon 6 nanofibre due to the drawing ratio induced by the electrospinning process and the molecular chains orientation induced by the alignment mechanism. When examining these mechanical properties we can conclude that a higher molecular orientation and a degree

of crystallinity are required to improve the structural characteristics of nylon 6 nanofibre. This is consistent with the trends in the alignment mechanism. Hence, as discussed in chapter 3, we have been able to obtain aligned nanofibres up to 10 cm long by spacing the collection disks up to 10 cm. Under these conditions, as the polymer nanofibre reaches the first collection disk; it travels a long distance before reaching the second collection disk. The use of collection disks with large space distance of 10 cm aligns the molecular chains in the direction of fibre axis, resulting in a higher degree of molecular orientation.

The discussed novel approach for tensile testing of single nanofibre based on an actuator and a micro spring as a transducer has been shown to be able to establish the mechanical behaviour of single nanofibres and nanofibre bundles. The tensile testing set-up demonstrated in this study can be used for the mechanical characterization of other polymer nanofibres. This set-up can be developed for nanomechanical testing of nanoscale fibres and other materials.

7.4.3 Future work

As pointed out in the above discussion, the mechanical properties of electrospun nylon 6 nanofibres are affected by fibre diameter, molecular geometry, molecular orientation and degree of crystallinity [7]. Within the fibre diameter category, it has been demonstrated that the finer the nanofibre, the higher orientation of the macromolecular chains will be achieved and thus high resistance to the axial tensile load [2, 8]. For improving the mechanical properties of electrospun nylon 6 nanofibres, the following processes have to be further considered. Firstly, based on the alignment mechanism, the mechanical properties of aligned nanofibres with lengths of 5 cm, 6 cm, 7 cm, 8 cm, 9 cm and 10 cm have to be established. Secondly, the relationship between the collection disks space distance ‘nanofibre length’ with respect to the diameter of the nanofibre has to be verified. Thirdly, to make matters more useful, wide angle x-ray diffraction (WAXD) and SEM/TEM- based fractography have to be used on bundles of aligned nanofibres with different lengths to establish their structural properties. Where, (WAXD) pattern performs the molecular chain orientation ‘orientation factor’ and degree of crystallinity and TEM fractographical image performs the tensile failure mechanism “‘brittle fracture or necking appearance”’.

Another key issue related to future work is to equip the tensile testing set-up apparatus with more effective and robust measurements parts. Resistive ‘semiconductors’ strain gauges integrated into the spring and a CCD camera mounted on a microscope for

observing the nanofibre alignment and the mode of failure are examples of set-up apparatus improvements. In addition, to achieve very high force sensing resolution, one can either find a spring with very low stiffness or, even better, employ very high resolution displacement sensors.

Finally, the specification standard for single nanofibres tensile testing can be established by optimizing the gauge length of the sample, the load and displacement resolution and the strain rate applied on the nanofibre. This is a fundamental stepping stone for nanomechanical testing of nanofibres.

7.5 References

- [7.1] E.P.S. Tan, C.T. Lim, *Mechanical characterization of nanofibres- a review*, Composites Science and Technology, **66**, 1102-1111 (2006)
- [7.2] F. Chen, X. Peng, T. Li, S. Chen, X.F. Wu, D.H. Reneker, H. Hou, *Mechanical characterization of single high-strength electrospun polyimide nanofibres*, Journal of Physics D: Applied Physics, **41**, 025308-1 - 025308-8 (2008)
- [7.3] B.P. Saville, *Physical testing of textiles*, Woodhead Publishing Ltd, Cambridge, UK (1999)
- [7.4] E.P.S. Tan, C.T. Lim, *A novel approach to tensile testing of micro and nanoscale fibres*, Review of Scientific Instruments, **75**, 2581-2585 (2004)
- [7.5] E.P.S. Tan, S.Y. Ng, C.T. Lim, *Tensile testing of a single ultrafine polymeric fibre*, Biomaterials, **26**, 1453-1456 (2005)
- [7.6] www.mts.com/stellent/groups/public/documents/library/dev_002170.pdf, accessed 05/ 11/2008
- [7.7] S.C. Wong, A. Baji, S. Leng, *Effect of fibre diameter on tensile properties of electrospun poly (ϵ -caprolactone)*, Polymer, **49**, 4713-4722 (2008)
- [7.8] C.T. Lim, E.P.S. Tan, S.Y. Ng, *Effects of crystalline morphology on the tensile properties of electrospun polymer nanofibres*, Applied Physics Letters, **92**, 141908-1 - 141908-3 (2008)
- [7.9] R. Inai, M. Kotaki, S. Ramakrishna, *Structure and properties of electrospun PLLA single nanofibres*, Nanotechnology, **16**, 208-213 (2005)
- [7.10] E.P.S. Tan, C.T. Lim, *Effects of annealing on the structural and mechanical properties of electrospun polymeric nanofibres*, Nanotechnology, **17**, 2649-2654 (2006)
- [7.11] Z.W. Pan, S.S. Xie, L. Lu, B.H. Chang, L.F. Sun, W.Y. Zhou, G. Wang, D.L. Zhang, *Tensile tests of ropes of very long aligned multiwall carbon nanotubes*, Applied Physics Letters, **74**, 3152-3154 (1999)

- [7.12] D.Y. Lee, Y. Kim, S.J. Lee, M.H. Lee, J.Y. Lee, B.Y. Kim, N.I. Cho, *Characteristics of chemo-mechanically driven polyacrylonitrile fibre gel actuators*, *Materials Science and Engineering: C*, **28**, 294-298 (2008)
- [7.13] X. Wang, K. Zhang, M. Zhu, B.S. Hsiao, B. Chu, *Enhanced mechanical performance of self-bundled electrospun fibre yarns via post-treatments*, *Macromolecular Rapid Communications*, **29**, 826-831 (2008)
- [7.14] R. Jalili, M. Morshed, S.A.H. Ravandi, *Fundamental parameters affecting electrospinning of PAN nanofibres as uniaxially aligned fibres*, *Journal of Applied Polymer Science*, **101**, 4350-4357 (2006)
- [7.15] Nanonics Imaging manual, <http://www.nanonics.co.il>, accessed 05/11/2008
- [7.16] Veeco[®] product manual, <http://www.veeco.com>, accessed 05/11/2008
- [7.17] E. Zussman, M. Burman, A.L. Yarin, R. Khalfin, Y. Cohen, *Tensile deformation of electrospun nylon-6,6 nanofibres*, *Journal of Polymer Science: part B: Polymer Physics*, **44**, 1482-1489 (2006)
- [7.18] E.P.S. Tan, C.N. Goh, C.H. Sow, C.T. Lim, *Tensile test of a single nanofibre using an atomic force microscope tip*, *Applied Physics Letters*, **86**, 073115-1 - 073115-3 (2005)
- [7.19] P.A. Yuya, Y. Wen, J.A. Turner, Y.A. Dzenis, Z. Li, *Determination of Young's modulus of individual electrospun nanofibres by microcantilever vibration method*, *Applied Physics Letters*, **90**, 111909-1 - 111909-3 (2007)
- [7.20] L. Meirovitch, *Principles and Techniques of Vibrations*, Prentice-Hall, Saddle River, New Jersey, USA, Page 7458 (1997)
- [7.21] U. Rabe, K. Janser, W. Arnold, *Vibrations of free and surface-coupled atomic force microscope cantilevers: theory and experiment*, *Review of Scientific Instruments*, **67**, 3281-3293 (1996)
- [7.22] J.E. Sanders, B.S. Nicholson, S.B. Mitchell, R.E. Ledger, *Polymer microfibre mechanical properties: a system for assessment and investigation of the link with fibrous capsule formation*, *Journal of biomedical materials research*, **67A**, 1412-1416 (2003)
- [7.23] G. Binnig, C.F. Quate, C. Gerber, *Atomic force microscope*, *Physical Review Letters*, **56**, 930-933 (1986)
- [7.24] R. Jumpertz, A.V.D Hart, O. Ohlsson, F. Saurenbach, J. Schelten, *Piezoresistive sensors on AFM cantilevers with atomic resolution*, *Microelectronic Engineering*, **41/42**, 441-444 (1998)

- [7.25] U. Rabe, K. Janser, W. Arnold, *Vibrations of free and surface-coupled atomic force microscope cantilevers: theory and experiment*, Review of Scientific Instruments, **67**, 3281-3293 (1996)
- [7.26] M.B. Bazbouz, G.K. Stylios, *Alignment and optimization of nylon 6 nanofibres by electrospinning*, Journal of Applied Polymer Science, **107**, 3023-3032 (2008)
- [7.27] S.B. Warner, A. Buer, S.C. Ugbolue, G.C. Rutledge, M.Y. Shin, *A fundamental investigation of the formation and properties of electrospun fibres*, In National Textile Center Annual Report, 83-90 (1998), available from:
<http://www.tesumassd.org/research/NTCprojects/M98-D01-01.pdf>
- [7.28] L. Yang, C.F.C. Fitie, K.O. Van der werf, M.L. Bennink, P.J. Dijkstra, J. Feijen, *Mechanical properties of single electrospun collagen type I fibres*, Biomaterials, **29**, 955-962 (2008)
- [7.29] S.Y. Gu, Q.L. Wu, J. Ren, G.J. Vancso, *Mechanical properties of a single electrospun fibre and its structures*, Macromolecular Rapid Communications, **26**, 716-720 (2005)
- [7.30] R.J. Roark, *Formulas for stress and strain*, 3rd edition, page 136, McGraw-Hill Book Company Incorporation, New York (1954)
- [7.31] M.K. Shin, S.I. Kim, S.J. Kim, S.K. Kim, H. Lee, G.M. Spinks, *Size-dependent elastic modulus of single electroactive polymer nanofibres*, Applied Physics Letters, **89**, 231929-1 - 231929-3 (2006)
- [7.32] L.M. Bellan, J. Kameoka, H.G. Craighead, *Measurement of the Young's moduli of individual polyethylene oxide and glass nanofibres*, Nanotechnology, **16**, 1095-1099 (2005)
- [7.33] S.H. Lee, C. Tekmen, W.M. Sigmund, *Three-point bending of electrospun TiO₂ nanofibres*, Materials Science and Engineering A, **398**, 77-81 (2005)
- [7.34] Y. Ding, P. Zhang, Y. Jiang, F. Xu, J. Yin, Y. Zuo, *Mechanical properties of nylon-6/SiO₂ nanofibres prepared by electrospinning*, Materials Letters, **63**, 34-36 (2009)
- [7.35] E.P.S. Tan, C.T. Lim, *Physical properties of a single polymeric nanofibre*, Applied Physics Letters, **84**, 1603-1605 (2004)
- [7.36] J.L. Duvail, P. Retho, C. Godon, C. Marhic, G. Louarn, O. Chauvet, S. Cuenot, B. Nysten, L. Dauginet-De Pra, S. Demoustier-Champagne, *Physical properties of conducting polymer nanofibres*, Synthetic Metals, **135-136**, 329-330 (2003)

- [7.37] L. Li, L.M. Bellan, H.G. Craighead, M.W. Frey, *Formation and properties of nylon-6 and nylon-6/montmorillonite composite nanofibres*, *Polymer*, **47**, 6208-6217 (2006)
- [7.38] R. Roy, Jr. Craig, *Mechanics of Materials*, 2nd edition, pages 389-395 and pages 448-504, John Wiley, New York (2000)
- [7.39] M. Wang, H.J. Jin, D.L. Kaplan, G.C. Rutledge, *Mechanical properties of electrospun silk fibres*, *Macromolecules*, **37**, 6856-6864 (2004)
- [7.40] F. Ko, Y. Gogotsi, A. Ali, N. Naguib, H.H. Ye, G.L. Yang, *Electrospinning of continuous carbon nanotube-filled nanofibre yarns*, *Advanced Materials*, **15**, 1161-1165 (2003)
- [7.41] J.J. Mack, L.M. Viculis, A. Ali, R. Luoh, G. Yang, H.T. Hahn, *Graphite nanoplatelet reinforcement of electrospun polyacrylonitrile nanofibres*, *Advanced Materials*, **17**, 77-80 (2005)
- [7.42] E.P.S. Tan, C.T. Lim, *Nanoindentation study of nanofibres*, *Applied Physics Letters*, **87**, 123106-1 - 123106-3 (2005)
- [7.43] A. Agic, B. Mijovic, *Mechanical properties of electrospun carbon nanotube composites*, *Journal of Textile Institute*, **97**, 419-427 (2006)
- [7.44] I.K. Kwon, S. Kidoaki, T. Matsuda, *Electrospun nano to microfibre fabrics made of biodegradable copolyesters: structural characteristics, mechanical properties and cell adhesion potential*, *Biomaterials*, **26**, 3929-3939 (2005)
- [7.45] Sigma-Aldrich, www.sigmaaldrich.com, accessed 19/11/2008
- [7.46] H. Hou, J.J. Ge, J. Zeng, Q. Li, D.H. Reneker, A. Greiner, S.Z.D. Cheng, *Electrospun polyacrylonitrile nanofibres containing a high concentration of well-aligned multiwall carbon nanotubes*, *Chemistry of Materials*, **17**, 967-973 (2005)
- [7.47] J. Ayutsede, M. Gandhi, S. Sukigara, M. Micklus, H.E. Chen, F. Ko, *Regeneration of Bombyx mori silk by electrospinning, part 3: characterization of electrospun nonwoven mat*, *Polymer*, **46**, 1625-1634 (2005)
- [7.48] H. Mahfuza, A. Adnan, V.K. Rangari, M.M. Hasan, S. Jeelani, W.J. Wright, S. J. Deteresa, *Enhancement of strength and stiffness of Nylon 6 filaments through carbon nanotubes reinforcement*, *Applied Physics Letters*, **88**, 083119-1 - 083119-3 (2006)
- [7.49] J.S. Jeong, J.S. Moon, S.Y. Jeon, J.H. Park, P.S. Alegaonkar, J.B. Yoo, *Mechanical properties of electrospun PVA/MWNTs composite nanofibres*, *Thin Solid Films*, **515**, 5136-5141 (2007)

- [7.50] S.D. McCullen, D.R. Stevens, W.A. Roberts, S.S. Ojha, L.I. Clarke, R.E. Gorga, *Morphological, electrical, and mechanical characterization of electrospun nanofibre mats containing multiwalled carbon nanotubes*, *Macromolecules*, **40**, 997-1003 (2007)
- [7.51] A. Allaoui, S. Bai, H.M. Cheng, J.B. Bai, *Mechanical and electrical properties of a MWNT/epoxy composite*, *Composites Science and Technology*, **62**, 1993-1998 (2002)
- [7.52] M.V. Jose, B.W. Steinert, V. Thomas, D.R. Dean, M.A. Abdalla, G. Price, G.M. Janowski, *Morphology and mechanical properties of nylon 6/MWNT nanofibres*, *Polymer*, **48**, 1096-1104 (2007)
- [7.53] R.J. Samuels, *Structured polymer properties*, Wiley InterScience, New York (1974)
- [7.54] <http://www.harvardapparatus.com>, accessed 22/01/2009
- [7.55] C.W. De Silva, *Vibration: fundamentals and practice*, CRC Press, London (2007)
- [7.56] B.C. Goswami, J.G. Martindale, F.L. Scardino, *Textile yarns: technology: structure and applications*, Wiley InterScience, New York (1977)
- [7.57] C.R. Carlisle, C. Coulais, M. Namboothiry, D.L. Carroll, R.R. Hantgan, M. Guthold, *The mechanical properties of individual, electrospun fibrinogen fibres*, *Biomaterials*, **30**, 1205-1213 (2009)
- [7.58] M.B. Bazbouz, G.K. Stylios, *The tensile properties of electrospun nylon 6 single nanofibres*, *Journal of Polymer Science Part B: Polymer Physics*, Submitted for publication, WILEY InterScience (2009)

CHAPTER 8: GENERAL DISCUSSION AND CONCLUSION

8.1 Overall project summary

In this thesis, we have aimed to investigate yarn spinning from electrospun nanofibres. We have based these studies on the staple yarn spinning concept by controlling the nanofibres morphology, aligning the nanofibres, inserting twist and taking up of a yarn. We have also aimed to optimize the geometrical and mechanical properties of the spun yarn by defining the yarn linear density, nanofibres twist per unit length and mechanical properties of every single nanofibre. This aim has been fulfilled by investigating the kinetic features of nanofibres entering into the spinning zone, theoretically and practically. It has also required studying the tensile testing behaviour of a single nanofibre. Typically, we have aimed throughout this investigation to provide a spinning strategy for yarn formation from electrospun nanofibres. This strategy can be applied to any polymers and it is outlined by the following findings:

- Controlling the electrospun nanofibre morphology (uniform nanofibre diameter and electrospinning nanofibres with approximately equal diameters).
- Aligning and paralleling the electrospun nanofibres by a mechanism designed to be compatible with the need of twist insertion.
- An effective mechanism for inserting twist into aligned nanofibres and taking up the yarn.
- Nanofibre orientation. The alignment mechanism must provide the required degree of chain orientation and crystallinity for nanofibre.
- Defining the velocity of the nanofibres and their linear density in order to control the yarn linear density and twist per unit length.

8.2 Summary of project results and suggestions for future work

Based on the above requirements, we have established the research findings in spinning nylon 6 nanofibre yarn. We have used nylon 6 polymer consistently for electrospinning of nylon 6 nanofibres and spinning them into yarn. We have designed and implemented the electrospinning set-up after good understanding of its operational principle and effects on process parameters.

We have investigated the physical properties of nylon 6/formic acid solution at different concentrations and the electrospinning process parameters in order to establish their

effect on the nylon 6 nanofibres morphology, average diameter and diameter uniformity. We have characterized the electrospun nylon 6 nanofibres at different concentrations, applied voltages and electrospinning distances by SEM. It has been found that the polymer solution concentration plays an important role in determining the nanofibre morphology. Particularly, polymer solution concentration of 20 wt. %, applied voltage of 15 KV , volume feed rate of 0.2 mL/h and electrospinning distance of 8 cm have been found optimum to make uniform nylon 6 nanofibres with uniform diameter.

After reviewing nano aligning mechanisms, we have redesigned a novel nano aligning and paralleling mechanism by introducing a gap 'space' between two grounded copper collector disks. This mechanism has generated a bundle of aligned three dimensional nylon 6 nanofibres and it has also been found suitable for nanofibres twist insertion. We have systematically scrutinized the degree of nanofibres alignment, nanofibres length and linear density of the collected nylon 6 nanofibres by varying the space between the disks and the collection time. The experiments have demonstrated that the number of the distributed nanofibres in the bundle can be controlled by altering the applied voltage, collection time and space between the disks. SEM images have indicated a greater degree of alignment as the space between the disks and collection time increases. The analysis has shown that the electrostatic repulsion forces between the deposited fibres also have a significant effect on the degree of alignment. The maximum length of the fibre bundle collected was 10 cm, depending on the collection geometry and processing parameters. We have found that the optimum distance between collector disks for spinning aligned nanofibres with acceptable density is 4-5 cm. This has provided the basis for twisting the nanofibre bundle into a yarn form. We have revealed that the strength of the stretching forces exerted on the nanofibres is related to the applied voltage, collection time and space between the disks. In other words, alignment and stretching of the nanofibres are derived by the electrostatic interactions between the positive electrode on the spinneret and the grounded disks.

The fibres have been characterized mechanically to ascertain their mechanical behaviour which is an indication of their chain orientation.

Before spinning the nanofibres into a yarn, we have aimed to functionalize and strengthen the nylon 6 nanofibres. We have opted in using multiwall carbon nanotubes (MWCNTs) as filler nanoparticles, due to their high hardness, strength, thermal and

electrical conductivity. We have used the shearing method (sonicating) to improve the dispersion of MWCNTs into the polymer solution. We have manipulated the electric forces of electrospinning and the stretching forces of the alignment mechanism to perform better alignment of the MWCNTs along the nanofibre axis. We have conducted SEM and TEM studies to characterize the morphology of nanofibres, the dispersion of MWCNTs and their alignment inside the fibre body. We have found that high speed shearing is a simple and convenient method to improve the dispersion of MWCNTs into a polymer matrix under a given loading. We have also noticed that the geometrical and electrical stretching of the collected nanofibres aligned the MWCNTs along the axis of the nanofibre, proving the alignment mechanism effective. We have also demonstrated that MWCNTs could not be completely embedded into the nanofibre when the loading concentration was increased above 3 wt. %. This indicates that the shearing method of dispersion could not perform higher loading concentration of MWCNTs in the polymer solution. In other words, further investigation for useful dispersion agents must be carried out in future work for improving CNTs/nanofibre composite.

After preparing aligned nanofibres and reviewing all nanofibre yarn spinning mechanisms and understanding their principles, a suitable yarn spinning mechanism was designed and used successfully. It was found that by controlling the geometrical shape and strength of the electric field between the spinneret and the collector, it is possible to control and achieve various nanofibrous architectures. Moreover, inserting twist and taking up the yarn requires grounded dynamic collection parts. Based on these requirements, we have implemented a novel mechanism for spinning continuous twisted yarn from aligned MWCNTs/ nylon 6 nanofibres. We have modified the alignment mechanism further (two faced disks separated by a distance of 4-5 cm) into a spinning mechanism by dynamically making the first disk as a twist inserting disk and the second disk as a taking up disk. SEM images have showed twisted nanofibres yarns with diameters ranging between 5 to 10 microns. We have found that twist speeds of 500 to 750 revolutions per minute and taking up speed of 8 m/min are optimum, provided that the electrospinning parameters remain constant. One important challenge we faced was the sticking of the yarn on the take up spool. This is attributed to the lack of evaporation of the solvent. Although we tried to overcome this problem taking into account the efforts of previous researchers, we still experience difficulties in winding of the yarn. Some suggestions for further research are outlined below.

- To control the evaporation rate of the solvent from the nanofibres until fully dried.
- To either change the take up spool material structure or coat the metallic spool with suitable lubricant.
- To coagulate the solvent during evaporation by putting the spinning zone devices in a liquid bath suitable to the polymer solution used, provided that the imparted twist in the liquid medium can be controlled during the nanofibre yarn formation.
- To change 'electrospinning' as 'electro dry spinning' to 'electro melt spinning' as it is more effective for spinning continuous yarn wound onto a take up spool without sticking.

Furthermore, for extending the nano yarn end use and based on the core spun yarn concept, we have also investigated and successfully fulfilled another new electro mechanical mechanism for spinning 'core electrospun nano yarn'. SEM images have shown that the deposited nanofibres are wrapped helically around the core filament resulting in a core electrospun nano yarn. We have analytically investigated the parameters of this mechanism such as feed-in angles, twist speeds and take up speeds for optimum spinning performance. Twist speeds at 500 to 750 revolutions per minute on core filament feed-in angle of 0° degree and take up speed of 1.5 cm/sec were found to be the optimum parameters for producing nano yarn under this new nano yarn spinning mechanism.

Some further suggestions to increase the take up speed and thus the core yarn production rate are as follows;

- By increasing the number of the spinnerets around the core filament.
- By improving the nanofibres-filament core adhesion such as: pre-treatment of the synthetic core with plasma.

We have found that core filaments that can be used include polymer, carbon, glass and elastomeric filament, monofilament, textured filament, high tenacity filament, metallic wire and staple yarn. Spinning continuous nanofibre yarn has great significance for many applications; medical and industrial such as filters, diapers, sanitary pads, protective and wiping clothing and light composites for automotive and aerospace use.

As mentioned previously, controlling the taken up yarn linear density and its twist per unit length has required defining of the entering nanofibres velocity into the spinning zone and their linear density. This point has been further explored aiming to define theoretically and practically the collected nanofibres velocity. We have reviewed the mathematical equations that govern electrospinning from the jet initiation to the nanofibres collection. We have examined the electrospinning modes theory and their kinetic features, and we have derived a novel mathematical model as necessity for calculating theoretically the jet velocity at its splitting point, the number of nanofibres generated from the jet and their velocities. The equations of the electrospinning jet and nanofibre velocity were obtained through deriving the mass, charge and linear momentum conservation laws using Cauchy's inequality, as the following.

$$\boxed{u_{j\text{Max}} = \frac{Q(\delta r_o^2 L_j + 1)}{\pi \rho r_o^2}}, \quad \boxed{u_f = \frac{u_{j\text{Max}}}{N_b} \left(\frac{a_j}{a_f}\right)^2 c_p}, \quad \boxed{N_b = \frac{L_j}{L_f} \left(\frac{a_j}{a_f}\right)^2 c_p}$$

$$\boxed{L_{\Sigma f} = L_j \left(\frac{a_j}{a_f}\right)^2 c_p}, \quad \boxed{L_{\Sigma f} = N_b \cdot L_f}, \quad \boxed{E_v = \frac{(Q - Mf_w)}{(Q - Mf_d)} \times 100}$$

Where, the first equation is for defining the maximum velocity of the jet at its splitting point based on the dimensional and operational features of the jet. The other equations are for defining the velocity and number of the nanofibres at the collection point based on the velocity and dimensions of the jet, dimensions of the collected nanofibre and evaporation rate of the solvent. We have found that these derived equations are convenient for theoretically predicting the density and kinematics of the electrospun nanofibres. To find out the accuracy of the model equations, we have determined practically the jet and the collected nanofibres velocities for PEO electrospun nanofibres. It has been shown that collecting the electrospun nanofibres by a rotating disk was an effective method for finding the actual velocity of the collected nanofibres. The experimental results of electrospinning PEO nanofibres have proved the jet splitting theory. It has been seen that the theoretical prediction was generally in reasonable agreement with the experimental evidence.

Upon aligning the nanofibres, we have aimed to mechanically characterize the nanofibres by tensile testing single nanofibres and nanofibre mats. The tensile test

method provides information about the mechanical properties of the nanofibre such as tensile strength, elastic modulus and strain at break. We have successfully performed the tensile test on nylon 6 and composite nylon 6/ MWCNTs nanofibre mats by a commercial tensile tester with a view to recognize the MWCNTs filling effect. The testing results have shown that electrospun nylon 6 nanofibre mat had a tensile strength of 10.45 MPa, Young's modulus of 19.4 MPa and strain at break of 250 %. After incorporating MWCNTs into the nanofibre, the nanofibre mat exhibited enhanced mechanical properties with a tensile strength of 13.05 MPa, Young's modulus of 28.34 MPa and strain at break of 205 %. The experimental stress - strain curves have shown that the nylon 6 nanofibre mat behaves like ductile material with obvious softening at the final failure, while the nylon 6/MWCNTs nanofibre mat behaves simply as a brittle material. However, it has been found that the tensile test for nonwoven nanofibre mat was not suitable for reflecting the exact mechanical properties of nanofibre. The architectural features of the fibre within the mat are random, fibre orientation is changed during the tensile test and also the nanofibre mat includes friction points between the fibres. A more accurate characterization can be achieved by conducting the tensile test on a single nanofibre or even aligned nanofibre bundles.

We have provided a critical review of the developed mechanical characterization testing methods for single nanofibres including tensile and bending test method and nanoindentation. Taking into account the efforts of previous researchers, we have designed and implemented a novel home made set-up for performing tensile testing of a single nanofibre. The load and displacement resolution of the set-up are found sufficient to determine the stress - strain response of the single nylon 6 nanofibre during deformation. As a result, we have plotted the experimental stress - strain curve for the single nylon 6 nanofibre in order to define the tensile strength, axial tensile modulus and ultimate strain. The testing results have shown that the aligned single electrospun nylon 6 nanofibre with 4 cm length had a Young's modulus of 901.65 MPa, a tensile strength of 304 MPa, a yield stress of 136.9 MPa and a yield strain of 15 % and a strain at break of 40 %. In other words, the simple tensile test set-up has proven to be successful for obtaining the nanofibre mechanical properties. However, the compared values of the tensile strength, axial modulus and ultimate strain for nylon 6 nanofibre with those of conventional nylon 6 microfibre have indicated that some of the nylon 6 nanofibre molecule chains have not been oriented well along the nanofibre axis during electrospinning and through the alignment mechanism. For further improving the

mechanical properties of electrospun nylon 6 nanofibre and spun yarn, the following suggestions may be useful for future work:

- Based on the alignment mechanism, the mechanical properties of the collected aligned nanofibres with length of 5 cm, 6 cm, 7 cm, 8 cm, 9 cm and 10 cm must be determined.
- The relationship between the collection disks space distance 'nanofibre length' with respect to the diameter of the nanofibre must be verified.
- Wide angle x-ray diffraction (WAXD) and SEM/TEM- based fractography must be conducted on a bundle of aligned nanofibres with different lengths to clarify their structural properties.
- A spring with very low stiffness constant, strain gauges integrated into the spring, very high resolution displacement sensors and a CCD camera mounted on a microscope must improve to the tensile set-up.
- Finally, optimizing the tensile test standards such as; gauge length of the sample, load and displacement resolution and strain rate applied on the nanofibre must be defined as they are important specifications for nanomechanical testing of nanofibres.

Lastly, to put this research in future context and clarify the industrial directions on nanofibre engineering, we have presented a critical account on the various modifications of the electrospinning designs to obtain different nanofibre architectures. We have illuminated by mechanism diagrams and nanofibre images the recent advances regarding nonwoven nanofibre fabrics, nanofibre fabric blends, nonwoven fabrics coated by nanofibre layers, three dimensional nanofibre fabrics and woven nanofibre fabrics. Moreover, we have investigated the industrial productivity of electrospinning. We have presented the experimental work in order to increase the electrospinning productivity and to verify the challenges associated with it. We have also provided a useful discussion on nanofibre engineering aspects and end uses such as core-shell, bicomponent, hollow, porous and fancy helical nanofibres.

In conclusion, although electrospinning is an important and promising technology for producing different nanofibre architectures, there is still further work to be done in process parameters, geometries, on nanofibre properties, manufacturing of continuous nanofibre yarn and nonwoven mats, as well as venturing towards woven fabrics and functional coatings.